2016 IWH

International Workshop on Holography and Related Technologies

全像暨應用技術國際學術研討會

Welcome message

Wen-Yih Isaac Tseng, MD, PhD
Director
National Taiwan University
Molecular Imaging Center

Dear Colleagues and Friends,

Welcome to the 2016 International Workshop on Holography (IWH) & Biomedical Molecular Imaging (BMI)! We are very glad to have you with us in the famous hot spring city of northeastern Taiwan, Jiaoxi, and share with us your recent progress in research.

The conference is organized jointly by the IWH and the National Taiwan University Molecular Imaging Center (NTU MIC). The aim of the conference is to create networking opportunities for exchanging research results and to stimulate new ideas. Every year, we hold the meeting in a resort area because we believe that novel ideas come from free interactions among relaxed minds.

There are 173 people attending the Conference of 2016 IWH & BMI. We have 69 keynote and invited speakers coming from China, Japan, Korea, Singapore, USA and Taiwan. The speakers are world-leading scientists in a wide spectrum of disciplines including holography, biomedical imaging, optical imaging, microscopy and spectroscopy.

I would like to thank all of you for your participation and sincerely hope that you will enjoy this three-day-event. I look forward to seeing you during the meeting to further strengthen our ties for future collaboration.

Contents

Committee

General Chairs
HSU, Ken-Yuh (National Chiao Tung University, Taiwan)
YATAGAI, Toyohiko (Utsunomiya University, Japan)
TSENG, Wen Yih Isaac(National Taiwan University, Taiwan)

Advisory Committee
HESSELINK, L. (Stanford University, USA)
ICHIOKA, Y. (Osaka University, Japan)
KODATE, K. (Japan Women's University, Japan)
KUBOTA, T. (Kyoto Institute of Technology, Japan)
KURODA, K. (Utsunomiya University, Japan)
YU, F. T. S. (Pennsylvania State University, USA) Francis Yu
You, Han-Hui (National Central University, Taiwan)
Cheng, Yih-Shyang (National Central University, Taiwan)

International Organizing Committee
HORIMAI, H. (Toyohashi University of Technology, Japan)
HOSHIZAWA, T. (Hitachi, Ltd., Japan)
IKEDA, J. (Kyoeisha Chemical Co., Ltd., Japan)
INOUE, A. (Mitsubishi Chemical Corporation, Japan)
INOUE, M. (Toyohashi University of Technology, Japan)
JIN, G. -F. (Tsinghua University, China)
LEE, S. -H. (Kwangwoon University, Korea)
NAYA, M. (Fujifilm Corporation, Japan)
NOMURA, T. (Wakayama University, Japan)
ORLIC, S. (Technical University of Berlin, Germany)
PARK, N.-C. (Yonsei University, Korea)
SAITO, N. (Nippon Housou Kyoukai (NHK), Japan)
SAKAMOTO, Y. (Hokkaido University, Japan)
XU, X. W. (DSI, Singapore)
YOSHIKAWA, H. (Nihon University, Japan)
FUJIMURA, R. (Utsunomiya University, Japan)
BARADA, D. (Utsunomiya University, Japan)
FUKUDA, T. (AIST, Japan)
YAMAMOTO, M. (Tokyo University of Science, Japan)
HASHIMOTO, N (Citizen)
MATOBA, O (Kobe University, Japan)
NOMURA, T (Wakayama University, Japan)
MATUSHIMA, K (Kansai University, Japan)
AWATSUJI, Y (Kyoto Institute of Technology, Japan)

Steering Committee
Chair
LUO, Yuan (National Taiwan University, Taiwan)
Co-Chair
SHIMURA, Tsutomu (the University of Tokyo, Japan)

Members
CHEN, Cheng-Huan (National Chiao Tung University, Taiwan)
CHEN, Chien-Yue (National Taiwan University of Science and Technology, Taiwan)
CHEN, Hui-Chi (Fu Jen Catholic University, Taiwan)
CHEN, Jing-Heng (Feng Chia University, Taiwan)
CHEN, Kun-Huang (Feng Chia University, Taiwan)
HSIEH, Chia-Lung (Academic Sinica, Taiwan)
LEE, Ju-Yi (National Central University, Taiwan)
GOSPODINOVA, Vera Marinova (National Chiao Tung University, Taiwan)
SU, Wei-Chia (National Changhua University of Education, Taiwan)
TU, Han-Yen (Chinese Culture University, Taiwan)

Program Committee
Chair
LIN, Shiuan-Huei (National Chiao Tung University, Taiwan)

Members
CHENG, Chau-Jern (National Taiwan Normal University, Taiwan)
SUNG, Kung-Bin (National Taiwan University, Taiwan)
HSIEH, Mei-Li (National Chiao Tung University, Taiwan)
HSU, Cheng-Chih (Yuan Ze University, Taiwan)
HSU, Wei-Feng (National Taipei University of Technology, Taiwan)
LIU, Jung-Ping (Feng Chia University, Taiwan)
SU, Wei-Hung (National Sun Yat-sen University, Taiwan)
YU, Ye-Wei (National Central University, Taiwan)

Program of the Symposium

Program of IWH 2016

Fri., November 11th, 2016			
Time	**Schedule**		
13:20-14:00	Opening Ceremony		
Time	**Title**	**Speakers**	**Chair**
14:00-14:30	**Keynote Speaker I** Computational Imaging : Seeing the Invisible	**BARBASTATHIS, George** Massachusetts Institute of Technology	**LIN, Shiuan-Huei** **LUO, Yuan**
14:30-15:00	**Keynote Speaker II** Holography for 3D Display – Status and Challenges	**LEE, Byoungho** Seoul National University	
15:00-15:40	Break		
15:40-16:00	Invited Speaker 1 **Multi-View Scanning Hologram**	**LIU, Jung-Ping** Feng Chia University	**ZHOU, Chang-He** **CHENG, Chau-Jern**
16:00-16:20	Invited Speaker 2 **Floating Image Generated with the Integration of Holographic and Geometrical Imaging**	**CHEN, Cheng-Huan** National Chiao Tung University	
16:20-16:40	Invited Speaker 3 **Phase-distortion Elimination of the Phase-only Read-out Signal of Holographic Data Storage System**	**YU, Yeh-Wei** National Central University	
16:40-17:00	Invited Speaker 4 **Three Dimensional Display Based on Volume Holographic Photopolymer**	**CAO, Liang-Cai** Tsinghua University	
17:00-17:20	Invited Speaker 5 **Phase Modulated Collinear Holographic Data Storage System**	**TAN, Xiao-Di** Beijing Institute of Technology	
17:20-17:40	Invited Speaker 6 **Improvement of Signal to Noise Ratio in Holographic Data Storage by Limiting Aperture Opening of Imager Pixels**	**FUJIMURA, Ryushi** Utsunomiya University	
18:00-21:00	Banquet (Invited)		
Sat., November 12th, 2016			
Time	**Title**	**Speakers**	**Chair**
08:30-09:00	**Keynote Speaker III** Holographic Data Storage System Enabling 2.4 Tbit/in.2 Recording	**HOSHIZAWA, Taku** Hitachi Ltd.	**SHIMURA, Tsutomu** **HSU, Ken-Yuh**
09:00-09:30	**Keynote Speaker IV** Optical Phase Conjugation Technology and the Application to Optical Information Processing	**SUN, Ching-Cherng** National Normal University	
09:30-09:50	Invited Speaker 7 **Graphene Based Organic-inorganic Holographic Elements and Devices**	**GOSPODINOVA, Vera Marinova** National Chiao Tung University	**FUJIMURA, Ryushi** **HSIEH, Mei-Li**
09:50-10:10	Invited Speaker 8 **The Application of Waveguide Holograms to Display Systems**	**SU, Wei-Chia** National Changhua University of Education	
10:10-10:30	Invited Speaker 9 **A Study of PQ:PMMA Photopolymer Recording Process Based on Rate Equations and Diffusion Equations**	**CHUNG, Te-Yuan** National Central University	
10:30-10:50	Break		
10:50-11:10	Invited Speaker 10 **Full-color High-definition CGH Employing RGB Color Filters**	**MATSUSHIMA, Kyoji** Kansai University	**NOMURA, Takanori** **LEE, Ju-Yi**
11:10-11:30	Invited Speaker 11 **Application of Head-mounted Computer Generated Holographic Display on the Human Visual Training**	**CHEN, Chien-Yu** National Taiwan University of Science and Technology	

Time	Title	Speakers	Chair
11:30-11:50	Invited Speaker 12 **Joint Wavelength and Position Multiplexing Using Optical Phase Only Image Encryption**	**CHANG, Hsuan-Ting** National Yunlin University of Science and Technology	**NOMURA, Takanori** **LEE, Ju-Yi**
11:50-12:10	Invited Speaker 13 **Magneto-optic Three-dimensional Holographic Display Composed of Artificial Magnetic Lattice**	**TAKAGI, Hiroyuki** Toyohashi University of Technology	
12:10-13:20	Lunch Session & Break		
13:20-13:40	Invited Speaker 14 **Incoherent Fourier Digital Holography**	**NOMURA, Takanori** Wakayama University	**CAO,Liang-Cai** **HSU, Wei-Feng**
13:40-14:00	Invited Speaker 15 **Depth of Field Multiplexing Microscopy by Multi-Focus Holographic Lens**	**CHEN, Hui-Chi** Fu Jen Catholic University	
14:00-14:20	Invited Speaker 16 **Focus Error Signal Obtained at the Far-field from a Rotational Disc and Measurement of its Positional Dependency**	**FUJITA, Teruo** Fukui University of Technology	
14:20-14:40	Invited Speaker 17 **Holographic Fluorescence Mapping Using Space-division Matching Method**	**HAYASAKI, Yoshio** Utsunomiya University	
14:40-15:40	Poster Session & Break		
15:40-16:00	Invited Speaker 18 **Simplified Modal Method for Deep-etched Fused Silica Gratings**	**ZHOU, Chang-He** Chinese Academy of Science	**TAN, Xiao-Di** **SU, Wei-Hung**
16:00-16:20	Invited Speaker 19 **Pixelization Error Reduction Algorithm (PERA): Inverse Optimization Algorithms for Design of Diffractive Optical Elements**	**HSU, Wei-Feng** National Taipei University of Technology	
16:20-16:40	Invited Speaker 20 **Displacement Measurement with Multiple Holographic Grating**	**HSU, Cheng-Chih** Yuan Ze University	
16:40-17:00	Invited Speaker 21 **Polarization-Selective Substrate-Mode Volume Holograms and Its Applications**	**CHEN, Jing-Heng** Feng Chia University	
17:00-17:20	Invited Speaker 22 **Differential Equations for Volume Hologram with Coordinate Conversion**	**BARADA, Daisuke** Utsunomiya University	
17:20-17:40	Invited Speaker 23 **A Study on Holographic Printing System using Shader**	**HONG, Sunghee** Korea Electronics Technology Institute	
18:00-21:00	Dinner		
Sun., November 13th, 2016			
Time	**Title**	**Speakers**	**Chair**
08:30-09:30	**Oral Presentations for Best Paper Award Competition**		**SUNG, Kung-Bin** **SITU, Guo-Hai**
09:30-09:50	Break		
09:50-10:10	Invited Speaker 24 **Ultrahigh-speed Interferometric Scattering (iSCAT) Microscopy**	**HSIEH, Chia-Lung** Academic Sinica	**HAYASAKI, Yoshio** **CHUNG, Te-Yuan**
10:10-10:30	Invited Speaker 25 **Measurement of Cornea Curvature by using Moiré Method**	**CHEN, Kun-Huang** Feng Chia University	
10:30-10:50	Invited Speaker 26 **3D Shape Sensing using a Phase Mask to Extend the Depth Measuring Range**	**SU, Wei-Hung** National Sun Yat-sen University	
10:50-11:10	Invited Speaker 27 **Common-path Tomographic Phase Microscopy for Studying the Morphology and Light Scattering Properties of Blood Cells**	**SUNG, Kung-Bin** National Taiwan University	
11:10-11:30	Invited Speaker 28 **Mode Decomposition of Multimode Fiber using Digital Holography**	**SITU, Guo-Hai** Chinese Academy of Science	
11:30-11:50	Invited Speaker 29 **Spatial and Temporal Imaging in Digital Holographic Microscopy for Quantitative Analysis**	**LIN, Yu Chih** National Taiwan Normal University	
11:50-12:10	Closing Ceremony		
Departure (Shuttle Service from JiaoXi JustSleep Hotel to Taipei NTU Campus)			

Keynote Speaker I

Computational Imaging: Seeing the Invisible

George Barbastathis
Massachusetts Institute of Technology, Mechanical Engineering Department
77 Massachusetts Ave, Cambridge, Massachusetts
& Singapore-MIT Alliance for Research and Technology (SMART) Centre
1 Create Way, Singapore

Computational imaging is the discipline of extracting maximum information from a “raw” intensity image, as it is formed on a camera, by using advanced computational techniques and prior knowledge on the class of imaged objects. The design of a computational imaging system can be radically different than traditional imaging system design, for example lens-less and distributed imagers become possible. This opens up ample opportunities of interest for many disciplines that deal with manipulating light (or sound, or other kinds of waves), from biology to architecture and defense/security.

In this seminar, I will describe in particular the flavor of computational imaging that deals with the “phase” of light, i.e. the delay that light waves experience as they go through matter. This delay cannot be seen by naked eye or traditional intensity-detecting cameras, and thus some form of computation is necessary for phase retrieval. This is usually considered as a hard “inverse problem” but recently, the use of sparsity priors has come to the rescue as a way to retrieve the information efficiently and accurately even in the presence of strong noise. I will briefly introduce the problem of phase retrieval, and then show examples from real experiments, as well present the caveats and design principles.

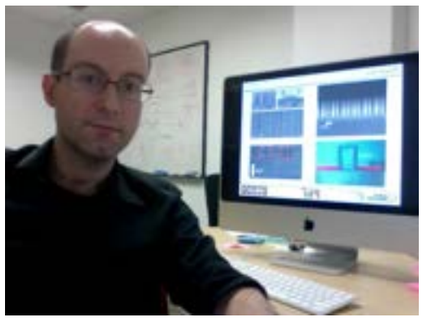

George Barbastathis received the Diploma in Electrical and Computer Engineering in 1993 from the National Technical University of Athens (Πολυτεχνείο) and the MSc and PhD degrees in Electrical Engineering in 1994 and 1997, respectively, from the California Institute of Technology (Caltech.) After post-doctoral work at the University of Illinois at Urbana-Champaign, he joined the faculty at MIT in 1999, where he is now Professor of Mechanical Engineering. He has worked or held visiting appointments at Harvard University, the Singapore-MIT Alliance for Research and Technology (SMART) Centre, the National University of Singapore, and the University of Michigan – Shanghai Jiao Tong University Joint Institute (密西根交大学院) in Shanghai, People’s Republic of China. His research interests are three-dimensional and spectral imaging; phase estimation; and gradient index optics theory and implementation with subwavelength-patterned dielectrics. He is member of the Institute of Electrical and Electronics Engineering (IEEE), and the American Society of Mechanical Engineers (ASME). In 2010 he was elected Fellow of the Optical Society of America (OSA) and in 2015 was a recipient of China’s Top Foreign Scholar (“One Thousand Scholar”) Award.

Keynote Speaker II

Holography for 3D Display – Status and Challenges

Byoungho Lee
School of Electrical and Computer Engineering, Seoul National University, Gwanak-Gu Gwanakro 1, Seoul 08826, South Korea
byoungho@snu.ac.kr

1.Introduction

Holography is a technique that records and reconstructs wavefront information of light. Due to these characteristics, holographic display is regarded as an ultimate three-dimensional (3D) display technique, since they can provide full 3D vision properties based on the wavefront regeneration. Despite this advantage, there are many limitations to be overcome for commercially successful display. In this presentation, I will explain the status of holographic 3D displays and challenges to overcome the limitations.

2.Spatial and time multiplexing techniques

The data amount of holography is determined by space-bandwidth product (SBP). The main problem of the holographic 3D display is that there is no display device that can express the holography’s huge amount of SBP. To display a high quality 3D images based on hologram, a large size spatial light modulator (SLM) with small pixel pitch is essential. However, current technical levels of SLMs cannot hold SBP for sufficient quality holograms. A simple way to solve the problem is using multiple SLMs to present more holographic information. Hahn et al. proposed a system with a curved array of spatial light modulators [1]. In the system, 12 SLMs, which are addressed in a curved array, present 36 views of hologram with large viewing angle of 22.8 degrees. Sasaki et al. proposed a large size holographic display system with tiling 16 4K-resolution SLMs [2]. With optical system consisting of polarization beam splitters, they implemented seamless full-color large size holographic display. Such spatial multiplexing methods can enlarge the amount of displayed information. However, they require numerous SLMs and the optical elements to align the many SLMs make the system bulky. Another way to increase the amount of information of holographic display is a time multiplexing technique. Takaki’s group presented a series of holographic 3D display systems a digital micro-mirror device (DMD) and scanning galvano mirror to enlarge screen size or viewing angle of holographic display [3, 4]. Since DMD can express only binary amplitude hologram, studies to improve the quality of the binary hologram are following [5, 6]. Li et al. proposed another type time multiplexing system using high order diffraction terms of a single SLM [7]. The high order terms are guided by holographic optical element (HOE) and sequentially displayed by electrical shutter and the screen size is enlarged. Even though they require mechanical synchronization, such time multiplexing techniques can enlarge the amount of displayed holographic information with a single SLM.

3.Holographic head-mounted display

Another important area where holographic 3D display can be utilized is head-mounted display (HMD) system. Since HMD display images only just in front of the human eye with fixed position,

the narrow bandwidth of the holographic display is not regarded as a big problem compared to conventional display system. Since HMD must be wearable, simplification is an important factor of holographic HMD. Moon et al. proposed a holographic HMD with LED light sources [8]. By using LED light sources, they achieved simple lightweight full-color holographic HMD system. Yeom et al. proposed a holographic HMD using HOE [9]. With in-coupler, out-coupler HOE and waveguide plate, the optical path of the holographic HMD can be simplified. Another important factor of holographic HMD is see-through property to achieve augmented reality (AR). Li et al. proposed a see-through AR holographic HMD using mirror-lens HOE [10]. By recording a mirror and a lens simultaneously on an HOE, see-through condition is easily achieved by holographic HMD.

4.Printed hologram

To overcome the fundamental limitation of SLM, some research groups print very high resolution hologram with lithography [11] or holographic printer [12] to obtain high resolution 3D images. Matsushima et al. generated four billion (216 × 216) high resolution computer generated hologram and fabricated it with laser lithography [11]. Kim et al. proposed seamless full color holographic printer for printing high quality 3D images on the holographic material [12] and Hong et al. proposed a hogel overlapping method to enhance the resolution of holographic printer [13]. Even though the printed holograms are static, the high resolution and small pixel pitch enables high quality and wide viewing angle 3D images.

5.Conclusion

Holography is considered as an ultimate technique for 3D display. However, current levels of display device cannot handle the large amount of information of holography. For the solutions, spatial and time multiplexing methods, HMD and holographic printing methods are introduced. Nowadays, a high tech SLM such as DMD and good quality holographic material such as photopolymer have been developed. These technological advances will brighten the future of holographic 3D display.

Reference:

[1] J. Hahn, H. Kim, Y. Lim, G. Park, and B. Lee, “Wide viewing angle dynamic holographic stereogram with a curved array of spatial light modulators,” Opt. Express 16, 12372-12386 (2008).

[2] H. Sasaki, K. Yamamoto, K. Wakunami, Y. Ichihashi, R. Oi, and T. Senoh, “Large size three-dimensional video by electronic holography using multiple spatial light modulators,” Sci. Rep. 4, 6177 (2014).

[3] Y. Takaki and N. Okada, “Hologram generation by horizontal scanning of a high-speed spatial light modulator,” Appl. Opt. 48, 3255–3260 (2009).

[4] Y. Takaki, Y. Matsumoto, and T. Nakajima, “Color image generation for screen-scanning holographic display,” Opt. Express 23, 26986-26998 (2015).

[5] Y. Matsumoto and Y. Takaki, “Improvement of gray-scale representation of horizontally scanning holographic display using error diffusion,” Opt. Lett. 39, 3433–3436 (2014).

[6] J. Jeong, J. Cho, C. Jang, G. Li, and B. Lee, “Simple quality improvement method for holographic display using digital micro-mirror device,” in Imaging and Applied Optics 2016, OSA Technical Digest, paper JW4A.43, July 2016. method,” Opt. Express 21, 14047–14055 (2013).

[7] G. Li, J. Jeong, D. Lee, J. Yeom, C. Jang, S. Lee, and B. Lee, “Space bandwidth product enhancement of holographic display using high-order diffraction guided by holographic optical element,” Opt. Express 23, 33170-33183 (2015).

[8] E. Moon, M. Kim, J. Roh, H. Kim, and J. Hahn, “Holographic head-mounted display with RGB light emitting diode light source,” Opt. Express 22, 6526–6534 (2014).

[9] H. J. Yeom, H. J. Kim, S. B. Kim, H. Zhang, B. Li, Y. M. Ji, S. H. Kim, and J. H. Park, “3D holographic head mounted display using holographic optical elements with astigmatism aberration compensation,” Opt. Express 23, 32025–32034 (2015).

[10] G. Li, D. Lee, Y. Jeong, J. Cho, and B. Lee, “Holographic display for see-through augmented reality using mirror-lens holographic optical element,” Opt. Lett. 41, 2486-2489 (2016).

[11] K. Matsushima and S. Nakahara, “Extremely high-definition full-parallax computer-generated hologram created by the polygon-based method,” Appl. Opt. 48, H54–H63 (2009).

[12] Y. Kim, E. Stoykova, H. Kang, S. Hong, J. Park, J. Park, and J. Hong, “Seamless full color holographic printing method based on spatial partitioning of SLM,” Opt. Express 23, 172–182 (2015).

[13] K. Hong, S.-g. Park, J. Yeom, J. Kim, N. Chen, K. Pyun, C. Choi, S. Kim, J. An, H.-S. Lee, U-i. Chung, and B. Lee, “Resolution enhancement of holographic printer using a hogel overlapping

Invited Speaker 1

Multi-View Scanning Hologram

Jung-Ping Liu[1)] and Hsuan-Hsuan Wen[1)]

[1)]Department of Photonics, Feng Chia University, 100 Wenhwa Rd., Seatwen, Taichung 40724, Taiwan

1.Introduction

Optical scanning holography (OSH) is a kind of digital holography [1]. In OSH, we can obtain a complex hologram, which contains three-dimensional (3D) information of the object target, with heterodyne scanning technique. Because of the scanning scheme of OSH, the recording time for OSH is proportional to the scanning resolution. For avoiding too long recording, the viewing angle as well as the resolution of the hologram is limited [2]. There are some methods to reduce the scanning time while at least the horizontal resolution remains [3-5]. Here we propose another optical method to increase the viewing angle. We record two scanning holograms at different viewing angles. The two holograms are synthesized to a single stereoscopic hologram for stereoscopic display. In addition, the reconstructed two views contain the depth cues, and thus there is no accommodation conflict in viewing the optical scanning stereoscopic hologram.

2.Experiment

The schematic setup of our optical scanning holographic system is shown in Fig. 1. The light source is a He-Ne laser (λ0=633nm). The laser beam is modulated by an electro-optic modulator (EOM) and then separated into two by polarizing beamsplitter 1. The two beams are manipulated and recombined by a beamsplitter, generating an interference pattern called time-dependent Fresnel zone plate (TDFZP) [1]. The object target is mounted on a two-dimensional (2D) scanner above a rotational stage. The rotation stage is to adjust the main viewing angle of the object and is static in the holographic recording. The 2D scanner moves to conduct 2D raster scanning using the TDFZP. The back-scattered object light is detected by photodetector 2, while photodetector 1 is applied to get a non-scanning reference signal. The electric signal is demodulated by a lock-in amplifier, generating a complex hologram

$$H(x,y)=\int_z h^*(x,y;z)\otimes R(x,y;z)dz\,, \tag{1}$$

where R(x, y, z) is the 3D intensity reflectivity of the object, and

$$h(x,y;z)=\exp\left[\frac{-jk}{z}\left(x^2+y^2\right)\right] \tag{2}$$

is the impulse response of the system. It should be noted that the phase of the object is not recorded in the hologram, and thus the recorded hologram is called incoherent hologram. We recorded two holograms of a real 3D figure as a demonstration. The hologram size is 20mm×20mm and the pixel pitch is 22μm. The object distance is about 110mm. We first rotated the object along the y-axis to □4° and recorded the first hologram, which is shown in Fig. 2(a) and (b). Subsequently, we rotated the object along the y-axis to □4° and recorded the second hologram, which is shown in Fig. 2 (c and (d). The two holograms are respectively reconstructed to the object plane. Reconstructed images are shown in Fig. 3.

3. Conclusion

We proposed to apply optical scanning holography to record two complex holograms at different viewing angles. The two holograms can be synthesized to a single stereoscopic hologram. The stereoscopic hologram can reconstruct two 3D images at two different angles, and thus generate a depth cue for the observer. This work is supported by MOST of Taiwan, under contract No. 103-2221-E-035-037-MY3

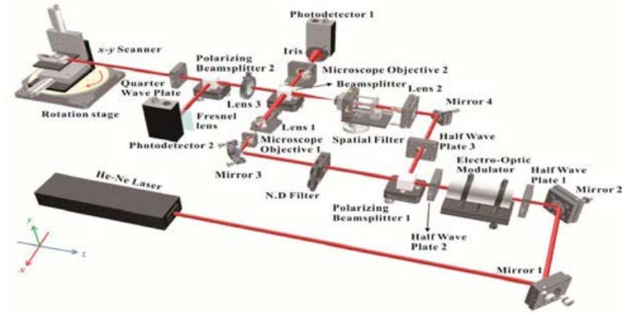

Fig. 1. Schematic of optical scanning holography

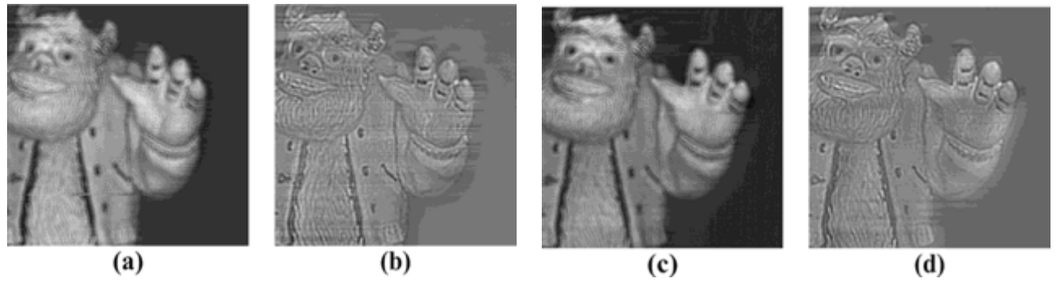

Fig. 2. Two complex holograms. (a) and (b) are respectively the real part and imaginary part of the hologram recorded at +4°□. (c) and (d) are respectively the real part and imaginary part of the hologram recorded at −4°.

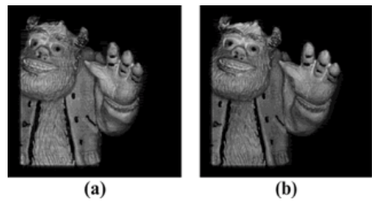

Fig. 3. Fig. Reconstructed images of the holograms recorded at (a) +4°□, and (b) −4°, respectively.

Reference:

[1] T.-C. Poon, Optical Scanning Holography with MATLAB, Springer, 2007.

[2] T.-C. Poon and J.-P. Liu, Introduction to modern digital holography with MATLAB, Cambridge University Press, 2014.

[3] J.-P. Liu, C.-C. Lee, Y.-H. Lo, and D.-Z. Luo, “Vertical-bandwidth-limited digital holography,” Opt. Lett. 37, 2574-2576, 2012.

[4] P. W. M. Tsang, J.-P. Liu, and T.-C. Poon, “Compressive optical scanning holography,” Optica 2, 476-483, 2015.

[5] P. W. M. Tsang, T.-C. Poon, and J.-P. Liu, “Adaptive optical scanning holography,” Scientific Reports 6, 21636, 2016.

Invited Speaker 2

Floating image generated with the integration of holographic and geometrical imaging

Cheng-Huan Chen[1)], Po-Sheng Chiu[2)] and Fu-Lung Chou[2)]
[1)]Department of Photonics, National Chiao Tung University, Hsinchu 30010, Taiwan, R.O.C.
[2)] Department of Power Mechanical Engineering, National Tsing Hua University, Hsinchu 30013, Taiwan, R.O.C.

1.Introduction

The sensation of an image floating in the air needs two features which are largely different from that of traditional displayed images, even 3D images. One is that the image should be located far away enough from the display devices, and the other one is that the background scene should still be visible while the viewers are looking at the image. There are two major technical approaches to generate floating image, one is geometrical imaging [1,2] and the other one holographical imaging[3,4]. Both have their own merit and limit. Geometrical image needs a solid object as the original source, or the image would look flat if the original source is a flat panel display. Holographic imaging has the limit on locating the image position, manipulating magnification due to the stringent requirement on the reconstruction source and spatial light modulator. The combination of these two technologies would give more degree of freedom for the construction of floating image display device.

2.System architecture

The architecture of the proposed floating image display device is shown in Fig. 1. A spatial light modulator(SLM) is located at the bottom of the whole device, and is surrounded by an array of reconstruction light source. The reconstructed image from the SLM, preferably a virtual image behind the SLM, is then imaged again by curved mirror to form a real image at the position of the floating cylinder as shown in Fig. 1. Because the field of view would be narrow, the reconstruction light sources can flash sequentially to generate different perspective view of an object, with the SLM flashing synchronizely for the corresponding fringe pattern.

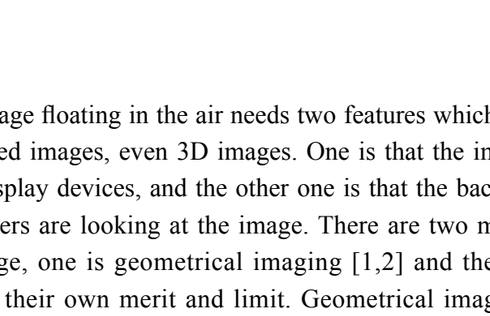

Fig. 1. Schematic architecture of the floating image display device

3.Prototype and demonstration

The prototype for one view has been built as shown in Fig.2, with the light path drawn with the green line. The SLM is a 1920×1080 phase modulation LCoS with the pixel size of 6.4μm from Jasper Display Co. The reconstruction light source is LED with a 30μm pinhole in the front to improve spatial coherence. The floating image is about 80mm from the concave mirror.

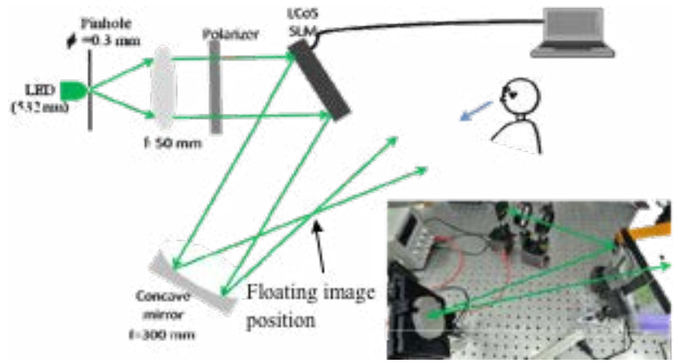

Fig. 2. Prototype and light path of floating image display device

A floating dot line cube has been generated with the prototype, as shown in Fig. 3. The image itself already has spatial depth, which can be indicated with the parallax of two vertical lines when viewing the cube from different viewing directions.

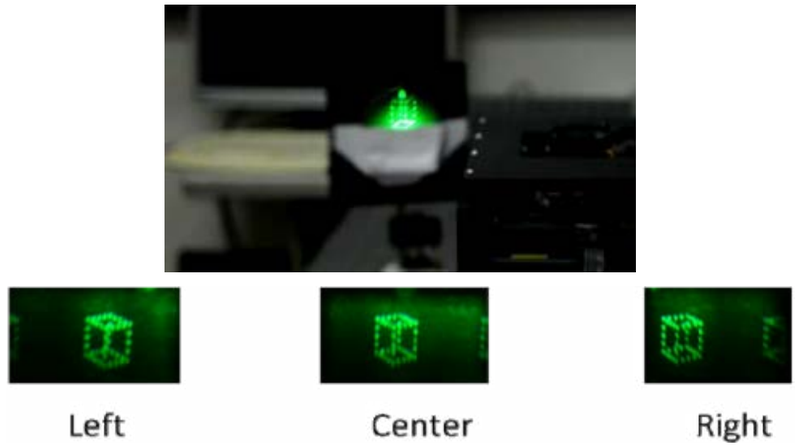

Fig. 3. Floating dot line cube generated with the prototype

References:

[1] S. Yoshida, “fVisiOn: Glasses-free Tabletop 3-D Display - Its Design Concept and Prototype -,” in Digital Holography and Three-Dimensional Imaging, OSA Techinal Digest, DTuA1.
[2] S.-W. Min, M. Hahn, J. Kim and B. Lee, “Three-dimensional electro-floating display system using an integral imaging method,” Opt. Express 13(12), 4358–4369 (2005).
[3] H. Yoshikawa, T. Yamaguchi, T. Ito and H. Ozawa, “Floating image display with a fine pixel pitchcomputer-generated hologram,” Opt. Eng. 51(4), 045801 (2012).
[4] J.-Y. Son, C.-H. Lee, O.O. Chernyshov, B.-R. Lee and S.-K. Kim, “A floating type holographic display,” Opt. Express 21(17), 20441–20451 (2013).

Invited Speaker 3

Phase-distortion Elimination of the Phase-only Read-out Signal of Holographic Data Storage System

Yeh-Wei Yu[1,2)], Shuai Xiao[1)] and Ching-Cherng Sun[1,2*)]

[1)]Department of Optics and Photonics, National Central University, Chung-Li, Taoyuan City, 32001 Taiwan

[2)]Optical Science Center, National Central University, Chung-Li, Taoyuan City, 32001 Taiwan

Holographic data storage (simplified HDS) is a promising technology for next-generation optical storage, because of its compatibility with various methods of holographic multiplexing [1]. In amplitude-encoded holograms, the strong DC term consumes around 2–10 times the M/# more than that required [2]. By contrast, the phase-only encoded hologram inherently removes the strong DC term and makes the M/# consumption effective [3]. Besides, since no energy is wasted by black signals, the phase-only encoded hologram has higher energy efficiency. Moreover, it was demonstrated to realize high visibility in the readout process [4, 5]. However, the phase distortion introduced by system error is a major concern. For example, the position misalignment of the disk is unavoidable in a HDS system. Slightly misalignment of the disk leads to dramatic disturbance to the signal. Based on the proposed optical model of collinear HDS, we simulate the inline interferogram for the HDS system with a 2mm storage disk, and 0.5 um of disk misalignment is introduced (Fig 1) [6, 7]. The phase distortion makes it impossible to readout the all signals through one-shot in-line interferometry. Hence, we propose a one-shot and aberration-tolerable scheme based on a double-frequency grating shearing interference (simplified DFGSI). The double-frequency grating (simplified DFG) is used to produce two diffraction images to create shearing interferometry. Fig. 2(a) presents the encoded binary phase distribution of the signal obtained through one-pixel shearing interference [Fig. 2(b)], and the bright and dark pixels in the interferogram correspond to constructive interference and destructive interference between two neighboring pixels, respectively, as illustrated in Fig. 2(c). Because the encoded phase of the first column is known, the encoded phase of the signal can be decoded by analyzing the interference pattern depicted in Fig. 2(c). The visibility of the interferogram enabled phase retrieval with high fidelity and simplicity in the optical system.

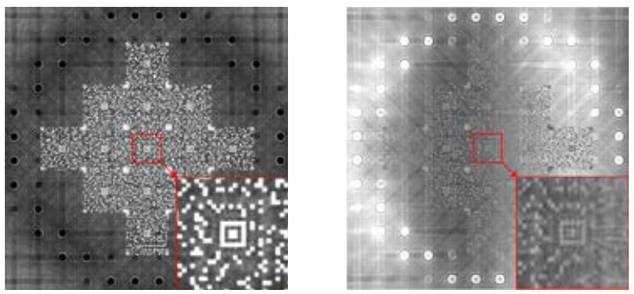

(a) (b)

Fig. 1. The simulated interferogram of homodyne detection obtained through inline interferogram for the HDS system with a 2mm storage disk. (a) No misalignment; (b) 0.5 um of disk misalignment is introduced.

An optical model for the DFGSI was developed and demonstrated experimentally. When DFGSI is applied to the read out signal in Fig. 1(b), a simulation based on the DFGSI optical model shows the phase distortion introduced by the disk misalignment can be successfully eliminated and the signal can be retrieved (Fig. 3).

Acknowledgments

This study was supported in part by the “Plan to Develop First-Class Universities and Top-Level Research Centers” of National Central University (Grants 995939 and 100G-903-2) and the Ministry of Science and Technology of the Republic of China (Contract MOST 104-2221-E-008-078-MY3 and 103-2221-E-008-063-MY3).

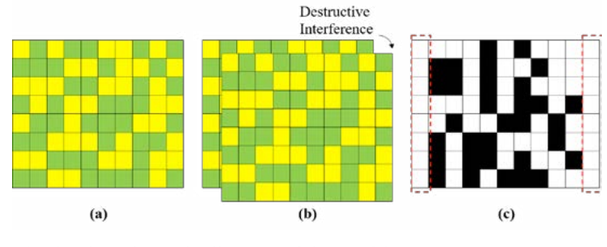

Fig. 2. The schematic diagram of the DFGSI

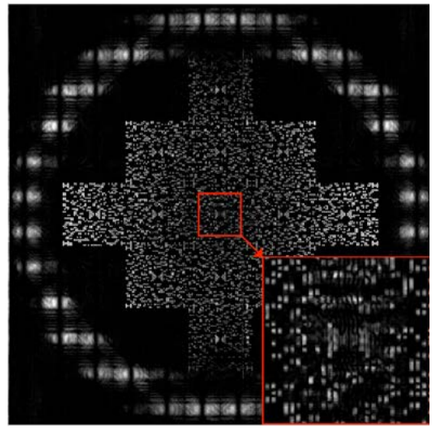

Fig. 3. The simulated inteferogram when DFGSI is applied to the readout signal of the HDS system with 0.5μm disk misalignment.

Reference:

[1] H. J. Coufal, D. Psaltis, G. T. Sincerbox, eds., Holographic Data Storage, Springer Series in Optical Sciences (Springer-Verlag, 2000)

[2] S. S. Orlov, W. Phillips, E. Bjornson, Y. Takashima, P. Sundaram, L. Hesselink, R. Okas, D. Kwan, and Raymond Snyder, “High-transfer-rate high-capacity holographic disk data-storage system,” Appl. Opt. 43, 4902 (2004).

[3] B. Das, J. Joseph, and K. Singh, “Phase-image-based sparse-gray-level data pages for holographic data storage,” Appl. Opt. 48, 5241-5250 (2009).

[4] M. Hara, K. Tanka, K. Tokuyama, M. Toishi, K. Hirooka, A. Fukumoto, and K. Watanabe, “Linear Reproduction of a Holographic Storage Channel using Coherent Addition of Optical DC Components,” Jpn. J. Appl. Phys. 47, 5885–5890 (2008).

[5] K. Curtis, L. Dhar, W. Wilson, A. Hill, and M. Ayres, Holographic Data Storage: From Theory to Practical Systems (Wiley, 2010).

[6] C. C. Sun, Y. W. Yu, S. C. Hsieh,T. C. Teng, and M. F. Tsai, “Point spread function of a collinear holographic storage system,” Opt. Express 15, 18111-18118 (2007).

[7] Y. W. Yu, C. Y. Chen, and C. C. Sun, “Increase of signal-to-noise ratio of a collinear holographic storage system with reference modulated by a ring lens array,” Opt. Lett. 35, 1130-1132 (2010).

Invited Speaker 4

Three dimensional display based on volume holographic photopolymer

Liangcai Cao*, Hao Zhang, Zheng Wang, Song Zong and Guofan Jin
Department of Precision Instruments, Tsinghua University, Beijing, 100084, P. R. China

1.Research motivation

A perfect three-dimensional (3-D) display technology should have the ability to offer all the depth cues of a 3-D scene. The data bandwidth of a 3-D scene is two or three orders of magnitude larger than that of traditional 2-D images. Conventional 3-D display techniques are normally based on binocular or multiview parallax with multiple 2-D images, at a bandwidth of several times of 1K by 1K. Holography directly addressing the wavefronts has the potential to record and display the whole information of a 3-D scene. If ordinary pixels are utilized and a planar surface is utilized in a computer generated hologram (CGH) based display, too many pixels of the spatial light modulator (SLM) are needed. A commercially acceptable quality may needs 64K by 64K pixels. Meanwhile, complex valued pixels with both amplitude and phase are not easily realized. Limited by materials and devices, the space-bandwidth product (SBP) of current CGH based display system can not meet the needs of high resolution display for big data.

Holographic printing technique on a holographic material is much closer to practical implementation of wide-viewing angle and high-SBP 3-D display since the optical resolution of holographic material allows the expansion of the SBP of the SLM[2, 3]. In traditional holographic printing systems, shift-multiplexing is utilized for the reconstruction of hogels in multiple locations as planar holograms. Volume holograms, due to the multiple sensitivities of volume Bragg gratings, have the potential for multiplexing for displaying huge amount of 3-D data. The holographic material used for printing, usually a photorefractive polymer or photopolymer, can expand the SBP since it has high dynamic range and good multiplexing capabilities[4]. In this work, an angular multiplexing based volume holographic display technology is employed to make full use of the dynamic range of the material and realized a high-resolution 3-D holographic display.

2.Multiplexed hogels for 3-D display

As is shown in Fig. 1, the wavefront of 3-D scene is encoded as the CGHs. The holograms are recorded in the gold nanoparticles doped photopolymer with the angular multiplexing. With the recorded holograms, 3-D scenes could be viewed at different viewing angles. There is no crosstalk between the channels due to the Bragg angular selectivity. The 3-D video is divided into multiple frames of 3-D scenes, encoded as multiple CGHs, loaded into the phase SLM sequentially, and carried by the object beams to write secondary CGHs in a volume holographic polymer. Angle-multiplexed hogels are recorded in the same recording spot with the same reference beam. Once all the CGHs are recorded, illuminating the hogel location of the polymer with the reference beam, all frames of the 3-D scenes can be reconstructed sequentially when the polymer is rotated to the corresponding angle-channels. Dynamic 3-D display can be achieved due to the persistence of vision by rotating the polymer with a time control program.

As is shown in Fig. 2, a video of a revolving clock is divided into 120 frames to be printed in the angle- multiplexed hogels. A solid-state laser at a wavelength of 532 nm is used. The thickness of the gold nanoparticles doped PQ/PMMA photopolymer is 1 mm. The SLM used in the system is LETO Phase-only Modulator (HOLOEYE Photonics AG) with 1920 × 1080 pixels. We obtain the reconstruction of all the 120 frames without crosstalk successfully. By controlling the rotation stage, a dynamic holographic video of 10 Hz is achieved. The results demonstrate the dynamic holographic display by volume holographic printing. In conventional printing technology, one hogel zone could support the resolution of 1920 × 1080 pixels. In this work, one hogel zone could support the resolution of 1920 × 1080 × 120 pixels.

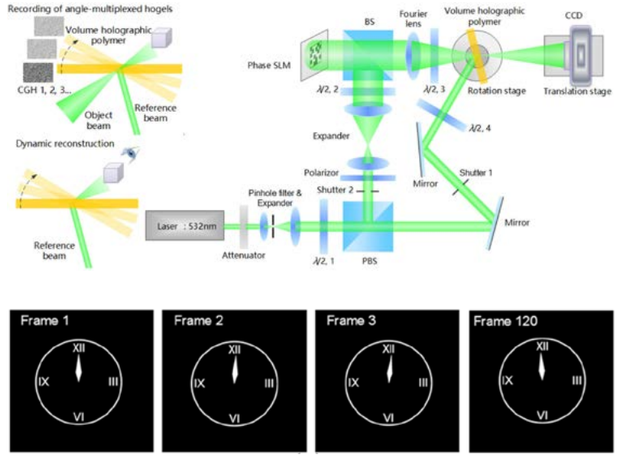

Fig. 1. Angular multiplexing for dynamic 3-D reconstruction. Left, Recording and reconstruction. Right, Optical setup.

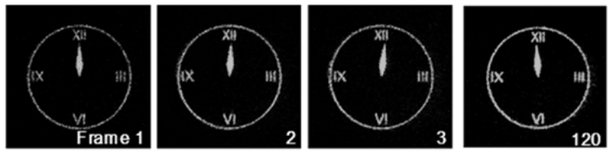

Fig. 2. The original frames and the displayed frames at different viewing angles

In conclusion, the wavefronts containing whole depth cues of 3-D scene can be recorded as hogels into the volume holographic polymer by the angle-multiplexing method. The SBP of the system is largely expanded because up to hundreds of hogels could be displayed. The printed holographic screen is capable of displaying a gigapixel 3-D datacube.

Acknowledgements

This work is National Basic Research Program of China (2013CB328801) and National Natural Science Foundation of China (NSFC) (61275013, 61505095, 61361160418, 61327902).

Reference:

[1] Y. Sando, D. Barada, and T. Yatagai, “Holographic 3D display observable for multiple simultaneous viewers from all horizontal directions by using a time division method,” Opt. Lett. 39, 5555–5557 (2014).

[2] H. Horimai, “Holographic 3D-image printer system with collinear optics,” International Workshop on Holography and Related Technologies (IWH 2015), Okinawa, Japan, Dec. 2015.

[3] K. Hong, J. Yeom, C. Jang, G. Li, J. Hong, and B. Lee, “Two-dimensional and three-dimensional transparent screens based on lens-array holographic optical elements,” Opt. Express 22, 14363-14374 (2014).

[4] L. Cao, Z. Wang, H. Zhang, G. Jin, and C. Gu, "Volume holographic printing using unconventional angular multiplexing for three-dimensional display," Applied Optics 55, 6046-6051 (2016).

Invited Speaker 5

Phase Modulated Collinear Holographic Data Storage System

Xiaodi Tan[1)], Hideyoshi Horimai[2)], Ryo Arai[3)], Junichi Ikeda[3)], Mitsuteru Inoue[4)]
Xiao Lin[1)], Jinpeng Liu[1)] and Yong Huang[2)]
[1)]Beijing Institute of Technology, 5 South Zhongguancun Street, Haidian District, Beijing 100081, China
Phone: +86-10-6891-9660, Fax: +86-6891-9060, E-mail: tan@bit.edu.cn
[2)]HolyMine Corporation, 2032-2-301 Ooka, Numazu, Shizuoka 410-0022, Japan
[3)]Kyoeisha Chemical Co., LTD, Sun Mullion Osaka Bldg., 6-12, 2-chome, Minamihonmachi, Chuo-ku, Osaka 541-0054, Japan
[4)]Toyohashi University of Technology, 1-1 Hibarigaoka, Tempaku-cho, Toyohashi, Aichi 441-8580, Japan

1.Introduction

High density, fast data rate and long lifetime data storage system is becoming more and more important with the increasing demand of the Big Data era. But, the main storage media we rely on currently are magnetic technology, like hard disk drives (HDD) and tape, which life times are several years only. They cannot satisfy the demand of prolonged preservation. Optical discs based on the bit-by-bit method, such as CD, DVD and Blu-ray Disc, for storing sound, movies, photos and other digital contents are widely used in our daily life. The long-term life time is one of the properties. The optical disc should be a good candidate of data storage system for big data preservation. However, the recording density limitation of the bit recording method are looming on the horizon.

Holographic data storage system (HDSS) is a different optical data storage system. In this technology, two coherent beams are necessary. One is information beam including user data we want to record, the other is reference beam. During the recording process, they interfere with each other and the interference pattern is recorded in the media, called hologram. In the reconstructing process, the information beam can be reconstructed when the reference beam incident on the hologram. Because the two beams are separate, we call this HDSS conventional 2-axis holography. This method was first proposed in the 1960s [1]. In this method, data are recorded in the media volumetrically (3-D) and transformed 2-dimensionally (2-D). Due to their large storage capacities and high transfer rates, HDSS should become a promising candidate of next-generation of storage system. Within the last decade, unique demonstration platforms using holography have been proposed [2–4]. However, these 2-axis HDSS still have essential issues for practicality [5]. Holographic recording has been known for 50 years and never been commercially available. It is clear that a technological breakthrough is necessary.

Collinear HDSS is very promising and differs from conventional 2-axis holographic data storage system [6]. With this technology, a small, practical HDSS can be produced more easily than conventional 2-axis holography. In this paper, we introduced collinear technology and reported the structure of media. And we discussed some methods to enlarge the recording density and increase data transfer rate of the collinear HDSS.

2.Phase Modulation to increase the recording density

There are generally several kinds of methods to increase the HDSS recording density on the recording media. These methods include multiplexing holograms to increase the number of holograms recorded in the same region of the media, saving the dynamic range of media, so called M number (M/#), to increase the multiplexing recording number, and increasing the amount of information in a data page, etc.

The amount of recording information in a data page is determined by its format. In the collinear HDSS, the data page format based on the subpage is designed to eliminate the problems of illuminated intensity distribution in a data page, of distortion and aberration of the optical system, of tilting, and of the estimation error caused by amplification. As shown in Fig. 8, the size of a subpage (24 x 24 pixels is used) depends on the parameters and the magnitude of the inhomogeneity of a system. In each subpage, there are 32- byte data symbols (4 x 4 pixels) and a synchronous mark (8 x 8 pixels) in its center. The synchronous symbol, which includes a 4 x 4 pixel rectangular block, is used to locate the subpage and to provide the necessary coordinate information for data decoding. The sorting method and correlation technique that differ from the threshold method are used to distinguish the ON-pixel and OFF-pixel states from the reconstructed image in the decoding process. In this data page format, 3 pixels ON and others are OFF, the code rate is 8/16 = 0.5; and the white rate is 3/16&19% approximately [6]. To improve the information content within a data page, an effective method is to elevate the code rate. The multiple gray coding method and phase modulated data page are used. In the format of the data page, there are only three ON-pixels in a symbol. If the gray coding method is used, if all 16 pixels are modulated by phase, the code rate should be increased [7-9].

3.Conclusions

In this paper, we have reviewed collinear HDSS. With its unique selectable capacity recording format of media shows both downward and upward compatibility of different disc capacities. Based on collinear technologies, we discussed many kinds of methods to increase the density and reduce the noise in the reconstruction process. These methods allow us to read low intensity hologram with high SNR. Further investigations are underway to develop the high power, small size and low cost laser, to test the reliability of the media, to balance the data density and the transfer rate by incorporating newly designed optical and electronic components. High density recording by phase modulated collinear HDSS has significant proved experimentally, the phase modulation can be used to increase code rate efficiently.

Reference:

[1] van Heerden P J., “Theory of optical information storage in solids”, Applied Optics, 1963, 2(4): 393–400
[2] Mok F H., “Angle-multiplexed storage of 5000 holograms in lithiumniobate”, Optics Letters, 1993, 18(11): 915–917
[3] Denz C, Pauliat G, Roosen G, Tschudi T., “Volume hologram multiplexing using a deterministic phase encoding method” Optics Communications, 1991, 85(2–3): 171–176
[4] Lande D, Heanue J F, Catrysse P, BashawMC, Hesselink L., “Digital wavelength-multiplexed holographic data storage system”, In: Summaries of papers presented at the Conference on Lasers and Electro-Optics. 1996, 142–143

[5] Horimai H, Tan X., “Collinear technology for a holographic versatile disk”, Applied Optics, 2006, 45(5): 910–914
[6] Horimai H, Tan X, Li J. “Collinear holography”, Applied Optics, 2005, 44(13): 2575–2579
[7] Li J, Cao L, Gu H, Tan X, He Q, Jin G, “Orthogonal-referencepattern-modulated shift multiplexing for collinear holographic data storage”, Optics Letters, 2012, 37(5): 936–938
[8] Lin X, Xiao X, Wu A, Tan X., “An effective phase modulation in the collinear holographic storage”, In: Proceedings of SPIE, Practical Holography XXVIII: Materials and Applications, San Francisco. 2014, 9006: 9006-1–9006-6
[9] Ke Xu, Yong Huang, Xiao Lin, Yabin Cheng, Xiaotong Li, Xiaodi Tan, “Unequally spaced four levels phase encoding in holographic data storage,” Optical Review, Vol.23, doi:10.1007/s10043-016-0263-1 (2016).

Invited Speaker 6

Improvement of Signal to Noise Ratio in Holographic Data Storage by Limiting Aperture Opening of Imager Pixels

Ryushi Fujimura[1,2], Yuya Nakamura[1] and Anna Odanaga[3]
[1]Department of Optical Engineering, Graduate school of Engineering, Utsunomiya University,
[2]Center for Optical Research and Education (CORE), Utsunomiya University,
[3]Faculty of Engineering, Utsunomiya University,
7-1-2 Yoto, Utsunomiya, Tochigi 321-8585, Japan

1.Introduction

Holographic data storage is an attractive solution for an archival memory system because of its large storage capacity, fast data transfer rate, and low energy consumption. In such a system, Nyquist aperture is usually inserted in the Fourier plane and limits the illumination area on the recording material, which is essential for improving the recording density. However, it also limits transmitted spatial frequency components, and thus increases the inter-pixel crosstalk noise.

In this paper we propose a method for improving the signal to noise ratio (SNR) deteriorated by the Nyquist aperture. The concept of our improving method is based on the limitation of the clear aperture of imager pixels. We numerically and experimentally investigated influence of such a limiting aperture on the SNR and discuss its effectiveness.

2.Phase Modulation to increase the recording density

Figure 1 shows schematic diagram of our proposed method in the holographic data storage. Since only a low spatial frequency component of the signal image can go through the Nyquist aperture at F1, the sharp edge of the original image will be lost and the transmitted image at O2 will blur depending on the size of the aperture opening (LF). As a result, a contrast in the output image obtained by the imager inevitably decreases, and thus the SNR is lowered. This is due to the fact that the intensity received by the imager is usually integrated over the whole area of imager pixel. An aperture array located at O3 is a key device in our method to improve the

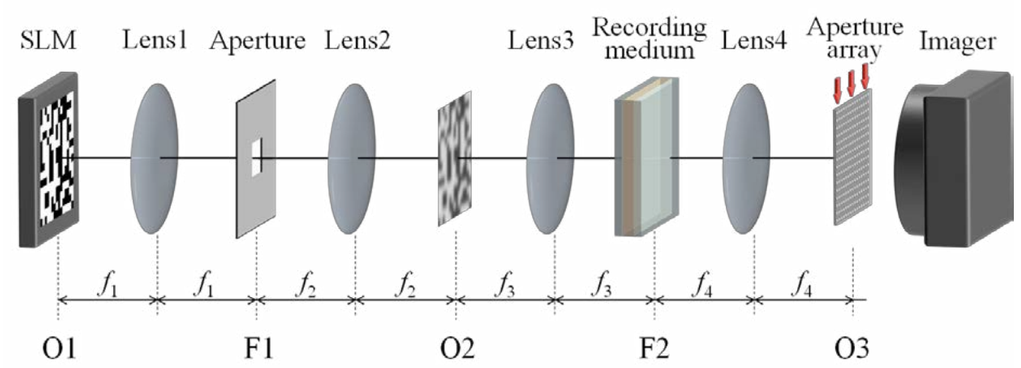

Fig. 1. Schematic diagram of our proposed method that improves SNR in binary-encoded intensity holographic data storage systems. Aperture array is inserted before the imager in the imaging plane to limit an aperture opening of imager pixels.

SNR. It limits the receiving area of the imager pixel only to a center part of each pixel area and avoids detecting the crosstalk noise near the pixel edge, as shown in Fig. 2. In this case, although the brightness of the output image becomes small, the resultant SNR is improved mainly due to the reduction of the variance.

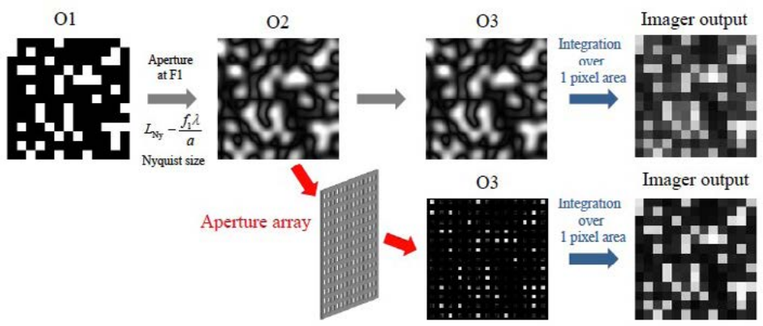

Fig. 1. Simulated results of the signal images at each location and resultant output image of the imager with and without aperture array. LNy is the Nyquist size that calculated with the signal pixel size a, the focal length f1, and the wavelength λ .

3.Experiments

To verify our proposed method, we performed a numerical simulation and an experiment without recording material in F2. In our experiment, an optical setup was arranged in such a way that the one pixel of the signal image was detected by using 35 × 35 imager pixels. It is because such a highly oversampling situation can virtually act as a variable aperture array by simply limiting the integration pixel. The results are shown in Fig. 3. The SNRs slightly but monotonically increased with decreasing the aperture opening ratio (L_D/a) when LF was equal to the Nyquist size (L_{Ny}). On the contrary, the SNR reached its maxima at a certain value of the LD/a when LF = 2LNy. This is because the decrease of the averaged intensity exceeds the gain from the decrease of the variance. Therefore, generally, there is an optimum values for LD/a in our proposed method.

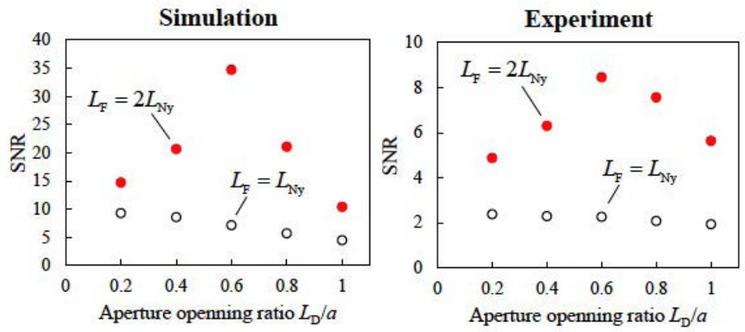

Fig. 1. The simulated and experimental results for our proposed method. The SNRs are plotted as a function of the aperture opening ratio LD/a. LD and LF represent the side length of aperture array at O3 and aperture at F1, respectively.

Keynote Speaker III

Holographic Data Storage System Enabling 2.4 Tbit/in.2 Recording

Taku Hoshizawa[1)] and Yukinobu Tada[2)]
[1)]Center for Technology Innovation - Information and Telecommunications, Hitachi Ltd., 292 Yoshida-cho, Totsuka-ku, Yokohama, Kanagawa, 244-0817 Japan
[2)]Development Division, Hitachi-LG Data Storage, Inc., 292 Yoshida-cho, Totsuka-ku, Yokohama, Kanagawa, 244-0817 Japan

1.Introduction

The demand for archival storage to preserve digital data for a long term is increasing. An angular-multiplexing holographic data storage system (HDSS) is one of the promising candidates for archival storage, because it has characteristics of a high transfer rate and a large disc capacity as well as longevity and high robustness, which are strongly requested for archival storage.

For the reason, we have been researching high density recording techniques in an HDSS. In 2009, we developed the monocular optical system passing both signal and reference beams through a single objective lens, and confirmed experimentally recording density of 663 Gbit/in.2.1) In 2012, we confirmed recording density of 1 Tbit/in.2 corresponding to 1 TB disc capacity by the recording technique obtaining a constant signal-to-scatter ratio (SSR).2) This paper presents several techniques to improve a recording density to 2.4 Tbit/in.2 required for 2 TB disc capacity.

2.RLL high-density recording

The hologram size corresponds to an aperture size of a spatial filter placed in a signal-beam path. Although the aperture size is limited by the Nyquist size which is inversely proportional to a pixel pitch of a spatial light modulator (SLM), it is unrealistic to enlarge the pixel pitch from physical constraints. Hence, we introduced run-length limited (RLL) modulation limiting the minimum length of runs of repeated polarity to 2 and having a code rate of 2/3. This RLL modulation produces the same effect as twice a pixel pitch of an SLM, and enables to reduce an aperture size of a spatial filter to half. Figure 1 shows the verification result of the effect of the RLL modulation obtained by an optical simulator. As a result, this RLL high-density recording method can reduce the hologram size to half, and increase the recording density to double.

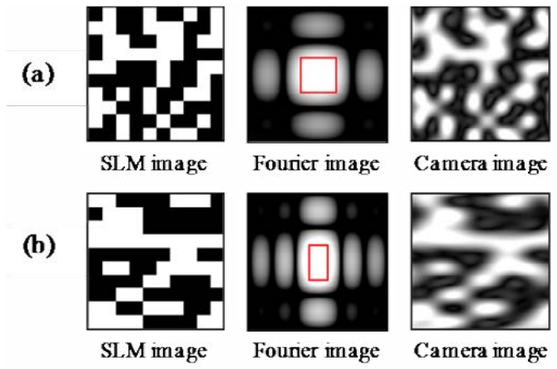

Fig. 1. Images on SLM Fourier plane, and camera Therectangular lines on each Fourier image indicate the Nyquist area. (a) Without RLL modulation (b) With RLL modulation

3.RLL turbo code

In the RLL high-density recording method, a half-size filter blocks the lower spatial frequencies of data patterns. Consequently, interpixel interference (IPI) in a page image captured by a camera, which degrades signal quality of the page image, occurs. To minimize influence of the IPI without decreasing a code rate, an RLL turbo code comprising a convolutional coding of a code rate of 2/3 and the RLL modulation was developed. In reproduction of a page, an error correction is executed alternately between an RLL demodulation and a convolutional decoding which use the BCJR algorithm, exchanging information each other. As a result, the RLL turbo code shows better performance than a low-density parity-check (LDPC) code of a code rate of 1/2, which was used in our conventional HDSS, in spite of more IPI, and enables error-free reproduction from a page image with a signal-to-noise ratio (SNR) of only 2.4 dB.

4.Servo system for reference beam angle

To capture a page image with an SNR of more than 2.4 dB, SNR degradation caused by Brugg mismatch of a reference beam angle must be minimized. Hence, a servo system for a reference beam angle comprising an optical error detecting system and two-degree-of-freedom control named adaptive final-state control (AFSC) was developed. A reference beam is split into a preceding beam and a reference beam, in accordance with polarization, using a Wollaston prism with a split angle θ, and is diffracted to the back of a disc. The preceding and reference beams are detected on optical electrical integrated circuits, and an S-curved angle servo signal is generated from the detected signals. However, since a reference beam angle to reproduce a next page ideally, or a target angle, is located at θ/2 degrees from the zero-cross point of the angle servo signal, it's unknown precisely before moving. Therefore, AFSC with a combination of feedforward and feedback control by using a final-state control (FSC) method, which obtains a feedforward input and a target trajectory, was introduced. The first FSC is performed to reveal the target angle by passing through the zero-cross point, and the second FSC is performed to move to the target angle as soon as the zero-cross point is detected. As a result, it enables to instantly access to a next page with a tolerance within ±5 mdeg.

5.Servo system for book tracking

A cluster of angular-multiplexed pages at the same location is called a book. A main function of the spatial filter placed in a signal-beam path is to block off undesired page images diffracted from neighboring books. Therefore, when a target book is off an expected position, signal quality of a page image is degraded because the spatial filter also interrupts a part of the page image. Nevertheless, it is almost impossible to move a target book to an expected position with a tolerance within ±5 μm our HDSS requires due to mechanical causes of a spindle motor rotating a disc, for example backlash. Hence, a servo system for book tracking comprising an optical system detecting a book position, a spatial filter mounted on a three-dimensional actuator, and three-dimensional spatial filter control was developed. This servo system controls the position of the spatial filter to compensate for relative position aberration between the target book and the expected position. As a result, it allows to access to a target book with a tolerance up to ±50 μm.

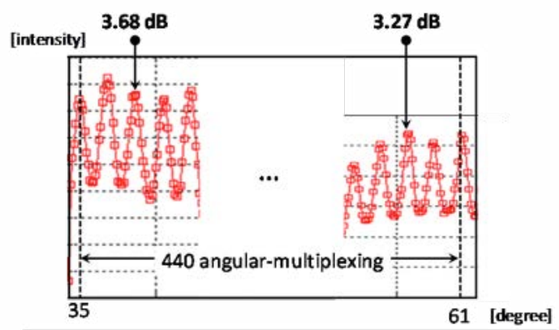

Fig. 2. Signal quality(SNR) of reproduced page images in 2.4 Tbot/in.^{2} recording

6.Results & discussion

We set up the evaluation equipment with an SLM of 4.4 M pixels, a camera of 8.4 M pixels, and a 405-nm external cavity laser diode (ECLD) having 100 mW output. In the equipment, we angular-multiplexed 440 pages from 61 to 35 degrees with an angle pitch from 64 to 57 mdeg. Figure 2 shows the experimental result of 440 angular-multiplexing recording. The SNR of 3rd and 438th pages was confirmed to be 3.27 and 3.68 dB respectively, which can be reproduced without error by the RLL turbo code, although deteriorated portions of the page images, for example disc surface reflection, were excluded from the SNR calculations.

In this experiment, the capacity of an RLL-modulated page was 2.7 M bits, and the hologram size was 0.00050 in.2. As the result, a recording density of 2.4 Tbit/in.2 was verified.

7.Conclusions

We have developed the technologies to realize an HDSS with a disc capacity of 2 TB, and confirmed experimentally a recording density of 2.4 Tbit/in.^{2}.

Reference:

[1]K. Shimada, T. Ishii, T. Ide, S. Hughes, A. Hoskins, and K. Curtis, ODS Tech. Dig., 2009, p. 61.
[2] M. Hosaka, T. Ishii, M. Yamaguchi, S. Koga, A. Tanaka, and T. Hoshizawa, ISOM Tech. Dig., 2012, p. 8.

Keynote Speaker IV

Optical Phase Conjugation Technology and the Application to Optical Information Processing

Ching-Cherng Sun[1,2], Yeh-Wei Yu[2], Che-Chu Lin[1], Sze-Yu Chen[1], and Tsung-Hsun Yang[1]
[1]Department of Optics and Photonics, National Central University, 32001 Chung-Li, Taiwan
[2]Optical Sciences Center, National Central University, 32001 Chung-Li, Taiwan

Abstract

Optical phase conjugation (OPC) is one of effective ways to retrieve wavefront when passing through a phase distortion medium.[1] Traditionally, OPC can be generated through four wave mixing in a nonlinear medium. In 1982, a self-pumped OPC, so-called Cat SPPCM (self-pumped phase conjugate mirror) was discovered in BaTiO3.[2] Such a way is in extremely low operation power. In advance, a faster SPPCM, called Kitty SPPCM, was proposed by taking the advantage of Cat SPPCM.[3] In this paper, a study of Kitty SPPCMs in various geometries (Fig. 1) will be introduced and the characteristic will be discussed.[4] In addition, we will introduce the development of digital-optical phase conjugator (DOPC) [5] technology. A new DOPC with the add of Kitty SPPCM will be proposed. The capability of the DOPC for passing through a turbid medium will be discussed. The other topic in the paper is to introduce a virtual objective inside a turbid medium such as biotissue. [6] As shown in Fig. 2, the virtual objective is formed through the phase conjugate wave by an optical phase conjugator and scattering sites across the tissue. A reverse focusing beam is observed, and the potential application in biomedical research will be introduced.

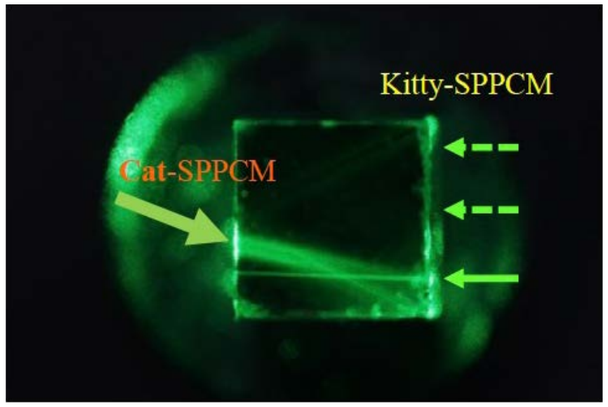

Fig. 2. A picture of a Kitty SPPCM based on a Cat SPPCM.

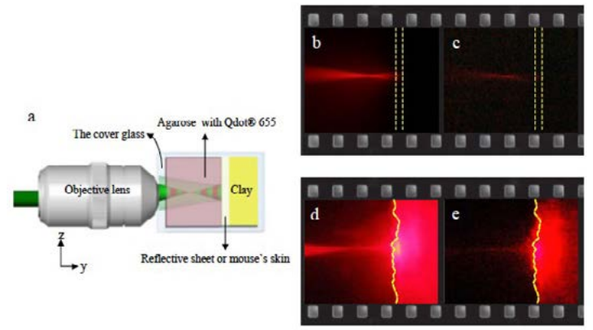

Fig. 2. (a) The schematic diagram of the virtual objective; (b) forward focusing light path in the diffuser sample; (c) inverse focusing light path in the diffuser sample by the virtual objective; (d) forward focusing light path in a skin sample; (e) inverse focusing light path in the skin sample by the virtual objective.

Reference:

[1] Z. Yaqoob, D. Psaltis, M. S. Feld, and C. Yang, Nat. Photonics 2, 110–115 (2008).
[2] J. Feinberg, Opt. Lett. 7, 486 (1982).
[3] C. C. Sun, R. H. Tsou, W. Shen, H. H. Chang, J. Y. Chang and M.W. Chang, Applied Optics 35, 1815 (1996).
[4] C. C. Lin, Y. W. Yu, C. Y. Cheng, C. C. Sun, Optical Engineering 54, 023101 (2015).
[5] M. Cui and C. Yang, Opt. Express 18, 3444 (2010).
[6] Y. W. Yu, S. Y. Chen, C. C. Lin, and C. C. Sun, Scientific Reports 6, 29452 (2016).

Acknowledgements

The authors acknowledge the assistance of Wei-Hsin Chen and Zhi-Shun Hou. The authors alsoacknowledge the support by Ministry of Science and Technology of ROC with the grant number MOST 104-2221-E-008-073-MY3, and by the National Central University's "Plan to Develop First-class Universities and Top-level Research Centers" with the grant number 105G-903.

Invited Speaker 7

Graphene based organic-inorganic holographic elements and devices

Vera Marinova[1,2], Shiuan Huei Lin[3] and Ken Yuh Hsu[1]

[1]Department of Photonics, National Chiao Tung University, University Str., 1001, Hsinchu 30010, Taiwan

[2]Institute of Optical Materials and Technologies, Acad. G. Bonchev Str. 109, Sofia, Bulgaria

[3]Department of Electrophysics, National Chiao Tung University, University Str., 1001, Hsinchu 30010, Taiwan

Abstract

We review varieties of graphene based organic-inorganic hybrid structures that can be used as holographic optical elements and devices. A high sensitive hybrid device working at transmission mode at near infrared spectral range is demonstrated supporting its role as optically addressed spatial light modulator by projecting a video image through it. In other type of structure all optical processes are controlled by the surface activated photorefractive phenomena where performed beam-coupling measurements at Bragg match regime show prospective amplification values and high spatial resolution.

1.Introduction

The challenge to modulate the light by light becomes a fundamental issue for photonic applications. This issue requires development of organic-inorganic devices operating with fast response time, in wide spectral sensitivity and allowing submicron resolution.

Basically, the organic-inorganic configurations are assembled using (i) photoconductive and photorefractive material (inorganic crystals as Bi12SiO20 (BSO) or Bi12TiO20 (BTO)), (ii) liquid crystals (LC) or polymer dispersed liquid crystals (PDLC) as strong birefringent organic materials and (iii) graphene as excellent transparent electrode or conductive nanoparticles. Such structures can be classified to two main types: electro-optically controlled and all optically controlled.

2.Electro-optically controlled holographic elements and devices

Electro-optically controlled structure consists of BSO:Ru crystal substrate and a glass substrate; LC layer (MLC-2070 type (Merck), nematic phase); polyimide alignment layers and graphene conductive layers. The structure is schematically illustrated at Fig.1. One side of BSO:Ru plate is covered by graphene conductive layer and the opposite side (contacting with LC molecules) with a photo alignment layer. The glass substrate has a graphene conductive layer and photoalignment layer.

Basic operation principle of the proposed device relies on electro-optically controlled birefringence of the liquid crystal molecules: the addressing beam activates the BSO:Ru photoconductive crystal to induce a corresponding charge field to the LC layer 1. As a consequence, at the exit of the device the light beam experiences a phase shift as a function of the applied voltage and the pump light intensity (Fig.1).

To demonstrate the optically addressed modulation properties we project a video image through the device and show the modulation of the pump light intensity, with the frame rate of 4 frames/sec.

1.All optically controlled holographic elements and devices

Among all-optically controlled structures, those based on photorefractive nonlinearity e.g. ability of some materials to modulate their refractive index in response to light, become of prime importance 2. In particular, the essential role in such applications plays so called space charge field (Esc) accumulated by photo-induced charge carriers redistribution within the photorefractive media.

All optically controlled structure consists of photoconductive BSO crystal substrate and a glass substrate arranged into a cell (10 μm thickness), filled with polymer dispersed liquid crystal (PDLC) doped

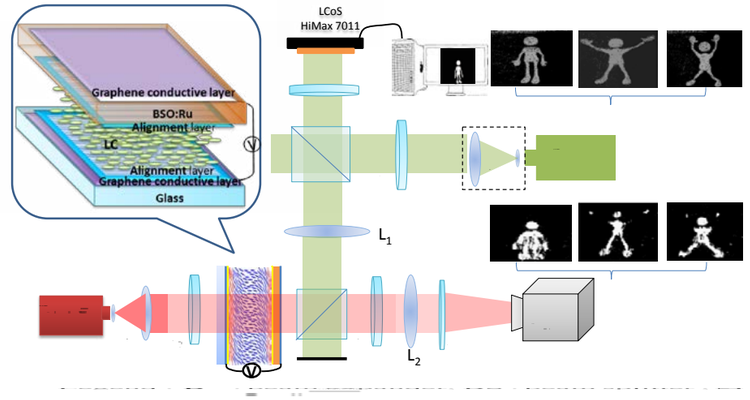

Fig.1. Structure of graphene based electro-optically controlled device and its OASLM properties.

with Graphene oxide (GrO). GrO nanoparticles (concentration of 10-4 wt%) were added into LC and after that the LC/GrO suspension was mixed with polymer matrix (NOA 65 UV glue) at 30:70 wt % ratio 3.

The light irradiation on BSO:Ru/PDLC:GrO structure lead to a reverse of its initial opaque state to the transparent state. Due to the BSO:Ru near-infrared absorption and high photoconductivity, the illumination with a Gaussian beam caused charge carriers generation, which migrate by diffusion to form an inhomogeneous distribution. This photo-induced field, generated inside the BSO:Ru plate, can be strong enough (estimated later) to spread out into the PDLC surface layer, realigning the LCs molecules orientation inside the droplets and thus to change the LCs director, consequently the refractive index and transparency of the structure. As a result, the refractive indices between the LC and polymer matrix changes, and thus the light intensity distribution through the BSO/PDLC:GrO structure could be switched 4.

In such all optically controlled BSO/PDLC:GrO hybrid structure, the charge migration, trap density and space-charge field come from the BSO substrate, whereas the high beam amplification is provided by the LC layer. Therefore, all processes are performed only by the action of light. The proposed novel structure does not require ITO contacts and alignment layers and all the processes are controlled by light, thus opens further potential for real-time image processing at the near infrared spectral range.

Financial support by the Ministry of Science and Technology (MOST), Taiwan under the contracts: MOST 104-2221-E-009-164; 104-2221-E-009-151 and ATU program under Ministry of Education, Taiwan are gratefully acknowledged.

Reference:

[1] P. Yeh and C. Gu, “Optics of liquid crystal displays”, Wiley, New Jersey (2010).

[2] P. Yeh, “Introduction to photorefractive nonlinear optics” (Wiley New York, (1993).

[3] R. C. Liu, V. Marinova, S. H. Lin, M. S. Chen, Y. H. Lin and K. Y. Hsu, Near infrared sensitive photorefractive device using PDLC and BSO:Ru hybrid structure, Opt. Lett., 39, 3320 (2014)

[4] V. Marinova, Z. F. Tong, S. Petrov, D. Karashanova, K. Y. H. Lin, S. H. Lin and K. Y. Hsu, Graphene oxide doped PDLC films for all optically controlled light valve structures, Proceed. SPIE, Vol. 9970 (2016)

Invited Speaker 8

The Application of Waveguide Holograms to Display Systems

Wei-Chia Su[1)], Wen-Kai Lin[1,2)], Shao-Kui Zhou[3)] and Bor-Shyh Lin[2)]

[1)]Graduate Institute of Photonic, National Changhua University of Education, Changhua, 50007, Taiwan

[2)]College of photonics, National Chiao Tung University, Tainan, 71150, Taiwan

[3)]Department of Physics, National Changhua University of Education, Changhua, 50007, Taiwan

1.Abstract

A holographic device called waveguide hologram is implemented by using a holographic optical element (HOE) and a planar waveguide. The probe light propagates through the waveguide with total internal reflection and then incident on this HOE, and then a signal wave is diffracted from the HOE. We demonstrate two applications of waveguide hologram in this study. One demonstration is an eyewear display system, and the other is a planar multifunctional display system.

2.Introduction

Waveguide holograms have received increasing attention owing to their potential in compact configuration and insusceptibility from extraneous lights [1-3]. The basic scheme of a waveguide hologram is shown in Fig.1. Basically, the waveguide hologram is fabricated by using a holographic optical element (HOE) and a planar waveguide. The HOE attached on the planar waveguide recodes the interference of the reference beam and the signal beam. Before interfering with the signal beam, the reference beam propagates through the waveguide with total internal reflection and then it was incident on the holographic recording material. And the signal beam propagates to the recording material with an almost normal incident angle. With proper arrangement of reference wave and signal wave, display systems with various functions can be implemented. In this study, an eyewear display system and a planar multifunctional display system is demonstrated based on waveguide holograms.

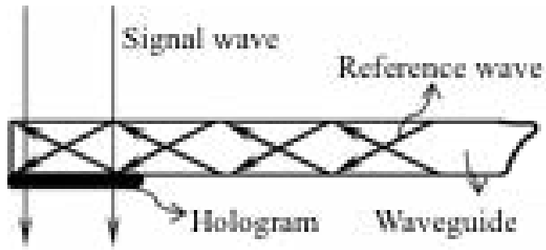

Fig. 1. The waveguide hologram

3.Eyewear display based on waveguide hologram

Fig.2 shows the basic architecture of the HMD system. A collimated beam is coupled into the waveguide, and then it is incident on a HOE. A converged spherical wave will be diffracted when a collimation beam probes the HOE. The diffracted converged spherical wave plays a role of backlighting for the LCD panel. And then the image on the LCD panel will be projected on the retina. Since the image is projected on the retina, the image quality will not be affected when human eye focus on different distance. Fig. 3 shows the observed diffracted virtual image when a binary amplitude pattern was used to replace the LCD pattern and placed in the front of the see-through window of the waveguide. A virtual image has been successfully obtained.

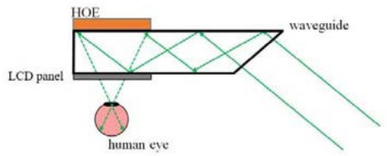

Fig. 2. The eyewear display based on waveguide hologram.

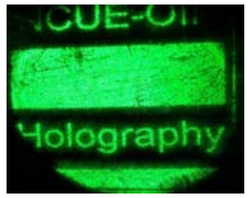

Fig. 3. The diffracted virtual image of the eyewear display

4.Planar multifunctional display based on Waveguide hologram

In this study, a compact waveguide hologram attached on a LCD panel has been successfully implemented to demonstrate a hybrid display system. This hybrid display aims to display 2D and 3D information simultaneously. The 2D information is produced by using a liquid crystal display (LCD) panel and the 3D image information is offered by using a waveguide hologram.

The schematic system is shown in Fig.5. The observer will see a 3D object in front of the LCD when the observer watches the display. The dimension of the hologram is 4 inch x 5 inch, and the thickness of the PMMA waveguide is 1 cm. The reference wave is a spot light source during recording. And the incident surface for the reference beam is a diffuser surface. In the reconstruction process, a LED light source is used for the image retrieved. Fig. 6 shows the reconstruction result of the planar multifunctional display.

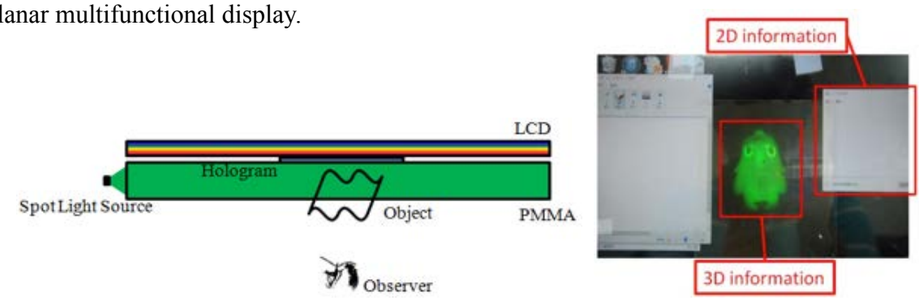

Fig. 4. a hybrid display system based on waveguide hologram.

5.Conclusion

We have successfully presented two compact display systems based on waveguide holograms. One of the demonstrations is a compact eyewear display system, and a virtual image diffracted from system has been successfully observed. The second demonstration is a hybrid display system. The 2D information from the LCD panel and the 3D image information from the waveguide hologram have been successfully observed.

Reference:

[1] A. Cameron, “The Application of Holographic Optical Waveguide Technology to Q-Sight TM Family of Helmet Mounted Displays,” Proc. of SPIE, Vol. 7326, 73260H (2009).

[2] H. Mukawa, K. Akutsu, I. Matsumura, S. Nakano, T. Yoshida, M. Kuwahara, K. Aiki, M. Ogawa, “A Full Color Eyewear Display using Holographic Planar Waveguides,” SID Symposium Digest of Technical Papers Vol. 39, No. 1, pp. 89–92 (2008).

[3] W.-C. Su and M.-H. Tsai, “A spectacle-type 3D display based on holographic optical element and planar waveguide,” 3D System and Applications Digest of Technical Papers, 2014-104 (2014).

Invited Speaker 9

A study of PQ:PMMA photopolymer recording process based on rate equations and diffusion equations

Te-yuan Chung[1)], Bao-Ren Shih[1)] and Chuan-Wen Chen[1)]

[1)]Department of Optics and Photonics, National Central University, No. 300 Chungda Rd, Chungli district, Taoyuan city, Taiwan 32001

1.Introduction

PQ:PMMA is known as an inexpensive photopolymer with low shrinkage. The recording wavelength of PQ:PMMA can be 532 nm or shorter which can be easily achieved by inexpensive solid-state laser and GaN-based diode lasers. In 2009, Gleeson et al. established a comprehensive chemical reaction dynamics model of PQ:PMMA [1]. This work established a set of simplified reaction rate equations along with diffusion equation to model the refractive index distribution in space during the recording process. With the model, a thorough simulation study and experiments on writing a 1D volume Bragg grating was performed and discussed.

2.Title section

By applying several practical considerations of PQ:PMMA reaction, the differential equations of 1D PQ molecular distribution and photochemical product distribution can be obtained as

$$\frac{\partial[PQ(x,t)]}{\partial t}=\frac{\partial}{\partial x}D_{PQ}\frac{\partial[PQ(x,t)]}{\partial x}-k_{PQ}[PQ(x,t)] \quad (1)$$

and

$$\frac{\partial[Product(x,y)]}{\partial t}=k_{PQ}[PQ(x,y)] \quad (2)$$

where “Product” indicates the compounds that change the refractive index of the photopolymer. Parameter D is the diffusion coefficient and k indicates the product generation rate. With these simplified equations, the distribution of the “product” can be simulated with given exposure conditions. In this work, the writing light intensity is a simple sinusoidal function. The simulation result is shown in Fig.1. The distribution of the photopolymer product directly proportion to the change of refractive index which can be used to calculate the diffraction efficiency if such a 1D refractive index distribution can be considered as a 1D volume grating.

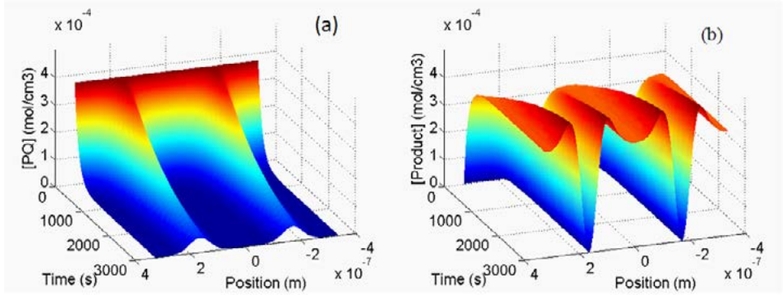

Fig. 1. (a) PQ and (b) Product density distributions as functions of exposure time.

1.Experiment

An experiment using 532 nm laser as the writing light source. The writing configuration is a typical two-beam interference scheme. A refractive type volume Bragg grating then was recorded in a piece of PQ:PMMA with thickness of 2 mm. The diffraction efficiency of the sample was monitored and compared by the simulation result as shown in Fig.2. The experimental result agree well with the simulation.

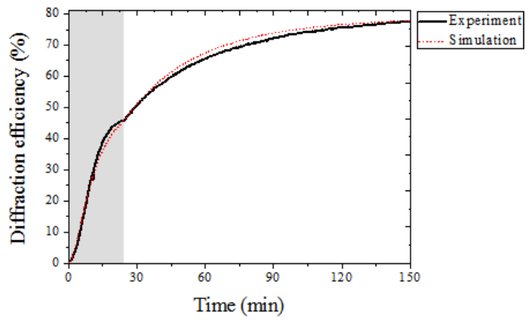

Fig. 2. The simulation and experimental results agree well with each other

Reference:

[1] S. Liu, M. R. Gleeson, J. Guo, J. T. Sheridan, E. Tolstik, V. Matusevich, and R. Kowarschik, "Modeling the photochemical kinetics induced by holographic exposures in PQ/PMMA photopolymer material," J. Opt. Soc. Am. B 28, 2833-2843 (2011).

[2] M. R. Gleeson, and J. T. Sheridan, "Nonlocal photopolymerization kinetics including multiple termination mechanisms and dark reactions. Part I. Modeling," J. Opt. Soc. Am. B 26, 1736-1745 (2009).

Invited Speaker 10

Full-color high-definition CGH employing RGB color filters

Kyoji Matsushima and Yasuhiro Tsuchiyama
Department of Electrical and Electronic Engineering, Kansai University, Yamate-cho 3-3-35, Suita, Osaka 564-8680, Japan

1.Introduction

For last several years, we have presented very large-scaled computer-generated holograms (CGHs) called high-definition CGHs (HD-CGHs), which reconstruct full-parallax high-quality 3D images[1-3]). However, these HD-CGHs could reconstruct only monochromatic images. Recently, we proposed the technique for their full-color reconstruction using RGB color filters and simulation to design appropriate filter properties[4,5]). The techniques make it possible to create high-quality full-color HD-CGHs[6]).

2.Principle and techniques

Our HD-CGHs work well as reflection hologram because their fringe pattern made of Cr thin films. RGB color filters are attached to each RGB fringe block, as shown in Fig.1. Here, gaps of the fringe, called guard gap, are made for increasing position tolerances of the filters as in Fig.2. One of key techniques is to use a multi-chip type white LED for the illumination light source. Fairly narrow spectra are obtained from combination of the light source and filters, as shown in Fig.3 (b). We adopt a vertical stripe pattern for the RGB color filters in order to avoid overlapping light diffracted by the filters with the reconstructed object image, because the light source is usually placed below the object for gaining higher diffraction efficiency.

3.Optical reconstruction and conclusion

The RGB color filters used are fabricated by the same technique as that of LCD panels. The filter properties are shown in Fig.3 (a). These properties are designed through the simulation technique[4,5]). An example of optical reconstruction and parameters of the full-color HD-CGH is shown in Fig.4 and Table 1, respectively. The HD-CGH is composed of 16 G pix, the fringe pattern is generated by using the polygon-based method[7]) and the silhouette method with the switch-back technique[3]).

Acknowledgement

The authors would like to thank Prof. Sakamoto and

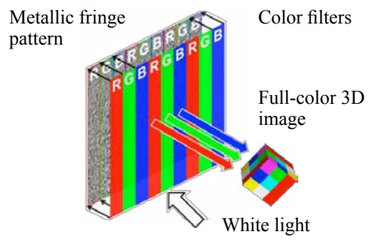

Fig. 1. The principle of full-color CGH using RGB filters.

Table 1 Parameters of the fabricated HD-CGH

No. of fringe pixels	131,072 · 131,072
Pixels pitches	0.8 □m · 0.8 □m
Size	10.5 · 10.5 cm²
Fringe type	Binary amplitude

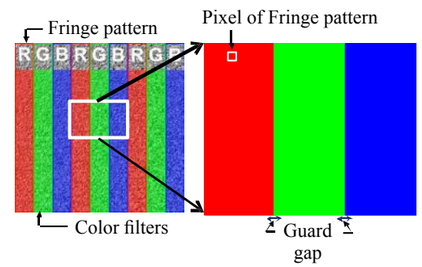

Fig. 2. Color filters attached to the fringe pattern with **guard gaps.**

Nakahara for their useful suggestions. This work was financially supported by the JSPS KAKENHI Grant Number 15K00512 and the MEXT strategic research foundation at private universities (2013-2017).

References:

[1] K. Matsushima, S. Nakahara, “Extremely high-definition full-parallax computer-generated hologram created by the polygon-based method,” Appl. Opt. 48, H54-H63 (2009).

[2] K. Matsushima, H. Nishi, S. Nakahara, “Simple wave-field rendering for photorealistic reconstruction in polygon-based high-definition computer holography,” J. Electron. Imaging 21, 023002 (2012).

[3] K. Matsushima, M. Nakamura, S. Nakahara, “Silhouette method for hidden surface removal in computer holography and its acceleration using the switch-back technique,” Opt. Express 22, 24450-24465(2014).

[4] Y. Tsuchiyama, K. Matsushima, S. Nakahara, Y. Sakamoto, “A Simulation technique for selection of color filter used for full-color high-definition CGH,” IWH2015, Th2-4 (2015).

[5] Y. Tsuchiyama, K. Matsushima, S. Nakahara, Y. Sakamoto, “Full-color high-definition CGH using color filter and filter design based on simulation,” OSA Digital Holography & 3-D Imaging, DW5I.4 (2016).

[6] Y. Tsuchiyama, K. Matsushima, “Full-color large-scaled computer-generated holograms using RGB color filters,” to be published.

[7] K. Matsushima, “Computer-generated holograms for three-dimensional surface objects with shade and texture,” Appl. Opt. 44, 4607-4614(2005).

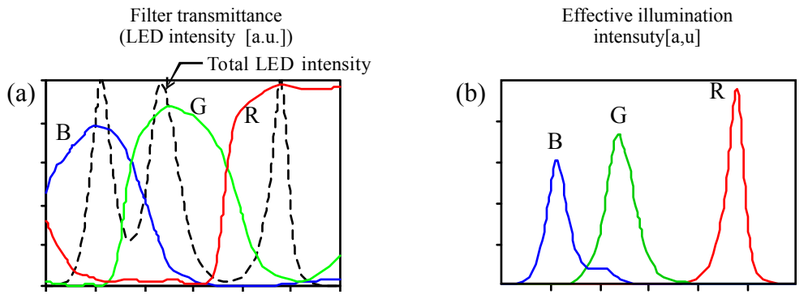

Fig. 3. Spectra of (a) transmission of the fabricated RGB filter and (b) effective illumination estimated by the white LED spectrum used for the light source.

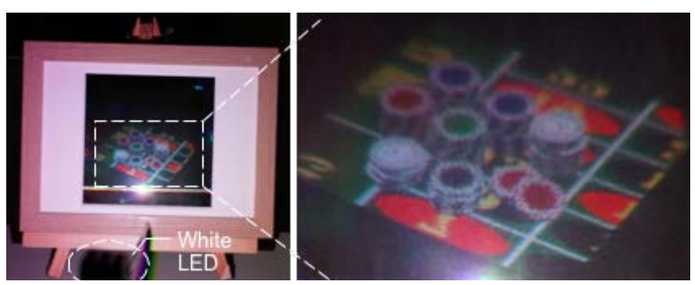

Fig. 4. Optical reconstruction of a HD-CGH named ‘Casino Chips

Invited Speaker 11

Application of head-mounted computer generated holographic display on the human visual training

Chien-Yu Chen[1)], Chi-Hao Chuang[2)]

[1)]Graduate Institute of Color and Illumination Technology, National Taiwan University of Science and Technology, Taipei 10607, Taiwan

[2)]Graduate Institute of Photonics and Optoelectronics, National Taiwan University, Taipei 106, Taiwan

1.INTRODUCTION

In recent years, vision trainings are applied to training eye muscles and reinforce the connection between the ciliary muscle and nerves Although it would spend longer time for improvement, it could avoid relevant medical risks; besides, trainings in pre-presbyopia could make more effective improvement [1]. General

vision trainings have the trainees view the left and the right picture cards with distinct distances and try to cross fuse the two images with focus as cyclopean vision [2]. Nonetheless, it might be difficult for the trainees recognizing the images with low contrast and blurred characterized images. In this research, the modified Gerchberg–Saxton algorithm [3] is used for the computer-generated hologram coding of fixation disparity image or changed disparity image. Here the fixation disparity is applied for accommodation training, and the changed disparity is applied for convergence training. In our system, the diffraction efficiency is over 85%, the visibility is about 90%, and RMSE is less than 0.04.

2.PRINCIPLE

Fixation disparity is defined as the characterized image whose left and right sizes are different but present same disparity. In the figure, when the characterized image with fixation disparity is located on the fixed image plane, it is regarded as the image projected from different distances. In other words, when both eyes viewing the left and the right images with the same disparity, the perception disorder is caused by the distinct sizes. The ciliary muscle therefore appears indirect accommodation because of monocular cues to complete fusional convergence [4].On the contrary, the changed disparity which is defined as the left and the right characterized images with the same size but changeable disparity. It aims to change the eyes’ vergence through the characterized image with distinct disparity for inducing the accommodation change. As a result, the above MGSA-type CGH is applied to coding image contents with fixation disparity and changed disparity for vision trainings.

3.EXPERIMENT AND ANALYSIS

Fig. 1(a) illustrates a prototype of MGSA-type CGH system with head-mounted display (HMD) for vision trainings. First, the DPSS laser (532 nm) is used for decrypting the coherence of light, which is adjusted to proper intensity with neutral density filters and then injected to the spatial light modulation (WUXGA, 8.1 m, HOLOEYE) through the collimating lens. SLM records POF with fixation disparity or changed disparity coded by MGSA. After the decryption, the image reconstructed by diffraction light is projected to CCD and transmitted to the head-mounted display for the trainee proceeding vision trainings through HMD. Fig. 1(b) shows a changed disparity image which is transmitted to HMD after the decryption. With cyclopean vision [2], the stereo image in the figure would extrude the screen when the dot viewed by both eyes would be convergent to a point. Moreover, in regard to the evaluation of diffraction efficiency, the decryption efficiency(85%) is

slightly lower than the result of computer computation (95%), but the image intensity can be accepted by human eyes. What is more, the reconstructed left and right images reveal the visibility 94.07% and 94.46%, respectively, showing the characteristic line of the decrypted image with favorable contrast, that the content could be clearly presented. Besides, the SNRs appear 8.44 dB and 7.94 dB, and the speckle is 20.23% after the random number phase multiplication that the noise disturbance has been reduced about a half, compared to traditional CGH [5]. Moreover, the computation average time is 60.28 s, revealing that the same or better image quality could be achieved by faster computation speed and less number of iteration times, compared to general holographic projection systems[5]–[7]

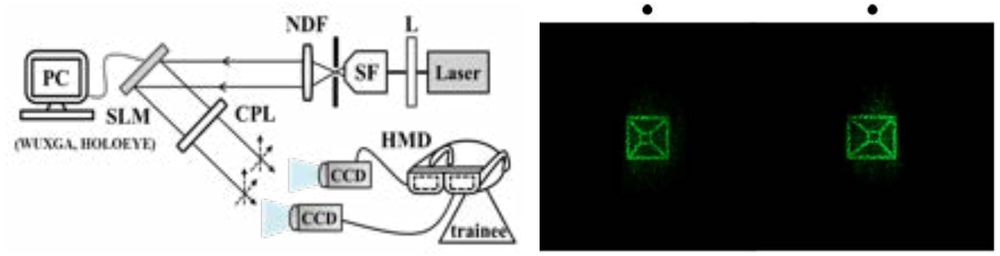

(a) (b)

Fig. 1. (a) Diagram of prototype MGSA-type CGH system (b) Stereo image pair with the changed disparity

4.CONCLUSION

The MGSA is used for the computer generated hologram coding of fixation disparity image or changed disparity image and the left and the right reconstructed image information is displayed on HMD. Such a method allows a trainee viewing the images with two different disparities through HMD and further changing the synkinesis of accommodation and convergence for effectively training ciliary muscle and extraocular muscle. Besides, the reconstructed images show the relative diffraction efficiency about 86% and visibility 94%. In comparison with traditional 2D cards, the images reconstructed by MGSA-type CGH present high contrast, high resolution, and changeable disparity that they could enhance the training effect and avoid crosstalk between the left and the right images.

Reference:

[1] J. Maxwell, J. Tong, and C. M. Schor, “Short-term adaptation of accommodation, accommodative vergence and disparity vergence facility,” Vision Res., vol. 62, pp. 93–101, 2012.

[2] B. Julesz, “Cyclopean perception and neurophysiology,” Invest. Ophthalmol. Vis. Sci., vol. 11, pp. 540–548, 1972.

[3] H. E. Hwang, H. T. Chang, and W. N. Lai, “Fast double-phase retrieval in Fresnel domain using modified Gerchberg–Saxton algorithm for lensless optical security systems,” Opt. Express, vol. 17, pp.13700–13710, Aug. 2009.

[4] J. M. Hillis andM. S. Banks, “Are corresponding points fixed?,” Vision Res., vol. 41, pp. 2457–2473, 2001.

[5] K. Choi, H. Kim, and B. Lee, “Synthetic phase holograms for autostereoscopic image display using a modified IFTA,” Opt. Express, vol.12, pp. 2454–2462, 2004.

[6] J. P. Liu, W. Y. Hsieh, T. C. Poon, and P. Tsang, “Complex Fresnel hologram display using a single SLM,” Appl. Opt., vol. 50, pp.H128–H135, 2011.

[7] J. Bu, G. Yuan, Y. Sun, S. Zhu, and X. Yuan, “Optimization of computer-generated holograms for dynamic optical manipulation with uniformstructured light spots,” Chin. Opt. Lett., vol. 9, pp. 061202–, 2011.

Invited Speaker 12

Joint Wavelength and Position Multiplexing Using Optical Phase Only Image Encryption

Yu-Ting Wang[1)] and Hsuan T. Chang[1)]

[1)]Photonics Information Laboratory, Department of Electrical Engineering, National Yunlin University of Science and Technology, Douliu Yunlin 64001 Taiwan

1.Introduction

Recently, the multiple image encryption methods based on the wavelength or position multiplexing schemes in the Fresnel transform domain have received great deal of attention [1]-[5]. Either the various wavelengths or the diffraction distance between the input and output planes are used in retrieving the phase-only functions (POFs) corresponding to the target images. In this study, we propose the joint wavelength and position multiplexing method, which simultaneously considers the manipulation of both parameters in the diffraction process. In decryption, therefore, both the correct wavelength and position parameters are required in order to reconstruct the corresponding target image at the output plane.

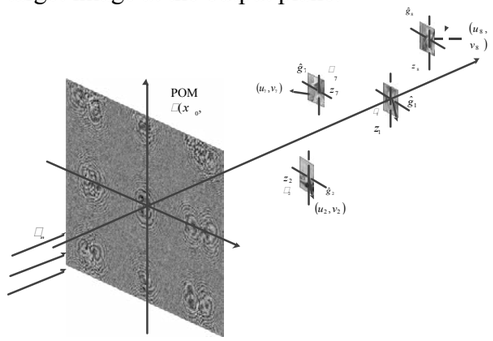

Fig. 1. Optical architecture of the proposed method

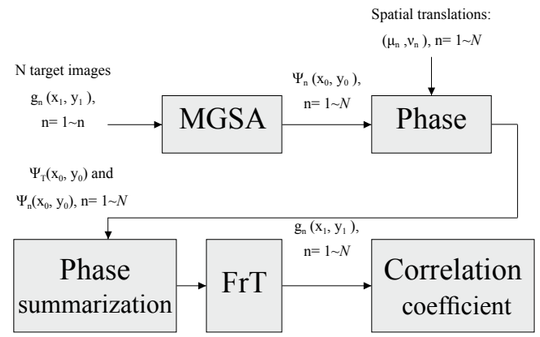

Fig. 1. Block diagram of the proposed method.

2.Method

Figure 1 shows the optical architecture of the proposed method. Given N target images, gi, i=1,…,N, for the multiplexing purpose, the main purpose is to retrieve a phase-only mask (POM) that can be used to reconstruct the target images in the corresponding diffraction distance Zn at the designated position (μi, νi) with a specific wavelength λn. Figure 2 shows the block diagram of the proposed method. For each target image, the modified Gerchberg and Saxton algorithm (MGSA) [6] is used to retrieve a POF $\Psi(x_0,y_0)$ that reconstruct the corresponding target image $g_n(x_1, y_1)$ through the diffraction distance zn with the wavelength λn at the output plane. Equation (1) shows the Fresnel transform (FrT) representing the diffraction process between the input POF and the output reconstructed image:

$$\mathrm{FrT}\{\exp[j\Psi_n(x_0, y_0)]; \lambda_n; z_n\}=\hat{g}_n(x_1, y_1)\exp\left[j\Psi_{\hat{g}_n}(x_1, y_1)\right]. \quad (1)$$

To reduce the crosstalk among all the target images, a phase modulation method [8] is used to shift the targetimages to the position (μ_i, ν_i) so that they are separated in the (xi, yi) coordinates. That is, given a shifting (μ_n,ν_n), the new phase $\Psi_n'(x_0, y_0)$, n=1~N, satisfying Eq. (2) can be determined by using Eq. (3).

$$\mathrm{FrT}\{\exp[j\Psi_n'(x_0, y_0)]; \lambda_n; z_n\} = \hat{g}_n(x_1 - \mu_n, y_1 - \nu_n)\exp[j\phi(x_1, y_1)], \quad (2)$$

$$\Psi_n'(x_0, y_0) = \Psi_n(x_0, y_0) + \frac{2\pi(\mu_n x_0 + \nu_n y_0)}{\lambda_n z_n}. \quad (3)$$

To achieve the multiplexing, all the POFs are summarized to become a POM with the POF $\Psi_T(x_0, y_0)$,

$$\exp[j\Psi_T(x_0, y_0)] = \exp\{\sum_{n=1}^{N}[j\Psi_n'(x_0, y_0)]\}, \quad (4)$$

To reconstruct a specific target image gn, the FrT with the corresponding wavelength and position is applied to the POM. Equation (5) describes the process.

$$\begin{aligned}|\mathrm{FrT}\{\exp[j\Psi_T(x_0, y_0)]; \lambda_n; z_n\}| &= \left|\hat{g}_n(x_1 - \mu_n, y_1 - \nu_n)\exp\left[j\Psi_{\hat{g}_n}(x_1 - \mu_n, y_1 - \nu_n)\right] + n_n(x_1, y_1)\right|, \\ &\approx |\hat{g}_n(x_1 - \mu_n, y_1 - \nu_n)| + |n_n(x_1, y_1)|,\end{aligned} \quad (5)$$

Finally, as shown in Fig. 2, the correlation coefficient (CC) ρ between the original and reconstructed images are determined to evaluate the system performance.

3.Results and Conclusion

In our simulation, nine target images of size 64 by 64 and placed at different coordinates (μ_i, ν_i) are used. Suppose that the SLM pitch is 8μm . In retrieving the POF for each target image, we search for the best wavelength and the diffraction position so that the highest CC of the reconstructed image can be obtained. Table 1 shows the best wavelength, position, and CC for each image. Compared with our previous wavelength or position multiplexing methods [3], the proposed method achieves higher CC values. In addition, the system security is also enhanced because both the wavelength and position parameters are required simultaneously in order to correctly reconstruct the target image at the output plane.

According to the simulation result, we have shown that the proposed method is superior to the previous methods that are only based on either wavelength or position multiplexing scheme. Our future work will focus on the error analysis of system parameters.

Image #	1	2	3	4	5	6	7	8	9
z(m)	3.1	3.2	3	3.2	3.2	3.2	3.2	3.1	3.2
λ(nm)	400	400	400	400	400	500	700	500	700
ρ value	0.954	0.959	0.925	0.913	0.950	0.971	0.938	0.982	0.964

Table 1. The wavelength and position parameters for reconstructing the target images with the best CC values.

4.Acknowledgment

This study is partially supported by the Ministry of Science and Technology, Taiwan, under the contract number MOST 105-2221-E-224-021-MY2.

Reference:

[1] G. Situ and J. Zhang, “Multiple-image encryption by wavelength multiplexing,” Opt. Lett., vol. 30, pp. 1306-1308, 2005.

[2] G. Situ and J. Zhang, “Position multiplexing for multiple-image encryption,” Journal of Optics A: Pure and Applied Optics, vol. 8, no. 5, p. 391, 2006.

[3] H.-E. Hwang, H.T. Chang, and W.-N. Lai, “Multiple-image encryption and multiplexing using modified Gerchberg-Saxton algorithm and phase modulation in Fresnel transform domain,” Opt. Lett., vol. 34, no. 24, pp. 3917-3919, 2009

[4] H.T. Chang, H.-E. Hwang, C.L. Lee, and M.-T. Lee, “Wavelength multiplexing multiple-image encryption using cascaded phase-only masks in Fresnel transform domain,” Appl. Opt., vol. 50, no. 5, pp. 710-716, 2011.

[5] H.T. Chang, H.-E. Hwang, and C.L. Lee, “Position multiplexing multiple-image encryption using cascaded phase-only masks in Fresnel transform domain,” Opt. Comm., vol. 284, no. 18, pp. 4146-4151, 2011.

[6] H.-E. Hwang, H.T. Chang, and W.-N. Lai, “Fast double-phase retrieval in Fresnel domain using modified Gerchberg-Saxton algorithm for lensless optical security systems,” Optics Express, vol. 17, no. 16, pp. 13700-13710, August 3, 2009

Invited Speaker 13

Magneto-optic Three-dimensional Holographic Display Composed of Artificial Magnetic Lattice

Hiroyuki Takagi[1)], Shoki Sakai[1)], Kazuki Nakamura[1)], Taichi Goto[1,2)], Pang Boey Lim[1)], Hironaga Uchida[1)] and Mitsuteru Inoue[1)]

[1)]Department of Electrical and Electronic Information Engineering, Toyohashi University of Technology, 1-1 Hibarigaoka, Tempaku, Toyohashi, Aichi 441-8580, Japan

[2)]JST, PRESTO, 4-1-8 Honcho, Kawaguchi, Saitama, 332-0012, Japan

1.Introduction

A holographic display is a realistic three-dimensional (3D) display because it produces an exact copy of the wave front of scattered light from 3D objects1). A holographic display demands a wide-viewing-angle for 3D visualization. However, the viewing angle of holographic displays based on conventional spatial light modulators (SLMs) is less than three degrees. The pixel pitch of conventional SLMs is in the range of 10-100μm. Recently, we developed a magneto-optic three-dimensional holographic display (MO-3DH-display) that had a two-dimensional magnetic pixel array with sub-micrometer-scale pixels for a wide-viewing holographic display. For controlling magnetic pixels, we used a thermomagnetic recording system to control the direction of magnetization by the optical addressing method. This method has the advantage that it is possible to fabricate sub-micrometer-scale pixel arrays without a driving line and pixel structure on the magnetic medium. The magnetic film of the first MO-3DH-display was an amorphous TbFe (a-TbFe) film, a material widely used in thermomagnetic recording applications. The MO-3DH-display could reconstruct 3D image over 22 degrees viewing angle. However, the reconstructed images had a low brightness: 4.4×10-2 cd/m2 with reconstruction illumination of 10.8 mW/cm2 at 532 nm. Display standard ISO13406 for liquid crystal displays recommends brightness of displays to be over 100 cd/m2. To represent a 3D image with 100 cd/m2 from the a-TbFe film would require reconstruction illumination of about 24 W/cm2. For improved diffraction efficiency, the magnetic film should have high transmittance and a large Faraday rotation angle. In this study, we developed a MO-3DH-display composed of an artificial magnetic lattice structure.

2.Experiments and results

We focused on the enhancement of the magneto-optic (MO) Faraday rotation by an artificial magnetic lattice structure of one dimensional magnetophotonic crystals (MPCs) 2). The MPC have two Bragg mirrors and a light localization layer of thin magneto-optic film. The MPCs enhance the Faraday rotation angle of the magnetic localization layer with high transmittance by Fabry-Pérot resonance. The thin MO film can obtain similar properties to thick MO film. However, the MPC has angular dependence that depends on the optical thickness of each layer in the MPC. Because optical thickness is changed when light angle is changed. The MPCs were designed to reduce angular dependence of diffraction efficiency by changing thickness of dielectric layers in Fresnel equation. The structure of MPCs for wide-viewing-angle was designed by the calculation. The structure was substituted GdGagarnet (SGGG) substrate / (Ta2O5/SiO2)out / (Ta2O5/SiO2)in / (BiDyY)3(FeAl)5O12 (BiDyYFeAlGarnet: BiDyYFeAlG) / (Ta2O5/SiO2)in / (SiO2/Ta2O5)out.

The thickness of (Ta2O5/SiO2)in was determined as λ/4n, where λ was the resonant wavelength of 532 nm and n is the refractive index of each material. The thickness of the BiDyYFeAlGarnet layer was 1.34 μm. The thickness of (SiO2/Ta2O5)out was 24 nm/ 16 nm for wide-viewing-angle. As results, the MPC has light intensity difference that was less than 3.15% when viewing-angle was less than ±15 degrees as calculation results. The diffraction efficiency of the MPC was over about 2,300 times higher than the a-TbFe film.

We fabricated an optical system using the tiling optical addressing method, which consists of a pulse laser, a digital micro mirror device (DMD), object lenses, an x-y-z stage, and magnetic media. The optical system for the tiling optical addressing method is shown in Fig. 1. A DMD (Discovery 1100, 1024 pixels × 768 pixels, maximum driving speed of 22 kHz/frame) was used for the tilling optical addressing method. The DMD showed part of 2D hologram pattern. To write the hologram, a pulse laser (Nd:YAG laser) operating at 355 nm with pulse width of approximately 10 nsec and a frequency of 10 Hz was used. The optical parametric oscillator was a MOPO-SL-1P (Spectra-Physics) to control wavelength. The 2D hologram pattern on the DMD was transferred to the magnetic film by two object lenses whose focal lengths are 100 mm and 10 mm. The pixel size was decreased to one-tenth of the original size of the DMD. Therefore, the magnetic pixel size was 1.36 μm. The reconstruction optical system consisted of a reconstruction illumination source, a polarizer and an analyzer with cross-Nicol configuration for separating zero order transmitted light and the reconstructed image. The MO-3DH-display composed of MPC could reconstruct high brightness 3D image and the viewing angle of the reconstructed image was 22°.

This work was supported by JSPS KAKENHI Grant Nos. 26220902.

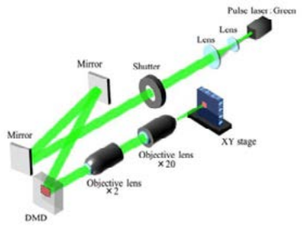

Fig. 1. The optical system for the tilling optical addressing method.

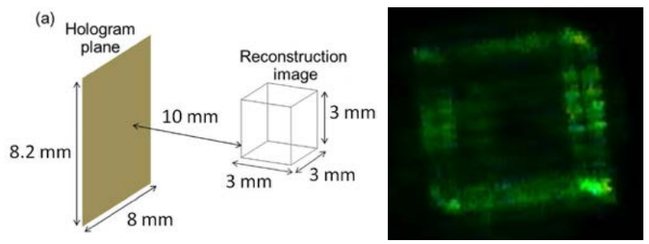

Fig. 2. (a) A model of 3D image for generating the hologram. The wireframe cube was constructed by point light sources. (b) A reconstruction 3D image from the MPC.

Reference:

[1] V. M. Bove, “Display Holography's Digital Second Act,” Proceedings of the IEEE 100, 918 (2012).

[2] M. Inoue, R Fujikawa, A. Baryshev, A. Khanikaev, P. B. Lim, H. Uchida, O. Aktsipetrov, A. Fedyanin, T. Murzina, and A. Granovsky, J. Phys. D 39, 151 (2006).

IWH Lunch Session

Jasper Display

Building the Eco-System for the Electro-Optics Platform

Kenneth Tai
Jasper Display Corp. Headquarter, TW, Hsinchu City 30059, Taiwan
Jasper Display Corp., Subsidiary, Santa Clara, CA, USA

2015 has already been claimed as International Year of Light by United Nations. Light and light-based technologies have received wide attention. United States and Europe were aware of this trend early and in 2013 they had proposed the White Paper and strategic roadmap about light-based technologies respectively. During the transition process of technology trends, many opportunities will arise inevitably. At this moment, it is necessary to find out the self-position and confirm the development direction quickly. With multi-party cooperation, the cornerstone of the industry could be raised and the time length of technology development could be folded up. Therefore, it would have a chance to grasp the world level market. In addition, education and training must also act simultaneously. This can provide the industry adequate engineering and R & D people.

Introduction

The UN has recognized the importance of raising global awareness about how light-based technologies promote sustainable development and provide solutions to global challenges. In fact, light plays a vital role in our daily lives. It becomes an imperative cross-cutting discipline of science in the 21st century. On 20 December 2013, the UN General Assembly 68th Session proclaimed 2015 as the International Year of Light and Light-based Technologies (IYL 2015). An International Year of Light is a tremendous opportunity to ensure that governments and people are made aware of the problem-solving potential of light technology. The proclamation obtained positive response and recognition from many countries immediately. This illustrated the science and technology of light is leading a new revolution. It will affect the development of the global civilization and the well-being of human. The UN declared that the 21st century is the century of light. The UN declared that the 21st century is the century of light. The influence of light to economy is so great, just like electronic technology had during the 20th century. Therefore, the economic development would be closely related to the development of both light and electronic. In 2014, the Nobel Prize in Chemistry and Physics were both awarded to the people whose researches are of light technology. For chemistry prize, it was awarded jointly to Eric Betzig, Stefan W. Hell and William E. Moerner "for the development of super-resolved fluorescence microscopy". For a long time optical microscopy was held back by a presumed limitation: that it would never obtain a better resolution than half the wavelength of light (0.2um). Helped by fluorescent molecules they ingeniously circumvented this limitation. Due to their achievements the optical microscope can now peer into the nanoworld. For physics prize, it was awarded jointly to Isamu Akasaki, Hiroshi Amano and Shuji Nakamura "for the invention of efficient blue light-emitting diodes which has enabled bright and energy-saving white light sources". Both red and green LED are already mature in technic and substantial in market, but limited to the

mismatched blue LED level,the white light LED was defective. This made corresponding LED lighting market was unable to be developed substantially. Now the high performance blue LED appears, so the key issues of white LED lighting is finally addressed and a substantial leap forward has been made in LED lighting market. By these two facts, light technology could bring human being more expansibility has been proven again.

Winning strategy

Since the trend is clear, to enter the light technology industry with a clear and definite strategy would be a safer way. By the strategy, people could examine themselves deeply and then find their position in market easily. I think a winning strategy should composite of three elements, innovation, domain know-how, and Electro-optics platform. Innovation is the key to competitive advantage. Domain know-how is the core to go deep and to differentiate for enterprises. As to Electro-optics platform, it would be a powerful tool to develop technology and product for startups and enterprises.

More than more

Taiwan has strong supply chain for silicon industry. Based on the accumulation of strength on both electronics and optics in Taiwan, the Electro-optics platform we proposed could derive many application for many fields, such as wearable, home, automobile, entertainment, medical treatment, and food. In semiconductor, there is a famous law to describe the progress for semiconductor process. It is Moore's law. Right now the barrier for mass production is 10nm. We could continue walking on technical path to overcome 10nm, 7nm, even 5nm. But there is a different path, application path. On this path, we could choose the branch for electronics, which continues to grow, or we could choose the branch for electro-optics. I also call it as “X-on silicon”. On this path, new elements, e.g. optics and material, are added into silicon industry. I think this could maximize the opportunities.

Technology Product Cycle

I was one co-founder of ACER Corp. I experienced many big changes for semiconductor. I am a witness to the revolution of computer. First was Mainframe, and then mini-computer. After mini-computer, PC came out. But now it is cell phone everyone has one. I think this is a typical technology product cycle and this cycle takes about 60 years. Mainframe is the step of B2B and B2G. Mini-computer is the step of B2B2commercial and PC is the step of B2B2consumer. Cell phone is the final step, B2consumer. US, EU and Japan have complete culture for these 4 steps but Taiwan entered this cycle from B2B2Consumer. As to China, it entered this cycle from B2Consumer. Now new trend appears, we have opportunities to run full cycle by introducing new elements without taking 60 years because the base is ready.

On Glass/On Silicon

Make a comparison for LCD (Liquid crystal on glass) and LCOS (Liquid crystal on silicon). LCD is capital intensive, and LCOS is technology centric. LCD is a mainstream industry, and LCOS is an emerging industry. However, LCOS could leverage the mature supply chain of LCD. Another difference between LCD and LCOS is their size. For example, typical TV is 55” right now, and cell phone is 5.5”. LCOS is 100 times smaller than TV and 10 times smaller than cell phone. LCOS has some advantages, including light, slim, short, small, speed. This could create imagination for talent people who have domain know-how.

X-on Silicon

Let’s talk about X-on silicon, I think X could be LC, microLED, OLED, or Polymer. For LC on silicon (LCOS), its applications could be classified into Display and Non-Display, or Amplitude modulation and Phase modulation. CGH-holography, near eye display, and projection are for Display. Digital optics, optical communication, holography data storage, and applied medical device are for Non-Display. The most interesting is about phase. A specific light at a point in space could be defined by its amplitude and phase. We always processed the amplitude of light only before. In fact, processing the phase of light could bring us more value. Many fantastic applications are about the phase of light. However, by the function of amplitude modulation and Phase modulation, the device was considered as “Spatial Light Modulator (SLM)”.

Electro-optics platform

About the Electro-optics platform we proposed, it is based on JDC technologies and services. JDC could provide hardware and software of LCOS, even including custom service, to partners for many fantastic applications. These applications are mainly about phase modulation for spatial light, such as WSS, optical computing, holography data storage, microscopy, beam shaping, optical tweezers, holographic HUD for automobile, digital grating, adaptive optics, and 3D manufacturing. As to Mini fab, it is a way to satisfy a special market for small volumes for very special and advanced need. We look for possible partners who have expertise to develop the corresponding recipe (LC recipe or other material). Combine with their recipe, JDC’s backplane may fit the very special and advanced need. We welcome this kind of cooperation to turn into seeds of startups. By the complementary, a complete LCOS industry chain will be build up. We consider Mini fab as the bridge which connects supply side and demand side. Not only to deepen the technologies, but also to expand the industry of light. In Taiwan, one alliance named “Things On Silicon Alliance” was established to support X-on silicon ECO-system. Its main functions includes education, market development, Infrastructure (Mini fab), and promotion for vertical application.

Enabling Disruptive Technology

In fact, there are many companies integrated SLM or X-on silicon technology into their products already, especially bio-medical field. Recently, the topic is active to

integrate light technology into bio-medical technology. Indeed, many new products and technologies emerge by this kind of combination, so we are confident that our SLM would be able to bring more opportunities for light industry.

Education

We realized one detail that optical technology must be rooted in education to establish a solid foundation. Experiments and theory are the same important. Through experiments, students become more familiar with the principles of optics, and they may find more details during experiments. This would be a great help to technology and product development when they enter industries in the future. We think that the traditional optical experiment equipments are not enough. In the generation of hard-soft combination, a important concept about “dynamic optics” should be established. It means we could use software to control the light. That is why we must develop “Educational Kit (EDK)” for education field. Also a compact optical system, “cage system”, has been developed to coordinate with EDK. Combining with the cage system, we think our EDK will lead a big change for students who are not optical background originally. Because it simplifies the process of optical experiments and makes these experiments more easily set up to those students. This can make more people to understand optics and enter this field. So far, our EDK could perform 10 optical experiments. They are sorted into 3 topics. The first topic is “Fundamentals of SLM”. The second topic is “Wave optics”. The third topic is “Fourier Optics”. But it is not limited. Teachers could design their own experiments and then Implement them on EDK. We believe that a solid optical education and training system can provide the industry adequate engineering and R & D people. This is very important to the whole eco-system of light industry.

Conclusions

Taiwan's capital-intensive and technology-intensive industry is its advantage. The best example is TSMC. It creates a very competitive industry chain. On the way to “High-Tech High-Touch”, many opportunities will arise inevitably. Light technology would be the key to grasp the opportunity. Just as the proclaim of the UN, “Light-based technology is a major economic driver with potential to revolutionize the 21st century”. In the history of technology development of human, people experienced “Mechanics century” and “Electronics century”. However, the foundation constructed by Mechanics and Electronics is ready. Optics will stand on their shoulder and grow up.

Mr. Kenneth Tai *– Mr. Kenneth Tai is one of the luminaries in Taiwan high-tech industry. As the chairman of Jasper Display Corporation, he dedicated himself to the optical research centers and photonic technology enterprises around the world.*

As a key enabler for industries of light technology, Mr. Tai made lots of efforts in the process of Taiwan becoming top level of ICT industry, and played an important role of approaching vertical integration and horizontal cooperation to participate in the development of this area.

Mr. Tai was the Co-Founder of Acer Group in 1976. During 1993-1995, he was the Vice Chairman of UMAX in US. At present, he is the Chairman of Avant (NASDAQ: AVNT), 21 Viant Group Inc.(NASDAQ:VNET), D-Link Corp., ALEEES, Evest Corp.. He is also the Chairman of Richtek, InveStar Capital, Digitimes.

Tel.: *e- mail:*

Invited Speaker 14

Incoherent Fourier Digital Holography

Takanori NOMURA[1] and Kaho WATANABE[2]
[1)]Faculty of Systems Engineering, Wakayama University, 930 Sakaedani, Wakayama, 640-8510, Japan
E-mail: nom@sys.wakayama-u.ac.jp
[2)]Graduate School of Systems Engineering, Wakayama University, 930 Sakaedani, Wakayama, 640-8510, Japan

1.Introduction

Incoherent digital holography as well as coherent digital holography is a technique to retrieve phase and am- plitude of an object. The possibility of incoherent digital holography has been widely studied. One of the simple optical setup to record an incoherent digital hologram is a rotational shearing interferometer. We have proposed the method to record a Fourier digital hologram of a spatially incoherent object using a rotational in- terferometer 1). The hologram is essentially obtained as the figure of cosine transformation. This feature causes degradation of the reconstructed image quality due to the dc term and a conjugate image. For the improvement of the quality, to remove a conjugate image, dual channel rotational shearing interferometer with a phase-shifting wave plate has been introduced 2). It enables us to realize phase-shifting with a help of polarization. Some experimental results are given to demonstrate the method.

2.Principle of recording incoherent Fourier digital hologram

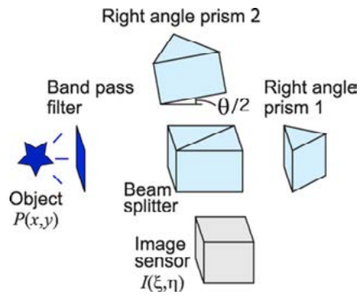

Fig.1 A rotational shearing interferometer to record incoherent Fourier digital hologram

Referring to Fig. 1, the proposed method is briefly reviewed. The right angle prism 2 is slightly rotated at an angle θ/2 around the optical axis of the interferometer. The incoherent lightwave from an object passes through a band pass filter to be set temporally coherent. The lightwave is separated by a beam splitter, and one is rotated at an angle of θ by the right angle prism 2. The other is reflected by a right angle prism 1. The hologram, of interference field intensity I(ξ, η) is given by

$$I(\xi,\eta)=\frac{1}{2}\iint_{-\infty}^{\infty}P(x,y)dxdy+\frac{1}{2}\iint_{-\infty}^{\infty}P(x,y)\cos\left[k\frac{2\sin\theta}{z_0}(-x\eta+y\xi)+k\Delta z\right]dxdy, \quad (1)$$

where P(x, y), k, z0, and Δz denote the brightness distribution of an object, the wavenumber, a harmonic mean of the distances of two optical paths, and a difference of them, respectively. For Δz = 0, we obtain the cosine transform of a brightness distribution of an object P(x, y). On the other hand, the sine transform is obtained for Δz = −λ/4. Here, λ denotes the wavelength. The cosine and sine transforms are equal to the real and imaginary parts of the Fourier transform, respectively.

To obtain both transforms simultaneously, we have proposed a dual channel rotational shearing interferometer 2). By introduction of polarization and a wave-plate, we have realized phase-shifting without any mechanical movements.

3.Experimental results

To demonstrate the proposed method, a preliminary optical experiment was performed. The optical setup was the same as shown in Fig. 1. A Chinese character shown in Fig. 2 displayed on the liquid crystal display with a blue backlight was used as an incoherent object. Its central wavelength was 448 nm with 10.0 nm full width at half maximum by contribution of the band pass filter. After recording a digital hologram, we reconstructed the recorded hologram numerically. The reconstructed image was shown in Fig. 3. You can see the object rotated by 90 degree with its conjugate and the dc. The rotation can be explained by Eq. (1). The reason is that the argument of cosine is not (xξ + yη) but (−xη + yξ).

Fig.2. A spatially incoherent object displayed on a liquid crystal display with a blue backlight.

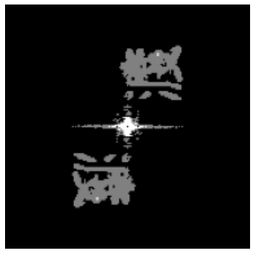

Fig.3. The numerical reconstructed image of the incoherent object

If we introduce an eighth wave plate between a right angle prism and a beam splitter in one arm of the interferometer, we can obtain sine transform of the object. This remove twin image of the reconstruction. In the workshop, more experimental demonstrations including a dual channel rotational interferometer will be given.

4.Conclusion

Incoherent Fourier digital holography based on a rotational interferometer was presented including an experi- mental demonstration. More application of this method can be found in the literatures[3–5]).

References:

[1] K. Watanabe, et al., IWH 2014 technical digest 16c03 (2014).
[2] K. Watanabe, et al., Appl. Opt. 54, A18 (2015).
[3] K. Watanabe, et al., Proc. SPIE. 9659, 96590D (2015).
[4] K. Watanabe, et al., Proc. SPIE. 9598, 95980D (2015).
[5] K. Watanabe, et al., Proc. SPIE. 9867, 986711 (2016).

Invited Speaker 15

Depth of Field Multiplexing Microscopy by Multi-Focus Holographic Lens

Ce Lee, You lan Li, Yu-Fan Cheng, Chia-Ling Tsao, Wun-Cherg Ding and Hui-Chi Chen
Department of Physics, Fu Jen Catholic University, 510 Zhongzheng Rd, Xinzhuang Dist., New Taipei City, 24205, Taiwan

1.Introduction

Traditional microscopy image the differenet depth of field within the sample by moving the axial position of the objective or sample. By combining the computer generated holography1, a multi-focus hologaphic lens2 was input to the microscopy system and image multiple sections onto the same detection plane3. To simulate a single hologram but with multiple foci, we used four methods to synthesize the multi-focus holographic lens. The comparisons of the optical results for the four method were discussed. Then, the liquid crystal display was used to be the spatial light modulator (SLM) and be input the phase-only hologram to the depth of field microcopy. The optical results of multiple-section images within the sample were also shown of this summary.

2.Theory and system setup

The depth of field multiplexing microscopy was shown as Fig.1, the laser light was expanded and illuminated on the sample area by a 4-f optical system and objective. A rotating diffuser was added to destroy the laser coherence. The fourier transform of sample image were projected on LCD by an objective and a 4-f system. A multi-focus holographic lens was display on the LCD. Then a CCD was placed on the focal plane of L5, to detect the multiple images at the different depth of the field from the sample area. The phase distribution of the lens is

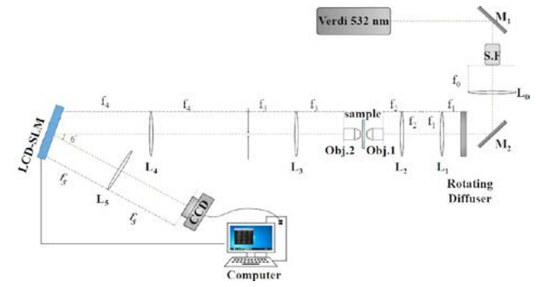

Fig. 1.

(1) $$L(x,y) = e^{\frac{-j\pi[(x-x_s)^2+(y-y_s)^2]}{\lambda f_s}}$$

where fs is the focus length, and (xs,ys) is the center location of the off-axis lens. To design the image from the depths of field Δz within the sample can be detect on the CCD, the focal length is

$$f_s = -M\frac{f_{obj.}^2}{\Delta z}$$

where M is the magnification of the optical system and fobj is the focal length of the objective. Moreover, the multiple images were arranged at the different location. The relations between the image location (xr,yr) on the CCD plane and the center location (xs,ys) of lens are $x_r = -\frac{f_5}{f_s}x_s \quad y_r = -\frac{f_5}{f_s}y_s$.

Of this summary, four methods were used to gnenrate the N-foci holographic lens. Area-partition method divides the LCD area to N parts for each holographic lens. Phase-adding method sum up the phase of the same pixel from each lens. Pixel-partition method is similar to the area-partition but unit in pixel. For example, Fig. 1 divide the LCD area to small parts each of 3×2 pixels for N=3×2 lens , the phase of each pixel is taken from the same pixel of each lens. Moreover, random methods simulate a random matrix of value r=1~N, then for each pixel take the phase from the rth lens.

3. Experimental results

We tested the multi-focus holographic lens of different N. The optical results of N=25 foci were shown as Fig. 2. Area-partition and phase-adding method show the higher intensity, however with the interference patterns between the lens. Furthermore, the interference of area-partition method overlap with the foci area, which increase the SN ratio. Moreover, the area-partition results show the larger focal spot than other methods, which is from the diffraction of the divided area. The results of the foci for the pixel-partition and random method show better focusing profile. However, when the number N of the lens increase to over 81, the result shows the pixel-partition method cann't generate the focal points. Therefore, the phase adding method was applied to produce the multi-focus holographics lens for the depth of field multiplexing microscopy. The deposion of 5μm polystyrene particle were used to verified the system performance. The 12-foci off-axis holographic lens was simulated by MATLAB. The optical images on the planes at the different depth of the field within the sample were shown as Fig.3.

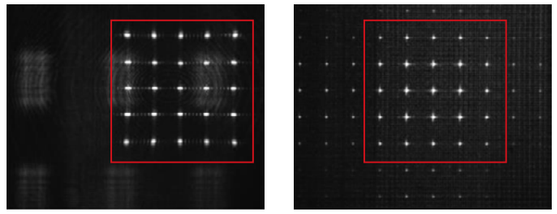

(a) Area-partition method

(b) Phase-adding method

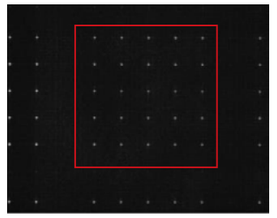

(c) Pixel-partition method

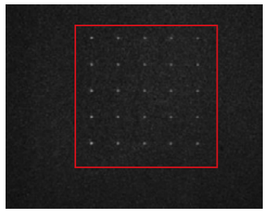

(d) Random method

Fig. 2.

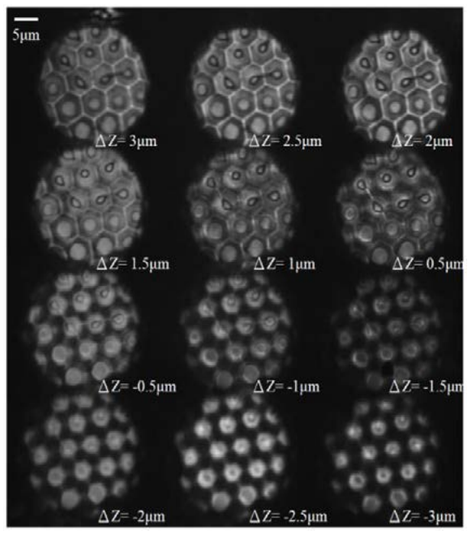

Fig. 3.

4.Conclusion

The results of four methods to produce the multi-focus holographic lens show, the phase-adding method has higher diffraction efficiency and random method has better focusing profile. Then the phase-adding method were applied to depth of field multiplexing microscopy, and the 12-section images within the sample were shown.

Reference:

[1] B. R. Brown, and A. W. Lohmann, IBM J. Res. Dev., 13, 160-168, 1969.
[2] C. Maurer, S. Khan, S. Fassl, S. Bernet, and M. Ritsch-Marte, Opt. Exp., 18, 3023-3034, 2010.
[3] C. Le, Master thesis, Fu Jen Catholic University, 2015.

Invited Speaker 16

Focus error signal obtained at the far-field from a rotational disc and measurement of its positional dependency

Akira Takagi, Takahiro Ishisaka, Satoshi Maruyama and Teruo Fujita
Department of Electrical and Electronics Engineering, Fukui University of Technology, 3-6-1 Gakuen, Fukui 910-8505, Japan

1.Introduction

Holographic data storage system (HDSS) has been studied as one of next-generation optical data storages to realize higher recording density and data transfer rate. Especially colinear HDSS1) can be promising one because of its optical stability and recording density. To realize a practical HDSS like a DVD-R recorder, controlling focal and radial positions of signal and reference beams should be necessary because the discs are exchanged in the optical disc jukeboxes. At ISOM'08 we proposed a new focus sensing method using the interference of far-field diffracted waves generated by embedded one-dimensional periodical structure in a disc2), which features no additional optics for those error signals' generation as well as non dependency of the irradiation beam's non-uniformity on the focus error signal. As the simulation showed expected results, building up an experiment system with bench optics, analog/digital processing circuits and a disc embedded one-dimensional grating followed to ensure its effectiveness experimentally3).

In this paper we brief the principle of this focus sensing method, explain a developed experiment system, and show the focus error signal (FES) obtained from a rotational disc. Also we report FES' dependence on the tangential position of a two element photo-detector (PD) located at the far-field.

2.Principle of the focus error generation

There are areas where the 0th and ±1st order diffracted beams are superimposed on the pupil of the objectives of optical heads for CD and DVD. When the focused spot crosses the grooves of those discs, the optical intensity distribution of those areas changes. If only defocus exists in the irradiation beam, moving linear fringes appear in those areas and its spatial frequency depends on the amount of defocus. Our system uses a two element PD located in the area and samples the intensity variation periodically (constant time period corresponding to $\pi/2$ phase shift of the PD signals). When the PD center in the tangential direction is x1 on the output pupil of the objective lens, detected intensity from PD element 1 and 2 (D1 and D2) are expressed as

$$I_{D1,D2} = I_{01,02} + I_{11,12}\cos\left[\beta_1 + \delta + 2\pi W_{20}\left\{-\frac{2}{q}\left(x_1 \mp \frac{\Delta}{2}\right) + \frac{1}{q^2}\right\}\right], \quad (1)$$

$$I_{DF} = I_{D1} - I_{D2}, \quad I_{SUM} = I_{D1} + I_{D2}, \quad (2)$$

where ID1, ID2 are the outputs of the two element PD, W20 is a defocus wavefront aberration, β1 is the initial phase, δ is the normalized lateral shift, q is the normalized groove pitch, Δ is the normalized spacing of the two PD elements' center so that the PD element's centers are expressed as x1- Δ/2 and x1+ Δ/2 respectively. Also I01,02 are the DC components and I11,12 are the modulation amplitudes. Then, from the difference/sum signals IDF, ISUM, we are able to obtain the FES as follows (FESb shows an opposite DC offset of FESa) ;

$$FESa = \left\{I_{DF}\left(-\frac{\pi}{2}\right) + I_{DF}(0)\right\}\cdot\left\{I_{SUM}\left(-\frac{\pi}{2}\right) - I_{SUM}(0)\right\} + \left\{I_{DF}(0) + I_{DF}\left(\frac{\pi}{2}\right)\right\}\cdot\left\{I_{SUM}(0) - I_{SUM}\left(\frac{\pi}{2}\right)\right\},$$

$$FESb = \left\{I_{DF}\left(\frac{\pi}{2}\right) + I_{DF}(\pi)\right\}\cdot\left\{I_{SUM}\left(\frac{\pi}{2}\right) - I_{SUM}(\pi)\right\} + \left\{I_{DF}(\pi) + I_{DF}\left(-\frac{\pi}{2}\right)\right\}\cdot\left\{I_{SUM}(\pi) - I_{SUM}\left(-\frac{\pi}{2}\right)\right\},$$

$$FES = FESa + FESb,$$

where $I_{DF}(\alpha)$ means the value of I_{DF} at $\delta = \alpha$.

3. Experiments

Figure 1 shows our experiment system we have been developing to verify the dynamic operation of this focus sensing method. First we prepared an optical disc with one-dimensional structure grooved in the radial direction (180,000 grooves/rotation ; groove pitch = 1.3 μm at r = 37 mm so that the 1st order is shifted by the radius of the beam) using a Compact Disc production process, and it was set on a turn table for SP/LP discs. When the disc rotates at 78 rpm (1.3 rps), the frequency of a groove crossing signal becomes 234kHz. To obtain sampling pulses, we use the stroboscopic pattern (160/rotation) caved on the outside perimeter of the rotation table. A He-Ne Laser beam irradiates this pattern so that the reflected light frequency is modulated at 208Hz. Then a Phase Lock Loop (PLL) circuit, which was composed of a digital VCO and MaxII CPLD, multiplies this signal by 4,500 for getting the sampling pulse whose frequency is 234KHz x 4 = 936kHz. The defocus fringes on the exit plane of the objective lens (NA=0.53) are projected onto the two-element PD through a macro lens with equal magnification. The PD width in the tangential direction is 155μm (width of 1 element) x 2 + 27μm (space between elements) = 337μm and the beam diameter is 4mm. ID1 and ID2 from the PD are sampled simultaneously at the rate of 936 kS/sec with two A/D converters and then 16 values of ID1 (ID2) which correspond to 4 periods, are transferred to a TI's DSP. The DSP averages those data to reduce the noise and calculates FES. Finally the FES is put out from a D/A converter with a period of around 17 μsec. We acquired well-shaped FES curves twice per one disc rotation due to the disc vertical vibration (Fig.2).

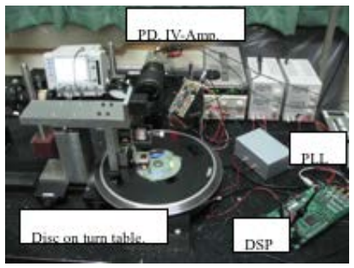

Fig. 1. Experimental setup. Red (690nm) laser beam comes from the left side, is reflected down by 90 degree and focused on the grating surface in the disc. Reflected/diffracted beams by the disc go up and are conducted to the PD by a beam splitter and a macro lens behind it.

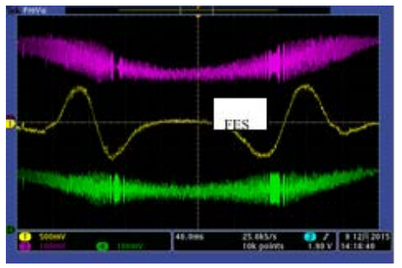

Fig. 2. obtained FES (yellow line in the middle) and input signals (upper and lower lines, proportional to ID1 and ID2). Horizontal grey line indicates a reference level for the FES, and the input signals are shifted up and down just not to be superimposed each other.

Next we evaluated the influence of the tangential location of the PD on the FES offset. In this experiment, PD was shifted ±300μm in the tangential direction from the best position (Fig.3(a)), where the offset was zero. The maximum offset case (around 1.5μm offset at -250μm PD shift) was shown in Fig.3(b). In these figures blue line is the modulated light intensity, and the distance

between a point of FES=0 and that of SUM=MAX gives the focus offset. Please note that the symmetry of the FES curves was not lost according to the PD position shift. As our simulation including the third order spherical/coma aberration had predicted such small offset4), residual aberrations of the diffraction-limited optics' components seem to cause this offset.

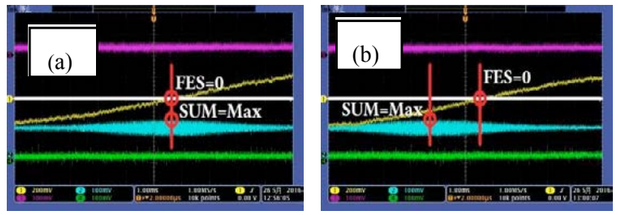

Fig.2. Focus offset dependency on the PD position, left: best position, right: shifted position by -250μm.

between a point of FES=0 and that of SUM=MAX gives the focus offset. Please note that the symmetry of the FES curves was not lost according to the PD position shift. As our simulation including the third order spherical/coma aberration had predicted such small offset4), residual aberrations of the diffraction-limited optics' components seem to cause this offset.

4.Summary

Focus offset of the FES generated by interference fringes at the far-field was verified by an actual optics and electronics system. A position where the offset became zero was confirmed, and small offset's dependence on the PD position was observed. Also FES curves' symmetry was not affected by the PD position.

Reference:

[1] H.Horimai et al. : Appl. Opt. 44, p.2575 (2005).
[2] T.Fujita and H.Horikoshi : Jpn.J.Appl.Phys. 48, 03A037 (2009).
[3] T.Sawada, A.Takagi and T.Fujita : ODF2016,1PDb-06 (2016).
[4] T.Fujita : Jpn.J.Appl.Phys.49, 08KD08 (2010).

Acknowledgment This work was supported by JSPS KAKENHI Grant Number JP15K06040

Invited Speaker 17

Holographic fluorescence mapping using space-division matching method

Ryosuke Abe and Yoshio Hayasaki
Center for Optical Research and Education (CORE), Utsunomiya University 7-1-2 Yoto, Utsunomiya 321-8585, Japan

1.Introduction

Fluorescence microscope is a well-known important tool in biology for visualizing the locations of biological molecules and fluorescence nanomaterials. Chemical reactions in life processes are localized in three-dimensions in contrast to those that take place in test tubes. Therefore, to understand the spatiotemporal dynamics of biological chemical reactions, the three-dimensional (3D) mapping of fluorescence light sources is indispensable for analyzing the biological phenomena. It is well known that one of the excellent tools for the 3D imaging of fluorescence was a laser confocal scanning microscope with the laser beam scanning mechanism.

A fluorescence digital holography [1-4] is another powerful tool for imaging a fluorescence object [5-9]. The optical arrangement is based on self-interference and there are some kinds of optical arrangements of self-interference digital holography [10-15]. The most excellent advantage is to obtain 3D image from a small number of image capturing without a laser scanning and a sample movement. We firstly demonstrated the 3D mapping of fluorescence sources using the fluorescence digital holography [16]. In the research, the position of the fluorescence source was measured by searching the peak intensity in the reconstructed images of a hologram, therefore it was difficult to measure many fluorescence sources.

In this paper, we demonstrate the space division matching method for measuring positions of densely-spread fluorescence nanoparticles under the framework of the fluorescence digital holography. The method is based on the spatial division of the reconstruction space and the search of a fluorescence source in each divided space.

2.Experimental setup

Figure 1 shows the experimental setup composed of a fluorescence digital holographic microscope and optical tweezers. In the fluorescence digital holographic microscope, excitation light was irradiated to a sample from an ultraviolet light emitting diode (UV-LED). The fluorescence was given to self-interferometer composed of two concave mirrors with the focal lengths of 400 and 500 mm for the axial shearing and the interference image was imaged on an electron-multiplying charge-coupled device image sensor. The hologram was obtained with the phase-shifting method and the diffraction was performed by the angular spectrum method. In the optical tweezers, the beam from a Yb-fiber laser with a

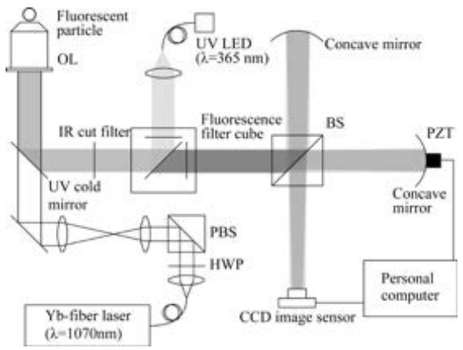

Fig. 1. Experimental setup. PBS; polarized beam splitter, HWP, half-wave plate; BS, beam splitter; OL, objective lens; PZT, piezoelectric transducer

wavelength of λ = 1070 nm was collimated and focused in a sample solution using a 60× oil-immersion microscope objective lens (OL) with a numerical aperture of NA = 1.25. The sample was fluorescence nanoparticles with a diameter of 500 nm fixed in gelatin.

3.Space-division matching method

The space-division matching method to measure 3D position of many fluorescence sources was proposed.

The procedure is performed by 3 steps as follows. Step 1: The whole observation space shown in Fig. 2(a) was equally divided to the search subspace shown in Fig. 2(b). Step 2: The peak fluorescence point was searched in the search subspace. Step 3: The measurement subspace put the point having the strongest fluorescence intensity on the center is made for each fluorescence source, as shown in Fig. 2(c). In the measurement subspace, the 3D positions of fluorescence sources was decided by the Gaussian fitting.

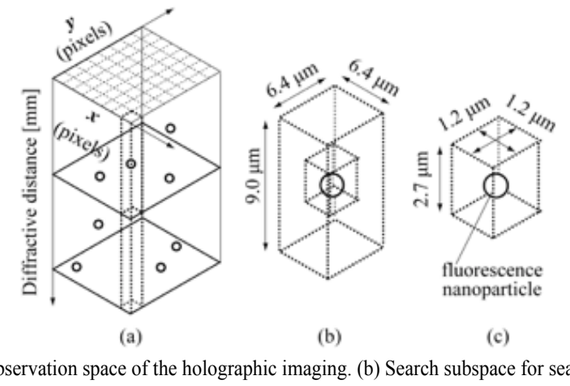

Fig. 2. (a) Whole observation space of the holographic imaging. (b) Search subspace for searching the strongest fluorescence light source. (c) Measurement subspace for detecting the 3D position.

4.Experiment results

Figure 3 shows the 3D mapping of the fluorescence nanoparticles. By using the space division matching method, the 12 fluorescence nanoparticles were searched. The mapping was obtained in the area with the radius of ~30 μm, because the fluorescence lights reflected from two concave mirrors with difference focal lengths were laterally deviated in the outside of this area.

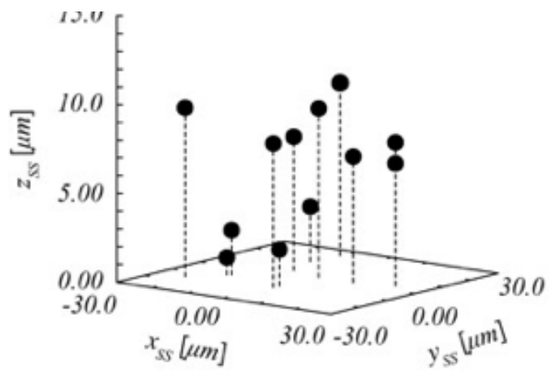

Fig. 3. Mapping of fluorescence point sources

FThe fluorescence lights from nanoparticles located around the focus plane had no interference according to the above same reason.

5.Conclusion

We demonstrated the quantitative 3D mapping of fluorescence nanoparticles using the space-division matching method. The method performed the 3D position measurement of many fluorescence nanoparticles. The measured area had cylindrical structure with the radius of ~30 μm.

References:

[1] A. S. Marathay, J. Opt. Soc. Am. A 4, 1861 (1987).
[2] E. Ribak, C. Roddier, F. Roddier, and J. B. Breckinridge, Appl. Opt. 27, 1183 (1988)
[3] S.-G. Kim, B. Lee, and E.-S. Kim, Appl. Opt. 36, 4784 (1997)
[4] J. Rosen and G. Brooker, Opt. Lett. 32, 912 (2007)
[5] B. W. Schilling, T.-C. Poon, G. Indebetouw, B. Storrie, K. Shinoda, Y. Suzuki, and M. H. Wu, Opt. Lett. 22, 1506 (1997).
[6] J. Rosen and G. Brooker, Opt. Express 15, 2244 (2007).
[7] J. Rosen and G. Brooker, Nat. Photonics 2, 190 (2008).
[8] N. Siegel, J. Rosen, and G. Brooker, Opt. Express 20, 19822 (2012).
[9] C. Jang, D. C. Clark, J. Kim, B. Lee, and M. K. Kim, Biomed. Opt. Express 7, 1271 (2016).
[10] D. Fu, S. Oh, W. Choi, T. Yamauchi, A. Dorn, Z. Yaqoob, R. R. Dasari, and M. S. Feld, Opt Lett. 35, 2370 (2010).
[11] G. Pedrini, H. Li, A. Faridian, and W. Osten, Opt. Lett. 37, 713 (2012).
[12] M. K. Kim, Opt. Lett. 37, 2694 (2012).
[13] D. N. Naik, G. Pedrini, and W. Osten, Opt. Express 21, 3990–3995 (2013).
[14] J. Hong and M. K. Kim, Opt. Lett. 38, 5196 (2013).
[15] M. K. Kim, Opt. Express 21, 9636 (2013).
[16] T. Yanagawa, R. Abe, and Y. Hayasaki, Opt. Lett. 40, 3312 (2015).
[17] A. Ashkin, J. M. Dziedzic, J. E. Bjorkholm, and S. Chu, Opt. Lett. 11, 288 (1986).
[18] T. Higuchi, Q. D. Pham, S. Hasegawa, and Y. Hayasaki, Appl. Opt. 50, H183 (2011).
[19] Y. Hayasaki and A. Sato, Opt. Commun. 322, 22 (2014)
[20] K. Goto, Y. Hayasaki, Opt. Lett. 40, 3344 (2015)
[21] J. W. Goodman, Introduction to Fourier Optics, 3nd ed. (McGraw-Hill, 1996), Chap. 3. 10.

Invited Speaker 18

Simplified modal method for deep-etched fused silica gratings

Changhe Zhou, Shubin Li, Changcheng Xiang, Yunkai Lu
Information Optics & Optoelectronics Lab, Shanghai Institute of Optics and Fine Mechanics, China
chazhou@mail.shcnc.ac.cn

1.Introduction

Simplified modal method is a theory to describe the modes inside a grating, particular a fused silica grating, which can vividly illustrate how a few modes are enough to determine the diffraction of different orders of a grating when its period is close to wavelength of light. It should be noted that simplified modal method is different from the well-known Rigorous Coupled Wave Algorithm (RCWA). The RCWA is a Fourier-mode method, whose coefficients are determined by matching the boundary condition of a grating, so RCWA is an essential numerical method.

The simplified modal method means a few lowest modes(usually two lowest modes) are used for analysis of deep-etched fused silica grating, it doesn't means that it is a scale method, in fact, the simplified modal method is a rigorous method, it comes from Maxwell equation, the modes are calculated from the eigenfunction, different from Fourier expansions used by RCWA, as shown in Fig.1. The lowest modes usually have the interesting property of even or odd symmetries used in Bragg diffraction, while the Fourier coefficients used by RCWA have no such symmetry.

Since the diffraction orders of deep-etched fused silica grating are mainly determined by two lowest modes, so simplified analytic equations might be obtained, the difference between the two lowest modes could illustrate the polarization-dependent, polarization-independent, the spectral-band diffraction with the changing opening ratio and depth of deep-etched gratings, which is not possible to obtain with RCWA.

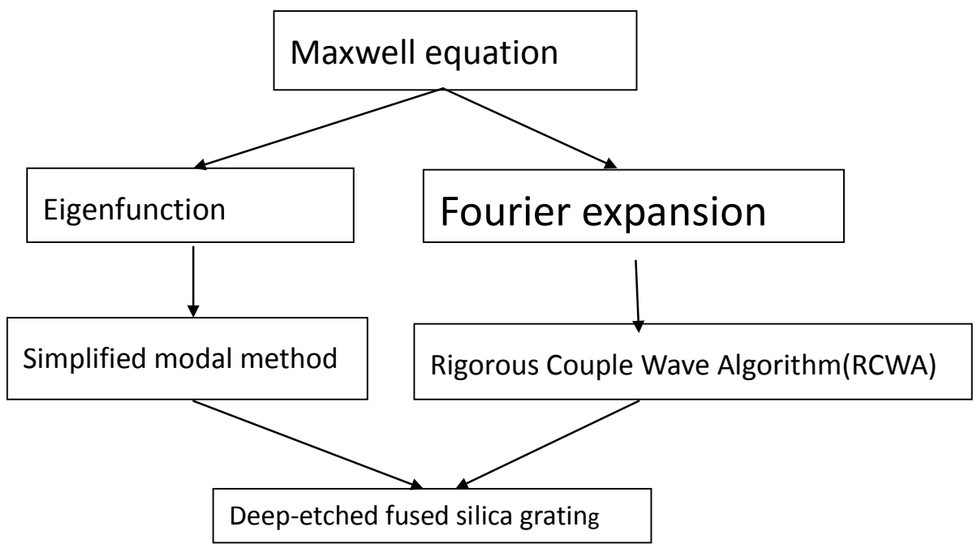

Fig. 1. Illustration of the equivalence of simplified modal method and RCWA for deep-etched grating.

2.Fused silica gratings

Deep-etched fused silica grating is a transmission grating with its depth and period optimized for a specific function[1,2]. There are basically two questions at the first glance, the first is what function a fused silica grating could behave; The second is how to fabricate such narrow and deep grooves.

Simplified modal method provides a convenient way to design the performance of a deep-etched fused silica grating. Fused silica gratings could function as a high-efficient grating, a 1×2 beam splitter, a 1×3 beam splitter, polarization-dependent, polarization-independent, and polarization-selective gratings, etc.

Fused silica is excellent optical material. So deep-etched fused silica grating has a wide transmission spectrum. Fused silica is hard, which is difficult to be etched intro optimized depth. We are using ICP facility to etch fused silica gratings. ICP means inductive-coupled plasma etching facility with different gases, such as CHF3, SF6, H2, O2, Ar, etc.. It should take a long-time to understand the etching characteristics of using the combination of these gases.

3.Applications

Simplified modal method is a powerful tool to analyze deep-etched silica grating. It could not only to predict the performance of deep-etched fused silica grating, but also, it could also be applied to volume grating, slanted grating, etc.. It is well-known that Kogelnik's coupled wave method is widely used for analysis of volume grating, it seems that simplified modal method might provide us a new view to analyse the inside physics of a volume grating[3]. Deep-etched fused silica grating could be widely used in beam combining of multiple laser beams, beam splitting from single beam into multiple laser beams,etc..

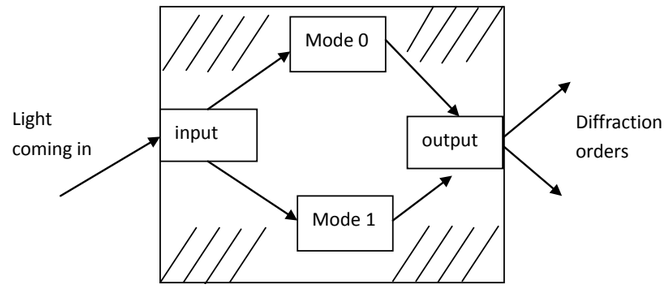

Fig. 2. Simplified modal method might provide a new view to see the inside physics of a traditional volume grating

Reference:

[1] J. Zheng, C. Zhou, B. Wang, and J. Feng, "Beam splitting of low-contrast binary gratings under the second Bragg angle incidence", JOSA A 25, 1075(2008).

[2] J. Feng, C. Zhou, J. Zheng and B. Wang, "Modal analysis of deep-etched low-contrast two-port beam splitter grating", Optics Communications 281,5298-5301(2008).

[3] S. Li, C. Zhou, Y. Lu, J. Wu, H. Cao, J. Yu, "Mode view of holographic grating", Journal of Optics, (accepted).

Invited Speaker 19

Pixelization Error Reduction Algorithm (PERA): Inverse Optimization Algorithms for Design of Diffractive Optical Elements

Wei-Feng Hsu* and Shih-Chih Lin

Department of Electro-optical Engineering, National Taipei University of Technology, Taipei 10608, Taiwan

* Correspondence: whsu@ntut.edu.tw

1.Introduction

Applications of diffractive optical elements (DOEs) or computer-generated holograms (CGHs) have considerably bloomed because of the advance of optical modulation techniques. Specifically, high-resolution spatial light modulators (SLMs) become user friendly in implementation of two- and three-dimensional imaging, optical communications, and biomedical applications. When a DOE is used to generate an image resembling a target image in a free-space optical system, it requires an optimization method to obtain a solution by minimizing the difference between the resultant image and the target image. Many optimization methods have been developed and applied to design of DOE, including Gerchberg-Saxton algorithm (GSA), iterative Fourier transform algorithm (IFTA), error diffusion method, direct search (DS) method, simulated annealing (SA) algorithm, generic algorithm (GA), and hybrid methods. No studies, however, have reported the influence of the determination of the difference between the resultant and the target image. In the presentation, we start with an introduction to a novel optimization algorithm, of which the alternatives can be related to several frequently-used optimization methods. These methods are briefly introduced and the comparisons are presented as well. In addition, the solution spaces of DOE parameters, determining the difference, are illustrated for their influences on the resultant DOE.

The solutions of DOE obtained in the optimizing processes are subject to the constraints in the optical element and the diffraction domains. The element constraint depends on the properties of the DOE, for examples, phase-only modulation, amplitude-only modulation, and a finite number of quantized phase levels. The constraint in the diffraction domain is typically the generation of an intensity distribution which approximates the target image. The two domains are connected by Fourier-transform based operations in free-space optical architectures. A direct method is consistent of the optimizing processes beginning with perturbations in the element domain, in which DOE pixels or element parameters are changed. The acceptance of the perturbation is determined on the difference between the resultant intensity distribution and the target image. The DS, SA, GA, and error diffusion approaches belong to the direct optimization method. The perturbation in the inverse method is generated in the diffraction domain in which the pixel values are changed in response to the perturbation setup and the element constraint. A typical inverse method is the IFTA in which the amplitude of the diffractive field is replaced by the squared root of the target image and the phase remains unchanged. Next, in the element domain, the element constrain is applied to the field transformed back from the diffraction domain. The updated field then transforms to the diffraction domain and conducts the diffraction constraint. The loop operations continue until evolution stagnates.

Generally speaking, the main advantage of the direct method is the quality of the resultant image generated by the DOEs, while effectiveness is the main advantage of the inverse method. As the number of pixels of DOE and target image increases to the order of millions, the advantages of these methods could no longer be held. For example, the searching for the global solution of DOE using an SA algorithm is too time-consuming to complete, and the signal-to-noise ratio of the resultant image of the DOE designed using an IFTA does not fulfill one's requirement. It is needed to develop the optimization method of DOE design that possesses the merits of the direct and inverse methods.

2.Pixelization error reduction algorithm (PERA)

The optimization approach presented here is originated from IFTA. The perturbation results from the change of a pixel in the diffraction domain. The change of the pixel value is deterministic since the target is a prior condition. The perturbed field transforms to the element domain, conducts the element constraint, and then transforms back to the diffraction domain. The double-transformed field is evaluated by calculating the performance parameters such as the root-mean-squared error, the signal-to-noise ratio, and the signal variation. When the performance is improved, the double-transformed field replaces the previous one. If not, the perturbation is discarded. Since the perturbation starts with the change of a pixel value, the proposed approach is called pixelization error reduction algorithm, and abbreviated to PERA. The comparisons of the DOEs using IFTA and PERA will be presented. The acceptance of a new state depends on the performance parameters, making this approach more flexible than the IFTA. The method of the selection of the perturbed pixel influences the resultant DOE which will be discussed in the presentation. The results are compared with the DS method. In addition, PERA can equip with a stochastic process which enables it to perform a search for the global solution, similar to the SA algorithm.

3.Solution space of DOE

Although the optimization methods gain most attention in design of DOE, the achievable performance of the resultant DOE and the diffractive image depends on the performance parameters used in the optimization operations. We will use a simple DOE, consisting three phase pixels, as an example to illustrate the solution spaces of the performance parameters of the DOE. The chosen performance parameters include the diffraction efficiency, the root-mean-squared error, and the signal-to-noise ratio. One example is shown in Fig. 1 for the phase-only DOE [ejφ1 ejφ2 ejφ3] and the target image [0.5 0.5 0]. According to the solution spaces, it is possible to understand the properties of the performance parameters, to determine the number of DOE solutions, and to select a cost function with a linear combination of the performance parameters. We will discuss some facts that we observed in these simulations and hope that they are helpful in the design of DOE.

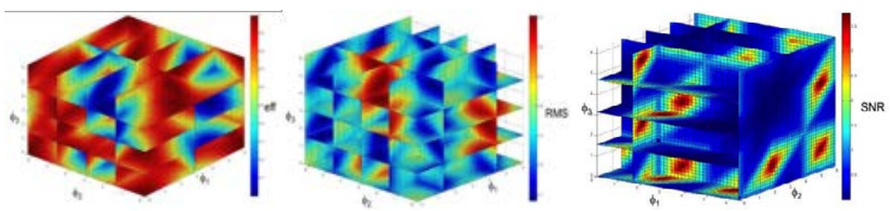

(a) (b) (c)

Fig. 1. Solution spaces of (a) the diffraction efficiency (eff), (b) the root-mean-squared error (RMSE), and (c) the signal-to-noise ratio (SNR) of a phase-only three-element DOE [ejφ1 ejφ2 ejφ3] to generate the diffractive image for the target [0.5 0.5 0]. The number of extreme values in the space of diffraction efficiency is two, the same as the number of signal pixels in the target image. The number of extreme values in the spaces of the RMSE and the SNR are three, identical to the number of the saddle points in the space of diffraction efficiency.

Invited Speaker 20

Displacement measurement with multiple holographic grating

Cheng-Chih Hsu[1*], Hang Chen[2], Chia-Wei Chiang[1], and You-Wei Chang[1]

[1)]Department of Photonics Engineering, Yuan Ze University, 135, Yuan-Tung Road, Chung-Li, 32003 Taiwan

[2)]Center of Ultra-precision Optoelectronic Instrument, Harbin Institute of Technology, Harbin 150080, China

E-mail: cchsu@saturn.yzu.edu.tw

1.Introduction

To achieve high resolution positioning, the displacement measuring methods [1-4] become more important and have attracted great attention over the past two decades, especially applied these techniques in nano-positioning systems such as semiconductor manufacture facilities, nano-handling, nano-manipulating and nanofabricating equipment. Grating interferometry is one of the most efficient methods of the displacement measurement. In such measurement method, the grating pitch is a critical issue, which affected to the sensitivity and resolution of the measurement. Small grating pitch provides high sensitivity; therefore, the grating pitch needs to be on a micron scale or lower [4]. In this study, we proposed a method for displacement measurement which integrated three gratings with two different grating pitches. Based on the arrangement of the measurement system, the effective grating pitches can be decreased 25% and down to 0.4 μm. The sensitivity enhancement can be reached 40%.

2.Experiment

Figure 1 showed the optical configuration of the proposed method. Obviously, the interference signal of path 1 was resulted from ±1 diffracted beam of the grating G1. Meanwhile, the interference signal of the path 2 was resulted from ±2 diffracted beam of the grating G1 and ±1 diffracted beam of the grating G2 and G3. Therefore, the effective grating pitches of the path 1 and path 2 can be measured and indicated in Fig. 2. Figure 3 showed that the round-trip displacement measurement obtained from these interference signals coming from paths 1 and 2. There was no significant difference between the measurement results coming from path 1 and HP interferometer. But there was a few sub-micrometer difference between the measurement results coming from path 2 and HP interferometer. The difference might come from the misalignment of gratings. We also demonstrated long-travel distance measurement and showed in Fig. 4. Figure 4(a) showed the results obtained from path 1 and the displacement was approximated of 100 μm. Figure 4(b) showed the results obtained from path 2 and the displacement was approximated of 1 mm. The results showed that no significant difference between the proposed method and comparison method.

3.Conclusion

In this paper, we demonstrated a method could reduce the effective grating pitch by using multiple holographic grating with suitable optical configuration. The results showed that the effective grating pitch could be approximated of 0.4 μm and the sensitivity would be enhanced 40% by theoretical prediction. We also demonstrated the round-trip and long-travel displacement measurements. The results showed good comparison between proposed method and HP interferometer.

Reference:

[1] W. J. Wu, C. K. Lee, C. T. Hsieh, Jpn. J. Appl. Phys. 38 (1999) 1725.

[2] C. W. Wu, Appl. Opt. 43 (2004) 3812.

[3] C. C. Wu, C. C. Hsu, J. Y. Lee, Y. Z. Chen, Opt. Express. 21 (2013) 13322.

[4] C. C. Hsu, C. C. Wu, J. Y. Lee, H. Y. Chen, Opt. Commun. 281 (2008) 2583.

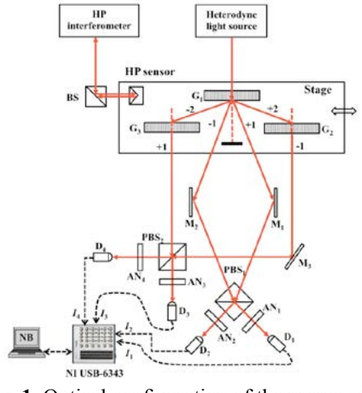

Fig. 1. Optical configuration of the proposed method

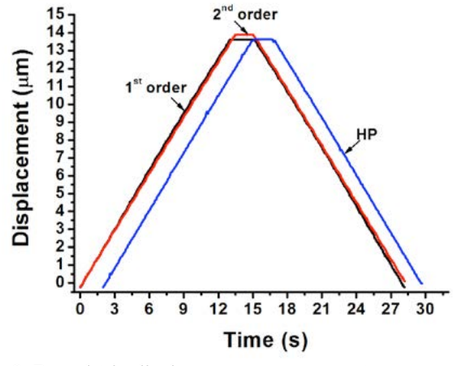

Fig. 3. Round-trip displacement measurement

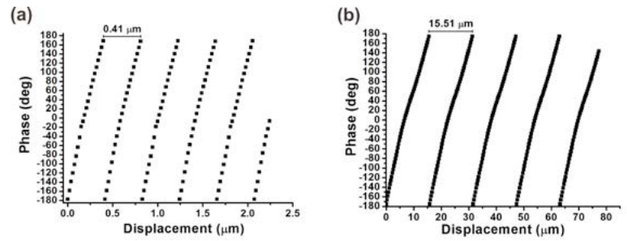

Fig. 2. Effective grating pitch measurement. (a) Path 1, (b) Path 2.

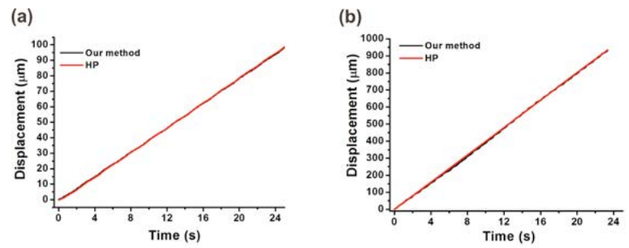

Fig. 4.ELong travel distance measurement. (a) Path 1, (b) Path 2.

Invited Speaker 21

Polarization-Selective Substrate-Mode Volume Holograms and Its Applications

Jing-Heng Chen[1)], Fan-Hsi Hsu[2)], Tai-Nan Guo[1)], Chien-Yuan Han[3)], Kun-Huang Chen[4)] and Ken-Yuh Hsu[2)]

[1)]Department of Photonics, Feng Chia University, 100 Wenhwa Road, Seatwen, Taichung 40724, Taiwan

[2)]Department of Photonics and Institute of Electro-Optical Engineering, National Chiao-Tung University, 1001 University Road, Hsinchu 30010, Taiwan

[3)]Department of Electro-Optical Engineering, National United University, 2, Lienda, Miaoli 36063,Taiwan

[4)] Department of Electrical Engineering, Feng Chia University, 100 Wenhwa Road, Seatwen, Taichung 40724, Taiwan

1.Introduction

Polarization-selective elements capable of splitting an optical beam into two orthogonally polarized beams play an important role in different kinds of optical systems such as optical sensing, optical data storage, imaging system, switching network, wavelength division multiplexing (WDM), and optical circulator. In different applications these elements are called as polarization beam splitter (PBS), spatial walk-off polarizer (SWP), or polarizing mirror. Presently several kinds of method and technique have been proposed to implement this function such as substrate-mode hologram, optical multi-layer coating, birefringent crystal, and micromachined integrated optic. In spite of the mature techniques, the elements fabricated with multi-layer coating, birefringent crystal, and micromachined integrated optic have drawbacks of complex fabrication processes and high cost. Especially, the crystal-type element is hard to fulfill the demand of compactness. Though, the conventional polarization-selective substrate-mode holographic elements have many advantages [1-2]. Its feasibility is usually limited by the finite refractive index modulation strength of a recording material. The common solution is to increase the thickness of the recording material in order to compensate the shortage of the refractive index modulation strength, in the phase modulation term. However, under the thickness condition of thick material, the distortion effect of interference fringe is worsened. An ideal holographic recording condition hinges on the thin thickness of a recording material with a high refractive index modulation strength. Actually these cannot be completed in both respects. Therefore, in this study we devoted to overcome the problems in fabrication of holographic optical elements and its applications. Based on the coupled-wave theory and the structure of substrate-mode holograms, a special design of polarization-selective substrate-mode volume holograms (PSVHs) and its recording method are proposed at a relatively large splitting angle near 90°. With this design, we need only a low refractive index modulation strength, which can be easily achieved with common recording materials. In addition, this design is applied to the generating of radially polarized beam which should bear all merits of conventional substrate-mode holographic elements such as compactness, plane structure, easily light collimation, easily fabrication, and low cost.

2.Experimental Results

A holographic radial polarizer was fabricated based on the coupled-wave theory [3] and the geometric structure of substrate-mode volume hologram. To show the feasibility of the method, a holographic radial polarizer was fabricated with C-RT20 photopolymer recording material. The prism-hologram-prism sandwiched recording setup was applied, as shown in Fig. 1. The diffraction efficiencies and the intensity distributions of generated radially polarized beam are shown in Fig. 2. The diffraction efficiencies ηs and ηp were 89% and 23.4% for at 443nm, respectively.

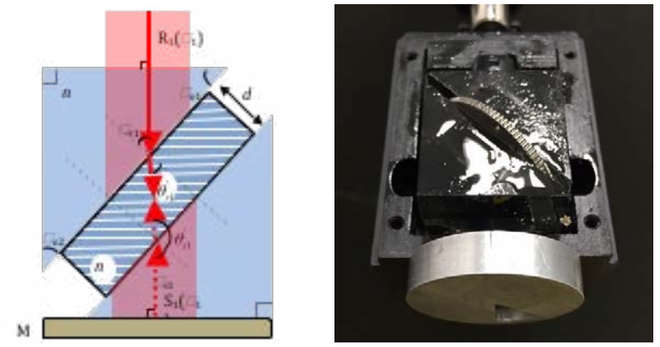

Fig. 1. Prism-hologram-prism sandwiched recording setup.

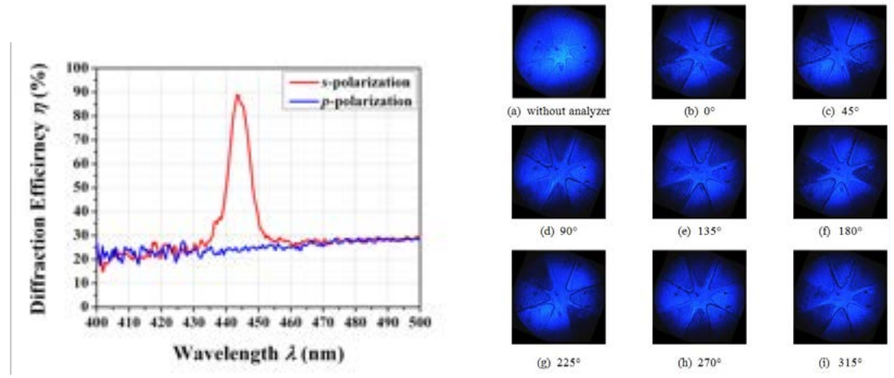

Fig. 2. (a) Diffraction efficiencies of PSVH and (b) intensity distributions of a radially polarized beam with and without an analyzer.

3.Conclusion

The research proposed a design of polarization-selective substrate-mode volume holograms and its application to radial polarizers. The proposed recording method belongs to a technique of longer wavelength construction for shorter wavelength reconstruction which can effectively solve the problems in conventional recording method. The holographic radial polarizer has considerable potential in application of radially polarized beams

Reference:

[1] Y. T. Huang and Y. H. Chen, “Polarization-selective elements with a substrate-mode grating pair structure,” Opt. Lett. 18, 921-923 (1993).

[2] Y. T. Huang, “Polarizing-selective volume holograms: general design,” Appl. Opt. 33, 2115-2120 (1994).

[3] H. Kogelnik, “Coupled wave theory for thick hologram gratings,” Bell Syst. Tech. J. 48, 2909-2947 (1969).

Invited Speaker 22

Differential Equations for Volume Hologram with Coordinate Conversion

Daisuke Barada[1,2] and Toyohiko Yatagai[2]

[1]Graduate School of Engineering, Utsunomiya University, 7-1-2 Yoto, Utsunomiya, Tochigi 321-8585, Japan

[2]Center for Optical Research and Education (CORE), Utsunomiya University, 7-1-2 Yoto, Utsunomiya, Tochigi 321-8585, Japan

1.Introduction

It is well-known that volume holograms are useful for diffractive optical elements, three-dimensional displays, and optical data storage with high data capacity. In theoretical analysis and numerical simulation for volume holograms, Kogelnik's coupled wave theory1) in general. However, a reconstructed beam is limited by the first order diffracted beam and polarization dependence is neglected in the theory because some approximation is used. In this study, a rigorous diffraction theory, in which polarization dependence is considerable, is proposed.

2.Theory

Maxwell's equations in the case of monochromatic light in Cartesian coordinate is represented by

$$\nabla \times \boldsymbol{E} = \mathrm{i}\omega\mu_0 \boldsymbol{H}, \tag{1}$$

$$\nabla \times \boldsymbol{H} = -\mathrm{i}\omega\varepsilon_0(\chi+1)\boldsymbol{E}, \tag{2}$$

where $\boldsymbol{E}=(E_x,E_y,E_z)$, $\boldsymbol{H}=(H_x,H_y,H_z)$, ε_0, μ_0, χ, and ω are electric field vector, magnetic field vector, permittivity of vacuum, permeability of vacuum, electric susceptibility of volume hologram, and angular frequency, respectively. In the case of transverse electric (TE) mode, that is, E_z=0, it is convenient that H_x and H_y are expressed by using a scalar potential function ${}^{e}u$ as

$$H_x = \frac{\partial\partial\ {}^{e}u}{\partial x \partial z}, \qquad H_y = \frac{\partial\partial\ {}^{e}u}{\partial y \partial z}. \tag{3}$$

Then, E_x, E_y, and Hz can be expressed by using ${}^{e}u$. Therefore, ${}^{e}u$ is satisfied differential equations as follows:

$$\left(\frac{\partial^2}{\partial x^2}+\frac{\partial^2}{\partial y^2}+\frac{\partial^2}{\partial z^2}\right)\frac{\partial\ {}^{e}u}{\partial x} = -k^2(\chi+1)\frac{\partial\ {}^{e}u}{\partial x}, \tag{4}$$

$$\left(\frac{\partial^2}{\partial x^2}+\frac{\partial^2}{\partial y^2}+\frac{\partial^2}{\partial z^2}\right)\frac{\partial\ {}^{e}u}{\partial y} = -k^2(\chi+1)\frac{\partial\ {}^{e}u}{\partial y}. \tag{5}$$

However, in the case of transverse magnetic (TM) mode, it is difficult to express electromagnetic field by using a potential function. In this paper, coordinates are converted and Maxwell's equations are expressed by

$$\frac{\partial E^3}{\partial x_2}-\frac{\partial E^2}{\partial x_3} = \mathrm{i}\omega\mu_0(\chi+1)H_1, \tag{6}$$

$$\frac{\partial E^1}{\partial x_3}-\frac{\partial E^3}{\partial x_1} = \mathrm{i}\omega\mu_0(\chi+1)H_2, \tag{7}$$

$$\frac{\partial E^2}{\partial x_1}-\frac{\partial E^1}{\partial x_2} = \mathrm{i}\omega\mu_0(\chi+1)H_3 = 0, \tag{8}$$

$$\frac{\partial H_2}{\partial x^2}-\frac{\partial H_2}{\partial x^3} = -\mathrm{i}\omega\varepsilon_0 E^1, \tag{9}$$

$$\frac{\partial H_1}{\partial x^3}-\frac{\partial H_3}{\partial x^1} = -\mathrm{i}\omega\varepsilon_0 E^2, \tag{10}$$

$$\frac{\partial H_2}{\partial x^1}-\frac{\partial H_1}{\partial x^2} = -\mathrm{i}\omega\varepsilon_0 E^3,$$

where

$$\boldsymbol{E} = E_x\boldsymbol{e}_x + E_y\boldsymbol{e}_y + E_z\boldsymbol{e}_z = E^1\boldsymbol{e}_1 + E^2\boldsymbol{e}_2 + E^3\boldsymbol{e}_3, \tag{12}$$

$$\boldsymbol{H} = H_x\boldsymbol{e}_x + H_y\boldsymbol{e}_y + H_z\boldsymbol{e}_z = H_1\boldsymbol{e}^1 + H_2\boldsymbol{e}^2 + H_3\boldsymbol{e}^3, \tag{13}$$

$$\boldsymbol{e}_x\frac{\partial}{\partial x} + \boldsymbol{e}_y\frac{\partial}{\partial y} + \boldsymbol{e}_z\frac{\partial}{\partial z} = \boldsymbol{e}^1\frac{\partial}{\partial x^1} + \boldsymbol{e}^2\frac{\partial}{\partial x^2} + \boldsymbol{e}^3\frac{\partial}{\partial x^3} = \boldsymbol{e}_1\frac{\partial}{\partial x_1} + \boldsymbol{e}_2\frac{\partial}{\partial x_2} + \boldsymbol{e}_3\frac{\partial}{\partial x_3}, \tag{14}$$

$$\boldsymbol{e}_1 = \boldsymbol{e}_x + \boldsymbol{e}_z\frac{\partial}{\partial x^1}\int\frac{1}{\chi+1}\mathrm{d}x^3, \quad \boldsymbol{e}_2 = \boldsymbol{e}_y + \boldsymbol{e}_z\frac{\partial}{\partial x^2}\int\frac{1}{\chi+1}\mathrm{d}x^3, \quad \boldsymbol{e}_3 - \frac{1}{\chi+1}\boldsymbol{e}_z, \tag{15}$$

$$\boldsymbol{e}^i = \sum_{j=1}^{3}(\boldsymbol{e}^i\cdot\boldsymbol{e}^j)\boldsymbol{e}_j. \tag{16}$$

When E^1 and E^2 are expressed by using a scalar function ${}^{m}u$ as

$$E^1 = \frac{\partial\partial^{\mathrm{m}}u}{\partial x^3\partial x_1}, \qquad E^2 = \frac{\partial\partial^{\mathrm{m}}u}{\partial x^3\partial x_2},$$

H^1, H^2, and E^3 can be expressed by ${}^{m}u$ and two differential equations are derived as follows:

$$\left(\frac{\partial\partial}{\partial x_1\partial x^1}+\frac{\partial\partial}{\partial x_2\partial x^2}+\frac{\partial\partial}{\partial x_3\partial x^3}\right)\frac{\partial^{\mathrm{m}}u}{\partial x_1} = -k^2(\chi+1)\frac{\partial^{\mathrm{m}}u}{\partial x_1},$$

$$\left(\frac{\partial\partial}{\partial x_1\partial x^1}+\frac{\partial\partial}{\partial x_2\partial x^2}+\frac{\partial\partial}{\partial x_3\partial x^3}\right)\frac{\partial^{\mathrm{m}}u}{\partial x_2} = -k^2(\chi+1)\frac{\partial^{\mathrm{m}}u}{\partial x_2}.$$

By solving eqs. (4), (5), (18), (19), polarization dependence of reconstructed beam can be evaluated.

3.Conclusion

In this paper, differential equations to express light propagation in volume holograms were derived by coordinate conversion. In future, volume holograms were evaluated by using the differential equations

Acknowledgment

This work has been partially supported by the Japan Science and Technology Agency (JST) under the Strategic
Promotion of Innovation Research and Development Program.

Reference:

[1] H. Kogelnik, Bell System Technical Journal, 48, 2909 (1969).

Invited Speaker 23

A Study on holographic printing system using shader

Sunghee Hong[1)], Kang Hoon Jong[1)], Kim Young Min[1)], Hong Ji su[1)], Chun Sung Shin[1)]
VR/AR Research Center
Korea Electronics Technology Institute Seoul, Republic of Korea

1.Introduction

Formulation of the holographic principle by Dennis Gabor in 1948 [1] and invention of lasers a decade later put foundations to holographic technology. Introduction of carrier frequency in holographic recording by Leith and Upatnieks in 1962 [2] and publication of Denisuyk [3] the same year on recording white light viewable reflection holograms pushed forward optical metrology and display holography of 3D still-images. Advents in computers and optoelectronics enabled development of holographic imaging technologies as holographic video and holographic printing. The current status of research on dynamic holographic display indicates that this technology still has a long way to go before the release of a commercial product. By comparison, technology of holographic printing of 3D still-images is the one closest to commercialization. The holographic stereogram printers, which are also known as direct-write digital holographic printers, have been developed and released as commercial products by Geola, Ultimate, and Zebra. As hologram printer's contents are fringe patterns, We have to calculation interference image with Rayleigh-Sommerfeld. But this calculation is so difficult .So we suggest that how to reduce processing time with computer. That is shader.

This paper is organized as follows. We first introduce the shader and hologram printer. And we explain how to use shader with R-S fringe pattern calculation.

As can be seen in Figure 1, the proposed Shader can generate fringe pattern quickly. Originally shader is developed for 3D rendering with GPU. And these days, GPU is composed with thousands core. That enable to use parallel processing

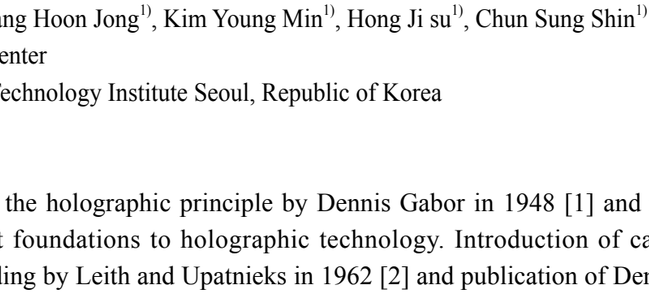

Fig. 1. Shader for fringe pattern image generation

2.Implementation

Center the title of the paper at the top of the page. It should be typed in capital bold letters. Below give the As we see Fig 2, we can design Shader pipeline for hologram fringe pattern. We input point cloud data into the vertex buffer object, and GPU chipset load the data into the vertex shader. But this is just transmission of point cloud data.

Next step is Geometry shader. That is hologram main numerical calculation .and fragment shader is blending of every fringe pattern.

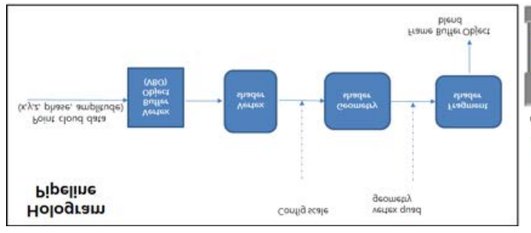

Fig. 2. Shader Pipeline for hologram

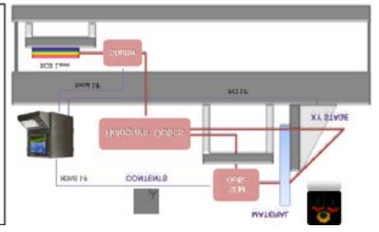

Fig. 3. Hologram printer hardware

As a Fig 3, we can print hologram fringe pattern with optic system. This system can make hologram 3D image. First of all we use R, G, B laser with light source. And we load fringe pattern image with SLM(Spatial Light Modulation). And we can use shutter with expose time. Optical shutter can control 10ms expose time. XY Stage move the material for every point printing. We use ultimate hologram film for material. Ultimate hologram film is made up of silver halide.

3.Conclusion

The paper presents a method for hologram generation with shader language. If we use Open MP for hologram generation, it take 1,854 second, But Shader takes a just 5 second. So we can reduce many time to generate hologram. That means we can print high quality hologram image. Before shader generation, it take a weeks or million polygon 3D object, so actually we can't generate high quality object.We can see a high quality hologram 3D image at Fig 4.

Fig. 4. Hologram printing

<Acknowledgment>

This work was supported by 'The Cross-Ministry Giga KOREA Project' grant from the Ministry of Science, ICT and Future Planning, Korea.

Reference:

[1] D. Gabor, "A new microscopic principle," Nature 161, 777–778 (1948).
[2] E. Leith and J. Upatnieks, "Reconstructed wavefronts and communication theory", J. Opt. Soc. Am. 52, 1123-30 (1962)
[3] Yu.N. Denisyuk, "On the reflection of optical properties of an object in the wave field of light scattered by it", Doklady Akademii Nauk SSSR 144, 1275-1278 (1962)

Invited Speaker 24

Ultrahigh-speed interferometric scattering (iSCAT) microscopy

Chia-Lung Hsieh[1)]

[1)]Institute of Atomic and Molecular Sciences, Academia Sinica, Taipei 10617, Taiwan

Tracking single particle by optical means has been a powerful tool to investigate dynamics without the need for ensemble average. In single-particle tracking (SPT), a small particle creates optical contrast from the surrounding environment, and thus its position can be spatially localized. SPT has made a great success in studying intriguing phenomena in the fields of physics, engineering, and biology. In most dynamic studies, high-speed detection is highly desirable because it offers the opportunity to discover new events. However, the signal-to-noise ratio generally decreases as the signal integration time becomes very short at a high acquisition rate. This difficulty is often overcome by using larger particles with stronger optical signal. Unfortunately, in many cases, large particles are not acceptable because they introduce heavy mass loading and steric hindrance, which obscures the original motion of the targets being labeled. Therefore, continuing effort has been made to track smaller particles with better spatial precision at higher speed. While fluorescence has been a convenient and widely used contrast mechanism in SPT, fluorescence is limited by its fundamental photophysical and photochemical properties, including photobleaching, blinking and saturation. As a result, fluorescence SPT struggles to support SPT with sub-millisecond temporal resolution and nanometer spatial precision.

Linear scattering is an alternative contrast mechanism for SPT. The photostable and unlimited signal allows for long-term and high-speed observation. The longstanding challenge in scattering-based SPT is to use smaller sized nanoparticles, as the scattering power scales with the sixth power of the size. In this talk, I will present an imaging technique called interferometric scattering (iSCAT) microscopy that allows for tracking very small nanoparticles with nanometer spatial precision within microseconds (1-3). Sharing the concept of detecting signal via interference with holographic microscopy, the clever design of iSCAT microscopy makes it a convenient and robust imaging modality with high sensitivity. A laser was used as the illumination light source of iSCAT microscopy. The light was projected on to the sample through a microscope objective (see Figure 1a). The reflection from the coverglass holding the sample served as the reference beam (see Figure 1b). The transmitted light illuminated the sample containing nanoparticles. The backscatterd light form the nanoparticles and the reflected reference beam were collected by the same objective and imaged onto an ultrahigh-speed CMOS camera. When the interference between the signal and the reference was set to be destructive, the particle appeared as a dark spot on a bright background (see inset of Figure 1a). Through this homodyne detection, shot-noise limited sensitivity, and therefore optimal localization precision are achieved at high speed. The common-path interferometry of iSCAT microscopy makes the signal less sensitive to the environmental noise. Using the weak reflection from the supporting coverglass as the local oscillator enhances the sensitivity by allowing more illumination light before the reference beam saturates the detector. By placing the object at the focal plane of the microscope objective, the particle can be seen in the iSCAT image without image reconstruction, which enables the real-time observation of highly rapid events.

We used iSCAT microscopy to set a new standard of SPT by tracking a 20 nm gold nanoparticle with 2 nm spatial precision at an ultrahigh acquisition rate of 500,000 frames per second (1). Using iSCAT microscopy, we investigated diffusion of single lipid molecules labeled by small gold nanoparticles in a supported bilayer membrane with unprecedented clarity (2, 3). When the membrane was composed of one lipid species and thus was homogeneous, simple Brownian motion was observed from microseconds to seconds (see Figure 1c). We then prepared a ternary membrane containing coexisting membrane domains of different phases: liquid-ordered (Lo) and liquid-disorder (Ld) phases. We were able to follow single molecules exploring both domains in a continuous manner with unprecedented clarity (3). Importantly, we observed anomalous subdiffusion in the Lo domains in the microsecond timescales. This result provides the first experimental evidence of nanoscopic substructures of the Lo phase, suggesting a new mechanism of regulating membrane dynamics at the nanoscale (3).

The combination of nanometer spatial precision and microsecond temporal resolution provides the opportunity to study rapid motions of nano-objects at the molecular scale. I will also discuss about the challenges of performing high-speed, high-precision iSCAT measurements in live cells.

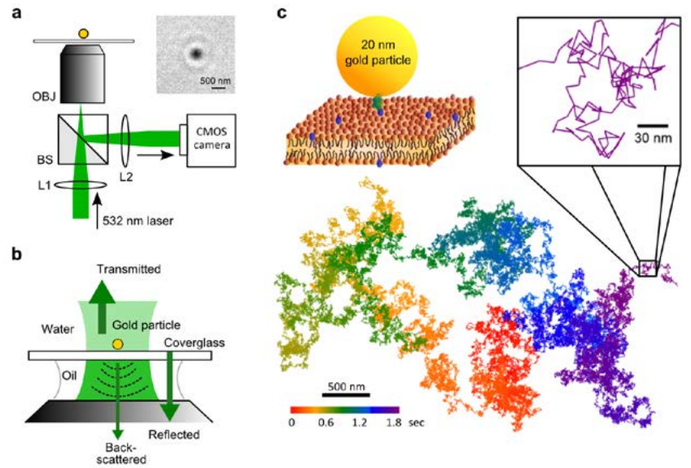

Fig. 1. (a) Schematics of iSCAT microscopy. Inset: iSCAT image of a 20 nm gold particle. (b) Close-up view of the schematics of iSCAT detection at the sample. (c) Tracking single lipid molecules in a bilayer membrane by ultrahigh-speed iSCAT microscopy. The image acquisition rate was 50,000 frames per second, corresponding to a temporal resolution of 20 microseconds. Long and precise diffusion trajectory was obtained from which diffusion characteristics can be analyzed with great detail.

Reference:

[1] Y.-H. Lin, W.-L. Chang, and C.-L. Hsieh, Shot-noise limited localization of single 20 nm gold particles with nanometer spatial precision within microseconds, Opt. Express 22, 9159 (2014).

[2] C.-L. Hsieh, S. Spindler, J. Ehrig, and V. Sandoghdar, Tracking single particles on supported lipid membranes: multimobility diffusion and nanoscopic confinement, J. Phys. Chem. B 118, 1545 (2014).

[3] H.-M. Wu, Y.-H. Lin, T.-C. Yen, and C.-L. Hsieh, Nanoscopic substructures of raft-mimetic liquid-ordered membrane domains revealed by high-speed single-particle tracking, Scientific Reports 6, 20542 (2016).

Invited Speaker 25

Measurement of Cornea Curvature by using Moiré Method

Yen-Chang Chu[1)], Wei-En Bi[1)], Chien-Hung Yeh[2)], Jing-Heng Chen[2)] and Kun-Huang Chen [1*)]
[1)]Department of Electrical Engineering, Feng Chia University, Taichung 40724, Taiwan
[2)]Department of Photonics, Feng Chia University, Taichung 40724, Taiwan

Abstract

Based on projection moiré method and heterodyne interferometry, a measurement system of cornea curvature was proposed. To show the validity of the proposed method, a corneal surface of the pig eyeball was measured in the experiment. The proposed system approach has the benefits of projection moiré method, Talbot effect, and heterodyne interferometery.

Keywords: Curvature radius, Cornea, Projection moiré, Talbot effect, Heterodyne interferometry.

1.Introdution

The cornea curvature is a very important parameter. A slight variation of the corneal surface can significantly affect the normal human vision. Therefore, the accurate measurement of cornea curvature provides important and essential information in vision diagnosis process [1-2]. In this study, we propose a simple method for measuring the cornea curvature. It is based on the Talbot effect, projection moiré method, and heterodyne interferometry. Because it applies the projection moiré method, the proposed method can inspect the larger degrees, and the longitudinal and lateral range on the sample surface. Additionally, using heterodyne interferometry ensures that this method is simple to implement, highly accurate, and achieves high resolution. The validity of this method was demonstrated experimentally, and the method has merits of high accuracy, high stability.

2.Principle

Fig. 1 shows the optical configuration of the proposed method. For convenience, the z-axis is the observation axis of CMOS camera, and y-axis is the direction perpendicular to the paper plane. A laser light of wavelength λ passes through an objective, a pinhole, and a collimating lens to form an expanded and collimated light, then impinges on a projection grating G1 at an angle α and forms a self-image on the tested sample with the self-image distance Z1. The projected fringes of the self-image can be distorted due to the non-plane tested sample. These distorted fringes are imaged on the reference grating G2 of the same pitch with G1 via a camera lens to form the moiré fringes and captured by the CMOS camera C. Next, when the motorized translation stage M moves the grating G1 along the x-axis at a constant velocity v within a time t, every pixel of CMOS camera can receive a continuously sinusoidal signal and be written as

$$I(x,y) = I_0(x,y) + \gamma(x,y)\cos[2\pi ft + \theta(x,y)], \quad (1)$$

where f=v/p denotes the heterodyne moiré frequency which results from the time-varying phase, and $\theta(x, y)$ is the phase of the height distribution h(x, y) on the tested sample and can be written as

$$\theta(x, y) = \frac{2\pi}{p} h(x, y)\tan\alpha. \quad (2)$$

The phase of the moiré fringes on the single pixel can be calculated by using the least-squares sine fitting algorithm. Applying the above procedures to the other pixels and using phase unwrapping to the acquired phases, the phase distribution θ(x, y) can be obtained, and the surface profile h(x, y) can subsequently be acquired. Accordingly, the cornea curvature can be calculated.

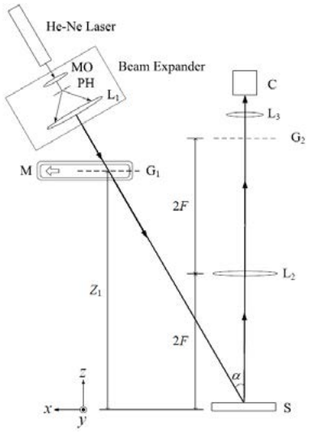

Fig. 1. The optical configuration of the proposed method.

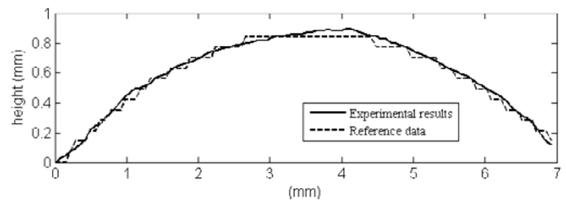

Fig. 2. Meridional curves of cornea cross-section from experimental result and reference data.

3.Experimental Results and Discussions

To show the validity of the proposed method, a corneal surface of a pig eyeball has been measured. The experiment setup includes: a diode laser of wavelength 473 nm, two linear grating of pitch 0.2822 mm, an imaging lens of focal length 200 mm, a motorized translation stage of resolution 0.05 μm to generate heterodyne moiré frequency f = 2 Hz (v = 0.5644 mm/s), a CMOS camera of 8-bit gray level and 1280×1024 resolution. The frame rate of CMOS camera fs=15 fps, the exposure time a = 66 msec, and total recording time T = 1 sec to record the heterodyne moiré signals in the different time points. Every recorded moiré image was filtered with 3×1 window by 2D median filtering to filter out the harmonic noise of moiré. To improve the visibility of the projected grating fringes, we stain the fluorescein on the corneal surface. The experimental results have been shown in Fig. 2. Fig. 2 shows the cross-section curve of the reconstructed corneal surface of the pig eyeball. Then, using the fitting curve can obtain the cornea curvature of pig eyeball as 0.222 mm-1.

4.Conclusion

This paper proposes a projection moiré method for measuring the cornea curvature. The validity of this method was demonstrated experimentally, and the method has the benefits of projection moiré method, Talbot effect, and heterodyne interferometery, including simple optical setup, ease of operation, high stability, and high resolution.

Acknowledgments

This work is partially supported by National Science Council of Taiwan under contract number MOST 105-2221-E-035-042.

Reference:

[1] M. C. Corbett, E. S. Rosen, and D. P. O'Brart, Corneal Topography: Principles and Applications, chap. 1-chap. 3 (1999).
[2] J. H. Massig, E. Lingelbach, and B. Lingelbach, Appl. Opt. 44(12), 2281-2287 (2005).

Invited Speaker 26

3D Shape Sensing using a Phase Mask to Extend the Depth Measuring Range

Chun-Hsiang Hsu, and Wei-Hung Su
Department of Materials and Optoelectronic Science, National Sun Yat-Sen University, Kaohsiung 804, Taiwan

1.Introduction

In this paper, we investigate an cubic phase mask [1] based on the iquid-crystal spatial light modulator (LC-SLM) to enlarge the depth measuring range for the projected fringe profilometry [2]. A microscope combined with a wide-angle eyepiece lens is employed to project a fringe pattern onto the inspected surface. At a different viewpoint, a CCD camera observes the projected fringes through another microscope and a cubic phase mask. Phase of the fringes is extracted by the Fourier transform method [2]. With the presented calibration schemes, depth information can be determined from the phase of the fringes. The cubic phase mask enlarges the depth of field of the image acquisition system, while the wide-angle eyepiece lens increases the depth of focus of the fringe projection system. It is found that the depth measuring range could be extended up to 1600μm, even though the DOF of the microscope was only 80μm.

2.Using the liquid crystal spatial light modulator (LC-SLM) as the phase mask

It has been shown that the depth-of-field of an incoherent optical system can be enlarged if the pupil function is a square aperture and is mathematically expressed as [1]

$$P(x,y)=\begin{cases}\frac{1}{\sqrt{2}}\exp[j\alpha(x^3+y^3)], & |x|\le L/2,\ |y|\le L/2\\ 0, & \text{otherwise}\end{cases}$$

An example for the phase of the pupil function is shown as Fig. 1(a), in which the α is 40. A liquid crystal spatial light modulator (LC-SLM) combined with an analyzer and a polarizer can be employed as a phase modulator. An example is shown as Fig. 1(b). We used HOLOEYE LC 2002 as the LC-SLM, in which the pixel resolution was 800 × 600 and the pixel pitch was 32μm × 32 μm. With the proper choice of the polarization angles θp and θa, phase was modulated by the input video signal. The LC-SLM modulated the phase linearly between 0 and 1.6π. Thus, phase of the pupil function should be wrapped with the 1.6π modulo operation. The residue of Fig. 1(a) after the modulo operation is shown in Fig. 1(c). This pattern is then used to be the input video signal.

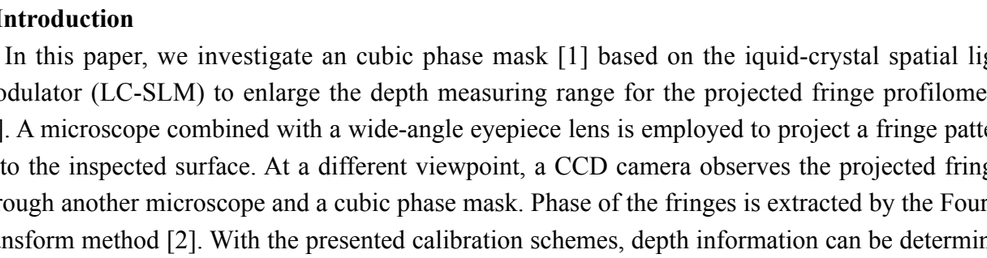

(a) (b) (c)

Fig. 1. (a) Phase profile of the pupil function. (b) Phase modulation using the LC-SLM. (c) Distribution of the input signals ranging from level 50 to 190: the brighter one represents the stronger input signal.

The LC-SLM was combined with a microscope to form an extended DOF system, as shown in Fig. 2(a). A square aperture with size of 15mm× 15mm was located on the LC-SLM, so that Eq. (1) was applicable to this system. To identify a suitable α value, a halogen lamp was selected as the incoherent light source. Lightwaves were launched into a pin hole to generate a point source. For a suitable value of α, the OTF obtained by the CCD camera should be not sensitive to defocus. Once the α value was identified, this extended DOF system could be used as the image acquisition system of the projected fringe profilometry.

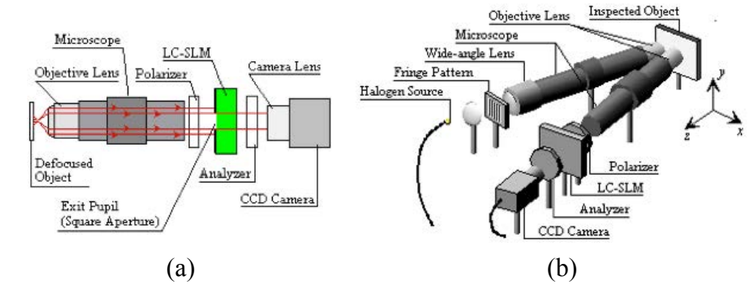

(a) (b)

Fig. 2. (a) Phase profile of the pupil function. (b) Phase modulation using the LC-SLM. (c) Distribution of the input signals ranging from level 50 to 190: the brighter one represents the stronger input signal.

A schematic diagram for 3D shape sensing is shown in Fig. 2(b). A sinusoidal fringe pattern is illuminated by the incoherent light source and projected by the microscope onto the inspected object. An object with size of 2000μm× 2000μm was selected as another inspected sample. Appearance of the fringes projected onto the tilted sample with its focus on the central region is illustrated as Fig. 3(a). The restored image is depicted as Fig. 3(b). Figure 3(c) shows the retrieved 3D surface profile. This object was also inspected by a standard scanning stylus profiler. The measurement results agreed very well, in the micron-range accuracy.

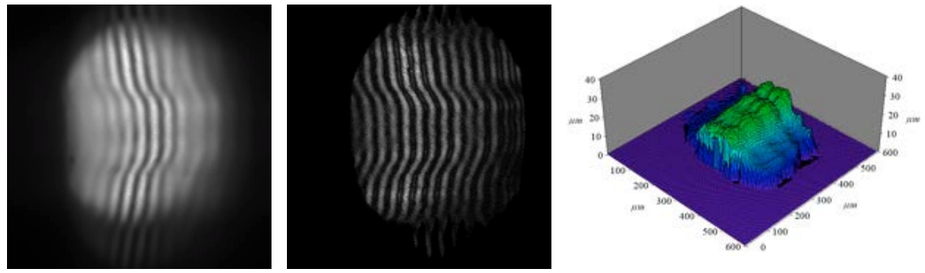

Fig. 3. (a) Diffraction efficiencies for various diffraction orders. (b) Diffraction efficiencies at different recording time for various θ

3.Conclusion

we investigated a unique projected fringe profilometry using the LC-SLM to enlarge the depth measuring range. The depth measuring range could be extended up to 1600μm, with accuracy in the micron-range.

Reference:

[1] D. Hong, K. Park, H. Cho, and M. Kim, “Flexible depth-of-field imaging system using a spatial light modulator,” Appl. Opt. 46, 8591-8599 (2007).
[2] M. Takeda, and K. Mutoh, “Fourier transform profilometry for the automatic measurement of 3-D object shaped,” Appl. Opt. 22, 3977-3982 (1983).

Invited Speaker 27

Common-path Tomographic Phase Microscopy for Studying the Morphology and Light Scattering Properties of Blood Cells

Kung-Bin Sung[1,2,3], Yang-Hsien Lin[1] , Shin-Shyang Huang[1] and Shang-Ju Wu[4]
[1]Institute of Biomedical Electronics and Bioinformatics,
[2]Department of Electrical Engineering,
[3]Molecular Imaging Center, National Taiwan University, No.1 Sec. 4 Roosevelt Road, Taipei 106, Taiwan
[4]Department of Internal Medicines, National Taiwan University Hospital, No.7 Zhongshan S. Road, Taipei 100, Taiwan

1.Introduction

Tomographic phase microscopy (TPM) and related techniques provide label-free three-dimensional (3D) visualization of sub-cellular refractive index (RI) distributions of living cells. The RI of biological specimens represents the local mass density of biomolecules. 3D RI mapping of a biological sample is achieved by reconstruction, based on either filtered backprojection or optical diffraction tomography, from two-dimensional (2D) quantitative phase and amplitude images of the sample under multiple illumination directions. One of the main experimental challenges is to obtain high-quality phase images of the sample in the presence of phase noise due to various sources. We have demonstrated a common-path configuration to acquire 2D scattered-field images of the sample via single-shot off-axis digital holographic microscopy [1]. Results of imaging red blood cells (RBC) and white blood cells (WBC) will be presented. In addition, RI images of thin slices of esophageal mucosa from 14 patients were collected and analyzed to investigate the light scattering properties of both normal and precancerous epithelial tissues.

2.Materials and Methods

Instrumentation – A schematic diagram of the common-path TPM (cTPM) system is shown in Fig. 1 [1]. Quantitative phase images of a transparent sample under plane-wave illumination are acquired with an off-axis Mach-Zehnder interferometer in which the beam scattered by the sample is split into different directions by a diffraction grating (80 grooves/mm). In the first diffraction order the illumination beam passing an empty region in the specimen provides a uniform reference wavefront which coincides at the CMOS sensor with the sample wavefront in the zeroth diffraction order. The image of the first-order beam is slightly shifted from that of the zeroth-order beam by adjusting the position of the grating. The phase shift caused by the specimen is retrieved using Hilbert transform. Two galvanometer-based scanning mirrors are used to change the incident angle of the illumination beam. 3D RI distributions of the sample are reconstructed using optical diffraction tomography with the non-negativity constraint [2]. The system has a transverse resolution of 0.35 μm and an axial resolution of 0.7 μm. The resolution of RI was estimated to be around 0.001, determined from the standard deviation of reconstructed RI values of polystyrene beads immersed in oil.

Red blood cell study – Whole blood samples were obtained from the NTU hospital, diluted 4,000 times in phosphate buffered saline and imaged with the cTPM system immediately. To convert 3D RI maps of living RBC into hemoglobin concentrations we experimentally determined the specific refractive increment (αHb) of hemoglobin. We filled hemoglobin solutions with various concentrations in a micro-trench and measured the RI value from phase images taken under normal-incidence illumination. Linear regression of the RI versus concentration yields αHb.

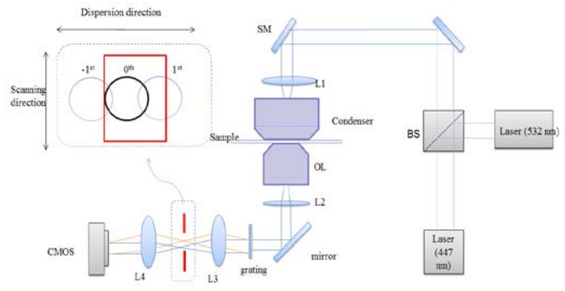

Fig. 1. Schematic diagram of the cTPM system. BS: beam splitter, OL: objective lens, SM: scanning mirror. The inset shows a window (red rectangle) allowing the full frequency content of the 0th-order beam to pass.

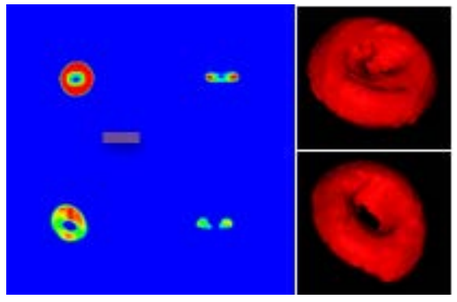

Fig. 2. Reconstructed RI images of a normal RBC (top row) and an RBC from a patient (bottom row). Scale bar 8 μm.

WBC study – After centrifuge of whole blood samples, a flow cytometry-based cell sorter was used to separate three major types of WBC including monocytes, lymphocytes and neutrophils. Based on experimentally determined 3D RI distributions of individual WBC, we used a 3D finite-difference time-domain (FDTD) simulation tool to study light scattering properties. The goal was to assess the feasibility of using light scattering features to distinguish the three major types of WBC.

3.Results and Discussion

We measured 3D RI images of RBC from normal volunteers and patients with mild thalassemia. Morphological features including the volume, surface area, sphericity and thickness were extracted. Additionally, we calculated the integrated phase and dry mass of each RBC from its phase image. The integrated phase and the ratio of surface area to volume was the best two features to discriminate thalassemic RBC from normal ones, achieving an area under the Receiver Operating Characteristic curve of 0.94 and 0.90, respectively.

On the results of the WBC study, backscattering spectra of lymphocytes matched well with spectra of homogeneous spheres as predicted by Mie theory. The other two types of WBC did not show this correlation due to irregular sizes of the cell body and nucleus. Nevertheless, the backscattering spectra of neutrophils are significantly more intense than those of lymphocytes and monocytes.

4.Conclusions

We successfully characterized 3D RI and morphological features of RBC and found that the integrated phase and surface-to-volume ratio are the best features to discriminate between RBC of patients with thalassemia and those of normal volunteers. The 3D RI tomograms of WBC and subsequent FDTD simulations indicated that backscattering characteristics of lymphocytes, monocytes and neutrophils are different each other. This suggests the possibility of classifying the three types of WBC based on backscattering measurements.

Reference:

[1] W.C. Hsu, J.W. Su, T.Y. Tseng, and K.B. Sung, “Common-path three-dimensional refractive-index microscopy of living cells,” Opt. Lett., 39, 2210-2213 (2014).

[2] J.W. Su; W.C. Hsu, C.Y. Chou, C.H. Chang, and K.B. Sung, “Digital holographic microtomography for high-resolution refractive index mapping of live cells,” J. Biophotonics, 6, 416-424 (2013).

Invited Speaker 28

Mode decomposition of multimode fiber using digital holography[1]

Meng Lyu[1,2)] and Guohai Situ[1)]

[1)]Shanghai Institute of Optics and Fine Mechanics, Chinese Academy of Sciences, Shanghai 201800, China

[2)]University of the Chinese Academy of Sciences, Beijing 100049, China

1.Introduction

Eigenmode decomposition of the field at the output of optical fiber can provide fundamental insights into the nature of electromagnetic-wave propagation, such as laser mode competition and oscillations, bend loss, and beam quality of optical fibers. In the past few years, several modal decomposition (MD) approaches have already been developed [1]. These methods can be divided into two categories. The first category is iterative approach [2, 3], which is time-consuming. The other one is direct measurement [1], which is costly or hard to apply. In this talk, we propose and demonstrated a fast and accurate MD measurement technique based on digital holography (DH).

2.Mode decomposition for step-index fiber modes

Considering a step-index fiber with an assumption of weak guiding, the eigensolution of the Helmholtz equation take the approximated form of LP modes,

$$\psi(r,\varphi)=R(r)\Phi(\varphi) \tag{1}$$

where $R(r)=C\begin{cases}\dfrac{J_l\left(Ur/a\right)}{J_l(U)} & r\le a\\ \dfrac{K_l\left(Wr/a\right)}{K_l(W)} & r>a\end{cases}$ and $\Phi(\varphi)=\begin{cases}\cos(l\varphi) & \text{for "even" mode}\\ \sin(l\varphi) & \text{for "odd" mode}\end{cases}$ (2)

The symbol a denotes the fiber core radius and C is a constant so that $\psi(r,\varphi)$ fulfills the normalization condition. The values for U and W can be calculated from the characteristic equations of step-index fiber. Any propagating field of a fiber can be projected on the Eigen modes of the fiber. It can be mathematically expressed as a superposition of eigensolutions,

$$U(r,\varphi)=\sum_{n=1}^{m_{max}} c_n\psi_n(r,\varphi) \tag{3}$$

and fulfill the equation

$$\sum|c_n|^2=\sum\rho_n=1 \tag{4}$$

where ρ_n is the weight of the n-th eigenmode. As eigenmodes are orthonormal [1]

$$\langle\psi_m,\psi_n\rangle=\iint_R\psi_m*\psi^*{}_n\,d\varphi dr=\delta_{mn} \tag{5}$$

after obtaining the propagating field U at the output end of the fiber by off-axis DH, the modal coefficient

[1]This work was supported by the NSFC (61377005) and the Chinese Academy of Sciences QYZDB-SSW-JSC002

c_n can be given by $c_n=\langle U,\psi_n\rangle$.

3.Experimental verification

The experimental setup is shown in Fig. 1. The test fiber is a SMF-28 fiber (NA =0.14, core diameter is 8.2 μm). The fiber is excited by a He-Ne laser (wavelength is 633 nm).

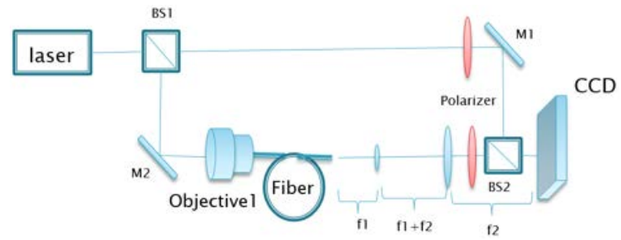

Fig. 1. Experimental setup

As two sets of polarizations are mutually perpendicular in fiber, we can consider only one polarization at a time without loss of generality. Due to the Helmholtz equation, the LP modes in this experimental condition are LP01even, LP02even, LP11even, LP11odd, LP12even, LP12odd, LP21even, LP21odd, LP31even and LP31odd. Figures 2 and Fig. 3. show the results of the experiments.

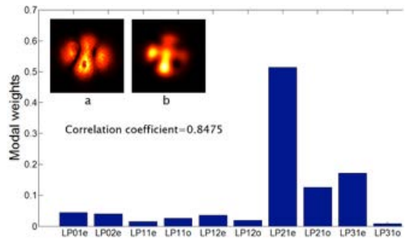

Fig. 2. Results of the experiments

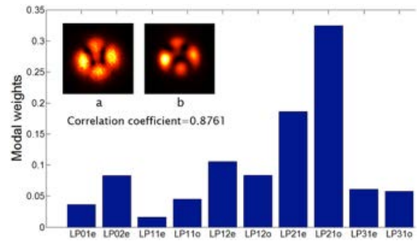

Fig. 3. Results of the experiments

Images a in Fig.2. and Fig.3. are the measured beam profiles by DH, and images b are the reconstructed beam profiles. The correlation coefficient of two beam profiles are 0.9534 and 0.9617, respectively. Then we find the new MD method is feasible.

4.Conclusion

We have proposed and demonstrated a novel MD method by DH approach. As a one-shot and non-iterative approach, the proposed method is fast. Meanwhile, the results show that the method is accurate.

Reference:

[1] Kaiser T, Flamm D, Schröter S, et al. Complete modal decomposition for optical fibers using CGH-based correlation filters. Optics Express, 2009, 17(11): 9347-9356.

[2] Shapira O, Abouraddy A F, Joannopoulos J D, et al. Complete modal decomposition for optical waveguides. Physical Review Letters, 2005, 94(14): 143902.

[3] Huang L, Guo S, Leng J, et al. Real-time mode decomposition for few-mode fiber based on numerical method. Optics Express, 2015, 23(4): 4620-4629.

Invited Speaker 29

Spatial and temporal imaging in digital holographic microscopy for quantitative analysis

Yu-Chih Lin[1)], Xin-Ji Lai[1)], Han-Yen Tu[2)], and Chau-Jern Cheng[1)]

[1)]Institute of Electro-Optical Science and Technology, National Taiwan Normal University, Taipei 11677, Taiwan

[2)]Department of Electrical Engineering, Chinese Culture University, Taipei 11114, Taiwan

[*)]E-mail: yclin_ioplab@ntnu.edu.tw

Abstract

This study presents the spatial and temporal imaging in digital holographic microscopy for high resolution quantitative analysis. The applications in biological and physics research has been achieved with sub-micron and picoseconds resolution. The novel method and potential applications for ultrafast, super-resolution wavefronts recording and reconstruction will be discussed in this study.

Keywords— resolution, time-resolved, digital holographic microscopy

1.Introduction

Digital holographic microscopy (DHM) [1-3] has been wid ly used in quantitative measuremen s for optical micro-elements or biological samples. Quantitative complex imaging (amplitude and phase) is an important issue in recently studies, becaus the complex wavefronts can serve the analysis for detecting the three-dimensional optical thickness profile with high phase accuracy in sub-wavelength range. Compare to the high phase accuracy in DHM, the spatio-temporal resolution becomes more and more important when applied DHM system to the precise researches as biological and physics applications. For spatial domain, the infinite aperture size and wavelength of light have restricted the spatial resolution of optical imaging system. In recent, the synthetic aperture (SA) method is widely used in quantitative imaging for overcome the diffraction limit and resolution enhancement [4]. Then, the Ultrashort pulse laser is well established as a convenient tool for surface processing and optical excited of several different materials [5,6], such as optical absorption, heat conduction, phase transitions, evaporation kinetics and plasma dynamics. And the ultrashort duration in pulse laser has a good potential for ultrafast time-resolved measurement and improve the temporal resolution up to sub-picoseconds time scales [7].

2.Resolution enhancement in spatial imaging

The schematic representation of the resolution enhancement by synthetic aperture in digital holographic microscopy is indicated in Fig. 1(a). The synthetic aperture task was achieved by the scanning of the galvo mirror with the 4-f imaging architecture in object arm. In this experiment, the scanning angles could attain a scanning range of ±65°. Experimental results of the resolution enhan ement are shown in Fig. 1(b). The spatial resolution was improved to 200 nm and the finest structure in the cell body can be observed as in he magnified area in Fig. 1(b) after employed the synthetic ape ture in digital holographic microscopy.

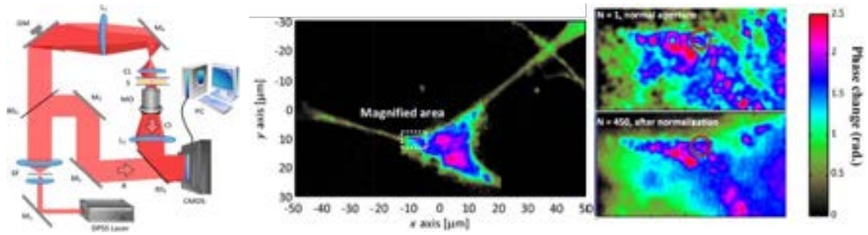

Fig. 1. (a) experimental setup of synthetic aperture DHM and (b) its resolution enhancem nt results for measuring the living cell.

3.Ultrafast time-resolved imaging by pulsed digital holographic microscopy

Digital holographic microscopy (DHM) [1-3] has been wid ly used in quantitative measuremen s for optical micro-elements or biological samples. Quantitative complex imaging (amplitude and phase) is an important issue in recently studies, becaus the complex wavefronts can serve the analysis for detecting the three-dimensional optical thickness profile with high phase accuracy in sub-wavelength range. Compare to the high phase accuracy in DHM, the spatio-temporal resolution becomes more and more important when applied DHM system to the precise researches as biological and physics applications. For spatial domain, the infinite aperture size and wavelength of light have restricted the spatial resolution of optical imaging system. In recent, the synthetic.

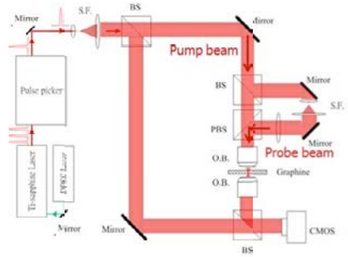

Fig. 1. Experimental setup of the time-resolved pump-probe pulsed digital holographic microscopy. S.F.: spatial filter; BS: beam splitter; PBS polarized beam splitter; O.B.: objective.

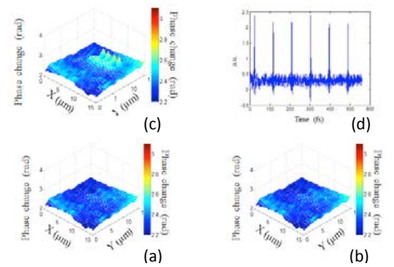

Fig. 2. Pulse-induced phase change with fringes structure in the sample at (a) 0 fs, (b) 50 fs, (c) 100 fs, and intensity of diffraction tem from the pulse-induced phase fringe on materia l by far-field measurement

4.Conclusions

We have proposed and demonstrated different techniques to enhance the spatial and temporal resolution in digital holographic microscopy an applied to biological and physics studies. The high spatial resolution information by synthetic aperture method is served for the living cell measurement. With employed the pulsed laser, the ultrafast time-resolved imaging can also applied to analyze the photoexcited phenomenon.

Acknowledgment This work was financially supported by the Ministry of Science and Technology, Taiwan (MOST 102-2221-E-003 -025 -MY3, MOST 105-2221-E-003 -015 -MY3, MOST 105-2923-E-003-001, and MOST 104-2221-E-034-01 -MY3).

Reference:

[1] P. J. van Heerden, Appl. Opt. 2, 393-400 (1963)

[2] H. J. Coufal, D. Psaltis, G. Sincerbox, Holographic data storage (Springer series in optical sciences, 2000).

[3] K. Kuroda, Y. Matsuhashi, R. Fujimura, T. Shimura, Opt Rev, vol. 18(5), pp. 374-382, 2011.

[4] S. H. Lin, P. L. Chen, C. I. Chuang, Y. F. Chao, and K. Y. Hsu, Opt. Lett. 36(16), pp. 3039-3041 (2011).

Faculty Positions Opening

The College of Photonics at the National Chiao Tung University invites applications for tenure-track faculty positions at all levels in Tainan Campus. We are seeking highly qualified candidates committed to a career in teaching and research in the areas of optics and photonic systems, novel laser systems and applications, optical metrology, sensing, imaging, optical information processing, storage, and displays using non-traditional technologies, solar energy systems, green energy technology and systems, optical systems for bio-medical and agriculture, optical designs and system integration.

Applicants are encouraged to apply by December 31, 2016, but applications will be accepted continuously until the positions are filled.

Instructions for Applicants

1.Website: http://www.cop.nctu.edu.tw/menu02_05_ii.html?nid=158

2.Submit the following Documents (e-mail is preferable):

- Filled Application form;
- Curriculum vita; includes research statement, teaching statement, and key publications
- 3 reference letters

3.Submit the following Documents (e-mail is preferable):

Contact person:

Professor Ken Y. Hsu ken@cc.nctu.edu.tw or

Ms. Lingching Chen (陳伶青小姐) lingching@nctu.edu.tw

Faculty Search Committee

College of Photonics

No. 301, Gaofa 3rd Road., Guiren District

Tainan City 71150

Taiwan

Poster Presentation Titles

1 . One-Shot Incoherent Complex Imaging by State-multiplexed Fourier Ptychography
Byounghyo Lee

2 . Optical Scanning Holographic Microscopy
Cheng-Hao Tsou

3 . Image Arrangement for Quasi-dynamic Display of Three-dimensional Image in Disk-type Multiplex Holograms
Chih-Hung Chen

4 . Virtual-image Replication from a Real-image Master in 360-degree Viewable Disk-type Multiplex Holography
Chih-Hung Chen

5 . Improvement Of Collinear Holographic Storage System By Micro Lens Array
Chi-Hsien Yang

6 . Polarization-switchable Meta-hologram with Dual Images
Chun Yen Liao

7 . Design of writing patterns for multi-level self-referential holographic data storage by phase-only modulation
Daiki Murozono

8 . Differential Equations for Volume Hologram with Coordinate Conversion
Daisuke Barada

9 . Light-sheet volume holographic microscopy
Dipanjan Bhattacharya

10.Fabrication of Holographic Devices with Azobenzene-based Materials
Fang-Yun Lee

11. Label-free analysis and identification of white blood cells using common-path tomographic diffractive microscopy
Fong-Jheng Lin

12. Characteristics of known phase embedded collinear holographic memory
Hajimu Nishimoto

13. Parallel Computing of Polygon-Based Computer-Generated Hologram
Heng-Kuang Liao

14. Computational microscopy of phase imaging based on transport of intensity
Hsi-Hsun Chen

15.Reflective-type Digital Holographic Microscopy with Self-pumped Phase Conjugation Mirror
Huang-Tian Chan

16. Fast calculation method for the polygon based computer generated hologram using sparse sampling
Jaebum Cho

17. Phase measurement of a tilted plane mirror using the derivative estimation of a single hologram
Jin Nozawa

18. Optical correlation system using simple structure holographic optical disk
Kanami Ikeda

19. Properties of Magnetic Volumetric Hologram with Magnetic Garnet/SiO_2 Multilayered Media
Kodai Kawazu

20. Volumetric display using bubbles induced by femtosecond laser pulses
Kota Kumagai

21. The study of synthesizing Images in screen imaging synthesis system
Kun-Zheng Lin

22. Michelson Interferometer for 3D Displacement Measurements
Lu-Yu Wang

23. Ultra-high speed goniophotometer for measuring the scattering light distribution of recording media used in holographic data storage
Ming Le

24. Reflection Conical Multiplex Holography using Optical System with Distorted Conical Object-Plane
Ming-Han Chan

25. Speckle Reduction in Holographic Projection Display Using Window Partition Method
Ming-Hong Weng

26. Effect of a quasi-continuous fringe-scanning on generalized phase-shifting digital holography
Nobukazu Yoshikawa

27. Digital Microscopy with Volume Hologram under Incoherent Light Source
Po-Hao Wang

28. Volume Hologram with Non-axial-scanning Confocal Microscope
Po-Hao Wang

29. Position Servo of Volume Holographic Disc by Self-Diffraction Signal
Po-Kai Hsieh

30.Optimal Angle of Tilted Plane for Diffraction Fields Generated by Diffractive Optical Elements Using Angular Spectrum Method
Shang-Hao Huang

31. Synthesis of PMMA/EGPEA Holographic Materials
Sheng-Kai Juang

32. Comparisons of Scanning Methods of Pixelization Error Reduction Algorithm (PERA) for Design of Diffractive Optical Elements
Shih-Chih Lin

33. Optimization of Dynamic Range of Pixelization Error Reduction Algorithm (PERA) for Design of Diffraction Optical Elements
Shih-Chih Lin

34. Optical data storage using volume polarization hologram
Shiuan Huei Lin

35. Scale Correction of Lens-Less Fourier Digital Holographic Microscope Based on Rayleigh-Sommerfeld Diffraction Integral
Shun Kashiwagi

36. A Simply Fabricating Technique for 3D Woodpile Photonic Crystal Structure
Shu-Yu Chen

37. Projected Fringe Profilometry using Binary-encoded Fringes
Sih-Yue Chen

38. Sub-micron resolution in graphene oxide doped PDLC layer combined with inorganic photorefractive crystal
Stefan Petrov

39. Generation of Depth-Cue-Added Holographic Stereogram with Look-up-Table Method
Sung-Lin Lu

40. Generation of Doughnut Mode Beam from Volume Holographic Optical Element
Sunil Vyas

41. Study of coherence wave using lensless Fourier transform holography
Sunil Vyas

42. Focus error signal obtained at the far-field from a rotational disc and measurement of its positional dependency
Teruo Fujita

43. Shift Multiplexed Recording in Holographic Data Storage Based on a Computer-generated Hologram with a Conical Wave
Teruyoshi Nobukawa

44. Ultra High Speed Printing of Large Size Holographic Optical Elements for Solar Power Generation Window Module
Tomoyasu Saigo

45. 1mm-thick See-through Holographic Lighting Unit ~ Ega-rim ~
Toshihiro Kasezawa

46. Wide wavelength range of Holographic Window for Solar Power Generation ~ Holo-Window II ~
Toshihiro Kasezawa

47. Study of 3D Human Face Imaging and Identification With Projection Grating Fringe
Wei-Wen Ni

48. Holographic Image Reconstruction in front of polarization-dependent Diffuser
Wen-Kai Lin

49. Generating 3D Photonic Crystal Structure by Holographic Lithography
Wen-Tse Shih

50. Photopolymerizable Silica using Ionic Liquids as Solvents by Sol-Gel Process
Xin-De Xie

51. Mirror-assisted Tomographic Phase Microscopy
Xing-Chen Liu

52. Resolution enhancement of digital holographic microscopy based on structured-illumination induced moiré fringes
Xin-Ji Lai

53. Synthetic aperture common-path digital holographic microscopy based on spiral phase filter
Xin-Ji Lai

54. GPU Implementation of Phase Retrieval with Fourier Transform
Yang-Hsien Lin

55. Single Light Source Tracking Method for Collinear Holographic Data Storage System
Yawara Kaneko

56. Scanning Projected Fringe Profilometry for Shape Measurements
Yi-An Lin

57. Multiwavelength Meta-hologram
Yi-Chieh Lai

58. Spatial and temporal imaging in digital holographic microscopy for quantitative analysis
Yu-Chih Lin

59. The Implementation of Real-Time Tracking and Time Reversal of Random Scattering in Diffused Media Based on Kitty Self-Pumped Phase Conjugate Mirror
Yu-Heng Chen

60. Multi-Layered Holographic Memory using Virtual Phase Conjugation
Yuta Goto

61. Panoramic 3-D Image Projection Using Computer Generated Phase-Only Hologram
Yu-Ting Wang

01.

One-Shot Incoherent Complex Imaging by State-multiplexed Fourier Ptychography

Byounghyo Lee, Jong-Young Hong, Jaebum Cho, and Byoungho Lee*
School of Electrical and Computer Engineering, Seoul National University, Gwanak-gu Gwanakro 1, Seoul 08826, South Korea
byoungho@snu.ac.kr

1. Introduction

Fourier ptychography (FP) is a recently developed microscopic imaging that can recover intensity as well as phase of the object by a set of variably illuminated images [1-3]. Compared with other phase retrieval method such as digital holography, FP has several advantages such as simple optical system and incoherent light sources [4]. However, the crucial disadvantage of FP is to require a lot of intensity images, which induces a long acquisition time. The use of lens array has been suggested to solve the problem in the field of ptychography [2]. Although they also mentioned the applicability of their method to the FP, the detailed reconstruction method and the algorithm is insufficient [2]. In this paper, we propose the concept of reconstruction method and structure to retrieve phase information with FP algorithm using lens array. The proposed system is verified by simulations.

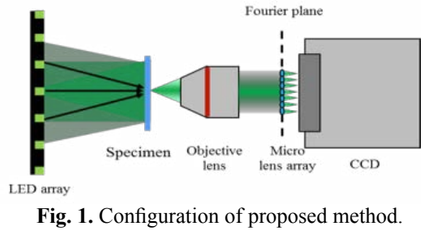

Fig. 1. Configuration of proposed method.

2. Principle and results

Figure 1 displays a configuration of proposed system. A micro lens array is placed at the Fourier plane of the objective lens and the charge coupled device (CCD) is located at the back focal plane of the micro lens array. Each micro lens transforms the different area of Fourier plane and generates a sub-image corresponding to Fourier transform of the area. A captured image consists of the sub-images without overlapping [5]. The sub-images can be used for FP because they include the different spectral information of the specimen. In other words, each sub-image corresponds with the captured image illuminated by the light emitting diode (LED) in conventional FP. When we use one LED, however, the complex information of specimen cannot be reconstructed because the sub-images are not overlapped in Fourier plane, which is essential requirement in FP [1, 3]. Therefore, the specimen is illuminated by multiple LEDs simultaneously to acquire spectrally overlapped images. The obtained image represents incoherent summations of images corresponding to each different illumination by LED in such a situation. Also, it has been known that the summations can be decomposed by state-multiplexed FP recovery algorithm [3]. Therefore, the summations of images can be separated by applying the algorithm to our system, and the decomposed sub-images which are overlapped in Fourier plane can be used to reconstruct the complex information of specimen by FP. We validated the system with simulations. Wavelength was 630 nm, an effective pixel pitch was 2.25 μm, and an objective

lens NA was 0.14 in this simulations. We used nine LEDs placed 6.8 mm under the specimen and the distance between LEDs is 6 mm. Figure 2(c) shows the Fourier spectrum of specimen which is incoherent summations of each spectrum corresponding to the different illuminations. The region of red box in Fig. 2(c) is summations of nine red boxes in Fig. 2(d). The distance between each box determines the part of overlapped area of decomposed images on Fourier plane, and is given by

$$\delta_{fx} = \frac{1}{\lambda}\sin\theta \tag{1}$$

where λ is wavelength and θ is given by the location and gap of LEDs. The simulation results of reconstructed amplitude and phase are shown in Figs. 2(g) and 2(h). From the results, it is verified that the proposed method is able to recover the complex information of specimen from a captured image.

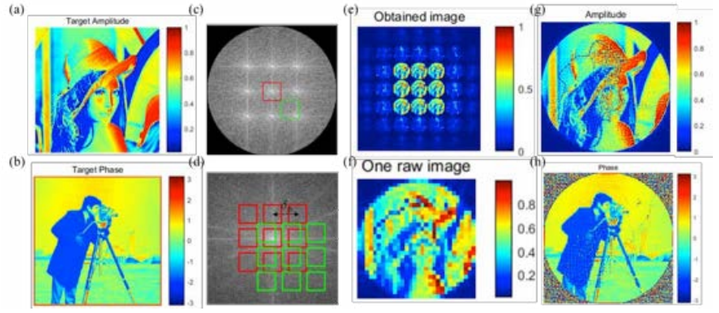

Fig. 2. Simulation results. (a), (b) The input amplitude and phase images. (c), (d) Fourier spectrum of specimen by proposed method. (d) Original Fourier spectrum of specimen (ground truth). (e) The obtained image. (f) The one raw sub-image of obtained image. (g), (h) The reconstructed amplitude and phase images.

3. Conclusion

We propose a new method of complex imaging microscopy by state-multiplexed FP. It has several advantages such as using incoherent light sources and simple optical system. And above all, it provides one-shot phase image. The simulation results show the feasibility of the system.

Acknowledgement

This research was supported by Projects for Research and Development of Police science and Technology under Center for Research and Development of Police science and Technology and Korean National Police Agency. (PA-H000001)

Reference:

[1]G. Zheng, R. Horstmeyer, and C. Yang, “Wide-field, high-resolution Fourier ptychographic microscopy,” Nat. Photonics **7**, 739-745 (2013).
[2] P. Sidorenko and O. Cohen, “Single-shot ptychography,” Optica **3**, 9-14 (2016).
[3] S. Dong, R. Shiradkar, P. Nanda, and G. Zheng, “Spectral multiplexing and coherent-state decomposition in Fourier ptychographic imaging,” Biomed. Opt. Express **5**, 1757-1767 (2014).
[4] Zhang, Tong, and I. Yamaguchi. “Three-dimensional microscopy with phase-shifting digital holography,” Opt. Lett. **23**, 1221-1223 (1998).
[5] J.-Y. Hong, J. Yeom, J. Kim, S.-g. Park, Y. Jeong, and B. Lee, “Analysis of the pickup and display property of integral floating microscopy,” Journal of Information Display 16, 143-153 (2015).

02.

Optical Scanning Holographic Microscopy

Cheng-Hao Tsou,[1] and Jung-Ping Liu [1]

[1] Department of Photonics, Feng Chia University, 100 Wenhwa Rd., Seatwen, Taichung 40724, Taiwan

1. Introduction

Optical Scanning Holography (OSH) is a kind of digital holography [1]. In OSH, a frequency shift is introduced to one of two mutual coherent light to generate a dynamic interference fringe, which is applied to two- dimensionally (2D) scan a three-dimensional (3D) object. The heterodyne scattered light of the 3D object is collected by the photodetector and generates a current output. We use Spatial-temporal Demodulation Technique (STDT) to demodulate the heterodyne signals in the current output [2]. OSH is able to acquire the hologram of fluorescent object because it can be operated in the incoherent mode. The conventional digital holography applies a CCD to acquire interference fringes, and thus the resolution of acquired digital hologram is limited by the CCD. In contrary, the image resolution of OSH can be better than conventional ones as the image resolution of OSH depends on the scanning speed and the time interval of the acquisition. In addition, OSH can be also applied to microscopy [3], spatial coherence analysis [4], sectional image reconstruction [5] and holographic encryption [6]. Therefore, OSH is a holographic technique with tremendous potential. Here we will demonstrate to apply OSH to record a fluorescence hologram of micro specimen.

2. Optical scanning holographic microscopy

Figure 1 is the schematic setup of optical scanning holographic microscopy (OSHM). We used a diode-pumped solid-state laser (λ_0=532.5nm) as the source. A laser beam passes through polarizing beam splitter (PBS) and is separated into two. We used half-wave plate (HWP) to rotate the reflected beam from s-polarized into p-polarized and coupled the beam into optical fiber 1 (OF1). When the transmitted beam passes through the electro-optic modulator (EOM), the frequency of the beam is shifted by Ω and then coupled into optical fiber 2 (OF2). The lights emitted from the other ends of the two fibers are respectively manipulated into a plane wave and a spherical wave, and are recombined by a beam splitter (BS). The beam is projected to the specimen, which is mounted on a 2D piezoelectric transducer (PZT). A dichroic mirror (DM) and a long-pass filter (LPF) are used to filtering out the pumping laser light. The fluorescent light emitted from the specimen is collected by lens 3 (L3) and lens 4 (L4), and detected by the photomultiplier 1 (PMT1) and photomultiplier 2 (PMT2), for obtaining a transmission hologram and a reflection hologram, respectively. We sent the signal into personal computer (PC) by analog-to-digital convertor (ADC). Finally, we used STDT to demodulate the raw data.

The hologram recorded in the transmission mode can be expressed as [7]

$$H(x,y)=\int h^{*}(x,y;z)\otimes T(x,y,z)dz \tag{1}$$

where ⊗ denotes correlation operation; $h(x,y;z)$ represents the point spread function (PSF), and is expressed as

$$h(x,y;z)=\exp\left[\frac{-jk}{z}\left(x^{2}+y^{2}\right)\right]; \tag{2}$$

$T(x,y,z)$ denotes the amplitude transmittance of the object target.

3. Experimental Results and Conclusion

We first measured the resolution of the OSHM by recording a hologram of pinhole with diameter

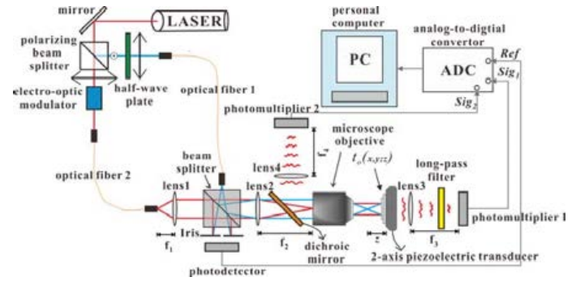

Fig. 1. Schematic of optical scanning holographic microscopy.

1μm (not shown). The estimated lateral resolution (Δx) and longitudinal resolution (Δz) are 0.78μm and 3.1μm , respectively. Subsequently, we recorded a reflection hologram of fluorescent beads, whose peak exciting wavelength is 533nm and peak emitting wavelength is 575nm. The hologram and its reconstructed image are shown in Fig. 2. We can see the reconstructed image in the Fig.2(c) are blurred. This is because the signal excited by fluorescence is very weak. In the future, we will optimize the system and increase the signal to noise ratio. This work is supported by Ministry of Science and Technology of Taiwan, R.O.C. under contract number 103-2221-E-035-037-MY3.

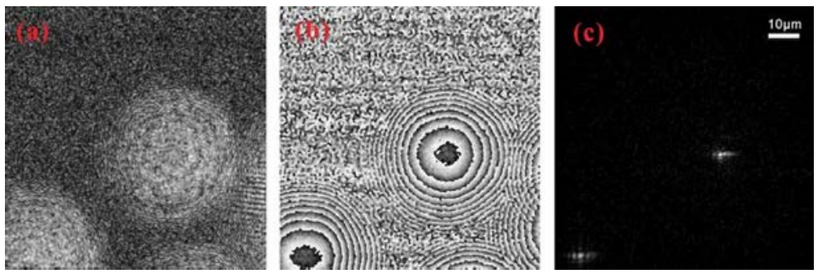

Fig. 2. (a) Amplitude, and (b) phase modulus 2π of the hologram of fluorescent beads. (c) Reconstructed image of the hologram at $z = 56\mu m$.

Reference:

[1] T.-C. Poon, Optical scanning holography with MATLAB, Springer, 2007.

[2] J.-P. Liu, D.-Z. Luo and S.-H. Lu, "Spatial–temporal demodulation technique for heterodyne optical scanning holography," Opt. Laser Eng. **68**, 42-49, 2015.

[3] J.-P. Liu, "Spatial coherence analysis for optical scanning holography," Appl. Opt. **54**, A59-A66, 2015.

[4] G. Indebetouw, A. E. Maghnouji, and R. Foster, "Scanning holographic microscopy with transverse resolution exceeding the Rayleigh limit and extended depth of focus," J. Opt. Soc. Am. A **22**, 892-898, 2005.

[5] E. Y. Lam, X. Zhang, H. Vo, T.-C. Poon and G. Indebetouw, "Three-dimensional microscopy and sectional image reconstruction using optical scanning holography," Appl. Opt. **48**, H113-H119, 2009.

[6] Y. Shinoda, J.-P. Liu, P.-S. Chung, K. Dobson, X. Zhou, T.-C. Poon, "Three-dimensional complex image coding using a circular Dammann grating," Appl. Opt., **50**, 838-845, 2011.

[7] T.-C. Poon and J.-P. Liu, Introduction to modern digital holography with MATLAB, Cambridge University Press, 2014.

03.

Image Arrangement for Quasi-dynamic Display of Three-dimensional Image in Disk-type Multiplex Holograms

Chih-Hung Chen and Yih-Shyang Cheng
Department of Optics and Photonics, National Central University, Chungli 32001, Taiwan

1. Introduction

Multiplex holography which combines off-axis holography and photography was first proposed by DeBitetto in 1969 [1], and it was developed into various types, including the cylindrical type, the conical type, and the disk type [2]. L. Cross developed the cylindrical-type multiplex hologram with its image appeared at the center of the cylinder and then Japanese scientists invented the conical holographic stereogram [3,4]. However, traditional holograms practically are composed of a series of long thin individual holograms which inevitably cause the reconstructed images overlaid with a fence structure. Recently, image-plane method has been designed to solve this problem, the so-called "picket-fence effect" [5-7]. We have developed image-plane disk-type multiplex holograms (IPDTMH) for both normal viewing and walk-around viewing [8-10]. Recently, optical copying system for these kinds of holograms was proposed to obtain high diffraction efficiency for multiple-exposure holograms [11,12]. Based on the planar-shaped recording and copying processes, this technique shows the distinguishing capability for duplication of the disk-type multiplex holograms.

In this paper, theoretical simulation and holographic process for making an IPDTMH are introduced. Proper spatial division of recoding area in a hologram disk is then illustrated for quasi-dynamic-image generation.

2. Concept, theory, and parameter design

To achieve an animation display in image-plane disk-type multiplex holography, we need to divide the recording area on a hologram disk into several portions (A_1~A_n), as shown in Fig. 1. Each portion contains M individual holograms for displaying a 3D image of one status belonging to our original object. In order to avoid image overlapping caused by two recording regions, we also need to design a proper interval between two adjacent recording sections.

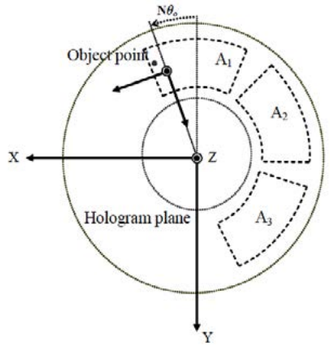

Fig. 1. Recording-area arrangement on the holographic recording plane.

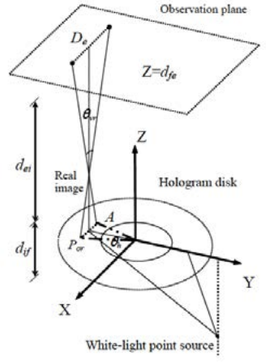

Fig. 2. Geometry of three-dimensional image display in an IPDTMH.

Adopting proper rotating speed for our hologram disk, we here introduce seven motions for generating a quasi-dynamic real image (Fig. 2). Our holographic process, including image reconstruction and optical recording can be described with the aid of Fig. 2 [10], and the finished IPDTMH is suitable for white light illumination. In numerical analysis, we can then theoretically find out the suitable parameters for fabricating this kind of hologram, including hologram number N_h as seen by one eye of an observer and the angle θ_r between two interfering beams.

3. Conclusion

Adopting normal-viewing image-plane disk-type multiplex holography, we introduce the arrangement of different frames on holographic recording plane. This technique can be extended to fabricate various formats of multiplex holograms. However, suitable number of frames and rotating speed of hologram need to be adjusted for better performance for this quasi-dynamic display and is worthy of further investigation.

Reference:

[1] D. J. DeBitetto, "Holographic panoramic stereograms synthesized from white light recordings," Appl. Opt. **8**, 1740-1741 (1969).
[2] Y. S. Cheng, W. H. Su, and R. C. Chang, "Disk-type multiplex holography," Appl. Opt. **38**, 3093-3100 (1999).
[3] G. Saxby, Practical Holography, 2nd ed. (Prentice-Hall, Englewood Cliffs, N.J., 1994).
[4] K. Okada, S. Yoshii, Y. Yamaji, J. Tsujiuchi and T. Ose, "Conical holographic stereograms," Opt. Commun. **73**, 347-350 (1989).
[5] Y. S. Cheng and R. C. Chang, "Image-plane cylindrical holographic stereogram," Appl. Opt. **39**, 4058-4069 (2000).
[6] Y. S. Cheng and C. M. Lai, "Image-plane conical multiplex holography by one-step recording," Opt. Eng.**42**, 1631-1639 (2003).
[7] Y. S. Cheng and C. H. Chen, "Image-plane disk-type multiplex hologram," Appl. Opt. **42**, 7013-7022 (2003).
[8] C. H. Chen, Y. S. Cheng, and Z. Y. Lei, "Single-beam copying system of 360-degree viewable image-plane disk-type multiplex hologram and polarization effects on diffraction efficiency," Opt. Exp. **15**, 10804-10813 (2007).
[9] Y. S. Cheng, Y. T. Su, and C. H. Chen, "360-degree viewable image-plane disk-type multiplex holography by one-step recording," Opt. Exp. **18**, 14012-14023 (2010).
[10]C. H. Chen and Y. S. Cheng, "Image design for normal viewing image-plane disk-type multiplex," Chin. Opt. Lett. **9**, 1200031-1200033 (2011).
[11]Y. S. Cheng, C. H. Chen, and Y. C. Hsieh, "Reflection disk-type multiplex holography using two-step recording," Jpn. J. Appl. Phys. **47**, 7173-7181 (2008).
[12]C. H. Chen and Y. S. Cheng, "Design of copying system for reflection disk-type multiplex hologram," Jpn. J. Appl. Phys. **50**, 09ME091-09ME093 (2011).

04.

Virtual-image Replication from a Real-image Master in 360-degree Viewable Disk-type Multiplex Holography

Chih-Hung Chen and Yih-Shyang Cheng
Department of Optics and Photonics, National Central University, Chungli 32001, Taiwan

1. Introduction

The concept of wavefront reconstruction was first invented by Gabor [1]. Rainbow hologram was proposed by Benton [2] and this technique makes it possible to display 3D images under white-light illumination. Multiplex holography, which combines rainbow holography and photography, was initiated by DeBitetto [3]. This technology then have been widely applied to several formats of multiplex holography, including the planar type, the cylindrical type [4], the conical type [5], and the disk type [6]. Image-plane disk-type multiplex holograms (IPDTMHs), which has the advantage of commercial mass production using the well-developed CD technology, was first proposed for the display type of normal viewing [7]. We have then developed IPDTMH for 360-degree viewable display [8]. Based on these two types of IPDTMHs, both virtual image and real image can be generated [9-10].

In order to obtain multiplex hologram with higher performance, two-step holographic process for the fabrication of IPDTMHs was developed in recent years [11-14]. In this paper, design of the optical setups for holograms replication of the 360-degree viewable IPDTMH is introduced. A simple optical replication system for virtual-image generation and preliminary experimental result are then demonstrated.

2. Image Display in a 360-degree Viewable Disk-type Multiplex Hologram

The left side of Fig. 1 indicates a real-image generation condition for an IPDTMH. Generally, a plane wave W_{RM} is used to generate 3D cube information from hologram H_1. Observers at d_{fe} away from H_1 can see a real image floating above the disk plane (W_{IM}). Right side of Fig. 1 is illustrated for virtual-image generation condition, in which a point source is adopted to produce the reconstruction reference beam W_{RT} (dotted line). In this observation condition, observers will see an image appearing underneath the hologram disk (W_{IT}). For mass-production application, a two-step holographic process for image transformation will be described in the next section.We will also propose a novel copying system for virtual-image generation.

3. Two-step Holographic Recording and the Experimental Result

Referring to Fig. 1, the left-side system nearby Lens L can be utilized for making a non-image-plane disk-type multiplex hologram, in which image plane is shifted to final recording film (H_2) for virtual-image display. The finished hologram is a real-image type master H_1.We here note that H_{2R} and H_{2V} planes are also the suitable candidates for H_2 plane in holographic copying.

A final recording film is designed to be on the H_2 plane, where image plane is situated.Object beam W_{OT} (dashed line) for holograms replication is generated from H_1 by illuminating with a reconstruction reference beam W_{RM}. The 2D information is finally imaged onto the film plane (H_2). A coherent reference beam W_{CT} is introduced with a lens L to form a diverging wave and propagates to the recording-film plane. Then a hologram for virtual-image generation can be obtained. Figure 2 shows one view of the reconstructed image from our transfer hologram (H_2).

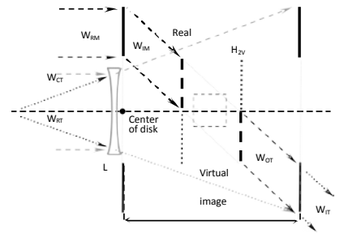

Fig. 1. Schematic diagram for real-image and virtual-image generation in a 360-degree viewable IPDTMH.

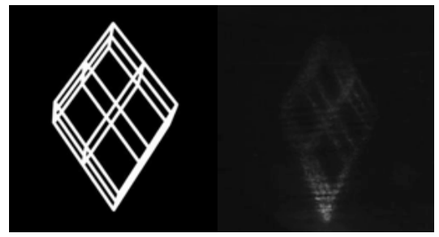

Fig. 2. Original simulated cube image and the experimentally reconstructed image from our duplicated hologram.

4. Conclusion

In this study, a two-step holographic process for the fabrication of a disk-type hologram is described. The first-step fabrication process is designed for real-image type master hologram and the second one is set for virtual-image type transfer hologram. By shifting the recording plane for the master hologram of real-image generation, optical setup of holographic replication for virtual-image display is introduced. Using a concave lens, simple optical systems for holographic replication of virtual-image displaying is also presented. Based on the copying method with one-shot recording described in this study, we can improve the optical performance of the duplicated holograms.

Acknowledgment:

Thanks are given to Meng-Ju Chen, Wan-Ting Hsieh, and Yuan-Ping Sung for performing optical experiment to obtain the image of Fig. 2.

Reference:

[1] D. Gabor, “A new microscopic principle,” Nature **161**, 777-778 (1948).
[2] S. A. Benton, “Hologram reconstructions with extended light sources,” J. Opt. Soc. Amer. **59**, 1545-1546 (1969).
[3] D. J. DeBitetto, “Holographic panoramic stereograms synthesized from white light recordings,” Appl. Opt. **8**, 1740-1741 (1969).
[4] L. Cross, “The multiplex technique for cylindrical holographic stereograms,” Proc. SPIE (1977).
[5] K. Okada, S. Yoshii, Y. Yamaji, and J. Tsujiuchi, “Conical holographic stereograms,” Opt. Commun. **73**, 347-350 (1989).
[6] Y. S. Cheng, W. H. Su, and R. C. Chang, “Disk-type multiplex holography,” Appl. Opt. **38**, 3093-3100 (1999).
[7] Y. S. Cheng and C. H. Chen, “Image-plane disk-type multiplex hologram,” Appl. Opt. **42**, 7013-7022 (2003).
[8] Y. S. Cheng, Y. T. Su, and C. H. Chen, “360-degree viewable image-plane disk-type multiplex holography by one-step recording,” Opt. Express **18**, 14012-14023 (2010).
[9] C. H. Chen and Y. S. Cheng, “Image design for normal viewing image-plane disk-type multiplex hologram,” Chin. Opt. Lett. **9**, 1200031-1200033 (2011).
[10]Y. S. Cheng, Z. F. Chen, and C. H. Chen, “Virtual-image generation in 360-degree viewable image-plane disk-type multiplex holography,” Opt. Express **21**, 10301-10313 (2013).
[11]C. H. Chen, Y. S. Cheng, and Z. Y. Lei, “Single-beam copying system of 360-degree viewable image-plane disk-type multiplex hologram and polarization effects on diffraction efficiency,” Opt. Express **15**, 10804-10813 (2007).
[12]Y. S. Cheng, C. H. Chen, and Y. C. Hsieh, “Reflection disk-type multiplex holography using two-step recording,” Jpn. J. Appl. Phys. **47**, 7173-7181 (2008).
[13]C. H. Chen and Y. S. Cheng, “Design of copying system for reflection disk-type multiplex hologram,” Jpn. J. Appl. Phys. **50**, 09ME091-09ME093 (2011).
[14]Y. S. Cheng and C. H. Chen, “Real-Image generation in normal viewing disk-type multiplex holography and design of replication method,” Jpn. J. Appl. Phys. **52**, 09LD101-09LD105 (2013).

05.

Improvement Of Collinear Holographic Storage System By Micro Lens Array

Yeh-Wei Yu[2], Chi-Hsien Yang[1], Shiuan-Huei Lin [3] and Ching-Cherng Sun[1]

[1]Department of Optics and Photonics, National Central University, Chung-Li, Taoyuan City 32001, Taiwan

[2]Optical Science Center, National Central University, Chung-Li, Taoyuan City 32001, Taiwan

[3]Department of Electrophysics, National Chiao Tung University, HsinChu 30010, Taiwan

Summary

The era of big data is followed by high demand of data storage, which is challenging current storage technologies. Holographic data storage is reckoned as one of the best solutions of cold data storage due to its ability to optical-parallel readout, store data in high density and resist EM pulse. Among technologies of holographic data storage, the collinear holographic data storage is less complicate to set up compare to off-axis holographic data storage, and is easy to miniaturize. However, collinear system has extremely strong DC term on the Fourier plane. It causes high M/# consumption, and thus the shift-multiplexing ability is limited and the storage capacity is reduced. High M/# consumption can even decrease the uniformity of readout signal.

In this paper, we propose a method using micro lens array to remove the strong DC term in Fourier plane. Figure 1 shows the schematic diagram of general collinear data storage system. The incident plane wave passes through the spatial light modulator (SLM) and carries on the signal to record, and is imaged by the 4-f system to the front focal plane of objective lens, and then focus onto recording media. During the recording process, the SLM generates a signal including a ring of reference beam and signal beam in the central area (figure 2). These two beams are focused onto the recording media and recorded by the media. In the reading process, SLM only generates reference beam to reconstruct signal beam. The reconstructed signal beam is then captured by CCD. The experimental result is shown in figure 3. Because of the strong DC term, the result image is not uniform and hence impossible to decode. We add a micro lens array into this system to reduce strong DC term in Fourier plane. The lens array on the SLM plane is to modulate the phase distribution of the signal and reference beam. As a result of phase modulation, the uniformity of reconstructed image is increased (figure 4). On the other hand, as the light pass through lens array twice, the image is a bit distorted by the border of each micro lens on lens array, so the result image is hard to locate and thus hard to decode. Decoding result shows that the bit error count is 852, and bit error rate is 4.42 %. To correct this issue, we add a 4-f system to image the phase distribution onto SLM plane (figure 5). The result image is shown in figure 6. The bit error count is 316, and the bit error rate is 1.63%. By this method, we can not only remove the DC term in Fourier plane to enhance the uniformity of reconstructed signal but also remain high image quality.

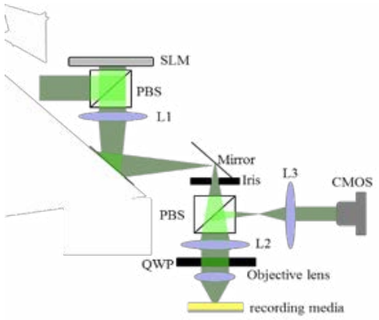

Fig. 1. schematic diagram of general collinear system

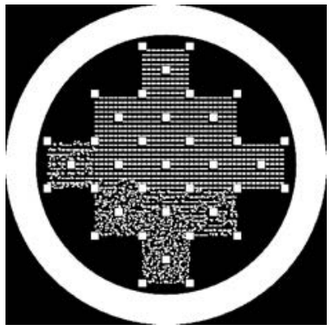

Fig. 2. the input signal

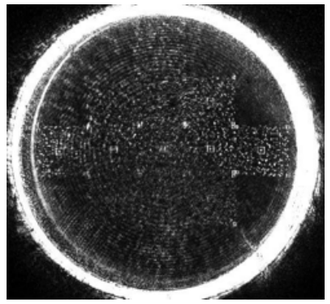

Fig. 3. result image (general system)

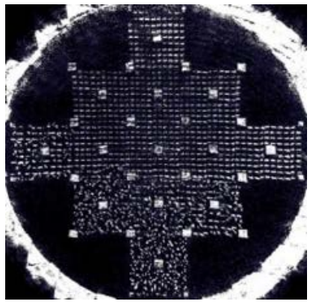

Fig. 4. result image (lens array attached on SLM)

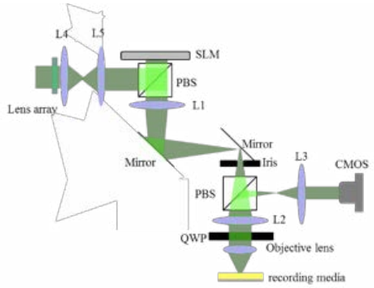

Fig. 5. schematic diagram (image lens array onto SLM plane)

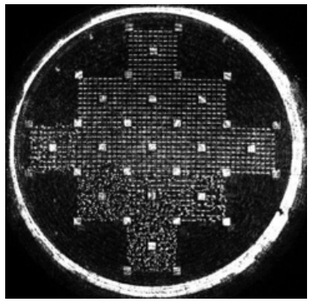

Fig. 6. result image (lens array imaged on SLM)

Acknowledgment:

The holographic recording media PQPMMA is supported by Prof. Shiuan-Huei Lin.

Reference:

[1] H. Horimai and J. Li, “A novel collinear optical setup for holographic data storage system,” in Proc. of SPIE 5380, 297–303 (2004).

[2] Y. W. Yu, C. Y. Chen, and C. C. Sun, “Lens array reference modulation in Collinear VHS,” IWH2012 Digest, 13A3 (2012).

[3] K. Curtis, L. Dhar, A. Hill, W. Wilson, and M. Ayres, *Holographic Data Storage: From Theory to Practical Systems* (Wiley, 2010)

06.

Polarization-switchable Meta-hologram with Dual Images

Chun Yen Liao[1)], Wei-Yi Tsai[1)], Yao-Wei Huang[2)], Pin Chieh Wu[1),2)], Cheng Hung Chu[2)], Hui Jun Wu[2)], Shulin Sun[3)], Lei Zhou[4)], Ai Qun Liu[5)], Chih-Ming Wang[6)], Greg Sun[7)], and Din Ping Tsai[1),2)]

[1)]Department of Physics, National Taiwan University, Taipei 10617, Taiwan [2)]Research Center for Applied Sciences, Academia Sinica, Taipei 11529, Taiwan [3)]Department of Optical Science and Engineering, Fudan University, Shanghai 200433, China

[4)]State Key Laboratory of Surface Physics and Key Laboratory of Micro and Nano Photonic Structures (Ministry of Education), Fudan University, Shanghai 200433,China

[5)]School of Electrical and Electronic Engineering, Nanyang Technological University, Singapore 639798, Singapore

[6)]Institute of Opto-electronic Engineering, National Dong Hwa University, Hualien 97401, Taiwan

[7)]Department of Engineering, University of Massachusetts Boston, Boston, Massachusetts 02125, United States

1. Introduction

Holograms, the optical devices to reconstruct pre-designed images, have been advanced dramatically with the development of today's nanotechnology [1, 2]. However, applications of hologram are still limited by the constituent materials, and their working range is rather narrow. In the past decade, metamaterials/metasurfaces composed of sub-wavelength artificial structures show tailored optical properties within flat optics in electromagnetic regions [3-5], such advances have led to demonstration of ultrathin invisibility [6], lens [7], wave plates [8], nonlinearity generation [9], et al. The spatial phase and amplitude modulation of metasurfaces exhibits a good candidate to achieve the spatial light modulators (SLM) [10] and plays a good candidate to realize the polarization-controlled dual images at arbitrary electromagnetic wave region in referred to as broadband metasurface hologram or metahologram [11-13]. In this paper, we report the high-efficiency and broadband meta-hologram consisted of plasmonic metamaterials, which functions for both coherent and incoherent light sources within a broad spectral range under a wide range of incidence angles [14].

2. Results and Discussions

We perform a high-efficiency broadband reflective meta-hologram in 4-level phase which is designed and fabricated in optical frequencies. There are 16 different nanocross pixels distributed on the meta-hologram sample because of the 16 combinations with 4 different length gold nanorods for each image. To characterize the performance of the fabricated meta-hologram, we use 780 nm diode laser as well as white light source to characterize the reconstructed images of proposed plasmonic meta-hologram. Figure 1(a) shows the schematic diagram of the functionalities of our designed metahologram under 45º linearly-polarized illumination. Figures 1(b) to 1(d) present three experimental reconstructed images of the meta-hologram under x-, 45º- and y-polarized incidence at wavelength λ = 780 nm, respectively. The projected patterns are selectively produced as "NTU" for x-polarization and "RCAS" for y-polarization incident light, and the intensities of two non-overlap patterns will be rise and fall according to the polarization, which is in excellent agreement with the design. For both x- and y-polarized incidence, the measured polarization contrasts are ~ 20 (the averaged intensity of "NTU" divided by the intensity of "RCAS" in the case of x-polarized illumination), confirmed the polarization-selective ability of our device. Furthermore, the reconstructed images of meta-hologram exhibit far more efficient (reaches 18% for 780 nm illumination).

3. Conclusions

We utilize the phase modulation at plasmonic resonance of gold cross nanoantennas to record two polarization-controlled images on a meta-hologram. Our meta-hologram is reflective type with significantly higher efficiencies than what have been designed and achieved so far using metamaterials. The reflective hologram has a number of advantages such as simple fabrication process, low metal absorption, broad working spectral range, and greater tolerance to variation of incident angle and light incoherence. By combining with the techniques of tunable metasurfaces, meta-hologram can potentially be used to realize the active hologram that works at arbitrary electromagnetic wave region.

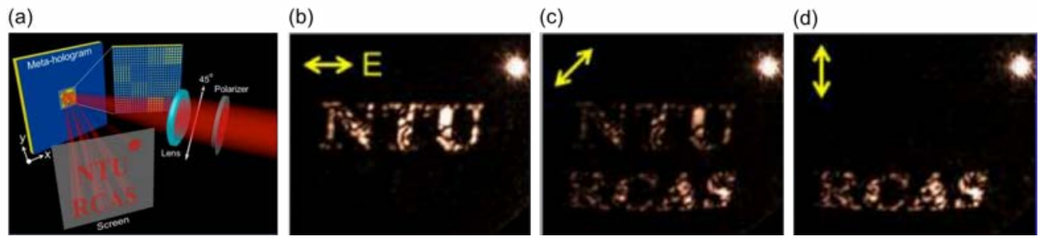

Figure 1. (a) The functionality of our designed meta-hologram under linearly-polarized illumination. Reconstructed images of meta-hologram for case of (b) x-polarized, (c) 45o-polarized, and (d) y-polarized incidence by a 780 nm laser.

Reference:

[1] D. Gabor, *Nature* **161,** 777-778 (1948).
[2] M. Ozaki et al., *Science* **332,** 218-220 (2011).
[3] S. Sun, et. al., *Nano Lett.* **12,** 6223-6229 (2012).
[4] N. Yu, et. al., *Nat. Mater.* **13,** 139-150 (2014).
[5] A. E. Minovich, et. al., *Laser Photon. Rev.* **9,** 195-213 (2015).
[6] X. Ni, et. al., *Science* **349,** 1310-1314 (2015).
[7] M. Khorasaninejad, et. al., *Nano Lett.* **16,** 4595-4600 (2016).
[8] F. Ding, et. al., *ACS Nano* **9,** 4111-4119 (2015).
[9] S. Chen, et. al., *Phys. Rev. Lett.* **113,** 033901 (2014).
[10] C. M. Watts, et. al., *Nat. Photon.* **8,** 605-609 (2014).
[11] D. Wen, et. al., *Nat. Commun.* **6,** 8241 (2015).
[12] M. Khorasaninejad, et. al., *Science Advances* **2,** e1501258 (2016).
[13] W. Ye, et. al., *Nat. Commun.* **7,** 11930 (2016).
[14] W. T. Chen, et. al., *Nano Lett.* **14,** 225-230 (2013).

07.

Design of writing patterns for multi-level self-referential holographic data storage by phase-only modulation

Daiki Murozono, Masanori Takabayashi, and Takashi Okamoto
Graduate School of Computer Science and Systems Engineering, Kyushu Institute of Technology, 680-4 Kawazu, Iizuka, Fukuoka 820-8502, Japan

1. Introduction

Self-referential holographic data storage (SR-HDS) is a new holographic recording technique, in which data can be holographically recorded and read without using a reference beam[1]. Since SR-HDS requires only a signal beam, a compact and stable optical system, compared with systems based on a two-beam geometry in which signal and reference beams are required, can be constructed. In our previous work, to improve the recording density, we showed that multi-level signal recording can be achieved by modulating not only the phase but also the amplitude of the writing beam, whereas only the phase distribution of the writing beam is modulated in basic SR-HDS[2]). However, the need for two spatial light modulators (SLMs) in multi-level SR-HDS introduces the challenges of high-precision alignment between the SLMs, beam power losses at the SLMs, and increased complexity of the optical system.

In this paper, we present a new realization method of multi-level SR-HDS, in which amplitude modulation of the writing beam is not required. Using the proposed method, multi-level recording can be realized by appropriately designing the phase distribution of the writing beam. First, we analytically clarify the conditions that should be satisfied for the writing beam. Next, we confirm that multi-level signal recording is possible by using the phase distribution designed based on the analytical result.

2. Self-Referential Holographic Data Storage

Figure 1 shows a conceptual diagram of SR-HDS. First, we consider the simplest case, in which only two pixels, P_1 and P_2, on the SLM function. Here, it is assumed that the phase modulation values at P_1 and P_2 during recording are ϕ_1 and ϕ_2, respectively, while they are both 0 during reading. When the hologram is illuminated by the reading beams, the amplitudes of the reading beams after passing through the hologram vary from each other. When the amplitude difference is defined as $\Delta A = A_1 - A_2$, ΔA is sinusoidally dependent on $\Delta\phi = \phi_1 - \phi_2$, as shown in Fig. 2. Therefore, after passing through the hologram, A_1 and A_2 can be written as follows:

$$A_1 = A_r + C_{12}\sin(\Delta\phi) \quad (1)$$

$$A_2 = A_r + C_{12}\sin(-\Delta\phi) \quad (2)$$

where A_r is the amplitude of the reading beam before it passes through the hologram. C_{12} is a coefficient that depends on the angle between two beams and the recording time, among other factors.

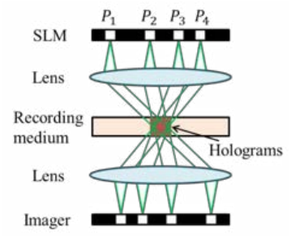

Fig. 1. Conceptual diagram of SR-HDS.

The principle when the pixels P_1, P_2, …, and P_n function can be regarded as the superposition of the case with two pixels. Therefore, under the assumption of negligible inter-pixel crosstalk, the amplitude of the i-th pixel A_i, can be approximated by

$$A_i = A_r + \sum_{i\neq j}^{n} C_{ij}\sin(\Delta\phi_{ij}) \quad (3)$$

where C_{ij} and $\Delta_{\phi ij}$ are the coefficients associated with the interaction between i-th and j-th pixels and the phase difference during recording between i-th and j-th pixels, respectively. From this equation, it is found that the output amplitudes, i.e. output intensities, of the pixels can be controlled by designing the phase values of the writing pixels. In other words, multi-level SR-HDS can be realized by phase-only modulation by designing the phase distribution of the writing beam such that the output amplitudes are different from each other.

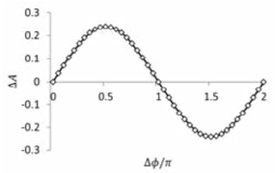

Fig. 2. Numerical simulation result of the relationship between ΔA and $\Delta\phi$.

3. Results

In this section, we clarify how the phase values of the writing pixels should be chosen so that the amplitudes of these pixels after the beam passes through the hologram are dependent on the phase distribution. For simplicity, we consider the case in which the datapage modulated to the writing beam consists of only four pixels and they have phase values of ϕ_1, ϕ_2, ϕ_3, and ϕ_4. Here, it is assumed that the coefficients C_{ij} are independent of both i and j. To determine the phase values ϕ_1, ϕ_2, ϕ_3, and ϕ_4, we define the minimum amplitude difference A_{MIN} as

$$A_{MIN} = \min\{|Ai - Aj|\}\ (i,j = 1,2,3,4, i \neq j) \quad (4)$$

First, we vary ϕ_1, ϕ_2, ϕ_3, and ϕ_4 from 0 to 2π in steps of 0.05π and calculate A_{MIN}. When $A_{MIN} \neq 0$, the amplitudes of these four pixels have four different values, i.e., multi-level recording is successfully realized. However, when $A_{MIN} = 0$, multi-level recording is not possible. Here, it should be noted that the greater the A_{MIN}, the better the reading quality that can be achieved. Figure 3 shows some combinations of the writing phases, ϕ_1, ϕ_2, ϕ_3, and ϕ_4, obtained by the analysis. We find that when the phases, $\{\phi_1, \phi_2, \phi_3, \phi_4\}$, satisfy the conditions of $\{0, \theta, \pi, \theta+\pi\}$ or $\{0, \theta, 2\theta, \theta+\pi\}$ $(0 < \theta < \pi)$, A_{MIN} becomes 0. In other words, multi-level SR-HDS can be realized when the signal phases do not satisfy these conditions.

Next, we confirm that the conditions clarified in the analysis are usable for multi-level SR-HDS even when the number of pixels is greater than four. In the following numerical simulation, the datapages have 64×64 pixels. In addition, the writing beam includes the four-level phases ϕ_1, ϕ_2, ϕ_3, and ϕ_4. Figures 4(a) and (b) show the histogram of the readout intensity distribution when the writing beam consists of the pixels with phase values $\{0, 0.5\pi, \pi, 1.5\pi\}$ and $\{0, 0.25\pi, 0.45\pi, 0.7\pi\}$, respectively. As we predicted, multi-level recording cannot be achieved when the writing phases, ϕ_1, ϕ_2, ϕ_3, and ϕ_4, satisfy the condition of $\{0, \theta, \pi, \theta+\pi\}$. It should be noted that we also confirmed that multi-level recording cannot be achieved when ϕ_1, ϕ_2, ϕ_3, and ϕ_4 satisfy the condition of $\{0, \theta, 2\theta, \theta+\pi\}$. As a result, it is shown that multi-level recording is possible without using amplitude modulation in SR-HDS, unless the writing phases satisfy the conditions that we have specified.

	ϕ_1	ϕ_2	ϕ_3	ϕ_4
$A_{MIN} = 0$	0	0.25π	0.5π	1.25π
	0	0.5π	π	1.5π
	0	0.3π	0.6π	1.3π
	0	0.45π	0.9π	1.45π
Maximum A_{MIN}	0	0.25π	0.45π	0.7π

Fig. 3. Example of the phase values when A_{MIN} is 0 and A_{MIN} is maximized.

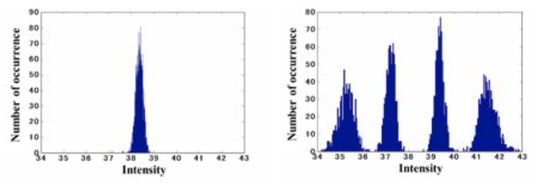

(a) (b)

Fig. 4. Histogram of four-level readout signal.
(a)Phases of the writing beam are 0, 0.5π, π, and 1.5π.
(b)Phases of the writing beam are 0, 0.25π, 0.45π, and 0.7π.

4. Conclusions

We investigated the conditions that the phase distribution of the writing beam should satisfy for multi-level SR-HDS. As a result of numerical analysis, we found that the phases of the writing beam must not satisfy $\{\phi_1, \phi_2, \phi_3, \phi_4\} = \{0, \theta, \pi, \theta+\pi\}$ or $\{0, \theta, 2\theta, \theta+\pi\}$ for four-level SR-HDS. In the future, we will investigate the conditions that should be satisfied in the case of other numbers of signal levels.

Reference:

[1] Masanori Takabayashi and Atsushi Okamoto, "Self-referential holographic and its applications to data storage and phase-to-intensity conversion," Opt. Express, **21**, 3669–3681 (2013).
[2] Masanori Takabayashi, Atsushi Okamoto, Masatoshi Bunsen and Takashi Okamoto, "Multi-level self-referential holographic data storage," ISOM'12 Technical Digest, 12–13 (2012).

08.

Differential Equations for Volume Hologram with Coordinate Conversion

Daisuke Barada[1,2] and Toyohiko Yatagai[2]

[1]Graduate School of Engineering, Utsunomiya University, 7-1-2 Yoto, Utsunomiya, Tochigi 321-8585, Japan

[2]Center for Optical Research and Education (CORE), Utsunomiya University, 7-1-2 Yoto, Utsunomiya, Tochigi 321-8585, Japan

1.Introduction

It is well-known that volume holograms are useful for diffractive optical elements, three-dimensional displays, and optical data storage with high data capacity. In theoretical analysis and numerical simulation for volume holograms, Kogelnik's coupled wave theory1) in general. However, a reconstructed beam is limited by the first order diffracted beam and polarization dependence is neglected in the theory because some approximation is used. In this study, a rigorous diffraction theory, in which polarization dependence is considerable, is proposed.

2.Theory

Maxwell's equations in the case of monochromatic light in Cartesian coordinate is represented by

$$\nabla \times \boldsymbol{E} = \mathrm{i}\omega\mu_0 \boldsymbol{H}, \tag{1}$$

$$\nabla \times \boldsymbol{H} = -\mathrm{i}\omega\varepsilon_0(\chi+1)\boldsymbol{E}, \tag{2}$$

where $\boldsymbol{E}=(E_x,E_y,E_z)$, $\boldsymbol{H}=(H_x,H_y,H_z)$, ε_0, μ_0, χ, and ω are electric field vector, magnetic field vector, permittivity of vacuum, permeability of vacuum, electric susceptibility of volume hologram, and angular frequency, respectively. In the case of transverse electric (TE) mode, that is, E_z=0, it is convenient that H_x and H_y are expressed by using a scalar potential function ${}^{e}u$ as

$$H_x = \frac{\partial\partial\ {}^{e}u}{\partial x \partial z}, \qquad H_y = \frac{\partial\partial\ {}^{e}u}{\partial y \partial z}. \tag{3}$$

Then, E_x, E_y, and Hz can be expressed by using ${}^{e}u$. Therefore, ${}^{e}u$ is satisfied differential equations as follows:

$$\left(\frac{\partial^2}{\partial x^2}+\frac{\partial^2}{\partial y^2}+\frac{\partial^2}{\partial z^2}\right)\frac{\partial\ {}^{e}u}{\partial x} = -k^2(\chi+1)\frac{\partial\ {}^{e}u}{\partial x}, \tag{4}$$

$$\left(\frac{\partial^2}{\partial x^2}+\frac{\partial^2}{\partial y^2}+\frac{\partial^2}{\partial z^2}\right)\frac{\partial\ {}^{e}u}{\partial y} = -k^2(\chi+1)\frac{\partial\ {}^{e}u}{\partial y}. \tag{5}$$

However, in the case of transverse magnetic (TM) mode, it is difficult to express electromagnetic field by using a potential function. In this paper, coordinates are converted and Maxwell's equations are expressed by

$$\frac{\partial E^3}{\partial x_2}-\frac{\partial E^2}{\partial x_3} = \mathrm{i}\omega\mu_0(\chi+1)H_1, \tag{6}$$

$$\frac{\partial E^1}{\partial x_3}-\frac{\partial E^3}{\partial x_1} = \mathrm{i}\omega\mu_0(\chi+1)H_2, \tag{7}$$

$$\frac{\partial E^2}{\partial x_1}-\frac{\partial E^1}{\partial x_2} = \mathrm{i}\omega\mu_0(\chi+1)H_3 = 0, \tag{8}$$

$$\frac{\partial H_2}{\partial x^2}-\frac{\partial H_2}{\partial x^3} = -\mathrm{i}\omega\varepsilon_0 E^1, \tag{9}$$

$$\frac{\partial H_1}{\partial x^3}-\frac{\partial H_3}{\partial x^1} = -\mathrm{i}\omega\varepsilon_0 E^2, \tag{10}$$

$$\frac{\partial H_2}{\partial x^1}-\frac{\partial H_1}{\partial x^2} = -\mathrm{i}\omega\varepsilon_0 E^3,$$

where

$$\boldsymbol{E} = E_x\boldsymbol{e}_x + E_y\boldsymbol{e}_y + E_z\boldsymbol{e}_z = E^1\boldsymbol{e}_1 + E^2\boldsymbol{e}_2 + E^3\boldsymbol{e}_3, \tag{12}$$

$$\boldsymbol{H} = H_x\boldsymbol{e}_x + H_y\boldsymbol{e}_y + H_z\boldsymbol{e}_z = H_1\boldsymbol{e}^1 + H_2\boldsymbol{e}^2 + H_3\boldsymbol{e}^3, \tag{13}$$

$$\boldsymbol{e}_x\frac{\partial}{\partial x} + \boldsymbol{e}_y\frac{\partial}{\partial y} + \boldsymbol{e}_z\frac{\partial}{\partial z} = \boldsymbol{e}^1\frac{\partial}{\partial x^1} + \boldsymbol{e}^2\frac{\partial}{\partial x^2} + \boldsymbol{e}^3\frac{\partial}{\partial x^3} = \boldsymbol{e}_1\frac{\partial}{\partial x_1} + \boldsymbol{e}_2\frac{\partial}{\partial x_2} + \boldsymbol{e}_3\frac{\partial}{\partial x_3}, \tag{14}$$

$$\boldsymbol{e}_1 = \boldsymbol{e}_x + \boldsymbol{e}_z\frac{\partial}{\partial x^1}\int\frac{1}{\chi+1}\mathrm{d}x^3, \quad \boldsymbol{e}_2 = \boldsymbol{e}_y + \boldsymbol{e}_z\frac{\partial}{\partial x^2}\int\frac{1}{\chi+1}\mathrm{d}x^3, \quad \boldsymbol{e}_3 - \frac{1}{\chi+1}\boldsymbol{e}_z, \tag{15}$$

$$\boldsymbol{e}^i = \sum_{j=1}^{3}(\boldsymbol{e}^i\cdot\boldsymbol{e}^j)\boldsymbol{e}_j. \tag{16}$$

When E^1 and E^2 are expressed by using a scalar function ${}^{m}u$ as

$$E^1 = \frac{\partial\partial^{\mathrm{m}}u}{\partial x^3\partial x_1}, \qquad E^2 = \frac{\partial\partial^{\mathrm{m}}u}{\partial x^3\partial x_2}, \tag{17}$$

H^1, H^2, and E^3 can be expressed by ^{m}u and two differential equations are derived as follows:

$$\left(\frac{\partial\partial}{\partial x_1\partial x^1}+\frac{\partial\partial}{\partial x_2\partial x^2}+\frac{\partial\partial}{\partial x_3\partial x^3}\right)\frac{\partial^{\mathrm{m}}u}{\partial x_1} = -k^2(\chi+1)\frac{\partial^{\mathrm{m}}u}{\partial x_1}, \tag{18}$$

$$\left(\frac{\partial\partial}{\partial x_1\partial x^1}+\frac{\partial\partial}{\partial x_2\partial x^2}+\frac{\partial\partial}{\partial x_3\partial x^3}\right)\frac{\partial^{\mathrm{m}}u}{\partial x_2} = -k^2(\chi+1)\frac{\partial^{\mathrm{m}}u}{\partial x_2}. \tag{19}$$

By solving eqs. (4), (5), (18), (19), polarization dependence of reconstructed beam can be evaluated.

3.Conclusion

In this paper, differential equations to express light propagation in volume holograms were derived by coordinate conversion. In future, volume holograms were evaluated by using the differential equations

Acknowledgment

This work has been partially supported by the Japan Science and Technology Agency (JST) under the Strategic
Promotion of Innovation Research and Development Program.

Reference:

[1] H. Kogelnik, Bell System Technical Journal, **48**, 2909 (1969).

09.

Light-sheet volume holographic microscopy

Dipanjan Bhattacharya[1,2,3†], Xiaomin Zhai[4†], Zhi Chen[1,5], Jau-Min Wong[7], George Barbastathis[1,8], and Yuan Luo[4,6,*]

[1] Singapore-MIT Alliance for Research and Technology (SMART) Centre, 1 CREATE Way, 138602, Singapore

[2] Centre for BioImaging Sciences (CBIS), Blk S1A, Level 2, National University of Singapore, 117546, Singapore

[3] MechanoBiology Institute (MBI), National University of Singapore, 117411, Singapore

[4] Institute of Medical Device and Imaging, National Taiwan University, Taipei, 10051, Taiwan R.O.C.

[5]Department of Biomedical Engineering, National University of Singapore, Singapore 117576

[6] Molecular Imaging Center, National Taiwan University, Taipei, 10055, Taiwan R.O.C.

[7] Department of Internal Medicine, National Taiwan University Hospital, Taipei, 10048, Taiwan, R.O.C.

[8] Department of Mechanical Engineering, MIT, Massachusetts, 02139, USA

1. Introduction

Three-dimensional (3D) fluorescent imaging of volumetric tissue samples is essential for quantifying and understanding mechanisms and processes within biological systems and organisms. The use of the term “volumetric imaging” typically implies sectioning ability, so that truly 3D image data can be acquired, ideally in real-time or at least at video-rate. Standard wide-field fluorescence microscopy of course has no optical sectioning capability. Light sheet microscopy (LSM) [1,2,3] based variants like, digital light-sheet microscopy (DSLM) [1,2], and selective plane illumination microscopy (SPIM) [3] are motivated by the desire to speed up volumetric imaging as well as reduce photo-bleaching due to prolonged illumination of the sample. As opposed to confocal, which uses spot-like excitation, in LSM the illumination is plane-wise and the camera axis is positioned orthogonally to the excitation beam axis, so as to capture the image of the entire fluorescing plane at once. Although LSM has improved the imaging speed and image quality, all these variants still require scanning each sectioning plane individually. Our proposed unique use of holography in this paper aims to ameliorate this problem.

On the other hand, in Multiple Volume-holography Microscopy (MVH), holographic gratings are superimposed in a volume recording material such that each grating obtains depth-resolved information from different depths within the object. Here, we present a variant of MVH microscopy that incorporates the LSM principle to still obtain sectioned images from multiple planes in one shot but with much improved contrast. The main idea is to use LSM to selectively excite fluorescence in two (or more) planes inside the sample; and then use MVH to image these two planes simultaneously onto corresponding non-overlapping areas of a digital camera. Compared to standard LSM techniques, the MVH method offers parallelism; compared to standard MVH, the selective illumination by LSM drastically reduces scattering from the rest of the sample and, hence, leads to improved contrast. However, as in any other hybrid, our proposed approach also presents certain tradeoffs: most notably, in return for parallelism we obtain poorer contrast than the original LSM, because the MVH does not offer perfect isolation of the simultaneously imaged planes. (In original LSM, only one plane at a time is illuminated.) Nevertheless, in our experiments we generally found the tradeoffs to be quite manageable and the quality of the images still comparable to those obtained by LSM, while still enjoying the parallelism offered by MVH.

2. Results

We overview the respective principles of LSM and MVH and describe how to combine them to design the optical arrangement that we used to implement our proposed hybrid approach. The prototype light-sheet MVH system, as shown in Figure 1, was built using dual-beam light-sheet excitation and a two multiplexed volume holographic imaging gratings. The performance of our MVH-LSM system is first investigated using fluorescently labeled microspheres. In our system, we have done the final alignment of both excitation-beams with similar sample mount geometry and embedded fluorescent beads. It is worth mentioning that the depth separation can be arbitrarily arranged with properly designed volume holographic multiplexing.

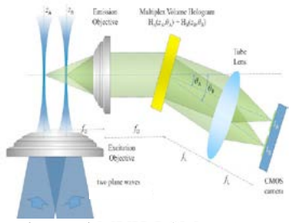

Fig.1. Schematic drawing of the experimental MVH-LSM system setup (BS: beam splitter; M: mirror).

Experimental results using tissue samples are further measured and also compared with conventional transmitted and reflective illumination. To verify system performance using fluorescently labeled microspheres and mice intestine samples, the experiment was configured such that a volumetric fluorescent sample could be excited either with two light sheet beams at the same time or with any one of the two beams (beam-1 or beam-2) on its own.

3. Discussion

We have developed a real-time, multi-plane, wide-field optical sectioning microscope, based on volume holographic multiplexing in combination with multiple light-sheet illumination. The proposed light-sheet based MVH is simple and robust to simultaneously observe images from different planes within a volumetric tissue sample while significantly suppressing out-of-focus background. MVH-LSM requires only one shot with no axial scanning to capture multiple planes simultaneously. In addition, as we use separated side illumination, the depth penetration of the present system is better compared to THIN system. Although the current light-sheet MVH observes two different planes, the system can be extended to obtain more planes simultaneously with more multiplexed volume holographic gratings ultimately enable real-time 3D video microscopy. For instance, a diffraction of element or spatial light modulator can be utilized to generate multiple diffraction beams to produce more light sheets for illumination. The proposed system can then be configured such that more light-sheet based illumination planes occur inside a volumetric sample, and also serve as the input focal planes for the subsequent multiplexed volume holographic imaging gratings.

Reference

[1] P. J. Keller, A. D. Schmidt, J. Wittbrodt, E. H. Stelzer, “Reconstruction of zebrafish early embryonic development by scanned light sheet microscopy”, Science, 322(5904), 1065–1069, 2008

[2] D. Bhattacharya, V. R. Singh, Z. Chen, P. T. C. So, P. Matsudaira, and G. Barbastathis, “Three dimensional HiLo-based structured illumination for a digital scanned laser sheet microscopy (DSLM) in thick tissue imaging”, Opt. Express. 20(25), 27337–27347, 2012.

[3] J. Huisken, D. Stainier, “Selective plane illumination microscopy techniques in developmental biology”, Development., 136(12), 1963-75, 2009

[4] Y. Luo, I. K. Zervantonakis, S. Oh, R. D. Kamm, & G. Barbastathis, “Spectrally resolved multidepth fluorescence imaging”, J. Biomed Opt., 16(9), 096015, 2011.

[5] Y. Luo, V. R. Singh, D. Bhattacharya, E. Y. S. Yew, J. C. Tsai, S. L. Yu, H. H. Chen, J. M. Wong, P. Matsudaira, P. T. C. So and G. Barbastathis, “Talbot holographic illumination nonscanning (THIN) fluorescence microscopy”, Laser & Photonics Reviews, 8(5), L71-L75, 2014.

10.

Fabrication of Holographic Devices with Azobenzene-based Materials

Fang-Yun Lee, Lu-Yu Wang, Tzu-Chien Hsu, and Wei-Hung Su Department of Materials and Optoelectronic Science, National Sun Yat-Sen University,

1. Introduction

The azobenzene-containing material can be ultilized as a holographic material for the sake of induction of dichroism and birefringence upon irradiation with polarized light [1-6]. The E-Z repeating photoisomerization and relaxation of azobenzene chromophores make it rewritable under holographic exposure.

In this paper, an azobenzene-containing material for optical storage are presented. It is fabricated by incorporating the azobenzene material (2-{[4-(dimethylamino)phenyl]diazenyl} benzoic acid, Methyl Red, MR) with Bis(3-aminopropyl)amine (BAA). The azobenzene composites were formed by ionic bonding, which reduces the oppertunity of the phase separation and enhances the thermal stability for long term preservation.

2. Fabrication method

Figure 1 depicts the molecular structures of the materials mentioned. The flow chart of the fabrication process for Azobenzene/BAA composites is illustrated as Fig. 2.

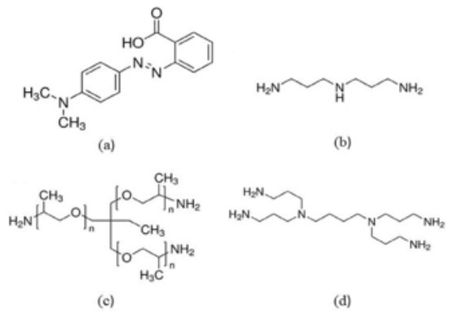

Fig. 1. The molecular structures of the materials used: (a) MR, (b) BAA, (c) TPGA, and (d) PPI

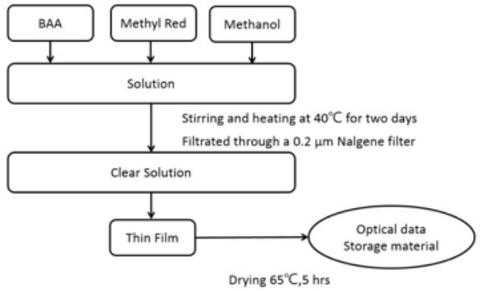

Fig. 2. Flow chart of the fabrication process

3. Experiments

Figure 3(a) shows the optical configuration for holographic recording. A DPSS laser with a wavelength of 532 nm was used as the light source. The azobenzene-containing material is illuminated by interference of the two plane waves. The power of the plane wave is 30 mW/cm2. A surface relief grating is therefore formed in films of the azobenzene-functionalized polymers under holographic exposure. The angles between the two light waves were 7o, resulting in a grating period of 4.35 μm. To evaluate the diffraction efficiency, a He-Ne laser with wavelength of 633 nm was used. Figure 3(b) depicts the optical configuration.

Figure 4(a) shows the diffraction efficiencies of Azobenzene/BAA composites for various diffraction orders. Appearance of the diffraction beams with different orders is shown in Fig. 4(b). Atomic force microscopy (AFM) revealed that surface variations of the composites Azobenzene/ BAA, was 758nm, while the sample thickness before holographic recording was 762nm.

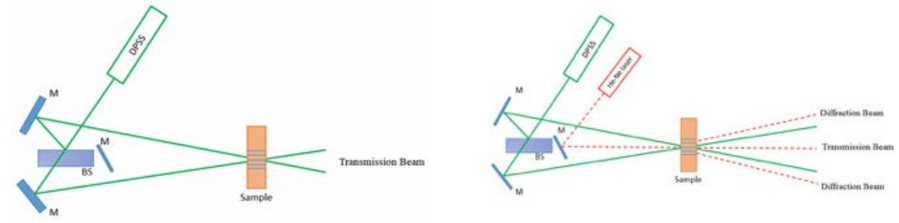

(a) (b)

Fig. 3. (a) Holographic setup in the recording proceedure.(b) Measurements of the diffraction efficeincy.

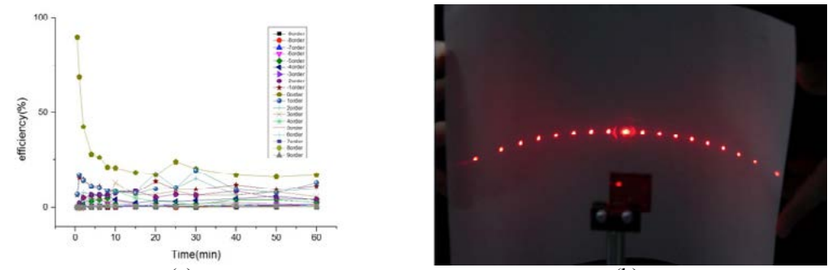

(a) (b)

Fig. 4.(a) Holographic setup in the recording proceedure. (b) Measurements of the diffraction efficeincy.

4. Conclusion

An azobenzene-based material has been fabricated for optical storage. Performances of its diffraction efficiencies have evaluated as well. It was found that the power sensitivity of Azobenzene/BAA composites was very high, in the order of minutes. Its surface variation due to holographic exposure was very large. The ratio of the variation amplitude to the sample thickness was approximately 0.5.

Reference

[1] W. Que, "Azobenzene-containing small molecules organic–inorganic hybrid sol–gel materials for photonic applications," Applied Physics B, vol. 91, 2008, pp. 539-543.

[2] K. G. Yager and C. J. Barrett, "All-optical patterning of azo polymer films," Current opinion in solid state and materials science, vol. 5, 2001, pp. 487-494.

[3] I. Khoo, et al., "Observation of orientational photorefractive effects in nematic liquid crystals," Optics letters, vol. 19, 1994, pp. 1723-1725.

[4] I. Khoo, "Holographic grating formation in dye-and fullerene -doped nematic liquid-crystal film," Optics letters, vol. 20, 1995, pp. 2137-2139.

[5] O. Kulikovska, et al., "Smart Ionic Sol. Gel-Based Azobenzene Materials for Optical Generation of Microstructures," Chemistry of Materials, vol. 20, 2008, pp. 3528-3534.

[6] N. Landraud, et al., "Near-field optical patterning on azo-hybrid sol–gel films," Applied physics letters, vol. 79, 2001, pp. 4562-4564.

11.

Label-free analysis and identification of white blood cells using common-path tomographic diffractive microscopy

Fong-jheng Lin[1)] Chao-mao Sie[1)], Kung-Bin Sung[1,2,3)]

[1)] Institute of Biomedical Electronics and Bioinformatics, National Taiwan University, Taipei, Taiwan

[2)] Department of Electrical Engineering, National Taiwan University, Taipei, Taiwan

[3)] Molecular Imaging Center, National Taiwan University, Taipei, Taiwan

1. Background

White blood cells (WBC) play main roles in defending the host against harmful pathogens and disease conditions [1]. Various subtypes of WBCs have been characterized to play different roles in the pathophysiology of diseases [2].Therefore, accounting the number of WBC in specific subtypes is important. We have developed common-path tomographic diffractive microscopy (cTDM) to acquire three-dimensional (3D) refractive index (RI) mappings of WBC without staining, thus getting morphological information of the cells when they are close to their natural state. Three main subtypes of WBC were analyzed, including monocyte, neutrophil and lymphocyte. We also analyzed the total phase integrated over the projected area of individual WBC, which is proportional to the dry mass. Finally, the scattering properties of WBC were obtained from 3D RI tomograms using the finite-difference time-domain (FDTD) method to demonstrate the feasibility of classifying the three subtypes of WBC based on their backscattering spectra.

2. Methods

2.1 Experimental Setup

The details of the system architecture were described in [3]. cTDM illuminates the sample using a 532 nm continuous-wave diode-pumped solid-state laser with angles ranging from -65° to 65°. The laser beam is expanded by a spatial filter and then focused by a scan lens to the back focal plane of an oil-immersion condenser to generate plane wave illumination. An oil immersion objective lens collects transmitted illumination light and forwardly scattered light of the specimen. A transmission grating is placed at about 70 mm in front of an intermediate image plane to generate multiple diffraction orders of the transmitted light.A window allows the zeroth-order and the first-order beams to pass. An image of the specimen in the zeroth- order beam interferes with a uniform first-order beam serving as the reference beam. Interference images of WBC are acquired by a high-speed CMOS camera. 2D images are recorded with various illumination angles and the retrieved amplitude and the phase images. From phase images,using 3D reconstruction to obtain 3D images.

2.2 Sample Preparation

WBCs were collected from the peripheral blood of human body. Isolated WBCs were not stained with specific antibodies. We add frobernectin in th slides to fix these WBCs to avoid suspension. Separated WBC subtypes kept on ice before experiments.

2.3 FDTD stimulation

We calculated backscattering spectra of three kinds of WBC. The backscattering was obtained by integrating the scattering intensity in the scattering angles between 164^{o}and 180^{o}.

3. Results

We used cTDM to get phase images and RI tomograms of the three kinds of WBC. Neutrophil's dry mass and RI are the largest. Monocytes have the largest diameter and volume; and lymphocytes have the smallest diameter and volume. From FDTD simulation, the oscillation frequency of the backscattering spectra is correlated with the diameter of spherical scattering subjects. For example, lymphocytes have the smallest diameter and the lowest oscillation frequency. Monocytes have the largest diameter and the highest oscillation frequency.

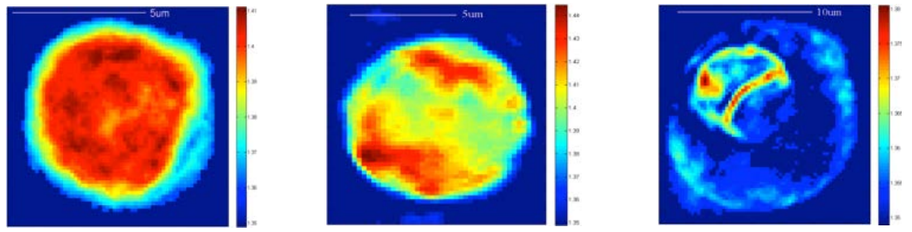

(a) (b) (c)

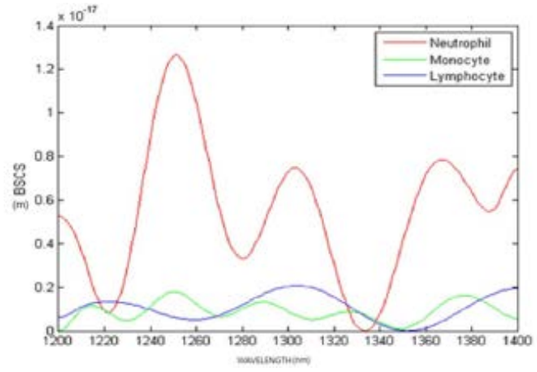

(d)

Fig. 1 (a)-(c) RI images and (d) FDTD simulation results of three subtypes of WBC, BSCS means backscattering cross section(unnormalized).

4. Conclusion

We measured 3-D RI tomograms of individual WBCs and retrieved quantitative structural information and also demonstrated classifications of measured WBC by FDTD stimulation. The methods enable classification of specific WBC subtypes, and it could not disturb WBCs cellular viability or functions.

Reference

[1] Balagopalan, L., Sherman, E., Barr, V.A. & Samelson, L.E. "Imaging techniques for assaying lymphocyte activation in action". *Nat Rev Immunol* **11,** 21-33 (2011).

[2] Edwards, J.C. & Cambridge, G. "B-cell targeting in rheumatoid arthritis and other autoimmune diseases".

[3] Hsu WC, Su JW, *et al* (2014). Opt Lett, 39(7):2210-13.

12.

Characteristics of known phase embedded collinear holographic memory

Hajimu Nishimoto[1)], Ryushi fujimura[2)], Masao Endo[1)], Shinsuke Umegaki1) and Tsutomu Shimura[1)]
[1)] Institute of Industrial Science, The University of Tokyo, 4-6-1 Komaba, Meguro-ku, Tokyo 153-8505, Japan
[2)] Department of Optical Engineering, Graduate School of Engineering, Utsunomiya University, 7-1-2 Yoto, Utsunomiya, Tochigi 321-8585, Japan

1. Introduction

Recently, demand for the new optical memories with high recording density is increasing due to the data explosion. A holographic memory is recognized as one of the new optical memory systems with high recording density and high transfer rate and low power consumption. Among the holographic memory, the collinear system, in which signal and reference beams go through a common path, have robustness for aerial and mechanical turbulence. For further increase of the recording density, the collinear systems with phase modulation for the data coding have been developed. Multi-level logic can be used in this system and multi-bit data can be expressed in one pixel. However, in the readout process in the phase information of each pixel, 4 step phase change of the reference wave is required with the phase shift method, or a set of 4 pixels is needed to express one phase information for the one shot readout. In these cases, the readout time is 4 times slower in the former case or the data density becomes 1/4 in the latter case. Thus, we proposed a new phase modulated collinear holographic memory with a new data coding method here. A limited number of known pixels are embedded in the page data format. Using these known pixels, we can know the absolute value of the phase and also determine the aberration of the reference wave. Using this information, we can readout the phase information of the data pixels. Only two pixels are needed to express the phase from 0 to 2π. In our method less than 3 pixels are required to express one data in the average, in contrast to the normal one shot phase shifting method, in which at least three pixels are required to express one phase information. In this paper, we will investigate some characteristics of this new method. We will estimate the signal to noise ratio and error rate numerically and experimentally.

2. Principle of known phase embedded collinear holographic memory

The optical system is shown Fig.1. In our system, some numbers of pixels with fixed phase are embedded in the data page. In recording process, LCOS-SLM displays phase pattern as reference and signal. In reading process, LCOS-SLM displays reference phase pattern and uniform phase at signal pixels which provides the plane reference wave to detect the phase. We use 4×4pixels which is defined 1 block as signal pattern. Among those pixels, the four known pixels are put at the corners. The phases of the known pixels are 0, π/2, π, 3π/2. Other pixels, hereinafter called unknown pixels, the phase φ is expressed with a pair of pixels. In 4 phase modulation level, the pair pixels are allotted φ-π/4 and φ+π/4. In analysis, we use 4 known pixels and 12 unknown pixels. First, we calculate parameters of expression which show a relationship between gray level and recorded signal phase from gray levels of 4 known pixels. Second, we calculate phase φ from gray levels of unknown pixels and the parameters.
Phase-shifting interferometry uses at least 3 pictures with different phase of illumination light to read 1 phase value. Using this method, known pixels are 4 pixels compared with 12 unknown pixels in 1 block. Thus, we can get 2 bits information in 3 pixels or less from one picture.

3. Simulation

A result of simulation calculated in 16 phase modulation level is shown in Fig.2. In this simulation, the number of the reference pixels, unknown pixels, and known pixels are 2342, 4816, and 225 respectively. We calculated the phase of the reference from intensity of all known pixels, and each unknown phases from pairs of unknown pixels. The result indicates that 16 level phase modulation can be resolved.

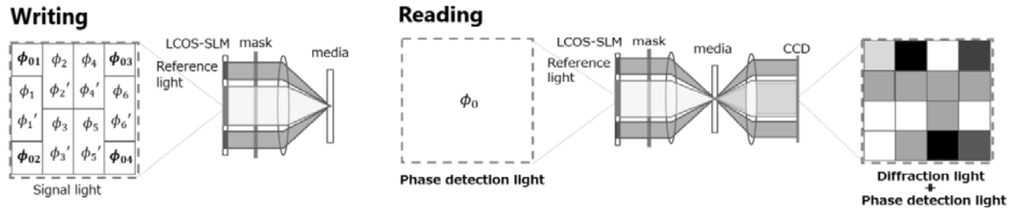

Fig.1 Writing and Recording process of known phase embedded collinear holographic memory

4. Experiment

We did experiment to verify the principle of known phase embedded collinear holographic memory. Fig.3 is the result of experiment in 4 level phase modulation. In this experiment, we use 8×8 pixels of LCOS to show 1 phase value and 56×56 pixels of CCD to determine intensity of 1 phase value. In this experiment, reference light neighbor on signal light unlike the simulation. As a result of analysis from CCD image (Fig.3), we got recorded unknown phase pattern without error.

5. Conclusion

The principle of known phase embedded collinear holographic memory is introduced. This method achieves one-shot phase reading using 3 pixels of LCOS or less. We have shown that 16 modulation level in simulation and 4 modulation level in experiment can be resolved.

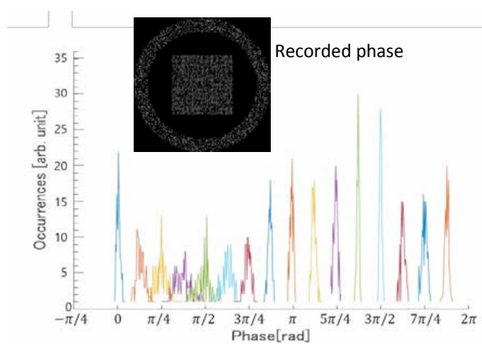

Fig.2 Result of simulation in 16 phase modulation level

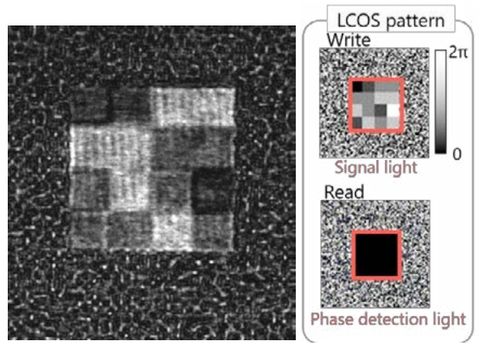

Fig.3 Result of experiment in 4 phase modulation level

Reference

[1] T. Nomura, and M. Imbe, “Single-exposure phase-shifting digital holography using a random-phase reference wave”, *Opt,lett*, Vol.35, No.13, pp.2281-2283, 2010.
[2] N. Ishii, N.Kinoshita, Eds., “Phase-code holographic multiplex recording method using symmetric phase conditions of discrete cosine transform“, J.Inst.Image Inform.TV.Engnr, Vol.59, No.12, pp.1869-1874.2005.

13.

Parallel Computing of Polygon-Based Computer-Generated Hologram

Heng-Kuang Liao [1)], and Jung-Ping Liu[1)]

[1)] Department of Photonics, Feng Chia University, 100 Wenhwa Rd., Seatwen, Taichung 40724, Taiwan

1. Introduction

Holography is a technique to record not only the amplitude but also the phase of object light. In the reconstruction, the optical field of the object can be correctly reconstructed. As a result, we can see through the hologram and observe the three-dimensional (3D) image of an object. In the last decade, the computer-generated hologram (CGH) attracts public's attention again because it is regarded as the next-generation technique for real 3D display. In the past, the full parallax computer-generated hologram was usually computed by point-based method. The calculation algorithm of the point-based method is straightforward and simple, but it cannot demonstrate the surface properties of object and the computing is relatively slow. Therefore, the point-based method was replaced by the polygon-based method, in which the object model consists of facets but not points [1-4]. Here we adopt the polygon-based method to generate a CGH and apply the parallel computing framework to reduce the computing time.

2. Generation of polyogon-based hologram

The flow chat of polygon-based method is shown in Fig. 1. First a 3D model composed of numerous facets is generated. In the polygon-based method, each polygonal surface represents a planar light source. The corresponding wave field $g(x, y)$ at this plane is expressed as

$$g(x, y) = a(x, y) \exp[i\phi(x, y)] \quad (1)$$

where $a(x, y)$ is the amplitude distribution which represents the shape, texture, and brightness of the polygonal surface; $\phi(x, y)$ is the initial phase distribution of the light. Usually, the plane of facet, which is referred to as the local tilted plane, is not parallel to the local parallel plane. The local parallel plane is parallel to the hologram plane, and its origin coincides with that of the local tilted plane. Thus, it is necessary to transform the function of wave field from the coordinate of local tilted plane to the coordinate of local parallel plane. In the polygon-based method, every facet is processed independently. Therefore all facets can be processed with the parallel computing framework.

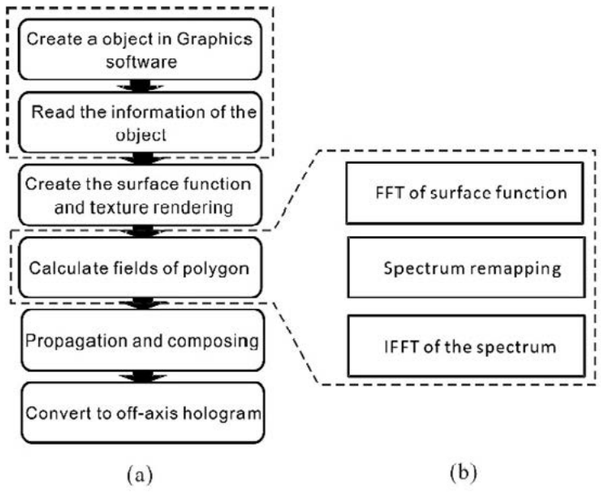

Fig. 1. The flow chat of the generation of polygon-based computer-generated hologram.

A high-definition polygon-based CGH named "Football" was generated and shown in Fig. 2(b). The status of football [Fig.2(a)] is composed of 3688 triangular facets but only 1640 facets face forward and thus contribute to the hologram. The size of the football is 4mm × 2mm × 2mm and the distance between the football and hologram plane is 250mm . The offset angle of the plane-wave reference light is 16.57° . The resulting amplitude hologram contains 1.6×10^9 pixels and the pixel pitch is 0.832μm . The "Football" was computed using a computer with quad-core intel i7 870 CPU and 32GB RAM. The total computing time without and with parallel computing framework are 28 mins and 18 mins, respectively. Finally, we used scalar diffraction to reconstruct the hologram [5]. High-definition reconstructed image is shown in Fig. 2(c).

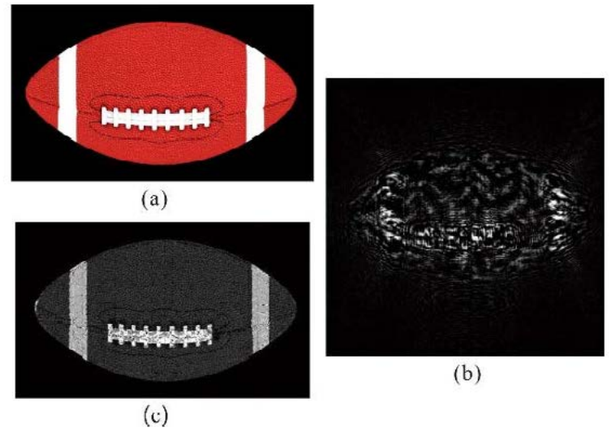

Fig. 2. (a) The object, "Football", (b) the real part of the complex hologram, and (c) the reconstructed image by simulation.

3. Conclusion

A high-definition and full-parallax computer-generated hologram of a computer-graphic model was generated by the polygon-based and texture-added method. We also applied parallel computing framework to speed up the hologram generation. In our demonstration, the computing time was reduced to nearly one half of the original. This work is supported by Ministry of Science and Technology of Taiwan, R.O.C. under contract number 103-2221-E-035-037-MY3.

Reference

[1] K. Matsushima and S. Nakahara, "Extremely high-definition full-parallax computer-generated hologram created by the polygon-based method," Appl. Opt., **48**, H54–H63, 2009

[2] H. Nishi, K. Matsushima, and S. Nakahara, "Rendering of specular surfaces in polygon-based computer- generated holograms," Appl. Opt., **50**, H245–H252, 2011.

[3] K. Matsushima, H. Nishi, and S. Nakahara, "Simple wave-field rendering for photorealistic reconstruction in polygon-based high-definition computer holography," J. Electron. Imaging, **21**, 023002–1, 2012.

[4] K. Matsushima, Y. Arima, and S. Nakahara, "Digitized holography: modern holography for 3D imaging of virtual and real objects," Appl. Opt., **50**, H278–H284, 2011.

[5] J.-P. Liu, "Controlling the aliasing by zero-padding in the digital calculation of the scalar diffraction," JOSA A, **29**, 1956–1964, 2012.

14.

Computational microscopy of phase imaging based on transport of intensity

Hsi-Hsun Chen,[1,2*)] and Yuan Luo[2,3)]

[1)] Department of Electrical Engineering and Graduate Institute of Photonics and Optoelectronics, National Taiwan University, Taipei 10617, Taiwan

[2)] Institute of Medical Device and Imaging, National Taiwan University, Taipei, 10051, Taiwan

[3)] Molecular Imaging Center, National Taiwan University, Taipei 10055, Taiwan

*email: d03941029@ntu.edu.tw

1. Introduction

Optical phase includes the information of optical path length as optical wave passes through refractive media. Quantitative phase images attract attention in the different research area, such as optical metrology and cell identification. However, a detector or CCD only detects intensity of samples, and thus phase information is lost due to no phase contrast in optical transfer function. To induce the phase contrast, one strategy with no need of interference is to use defocus measurement through optical axis near Fresnel region. This method is named as transport of intensity equation (TIE). Based on TIE, the phase information can be retrieved from multiple measurements through different depth quantitatively. However, the reconstructed phase is deviated from ground truth since the measured data is corrupt from the noise, at least shot noise. Moreover, the impulse response of TIE serves as a high-pass filtering, resulting in significant amplification of low frequency noise. In this paper, we propose a method to reconstruct the phase of sample based on the TIE using data from commercial microscopy. Meanwhile, we propose an algorithm to suppress cloudy effect due to low frequency noise. Our approach is able to reconstruct high quality phase information compared with that using direct solver in tradition method.

2. Method

The TIE for reconstructing phase ϕ (x, y) can be wrote as equation shown below

$$-k\frac{dI}{dz}=\nabla\cdot(I_0(x,y)\nabla\phi(x,y)) \tag{1}$$

where x,y and z denotes three dimensional coordinates, and k is the wave number. In the assumption of transparent sample, intensity I_0 ($\vec{r}$) can set as constant, therefore, the phase can be solved using the Possion solve as:

$$\phi(x,y)=\Im^{*}H\Im\{-\frac{k\partial I(x,y,z)}{I_0\partial z}\},\qquad H=\frac{-1}{u^2+v^2} \tag{2}$$

where u and v is the frequency coordinate along vertical and horizontal axis, respectively. $\Im$ and $\Im^{*}$ denotes the Fourier an inverse Fourier Transform pair. Since lower value (low frequency) in the denominator in eq. (2) would amplifier the low frequency noise, we introduce a regularizer into eq.(2) to address this problem. Associated with regularizer, the eq. (2) can be rewrote as:

$$\min\frac{1}{2}\left|\frac{k\partial I(x,y,z)}{I_0\partial z}-\Im H\Im^{*}\{\phi\}\right|^2+\tau\iint|\nabla\phi|dxdy \tag{3}$$

where τ is the parameter to weight the regularizer to suppress the noise as well as avoiding the under-fitting.

Result

In the experiment, we reconstructed phase of micro-lens array (MLA150-7AR, Thorlabs) [Fig. 1(a)], and the data is measured using commercial microscopy (DMI 3000 B, Leica). Solving via eq. (2) and alternative directional multiplier method (ADMM), we show the result in Fig. 1 below

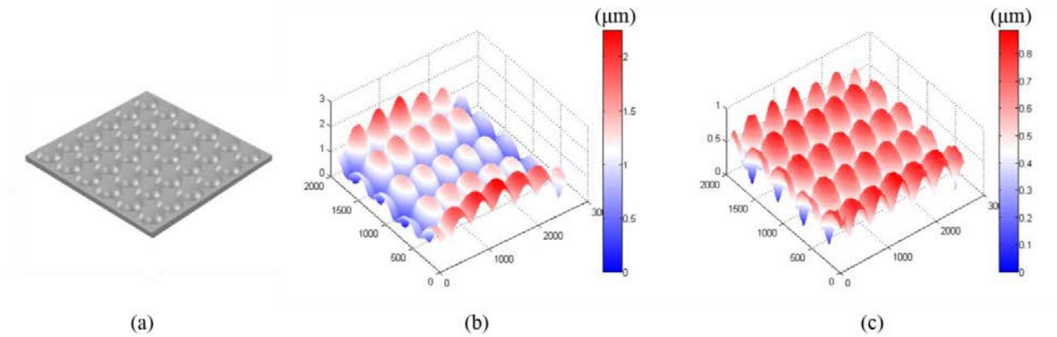

Figure.1. (a) The illustration of microlens array. (b) The reconstructed phase using Poisson solver. (c) The reconstructed phase using eq. (3).

In Fig.1, we can observe that the quantitative thickness (ground truth is 0.87 μm) of microlens solved from eq. (3) [Fig. 1(c)] is better than that in direct Poisson solver [Fig. 1(b)].

Discussion

In this paper, we propose a computational imaging to reconstruct the phase based on TIE. Compared with traditional Poisson solver, our approach with ADMM solver can retrieve phase information with higher accuracy.

Reference

[1] Jean Pierre Guigay, Max Langer, Renaud Boistel, and Peter Cloetens, "Mixed transfer function and transport of intensity approach for phase retrieval in the Fresnel region," Opt. Lett. 32, 1617-1619 (2007)

[2] Lei Tian, Jonathan C. Petruccelli, and George Barbastathis, "Nonlinear diffusion regularization for transport of intensity phase imaging," Opt. Lett. 37, 4131-4133 (2012)

[3] Boyd, S., Paikh, N., Chu, E., Peleato, B., And Eckstein, J. 2001. Distributed optimization and statistical learning via the alternating direction method of multipliers. Foundations and Trends in Machine Learning 3,1, 1–122.

15.

Reflective-type Digital Holographic Microscopy with Self-pumped Phase Conjugation Mirror

Huang-Tian Chan,[1] Yang-Kun Chew, [1] Min-Tzung Shiu, [2] and Chi-Ching Chang, [1],*

[1] Department of Materials and Energy Engineering, Ming Dao University, Changhua, Taiwan

[2] School of Defense Science, National Defense University, Taoyuan, Taiwan

*E-mail address: chichang@mdu.edu.tw

Abstract

Techniques that suppress noises derived from reference arm are maturely developed but not the object counterpart. Self-pumped phase conjugation technique which involves that use of BaTiO3 crystal was introduced unto reflective-type digital holographic microscopy to suppress scattering noise prior to recording stage.

Keywords: digital holographic microscopy, photorefractive, self-pumped phase conjugation

1. INTRODUCTION

Digital holographic microscopy (DHM) is a great tool in retrieving three-dimensional information of objects. With the use of digital means, zero-order and image-conjugate noise term that were initially encountered by conventional holography can be easily resolved. It is however that these techniques only suppress noises that are derived from reference arm. Object arm on the other hand, suffered scattering noise which is not being taken sufficient care. Therefore, this paper paid attention to the scattering noise in the object arm, by using phase conjugation techniques which involves self-pumping in photorefractive crystal [1]. Endeavors have showed that scattering noise can only be suppressed prior to recording stage with the use of phase conjugation techniques [2, 3], unlike reference wave. Thus, this study aimed to suppress scattering noise encountered in reflective-type DHM.

2. EXPERIMENT

An experimental setup of a reflective-type DHM, we refer as self-pumped phase conjugation digital holographic microscopy (SPPCDHM) as shown in Fig. 1. A DPSS Verdi laser of 532 nm in wavelength was used as light source. A half-wave plate (HWP) and polarizer were used to produce an extraordinary wave. A variable beam splitter (VBS) was used to adjust the intensity ratio of the object and reference wave. In the object arm, a polarized beam splitter (PBS) and a quarter-wave plate (QWP) was used to reduce intensity loss of object signal. The object (1951 USAF Resolution Target, Positive) was then magnified by a microscopic objective (MO). Again, a HWP was used to modulate the polarization state to extraordinary wave where a lens was used to focus the magnified image into the BaTiO3 crystal. In the reference arm, a spatial filter (SF) and a lens were used to match the quadratic phase term associated with the object wave. The hologram was recorded by a CCD (Pixera-150SS, 1392 × 1040 pixels, 0.650 × 0.484 cm^2). In order to show that SPPCDHM is capable in suppressing scattering noise, a transparency film was placed between the focusing lens and $BaTiO_3$ crystal, acting as scattering and phase distortion media. The whole experiment was repeated by using a conventional mirror instead of BaTiO3 crystal as a control set. The experiment was done in ambient surroundings of 27.5°C, 40% humidity.

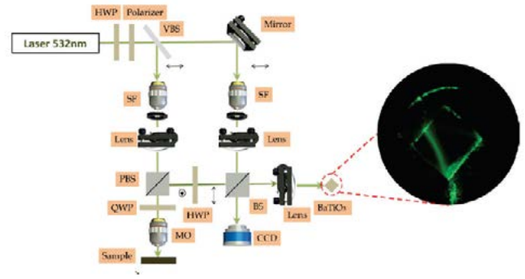

Fig. 1. Schematic diagram of a reflective-type SPPCDHM

3. RESULTS AND DISCUSSION

The holograms were subjected to reconstruction, results as shown in Fig. 2. It is clear that noises are being suppressed by employing phase conjugation technique into DHM. By using a 20x objective lens, the system is capable in achieving a net magnification of ~29x with a resolving power of 2.2μm.

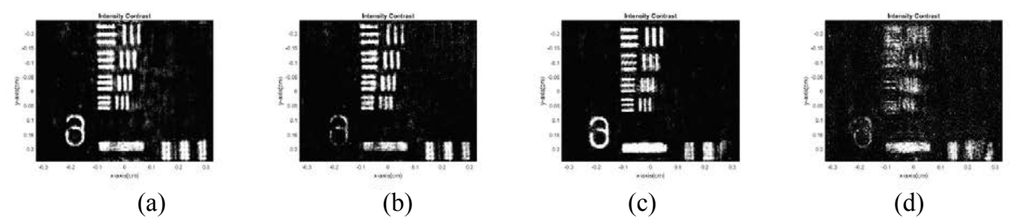

(a) (b) (c) (d)

Fig. 2. Reconstructed images of those using SPPCDHM (a) without additional noise, (b) with additional noise, and reconstructed images of those control set (c) without additional noise, (d) with additional noise.

4. CONCLUSION

To conclude this paper, we have employed optical phase conjugation technique into DHM to suppress scattering noise prior to recording stage, particularly in reflection-type configuration. The results proved that the idea is feasible capable in achieving a net magnification of ~29x with a resolving power of 2.2μm by using a 20x objective lens.

ACKNOWLEDGEMENTS

The authors thank Ministry of Science and Technology, Taiwan, ROC for financial support in this research, under grant no. (MOST 103-2221-E-451-006) and (MOST 104-2221-E-451-011).

Reference

[1] J. Feinberg, "Self-pumped, continuous-wave phase conjugator using internal reflection," Opt. Lett. **7**(10), 486 – 488 (1982).

[2] E. J. McDowell, M. Cui, I. M. Vellekoop, V. S. Z. Yaqoob, and C. H. Yang, "Turbidity suppression from the ballistic to the diffusive regime in biological tissues using optical phase conjugation," Journal of Biomedical Optics **15**(2), 025004-1 – 02554-11 (2010).

[3] T. R. Hillman, T. Yamauchi, W. S. Choi, R. R. Dasari, M. S. Feld, Y. K. Park, and Z. Yaqoob, "Digital optical phase conjugation for delivering two-dimensional images through turbid media," Scientific Reports **3**, 1909 (2013).

16.

Fast calculation method for the polygon based computer generated hologram using sparse sampling

Jaebum Cho, Jinsoo Jeong, Dukho Lee, Byounghyo Lee, and Byoungho Lee*
School of Electrical and Computer Engineering, Seoul National University, Gwanak-gu Gwanakro 1, Seoul 08826, South Korea
* byoungho@snu.ac.kr

1. Introduction

Computer generated hologram (CGH), contents for a holographic display, can be distinguished in several methods. The point based method requires a lot of computation power, but it is easy to understand and implement [1]. The polygon based method is complicated to implement, but it is efficient to express a plane surface [2, 3]. The ray sampling based method is easy and efficient, but it sacrifices some properties of holographic images [4]. Some studies are trying to save computation power by reducing computation region [1, 2]. These methods utilize light field confinement in the spatial domain. In this paper, we propose a method to reduce computation region by using sparse sampling in the spatial frequency domain, so the confinement of light field in the spatial domain can be considered in the frequency domain as well.

2. Principle

An ordinary computer graphic scene includes enormous polygon facets, and single facet is relatively small for the whole image size. In the polygon based method, CGH of each polygon is calculated independently. In most cases, single polygon is surrounded by zero region.

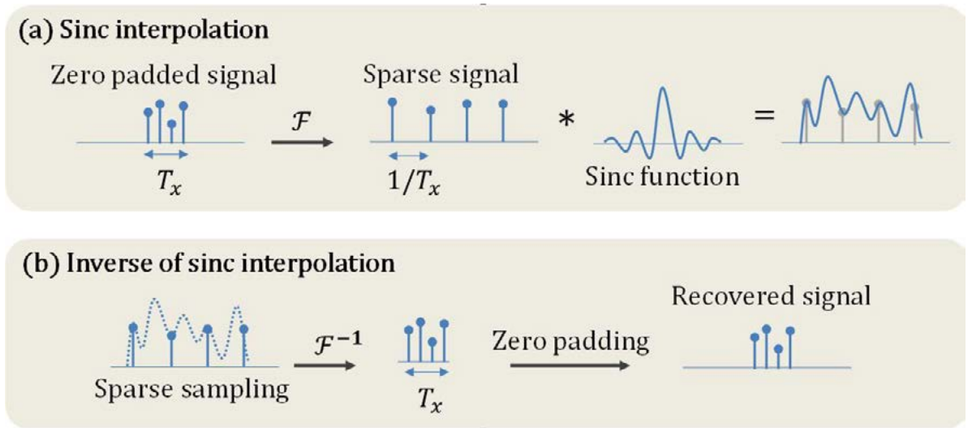

Fig. 1. (a) Sinc interpolation by the zero padding, and (b) inverse process of sinc interpolation which is utilized for the proposed algorithm.

As seen in Fig. 1(a), it is well known that zero padding in the spatial domain causes sinc interpolation in the frequency domain, when two domains are related by fast Fourier transform (FFT). That is, the spatial domain signal can be recovered from the sparsely sampled signal in the frequency domain as seen in Fig. 1(b).

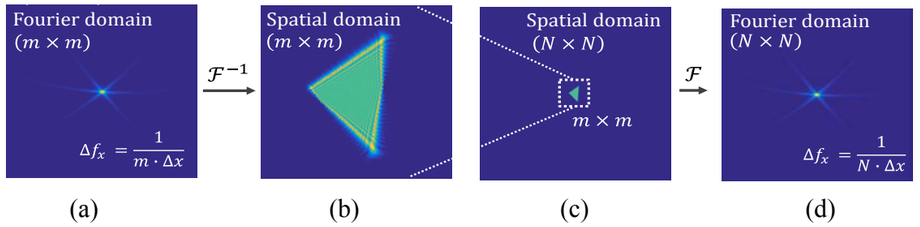

Fig. 2. The proposed algorithm workflow: (a) Only small number of key values in frequency domain are calculated. (b) Non-zero signal region is recovered by FFT. (c) All processes are completed by zero padding. (d) The final whole CGH is sinc interpolated form of the initially calculated field.

If the signal is isolated in spatial domain, only small number of key signal in the frequency domain is required to recover the signal. In Fig. 2, the numerical results of the proposed algorithm are represented. In this simulation, total computation grid size N is set to 1024, and local grid size m is set to 128, and the integral equation is summated directly to avoid interpolation error. In this case, the computation region is reduced to 64 times less and the computation time is reduced to about 61.1 times less.

3. Conclusion

We show that isolated signal in the spatial domain can be recovered with sparsely sampled signal in the frequency domain. The proposed method can divide the computation load into many small independent pieces without errors, so it is expected to be implemented to GPGPU computation. It is not the most efficient algorithm relative to other algorithms [2], but it is easy to implement and generalize. For example, the computation load of the proposed algorithm is nearly unrelated with the number of facets.

Acknowledgement
This work was supported by the Brain Korea 21 Plus Project in 2016.

Reference

[1] T. Shimobaba, N. Masuda, and T. Ito, "Simpleand fast calculation algorithm for computer-generated hologram with wavefront recording plane," Opt. Lett. **34**, 3133–3135 (2009).
[2] K. Matsushima, "Computer-generated holograms for three-dimensional surface objects with shade and texture," Appl. Opt. **44**, 4607–14 (2005).
[3] H. Kim, J. Hahn, and B. Lee, "Mathematical modeling of triangle-mesh-modeled three-dimensional surface objects for digital holography," Appl. Opt. **47**, D117-27 (2008).
[4] K. Wakunami and M. Yamaguchi, "Calculation for computer generated hologram using ray-sampling plane," Opt. Express **19**, 9086–101 (2011).
[5] A. Kondoh and K. Matsushima, "Hidden surface removal in full-parallax CGHs by silhouette approximation," Syst. Comput. Japan **38**, 53–61 (2007).

17.

Phase measurement of a tilted plane mirror using the derivative estimation of a single hologram

Jin Nozawa,[1] Atsushi Okamoto,[1] Yasuyuki Kuno,[2] Masataka Toda,[2] Kazuhisa Ogawa,[1] and Akihisa Tomita[1]

[1] Graduate School of Information Science and Technology, Hokkaido University, N14-W9, Kita-ku, Sapporo,060-0814, Japan

[2] Trial Manufacturing Pla nt, Aisin Seiki Co., Ltd. 2-1, Asahi-machi, Kariya, Aichi, 446-8524, Japan

1. Introd uction

Recently, digital holography (DH) [1,2] is attracted in many fields, such as biomedical field [3] and industrial field [4]. DH can measure the optical phase distribution by capturing interferograms between a signal beam and a reference beam with an image sensor. We proposed the holographic diversity interferometry (HDI) [5], which can achieve high speed and high resolution phase measurement by utilizing multiple image sensors. However, HDI needs at least two image sensors for capturing the two phase-shifted interferograms, and the alignment accuracy of these two image sensors have to be within the submicron order.

In this paper, we propose the phase measurement method using the derivative estimation of a single hologram. In the proposed method, we assume the phase deviation of the measuring object to be constant and measure the phase of signal beam from an interferogram and its partial differentiation. Although the proposed method severely restricts the measurable object, such as the tilted plane mirror, the additional image sensor, the phase modulation device, and bandpass filter are not needed. Thus, the proposed method can measure the phase of signal beam in a simple optical setup without deteriorating the measuring speed and the spatial resolution. The experiment showed the basic operation of the proposed method.

2. Derivative estimation of a single hologram

In this section, we explain the basic principle of the proposed method. We assume the signal amplitude is A_o, the reference amplitude is A_r, and the signal phase distribution is ϕ(x,y), the interferogram between the signal beam and reference beam H_1 is described as

$$H_1 = A_o^2 + A_r^2 + 2A_oA_r\cos\phi(x,y)\,. \tag{1}$$

By extracting the cosine term,

$$\cos\phi(x,y) = \{H_1 - (A_o^2 + A_r^2)\} / 2A_oA_r\,. \tag{2}$$

Here, we assume that the $\phi(x,y)$ is linear coupling of the 1D function of the horizontal x direction and the transverse y direction, and the direction of derivation and that of the phase increment are the same. Partial differentiations along the x direction and the y direction of the equation (2) is described as

$$\partial/\partial x\cos\phi(x,y) = -\phi_x\sin\phi(x,y) \tag{3}$$

$$\partial/\partial y\cos\phi(x,y) = -\phi_y\sin\phi(x,y) \tag{4}$$

ϕ_x, ϕ_y are derivatives of the $\phi(x,y)$ along the x direction and the y direction. In this situation, the ϕ_x and ϕ_y should be positive constant values. Thus, the maximum value and the minimum value of the right side of equation (3) are defined as $I\max_x$ and $I\min_x$, and those of the equation (4) are defined as Imaxy and Iminy, respectively. The derivative of the phase distribution can be estimated as

$$\phi_x = (I_{\max x} - I_{\min x})/2 \tag{5}$$

$$\phi_y = (I_{\max y} - I_{\min y})/2\,. \tag{6}$$

These four values of Eqs. (3)-(6) can be easily estimated by the computer, sine term can be described as

$$\sin\phi(x,y) = -\{\partial/\partial x\cos\phi(x,y)/\phi_x + \partial/\partial y\cos\phi(x,y)/\phi_y\}/2 \tag{7}$$

Therefour, the phase distribution of signal beam $\phi(x,y)$ is described as Eq.(7)

$$\phi(x,y) = \arctan(\sin\phi(x,y)/\cos\phi(x,y))\,. \tag{8}$$

3. Experiment

Figure 1 shows the experimental setup. In this experiment, the plane mirror was used as the measuring object. At first, a green laser was irradiated from diode pumped solid state (DPSS) laser. Then, the plane wave was generated by passing through an isolator and spatial filter. This plane wave was divided into the signal beam and the reference beam. Reference beam was set to linear polarization at 45 degrees and irradiated to the mirror. The reflected light was delivered to the charge coupled device (CCD) by the imaging system consisting from lens 3 to lens 6. The signal beam was set to the circular polarization and delivered to CCD. Here, the incident angle of signal beam is tilted by another mirror. We calculated the phase distribution of tilted plane mirror by the proposed method and HDI, and compared with the results.

Figure 2 shows the experimental results. Figs. 2(a) and 2(b) show the phase image calculated by the HDI and the proposed method, respectively. Almost same phase image was calculated by the proposed method and the correlation between Figs. 2(a) and Fig. 2(b) was 0.82. This suggests that the proposed method can measure the phase of tilted plane mirror. Moreover, the unwrapped phase image, shown in Fig. 2(c), clearly described the profile of plane mirror. Therefore, the basic operation of the proposed method was confirmed.

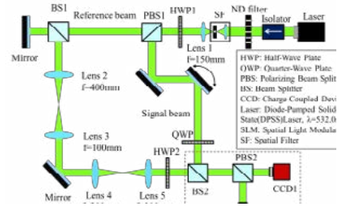

Fig. 1. Experimental setup

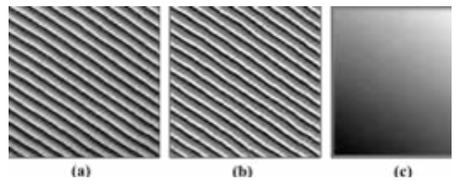

Fig. 2. Experimental results; (a) phase image of HDI. (b) phase image of proposed method. (c) unwrapped phase image of Fig. 2(b).

4. Conclusion

We showed that the proposed method can measure the signal phase from a single hologram without using the bandpass filter. The extension of proposed method using higher order differentiation is the next step.

Reference

[1] I. Yamaguchi, et al., Opt. Lett., **22**, pp.1268-1270 (1997).
[2] M. Takeda, et al., J. Opt. Soc. Am, **72**, pp.156-160 (1982).
[3] P. Guo, et al., Opt. Lett., **29**, pp.857-859 (2010).
[4] Y. Kikuchi, et al., Opt. Lett., **35**, pp.1548-1550 (2010).
[5] A. Okamoto, et al., Opt. Express, **19**, pp.13436-13444 (2006).

18.

Optical correlation system using simple structure holographic optical disk

Kanami Ikeda, Toshihiro Sugaya and Eriko Watanabe
Department Engineering Science, University of Electro-Communications, 1-5-1 Chofugaoka, Chofu, Tokyo 182-8585, Japan

1. Introduction

The volume of information generated not only by people but also by sensors such as those in cameras has been dramatically increasing. Faster technologies that can analyze enormous amounts of data are required. We have developed an optical correlator using a coaxial holography system[1] for this requirement. This optical correlator has a simple configuration and is compatible with the control technique of conventional optical disks such as CDs and DVDs. We achieved 2.4 Mfps in an optical correlation experiment, which is equivalent to 143 Gbps data transfer speed[2] by improving the disk rotation speed via weight reduction of the objective lens and reducing the shift pitch of the shift multiplex recording to 2 μm. We also developed a demonstration system using the optical correlator in a cloud environment[3].

In this study, for practicality, a simple structure disk without a dichroic layer was designed and fabricated on an experimental basis for the tracking servo system, despite using two different color lasers. More than 1000 holograms were written with tracking on a single circular groove track, and stable optical correlation signals were obtained from the written holograms.

2. Disk structure and servo system of the coaxial holography

2.1. Servo system

The coaxial holography system[4] in a simple configuration was employed for our optical correlator. Figure 1(a) shows the configuration of the disk control system. The objective lens was held by a leaf spring of an actuator and moved for focusing and tracking the direction by flowing a current in coils. The astigmatism method and push-pull method were used for focal error detection and tracking error detection, respectively.

2.2. Disk structure

Red and green lasers were employed for the servo system and hologram writing and reading of the optical correlator, respectively. Figures 1 (b) and (c) show the holographic versatile disc (HVD) structure that was proposed for the coaxial holographic system and the simple structure disk without a dichroic layer that was designed in this study, respectively. The HVD consists of glass, 2P+ reflective, gap1, dichroic mirror, gap2, recording (photopolymer), anti-reflection (AR), and cover layers. The dichroic mirror layer was utilized for the preventing degradation of the correlation signal by the preformat used for the tracking and addressing in the optical correlation process. However, the dichroic layer has been a factor in increasing the costs of the holographic disk. For optical correlation, we think that the efficiency of the grooves is lower than the holographic memory for the experiment because the optical correlation signal was not obtained by the two-dimensional imaging devices. The simple structure disk consisting of glass, 2P+ reflective, gap, recording, AR, and cover layers without a dichroic layer was designed and fabricated on an experimental basis for the tracking servo system, despite using two different color lasers.

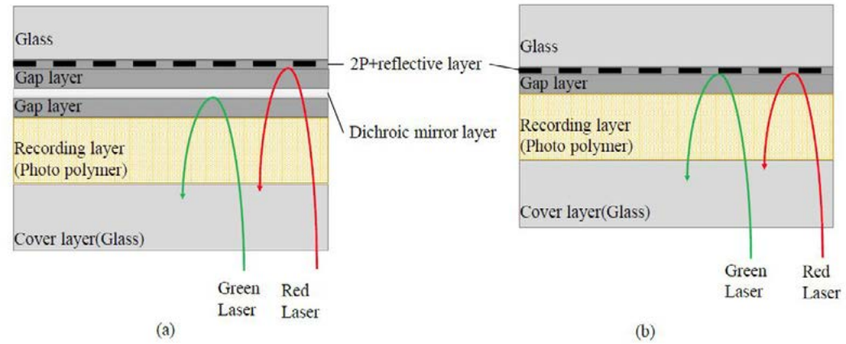

Fig.1. Disk structure (cross section) of (a) HVD format and (b) designed in this study.

3. Experiment

A track with a groove pitch of 1 mm on the new disk was used on this experiment. Figure 2 (a) shows the experimental setup for this experiment. When we recorded more than 1000 data with a size of 180 × 240 pixels and a shift multiplex recording pitch of 2 μm, the tracking on a single circular groove track and focusing were executed by a red laser. The recording holograms was time consuming, but we succeeded in recording stable holograms using a pulse laser in the experiment. The stable optical correlation signals were obtained from the written holograms using a green CW laser (Fig. 2(b)). Therefore, the optical correlation system enabled us to demonstrate image matching for a large number of database images.

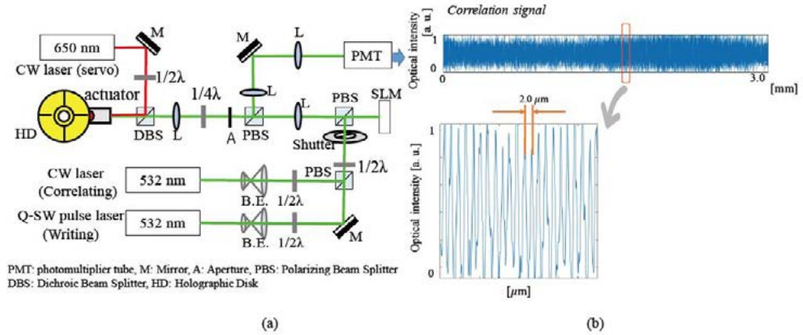

Fig.2. (a) Experimental setup and (b) results (Auto-correlation signals).

4. Conclusion

A tracking servo was introduced for a high-speed holographic optical correlation system. A simple structure disk without a dichroic layer was designed. More than 1000 holograms with 2 μm pitch were written by tracking on a single circular groove track and stable auto-correlation signals were obtained.

Acknowledgement

This study is partly supported by Strategic Information and Communications R&D Promotion Program.

Reference

[1] H. Horimai, X. Tan, and J. Li: Appl. Opt. 44, 2575 (2005).
[2] K. Ikeda and E. Watanabe: Jpn. J. Appl. Phys. 55, 09SC01 (2016).
[3] K. Ikeda, K. Kodate and E. Watanabe: Jpn. J. Appl. Phys. 55, 09SC03 (2016).

19.

Properties of Magnetic Volumetric Hologram with Magnetic Garnet/SiO_2 Multilayered Media

Kodai Kawazu[†], Zen Shirakashi[†], Taichi Goto[†,‡], Hiroyuki Takagi[†], Yuichi Nakamura[†], Pang Boey Lim[†], Hironaga Uchida[†], Mitsuteru Inoue[†]

[†]Toyohashi University of Technology, 1-1 Tempaku-cho, Toyohashi, Aichi, 441-8580, Japan

[‡]JST PRESTO, 4-1-8 Honcho, Kawaguchi, Saitama, 332-0012, Japan

1. Introduction

Hologram memory is an attractive storage technology with high recording density and fast data-transfer rate. We have studied to realize magnetic hologram using a transparent polycrystalline magnetic garnet films with long-term stability, and succeeded to record and reconstruct magnetic holography using the garnet film[1)]. However, the reconstructed image was unclear due to small diffraction efficiency. To improve the diffraction efficiency, the formation of deep and clear magnetic fringe is required. Recently, we reported that stacking structures composed of magnetic garnet and heat sink layers allow to diffuse excess heat generated in garnet layers into heat sink layers and prevent a merge of magnetic fringes[2)]. In this paper, we fabricated magnetic garnet/SiO_2 multilayer structures to see the effect on diffraction efficiency.

2. Experimental method

The magnetic garnet layer (Bi:YIG) and SiO_2 layers were deposited by ion beam sputtering. Figure 1 showed a structure of fabricated Bi:YIG/SiO_2 multilayer. We fabricated 4 and 8 pairs of SiO_2/Bi:YIG layers on a substituted gadolinium gallium garnet (SGGG) substrate/Bi:YIG structure. The total Bi:YIG thickness of the 4 pair medium was about 1 μm and that of 8pair was about 2 μm. For comparison, Bi:YIG single-layer films were also prepared by RF-magnetron sputtering. The fundamental properties of the fabricated media were summarized in Table 1. The diffraction efficiency was evaluated using two beam interference system with a spatial frequency of 1500 linepair/mm.

3. Results & discussion

Figure 2 shows the diffraction efficiency of the multilayer and single layer media. As shown in Fig. 2, the diffraction efficiency of the 4 pair multilayer and single layer film with about 1 μm thick Bi:YIG was almost same. In contrast, the diffraction efficiency of 8 pair multilayer medium was smaller than that of 2.7 μm thick single layer film. In this experiment, the improvement of diffraction efficiency due to the suppression of thermal diffusion in the garnet layer was not obtained. This may attribute to the reduction of stray magnetic field since it decreases as decreasing the thickness of a garnet layer from the numerical calculation, which results the small reversed magnetization. To increase the strength of reversed magnetization, magnetic assist recording was carried out, and the diffraction efficiency was evaluated. Figure 3 shows the dependence of the assist magnetic field on the maximum diffraction efficiency. The diffraction efficiency was improved by the magnetic assist in all the samples, and the 8 pair multilayer medium showed the higher diffraction efficiency than 2.7 μm single layer film at higher assist magnetic field. This supports that the reversed magnetization without the magnetic assist was insufficient. This suggests the multilayer media could be applied for magnetic hologram memory, and the optimization of the multilayered structure may result higher properties.

4. Conclusions

We fabricated Bi:YIG/SiO_2 multilayer media to see the effect on diffraction efficiency. As a result, the thick 8 pair multilayer media showed smaller diffraction efficiency than that of 2.7 μm single layer film probably due to small stray magnetic field, and the effect of heat sink layer for thermal diffusion suppression was not observed unfortunately. To improve the diffraction efficiency, the magnetic assist recording was carried out, and the 8 pair multilayer medium showed the highest diffraction efficiency. So the optimization of the multilayered structure may result much high diffraction efficiencies and clear reconstruction images. This work was supported in part by the Grants-in-Aid for Scientific Research (S) 26220902 and (A) 15H02240.

Reference

[1] Y. Nakamura, H. Takagi, P. B. Lim, and M. Inoue, Opt. *Exp*. **22**, 16439-16444 (2014).

[2] R. Isogai, Y. Nakamura, H. Takagi, T. Goto, P. B. Lim and M. Inoue., Opt. *Exp*, **24**, 522-527 (2016).

Table.1 The properties of SiO_2/Bi:YIG multilayer and Bi:YIG single-layer media

	Transmissivity T (%)	Reflectivity R (%)	Faraday rotation θ_F (deg.)	Coercive force H_c (Oe)	Maximum diffraction efficiency η ($\times 10^{-2}$%)
Single layer film (1.2 μm)	44.7	-	2.95	210	0.58
Single layer film (2.7 μm)	18.8	-	6.55	160	2.50
4 pair multilayer medium	45.5	15.4	3.61	370	0.70
8 pair multilayer medium	15.4	15.4	6.28	470	1.82

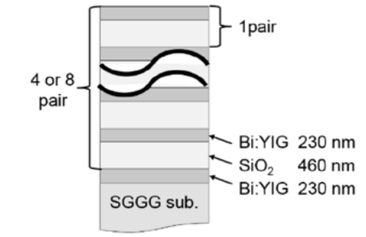

Fig. 1. Structure of Bi:YIG/SiO2 multilayer

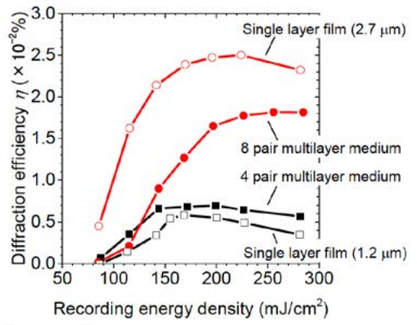

Fig. 2. The diffraction efficiency of the multilayered and single layer media

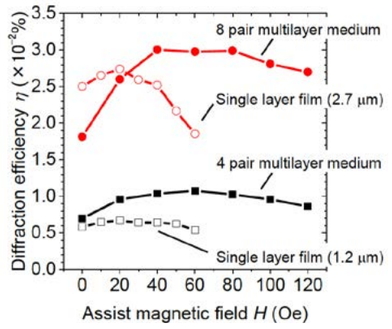

Fig. 3. The dependence of the assist magnetic field on the maximum diffraction efficiency

20.

Volumetric display using bubbles induced by femtosecond laser pulses

Kota Kumagai and Yoshio Hayasaki
Center for Optical Research and Education (CORE), Utsunomiya University 7-1-2 Yoto, Utsunomiya 321-8585, Japan

1. Introduction

Volumetric display has paid much attention for three-dimensional (3D) display in fields of optics and computer graphics. This display can render the 3D graphics that is observed from any surrounding viewpoints without to wear any special devices and physiologic discomfort unlike holographic, stereoscopic, and head-mounted display are based on planer two-dimensional (2D) screen for displaying visual information having binocular parallax. Volumetric displays render volume pixels, which are generally called voxels. These displays are classified into two types, depending on the characteristics of the voxels: the light-reflecting type and the light-emitting type. The laser irradiation type has a wide viewing angle and does not require any physical connection between the light source and the display volume. Laser-irradiation-based volumetric displays have been demonstrated by using various media. With these previous approaches, however, the number of voxels in the volumetric display is not high enough for rendering practical volumetric images because they are limited by the repetition frequency of the laser and the speed of the 3D scanning system. In our previous work, we proposed the volumetric display systems based on holographic parallel optical access and multi-photon excitation using a computer-generated hologram (CGH) displayed on a liquid crystal spatial light modulator (LCSLM). The screen materials were the multilayer fluorescent screen [1] and air [2]. The holographic method has not only increased the maximum number of voxels that can be rendered but also enabled the formation of brighter volumetric images. In addition, two-color display composed of red voxels and blue-green voxels has been achieved. In this paper, we demonstrated volumetric display with femtosecond-laser induced microbubbles.

2. Experimental setup

Figure 1 shows the system configuration of the holographic-laser-drawing volumetric display using the Fourier CGHs displayed on LCSLM. It consists of an amplified femtosecond laser source (Micra and Legend Elite Duo, Coherent), a 2D galvanometer mirror (GM-1010, Canon) and varifocal lens (EL-10-30-C, Optotune) that constitute a 3D beam scanner, an LCSLM (X8267, Hamamatsu). A femtosecond laser has a center wavelength of 800 nm, a repetition frequency of 1

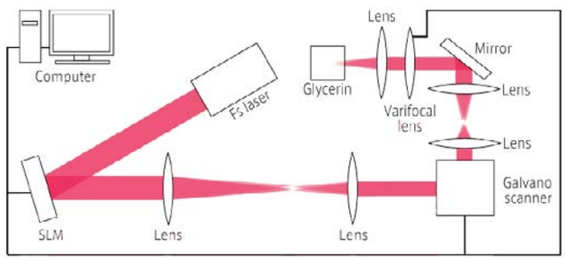

Fig. 1. Volumetric display system with holographic parallel optical access and a multilayer fluorescence screen.

kHz, a pulse duration of < 100 fs, and a maximum pulse energy of up to 7 mJ.

3. Experimental results

Figure 2 shows the generated area of micro-bubbles in the axial direction for the energy of the irradiated pulses. Femtosecond laser-induced micro-bubbles were observed with a cooled charge-coupled device (CCD) image sensor

(BU50LN, Bitran) and illumination of a halogen lamp. The frame rate of the CCD image sensor was 33 fps. The threshold of generated micro-bubbles for a single pulse was 1.8μJ. The bubble was not generated for 0.5 μJ or lower even though 1000 pulses were irradiated. As the pulse energy and the number of irradiated pulses are increased, the generated area expanded along the axial direction of the laser pulse irradiation.

Figure 3 shows a sequence of images of the 2D graphics rendered by femtosecond laser-induced micro bubbles. This picture has taken in ambient room light. The repetition frequency of the laser

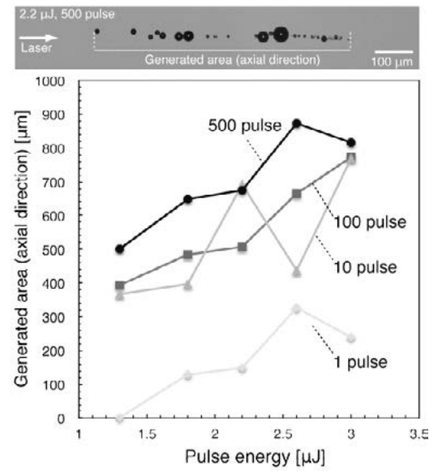

Fig. 2. Axial length of generated area of femtosecond laser-induced bubbles versus the energy of irradiated pulses.

Fig. 3. 2D graphics of "Whale" rendered by femtosecond laser-induced microbubbles.

pulses was 1 kHz, and the irradiation energy was 1.8 μJ.

4. Conclusion

We demonstrated a display with femtosecond laser-induced micro bubbles and holographic-laser-drawing technique using the CGH displayed on LCSLM.

References

[1] K. Kumagai, D. Suzuki, S. Hasegawa and Y. Hayasaki, "Volumetric display with holographic parallel optical access and multilayer fluorescent screen," Opt. Lett., **40**, 3356–3359 (2015).

[2] Y. Ochiai, K. Kumagai, T. Hoshi, J. Rekimoto, S. Hasegawa, Y. Hayasaki, "Fairy lights in femtoseconds: aerial and volumetric graphicsrendered by focused femtosecond laser combined with computational holographic fields," ACM Trans. Graph. **35**, 1-14 (2016).

21.

The study of synthesizing Images in screen imaging synthesis system

Yeh-Wei Yu[1], Kun-Zheng Lin[2], Yun-Hsuan Lin, Che-Chu Lin, Yu-Heng Chen, Ming Le[2], Tsung-Hsun Yang[2], and Ching-Cherng Sun[2]

[1]Optical Science Center, National Central University, Chung-Li, Taoyuan City 32001, Taiwan

[2]Department of Optics and Photonics, National Central University, Chung-Li, Taoyuan City 32001, Taiwan

Summary

In the study of holography, the quality of hologram is very important. The BSDF is used to describe scatter behavior of object surface or diffuser [1-3]. The screen imaging synthesis system (SIS) can measure BSDF of hologram quickly and correctly. It uses a camera to get image which records the information of light distribution and uses rotators to change the picturing aspect. By using image fusion, we can get the whole field light distribution [4]. It is a powerful instrument to check the quality of hologram. The SIS system consists of a camera, a screen, a light source and three motors. Figure 1 show the structure of the SIS system. For example, we measure the BSDF of a diffuser. First, we define the coordinate plot. The coordinate plot on SIS system is (x, y, z) which does not change when the motors rotates. The coordinate plot (x1, y1, z1), (x2, y2, z2) and (x3, y3, z3) are on the motor 1, motor 2 and motor 3. The screen and the camera are all on the coordinate plot (x, y, z). The light source is on the coordinate plot (x2, y2, z2) and the diffuser is on the coordinate plot (x3, y3, z3). If the point P0 (α, β, γ) which the point P3 (α3, β3, γ3) on (x3, y3, z3) projects onto the screen will change the position when three motors rotate. We can use rotation matrices to describe how three motors affect the coordinate position. Equation 1 shows the rotation matrices for three motors.

$$R_{1\beta 0}=\begin{bmatrix} cos\theta_y & 0 & sin\theta_y \\ 0 & 1 & 0 \\ -sin\theta_y & 0 & cos\theta_y \end{bmatrix}, R_{2\beta 1}=\begin{bmatrix} 1 & 0 & 0 \\ 0 & cos\theta_{x1} & -sin\theta_{x1} \\ 0 & sin\theta_{x1} & cos\theta_{x1} \end{bmatrix}, R_{3\beta 2}=\begin{bmatrix} cos\theta_{y2} & 0 & sin\theta_{y2} \\ 0 & 1 & 0 \\ -sin\theta_{y2} & 0 & cos\theta_{y2} \end{bmatrix} \quad (1)$$

The three rotation matrices have different bases, so we use similarity transformation to change bases of rotation matrices. Equation 2 and equation 3 show the relation equation between P0 and P3.

$$\mathrm{P3} = R_{3\beta 0}R_{2\beta 0}R_{1\beta 0}\mathrm{P0} = R_{1\beta 0}R_{2\beta 1}R_{3\beta 2}\mathrm{P0} \quad (2)$$

$$\begin{bmatrix} \alpha_3 \\ \beta_3 \\ \gamma_3 \end{bmatrix} = \begin{bmatrix} \cos\theta_y & 0 & \sin\theta_y \\ 0 & 1 & 0 \\ -\sin\theta_y & 0 & \cos\theta_y \end{bmatrix}_y \begin{bmatrix} 1 & 0 & 0 \\ 0 & \cos\theta_{x1} & -\sin\theta_{x1} \\ 0 & \sin\theta_{x1} & \cos\theta_{x1} \end{bmatrix}_y \begin{bmatrix} \cos\theta_{y2} & 0 & \sin\theta_{y2} \\ 0 & 1 & 0 \\ -\sin\theta_{y2} & 0 & \cos\theta_{y2} \end{bmatrix}_y \begin{bmatrix} \alpha \\ \beta \\ \gamma \end{bmatrix} \quad (3)$$

In the process of image fusion, we find that some sections are overlapped up to 10 times. The repeated data will slow down the system speed and the large angle image will have less information. So we try to reduce the image number to optimize system. We give up some large angle images and the total image number is reduced from 35 pictures to 23 pictures. We compare the result of the 35 pictures to the 23 pictures of measuring XM-L LED. The two results are very similar and their NCC of one- dimension intensity distribution between 35 pictures and 23 pictures are 99.97%. Figure 2 shows the one-dimension intensity distribution of 35 pictures and 23 pictures.

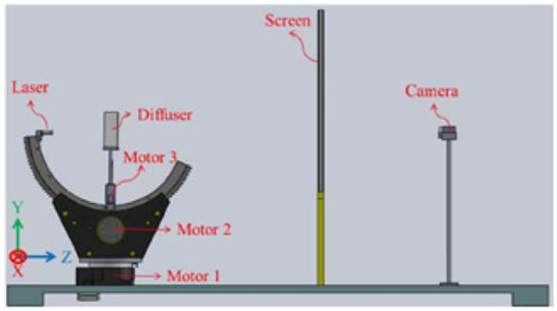

Fig. 1. The structure of the SIS system.

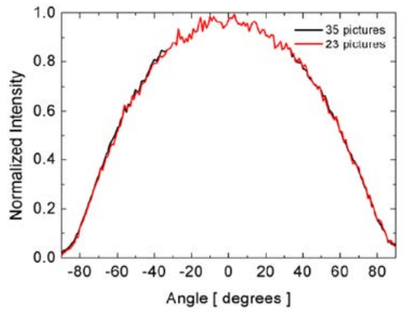

Fig. 2 .one-dimension intensity distribution of 35 pictures and 23 pictures.

Acknowledgments

This work was supported in part by the Aim for the Top University Project of National Central University Grant 105G903-2 and 105G705-3, and Ministry of Science and Technology of Taiwan (Contract MOST104- 2812-8-008-001 and MOST104-2221-E-008-078-MY3).

References

[1] F. E. Nicodemus, “Directional reflectance and emissivity of an opaque surface,” Appl. Opt. 4, 767 (1965)

[2] F. E. Nicodemus, J. C. Richmond, J. J. Hsia, I. W. Ginsberg, and T. Limperis, *Geometric Considerations and Nomenclature for Reflectance* (U.S. Dept. Commerce, Washington, D.C., NBS Monograp 160, 1977).

[3] Commission International de l’Eclairage, *Radiometric and photometric characteristics of materials and their measurement*, 2nd Edition (CIE 38(TC-2.3), 1977).

[4] Y. W. Yu, Y. L. Chen, W. H. Chen, H. X. Chen, X. H. Lee, C. C. Lin and C. C. Sun, “ Bidirectional Scattering Distribution Function by Screen Imaging Synthesis,” Optics Express 20, 1268-1280 (2012).

22.

Michelson Interferometer for 3D Displacement Measurements

Lu-Yu Wang,[1] Hui-Hung Lin,[1] Kuo-Kai Hung,[1] and Wei-Hung Su[2]

[1] Noporvis Co., Ltd., Kaohsiung 811, Taiwan

[2]Department of Materials and Optoelectronic Science, National Sun Yat-Sen University, Kaohsiung 804, Taiwan

1. Introduction

Michelson interferometer is a powerful tool in the field of optical metrology. With the help of Michelson interferometer, several optical detections are achievable, such as precise inspection of moving distances, characterization of spectral bandwidth, determination of the refractive index, identification of the surface profile, and study of the coherence for the optical sources [1].

In this paper, we use the Michelson interferometer to perform the distance measurement for a 3-dimensional translation stage. Our purpose is to design a movable stage, which meets the requirement of the next-generation lithography. The displacement accuracy should be in the order of nanometers. With the help of Michelson interferometer, accuracy of the presented setup better than 1 nanometer is desirable.

2. Principle and experiment

Figure 1(a) shows the configuration of a Michelson Interferometer, which are mainly composed of (1) a laser light source, (2) a beam splitter, (3) a fixed mirror M2 and a movable mirror M1 which is mounted on a translation stage, (4) a object lens, and (5) a screen.

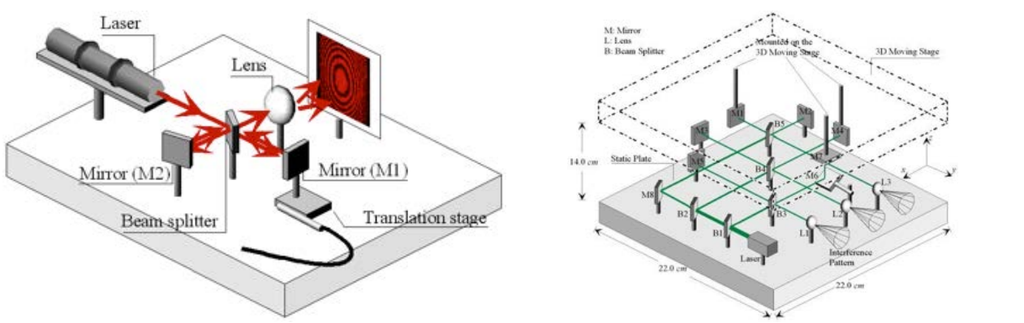

(a) (b)

Fig. 1. (a) Schematic setup of the scanning fringe projection. (b) Appearance of the optical setup for the 3D moving stage.

Light from a laser source is divided by a beam splitter, which is oriented at an angle 45° to the beam. One half of the light wave is reflected from the beam splitter to the fixed mirror M2, and then is back to the beam splitter. The other half passing through the beam splitter is reflected by the movable mirror M2 and is then back to the beam splitter. The resulting reflected and transmitted waves are focused by an objective lens to form two point sources, and projected to a screen where they superimpose to create fringes. With the Michelson interferometer, the displacement of the movable mirror M1 can be determined. The movement of M1 is discerned by counting the shift of the phase on the screen. The relation between the moving distance and the shifted phase can be expressed as

$$d = \frac{\lambda}{4\pi}\Delta\varphi \cdot \tag{1}$$

A 3D moving stage with size of 220mm 220mm was selected as the tested sample. This stage was actuated by piezo flexure materials and could be translated in x-, y-, and z-directions. A Michelson interferometer was built beneath the stage to measure the moving distance in x-, y-, and z-directions. Figure 1(b) shows the optical setup, in which the 3D moving stage is addressed with dotted lines. The mirrors M4, M1, and M7 were mounted on the moving stage. The other mirrors M3, M2, and M5 were mounted on the fixed plate. To perform the displacement measurement in x-, y-, and z-axis, three interference patterns were formed. When the tested stage was moving along a desired axis, the corresponding interference pattern shifted its phases to a specific position. Phase of the interference pattern can be extracted by the Fourier transform method [2]. Thus, the shifted phase caused by the displacement was determined. Displacement in that axis could be identified by Eq. (1).

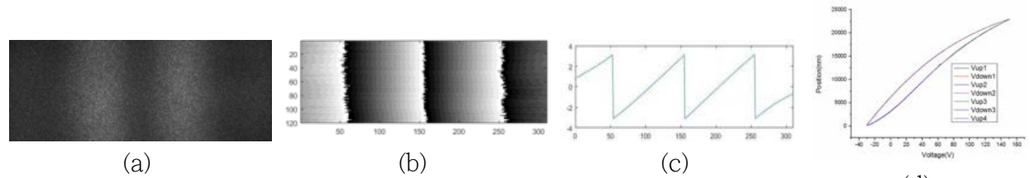

(a) (b) (c) (d)

Fig. 2. (a) Appearance of the interference pattern on the screen. (b) The extracted phase map. (c) Its distribution along one image row. (d) Correspondence between the moving distance and the voltage applied to the piezo flexure material.

Figure 2(a) shows the interference pattern observed by a CCD camera. Figure 2(b) illustrates the extracted phase map. Its phase distribution along one image row is shown as Fig. 2(c). By actuating the piezo flexure material, the stage was located at another location, and the phase of the interference pattern was shifted. Figure 2(d) illustrates the position of the translation stage when a voltage is applied to the piezo flexure material. A Michelson interferometer is employed to identify the moving distance. The displacement is not linearly proportional to the applied voltage. As a result, the trace of the positions when the voltage was applied incrementally is different from that when the voltage was applied decreased. The measurement was repeated more than three times. All the obtained results were consistent. It is found that the stage's location can be precisely identified with the interferometer. Accuracy in the order of nanometers is desirable.

3. Conclusion

A configuration of a 3D translation stage calibrated by Michelson interferometers has been proposed. With the help of Michelson interferometer, the location of the 3D translation stage actuated the piezo flexure material can be precisely described. It is found that the moving distance of the translation stage is not linearly proportional to the applied voltage. Accuracy in the order of nanometers is desirable.

References

[1] T. Li, A. Wang, K. Murphy, and R. Claus, "White-light scanning fiber Michelson interferometer for absolute position–distance measurement," Optics Letters, Vol. 20, Issue 7, 1995, pp. 785-787.

[2] M. Takeda, and K. Mutoh, "Fourier transform profilometry for the automatic measurement of 3-D object shaped," Appl. Opt. 22, 1983, pp. 3977-3982.

23.

Ultra-high speed goniophotometer for measuring the scattering light distribution of recording media used in holographic data storage

Yeh-Wei Yu[1)], Ming Le[2)], Yun-Hsuan Lin[2)], Che-Chu Lin[2)], Tsung-Hsun Yang[2)], and Ching-Cherng Sun*

[1)] Optical Science Center, National Central University, Chung-Li, Taoyuan City, 32001 Taiwan. Correspondence and requests for materials should be addressed to C.-C.S. (email: ccsun@dop.ncu.edu.tw)

[2)] Department of Optics and Photonics, National Central University, Taoyuan City 32001, Taiwan

Summary

Because of rapidly growing amount of data. The needs of cold data storage keep increasing. Holographic data storage technique is undoubtedly the best solution. But the scattering noise of photopolymer used as recording media restricts the storage capacity. In order to analyze the scatting characteristics of recording media, we develop an innovative machine which can rapidly measure the bidirectional scatting distribution function (BSDF) of a recording media used in holographic data storge [1, 2].

Figure 1 shows the set-up of the measuring machine. This machine can not only measure the BSDF by replacing the diffuser with a light source, it can also measure the light distribution of a small light source, so the distance between the light source and screen allows us to measure the light source under 5 cm [3]. The screen is made by a white lambertian sticker glued on a 601 by 496 by 3 (mm) anti-reflective glass and the motor 1 and motor 2 rotate the diffuser and laser to 60 different positions. As a result, we can use the screen and the camera to capture the whole light field distribution, and the motor 3 changes the incident angle of the diffuser.

After finishing the parameter optimization and calibration of the system [4, 5], we can use the image fusion algorithm developed by our team to get the 2-D light distribution or BSDF [6]. When the incident angle is 0º and the angular resolution is 2º, we can get the result in only 10 minutes. Compared to 7 hours that the goniophotometer takes, it can dramatically enhance the measurement time by 97.6%. If the amount of the incident angle is 9 (0~80), the machine takes only 1 hour to finish the measurement, and the 2-D result is shown in Fig. 2.

Figure 3 is the comparison of 1-D BSDF result between our machine and a traditional goniophotometer. Except the unmeasurable angle in the goniophotometer, the two curves are highly similar. We verify the accuracy of machine with 4 different diffusers, whose incident angle is form 0 to 70, and all the normalized cross correlation (NCC) of 1-D BSDF results between our machine and the goniophotometer are higher than 98.5%. It demonstrates the high accuracy and feasibility of the machine for measuring scattering light distributions.

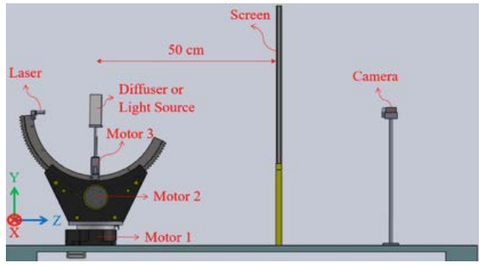

Fig. 1. Side view of the machine

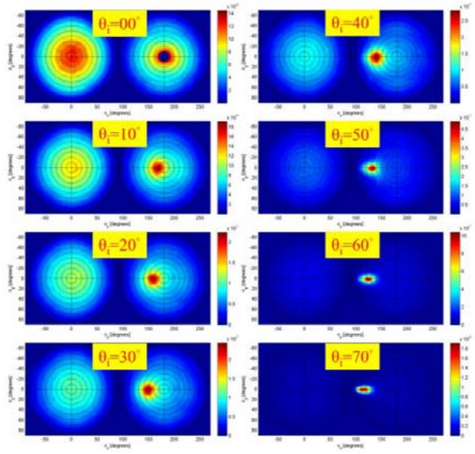

Fig. 2. BSDF result of diffuser

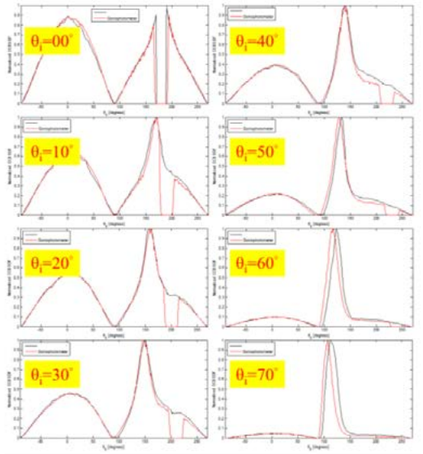

Fig. 3. Comparison of 1-D BSDF result between machine (black) and goniophotometer (red).

References

[1] K. Curtis, L. Dhar, A. Hill, W. Wilson, and M. *Ayres, Holographic Data Storage: From Theory to Practical Systems* (Wiley, 2010).

[2] J. C. Stover, *Optical scattering measurement and analysis* (McGraw-Hill , 1990).

[3] C. C. Sun, W. T. Chien, I. Moreno, C. C. Hsieh, and Y. C. Lo, “Analysis of the far-field region of LEDs,” Opt. Express 17, 13918–13927 (2009).

[4] V. N. Mahajan, *Optical Imaging and Aberrations, Part I Ray Geometrical Optics* (SPIE PRESS , 1998).

[5] J. M. Palmer, *Barbara Geri Grant, The art of radiometry* (SPIE, 2009).

[6] Y. W. Yu, Y. L. Chen, W. H. Chen, H. X. Chen, X. H. Lee, C. C. Lin, and C. C. Sun, “Bidirectional scattering distribution function by screen imaging synthesis, ” Opt. Express 20(2), 1268-1280 (2012).

24.

Reflection Conical Multiplex Holography using Optical System with Distorted Conical Object-Plane

Yih-Shyang Cheng and Ming-Han Chan

Department of Optics and Photonics, National Central University, Chungli, Taiwan 320, R.O.C.

1. Introduction

Multiplex holography was originally proposed to overcome the limitation on the subjects which can be used for holographic recording. A series of 2D photographs was generated by computer or taken from a 3D object and then fed into the optical system for synthesizing as a composite hologram. Besides the original flat format, multiplex hologram was also developed into the cylindrical type [1], the conical type [2], and the disk type [3]. These later types of multiplex holograms are capable of generating 3D images for walk-around viewing. Multiplex hologram fabricated with the tradition method would generate image superimposed with vertical dark lines, called picket-fence effect. To solve this problem, the image-plane technique was introduced. Due to the possible emerging of flexible display device, the possibility of using it as the input object plane was considered [4]. In that investigation, since the scale of the object was small, the input object plane was approximated to be a partial cone. Here, we consider the object plane in more detail and fabricate a reflection conical multiplex hologram. The experimental result is compared with the previous result.

2. Holographic Process and Experimental Result

Figure 1 shows the optical system for the object beam in holographic recording. Laser light is expanded by the spatial filter SF_1 before focused by the lens L_1 onto the center of the lens L_2. On its way toward the lens L2, it carries the information displayed on the object plane, a curved surface. The diverged wave is further focused by the lens L_3 to a distance q_3+d_{fe} downstream. The object plane corresponding to the image plane is a compressed asymmetric conical surface due to different magnification for different image distance.

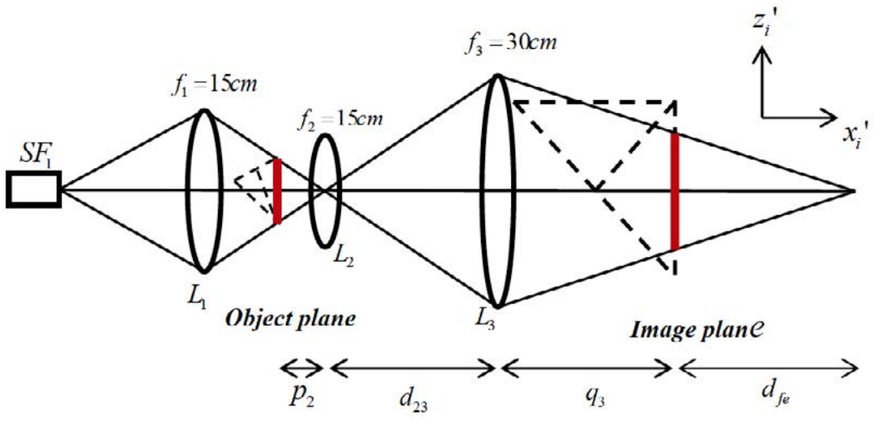

Fig.1. Optical system for object wave in recording of image-plane conical multiplex hologram.

The holographic recording for individual image-plane hologram is with a coherent reference wave diverging on the axis and above the tip of the recording conical film. After each recording, the object is replaced by the next image and the conical film is rotated by a small angle for making the next exposure till all the images are used up. This reflection holographic geometry guarantees the reproduction of a single-colored 3D image, with wavelength bandwidth limited by the thickness of the recording medium, for the observer. The original 2D object is prepared by the information flattened from the compressed conical surface and photo-reduced on the black-and-white photographic film. The mount of the compressed conical shape to clamp the 2D object information into the right shape is fabricated by 3D printing.

An ideal cube object of 4cm on each side is first projected by the eye onto the hologram cone to obtain the original 2D object. With geometrical optical ray-tracing, the 2D object information is traced back to the object plane in Fig.1 for recording. Following the above-described procedure, we can then obtain the final observed images generated from the conical hologram. Fig.2 left shows the image observed at the designated viewing distance of 50cm. The figure on the right-hand side is from the previous result when the 2D object in the hologram recording system is prepared on a conical surface. We note that, with the method proposed in this paper, the regenerated image is free from distortion.

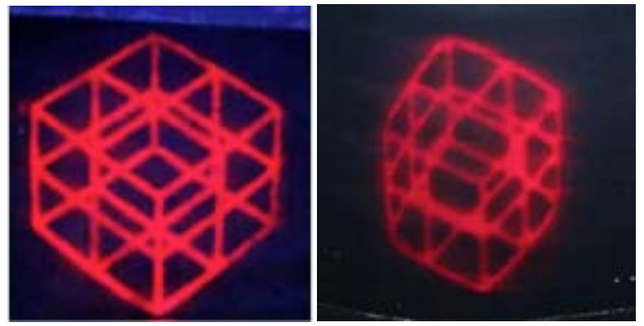

Fig.2. Images observed at the designated viewing distance of 50cm. The left figure is the result from this paper and the right figure is from the previous result when the object plane is approximated as a conical surface.

the hologram recording system is prepared on a conical surface. We note that, with the method proposed in this paper, the regenerated image is free from distortion.

3. Summary

With the holographic film pre-bent into a conical shape before recording, the interfering-ray directions on the film would not be changed after development process. Hence, the holographic process is considerably simplified. The device to mount the distorted 2D object plane can easily be fabricated by using the 3D printer. The final result shows that the regenerated image from the hologram is free from distortion.

References

[1] L. Huff and R. L. Fusek, " Color holographic stereograms," Opt. Eng. 19, 691-695 (1980).

[2] K. Okada, S. Yoshii, Y. Yamaji, J. Tsujiuchi, and T. Ose, "Conical holographic stereograms," Opt. Commun. 73(5), 347-350 (1989).

[3] Y. S. Cheng, Y. T. Su, and C. H. Chen, "360-degree viewable image-plane disk-type multiplex holography by one-step recording," Opt. Exp. 18(13), 14012-14023 (2010).

[4] Y. S. Cheng and S. Y. Lin, "Reflection image-plane conical multiplex holography using optical system with curved object-plane," Proc. Digital Holography and 3D Imaging, Shanghai (2015).

25.

Speckle Reduction in Holographic Projection Display Using Window Partition Method

Ming-Hong Weng, Hsin-Chuan Chen, and Wei-Feng Hsu*

Department of Electro-optical Engineering, National Taipei University of Technology, Taipei 10608, Taiwan

*Email: whsu@ntut.edu.tw

1. Introduction to system schematic of holographic projection display (HPD)

We present a scheme of a holographic projection display in which a phase-only spatial light modulator (SLM) performed three functions: beam shaping, image display, and speckle reduction [1]. Figure 1 illustrates the schematic diagram of the entire system and the functionality. The functions of beam shaping and image display were performed by dividing the SLM window in to four sub-windows which were loaded with different diffractive phase elements (DPEs). Three sub-windows show DPEs to shape red, green, and blue lasers into rectangular distributions and become the incident field to the imaging DPE loaded in the sub-window. The field modulated by the DPE to generate a display image through a Fourier transform lens. The functions of speckle reduction and color combination were performed by temporally integrating the display images. The DPEs were calculated using a modified iterative Fourier transform algorithm (IFTA) [2]. Initializing with different random phases, the IFTA program resulted in DPEs which generate resemble images with random phases. Integrating the images reduces the speckle phenomenon in the resultant image.

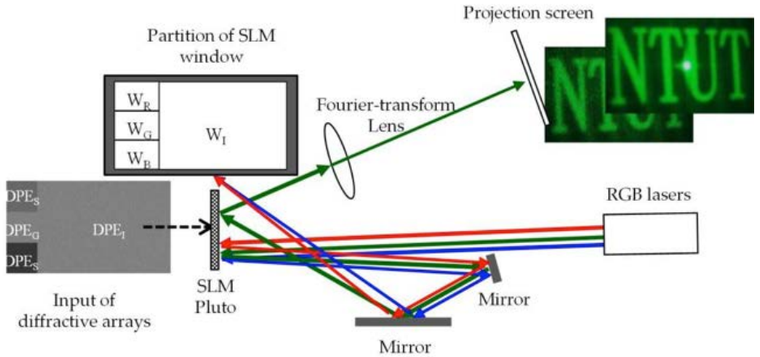

Fig. 1. Schematic diagram of the diffractive projection display system. When a green image is produced, for example, the green laser beam becomes rectangular as it reflects back to the spatial light modulator (SLM). The diffractive phase element, DPEI, in sub-window WI modulates the rectangular beam and produces a display image in the projection screen. Using temporal integration of multiple speckled images reduces the speckle effect in the display image.

2. Window partition method for HPD

The first function performed by the SLM is beam shaping of the incident lasers. The cross section of the incident beam is circular and will be changed into rectangular by the SLM. The left side of the SLM window is divided into three sub-windows W_R, W_G, and W_B, sequentially from top to bottom, and each contains 360×360 pixels. Each sub-window modulates a laser beam to generate rectangular distribution of intensity that will cover the right side of the SLM window W_I.

The second function performed by the SLM is diffractive imaging by means of an optical Fourier transform system. Loaded in sub-window W_I, the phase elements DPE_I containing 1560×1080 pixels to generate the display images are calculated using the IFTA programs which are the same as the programs for beam shaping DPE. Although the optical wave incident to W_I is not uniform and contains speckles, the quality of the diffractive image of the illuminated DPE_I is approximately close to that illuminated by uniformly plane waves.

The third function performed by the SLM is speckle reduction by temporally integrating many statistically independent specked images. Speckle phenomenon in an image can be evaluated by the

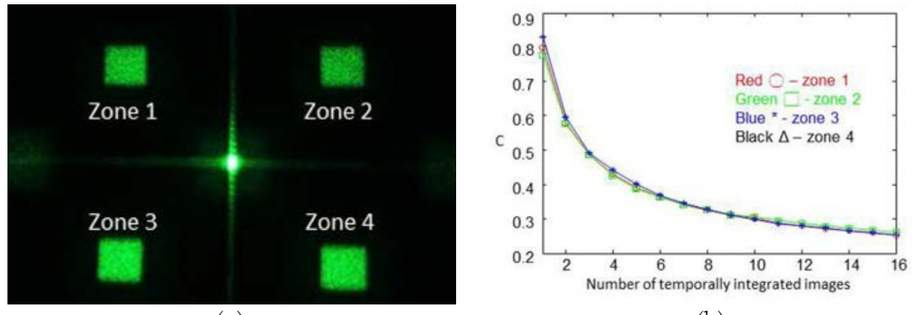

Fig. 2. (a) Test image for speckle reduction and (b) Speckle contrast of the resultant images by temporal integration of multiple speckled images

speckle contrast C, defined by $C = \sigma_I / \bar{I}$, where σ_I and $\bar{I}$ are the standard deviation and the mean of the speckle intensity of image, respectively [3]. Figure 2 shows the test pattern which we used to evaluate the effect of our method of speckle reduction and the speckle contrast of the resultant images.

3. Summary

We have presented a holographic projection display scheme that requires very limited volume because it needs only a phase-only SLM, a Fourier-transform lens, and two mirrors. The beam shaping and image display functions were performed by dividing the SLM window into four sub-windows. Speckle reduction was achieved by displaying the DPEs in temporal sequence. The DPEs were calculated using a modification of IFTA. Speckle in the resultant image was reduced through the temporal integration of the diffractive images. Sixteen images were used to produce speckle contrast values of 0.26.

References

[1] W.-F. Hsu and M.-H. Weng, “Compact holographic projection display using liquid-crystal-on-silicon spatial light modulator,” *Materials 9*, 768 (2016).

[2] F. Wyrowski and O. Bryngdahl,” Iterative Fourier-transform algorithm applied to computer holography,” *J. Opt. Soc. Am.* **A5**, 1058–1065 (1988).

[3] J. W. Goodman, *Speckle Phenomena in Optics: Theory and Applications*; Roberts & Company: Englewood, CO, USA, 2007, p. 28.

26.

Effect of a quasi-continuous fringe-scanning on generalized phase-shifting digital holography

Nobukazu Yoshikawa, Syouma Namiki, and Keisuke Kasai Graduate School of Science and Engineering, Saitama University, 255 Shimo-Okubo, Sakura-Ku, Saitama, 338-8570, Japan

1. Introduction

A continuous fringe-scanning scheme combined with a generalized phase shifting approach is an effective way to perform a high-speed measurement in phase-shifting digital holography (PSDH) because highly precise phase shift control and synchronization between a digital camera and a phase shifter are not required [1]. The recent piezoelectric transducer (PZT) controller is often equipped with a programmable control function for stage positioning. Although a linear phase shift can be created by such functions, if only simple program functions such as move, stop and wait are used, we may obtain a quasi-linear phase shift. The problem on the phase shift error can be almost negligible in the generalized PSDH. However, the nonlinearity of the phase shift will affect the integrating intensity of the interference fringe captured by the continuous fringe scanning scheme. In this study, we develop the generalized PSDH with the continuous fringe-scanning scheme using a quasi-linear phase shift that is created by the simple program function of the PZT controller. Furthermore, we experimentally investigate the effect of the quasi-linear phase shift.

2. Method

We consider a color PSDH system shown in Fig. 1. The phase shift is created by a reference mirror mounted on a piezo stage (SIGUMA KOKI, SFS-H40X) controlled by a PZT controller (SIGUMA KOKI, FINE-01γ). The simple motion can be controlled by a programmable control function. The minimum step size is 1 nm and the wait time pitch width is 0.01 sec. Three phase-shifted color interference fringes are captured by a color CCD camera (SONY XCL5005CR, 2048×2048 pixels, 15fps). After color decomposition, the statistical generalized phase-shifting approach is independently applied to the interference fringes of each wavelength. As a result, the phase shift values of each wavelength are estimated [2]. We use an interference fringe between two plane waves to verify the effect of the quasi-linear phase shift. Therefore, the phase shift value and the moving distance of the reference mirror can be obtained correctly using the Fourier transform method. The quasi-linear phase shift is created using an approximate ramp signal consisting of a small step movement and a subsequent short stopping state. We use the ramp signal designed by the

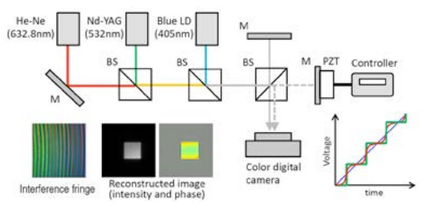

Fig. 1. Color PSDH system using the quasi-linear phase shift.

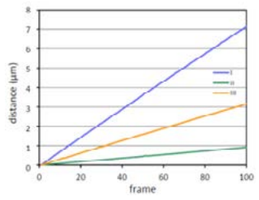

Fig. 2. Moving distance of the reference mirror.

conditions of (I) 1

nm increment without stopping state, (II) 1nm increment with stopping state of 0.01sec, and (III) 4nm increment with stopping state of 0.01 sec.

3. Experimental results

Figure 2 shows the moving distance of the reference mirror as a function of the frame. The moving distance per 1 frame was I: 72.0±10.8nm, II: 9.2±3.4nm, and III: 32.0±6.7nm. The reference mirror moved almost linearly though small fluctuations occurred when the piezo stage is accelerated or decelerated. Figure 3 shows the phase estimation error of generalized PSDH. The typical reconstructed phase image is shown in Fig.4, where the phase is compensated by the initial phase of the first reconstructed frame.

In the condition I, phase estimation was successfully performed except for some frames in which a large estimation error occurred. The phase estimation error may be caused by the nonlinearity of the quasi-linear phase shift. However, almost the same reconstructed wave was obtained in all frames in the case of the He-Ne and the Nd-YAG lasers. For the blue LD, the exchange between the object and conjugate waves sometimes occurred though the object wave was clearly reconstructed. In such case, the direction of phase rotation may be inverted due to the excessive increase of the phase shift in the phase shift estimation. Therefore, the influence of a quasi-linear phase shift is small as long as a long wavelength light source is used. In the condition II, there were phase errors of approximately 0.3 radian in all frames. Moreover, significant phase estimation error occurred at frames around the stop state. The reconstructed image was distorted because the object and conjugation waves were reconstructed at the same time as shown in Fig.4(b). The cause of that may be due to the vibration noise caused by the stage stop, the increase of the nonlinear phase shift component due to the repetition of the rapid acceleration or deceleration, and the small amount of the phase shift. At the large error frames, the distortion of the reconstructed image was improved because the phase shift became large. In contrast, the phase estimation error was less than 0.02 radian in the condition

III. The object wave was clearly reconstructed except for some frames in which a large phase estimation error occurred. The phase of the reconstructed image was slightly increased with increasing the frame number, which may be caused by the nonlinear phase shift component.

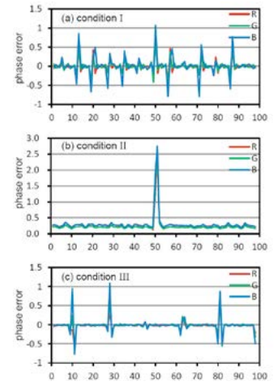

Fig.3. Phase estimation error of generalized PSDH.

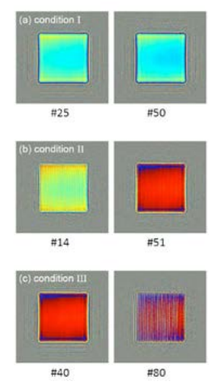

Fig.4. Reconstructed phase image.

4. Conclusion

We verified the effect of the quasi-linear phase shift in generalized PSDH with the continuous fringe-scanning scheme. When the quasi-linear phase shift was created by the phase shift schedule consisting of successive minute movement without the stopping state, the phase shift estimation can be successfully performed. When the stopping state was used to create the linear phase shift, the effect of the quasi-linear phase shift was significantly different depending on the combination of the move and wait time.

References

[1] N. Yoshikawa and K. Kajihara, Opt. Lett. 40, 3149-3152 (2015).
[2] T. Shiratori and N. Yoshikawa, IWH 2015 Digest, We5-P13 (2015).

27.

Digital Microscopy with Volume Hologram under Incoherent Light Source

Po-Hao Wang,[1)]* Hsi-Hsun Chen,[1)] Wei-Tang Lin,[1,2)] Yuan Luo[1,3)]

[1)]Institute of Medical Device and Imaging, National Taiwan University, Taiwan

[2)]National Taiwan University School of Medicine, Taiwan

[3)]Molecular Imaging Center, National Taiwan University, Taiwan

1. Introduction

Digital holographic microscopy (DMH) has great potentials in biomedical imaging applications. By computational reconstruction, in-focus three-dimensional images can be easily reconstructed without time consuming vertical optical axis scanning. In general, DHM requires coherent condition when format a hologram by CCD camera. Thus, it can not reconstruct 3D images under incoherent sources, such as white light or emitted fluorescent light.

To generate interference pattern for digital holography, a pinhole can be used in lensless system with LED light source, but it is difficult to use in bio-fluorescent sample [1] [2]. Several techniques have been proposed to cross this barrier by using incoherent light such as Fresnel incoherence correlation holography [3][4] and incoherent digital holographic adaptive optics [5][6][7]. However, the former requires spatial light modulators with limited pixel resolution and expensive price, while the later needs mechanical scanning in their Mach–Zehnder setup to match short optical path length.

2. Experimental results

In this article, a self-interference 4-f imaging system with two multiplexed volume holographic pupils is proposed. PQ-PMMA volume hologram can be used as a thick recording material to record wavefronts [8] [9] [10]. Through the recording exposure process, two multiplexed volume holographic pupils can diffract two different wavefronts along the same path, as shown in Fig.1. The diffracted signal beam from the sample will interfere with its corresponding common-path reference beam after volume holographic pupils. Therefore, self-interfered pattern will be generated and recorded at the CCD plane. Fresnel propagation method then can be utilized for computational reconstruction.

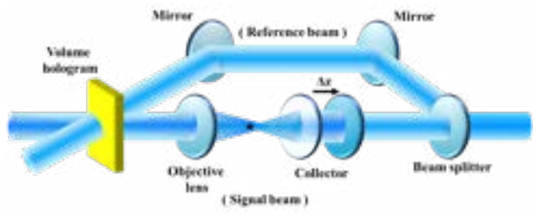

Fig.1. Recording process.

In the experiment, we used a white light LED as an incoherent light source. An air-force resolution target was used in our microscopic imaging system to test the system property. The multiplexed volume holographic pupil is located at the center position (i.e. Fourier plane) in microscopy system. With multiplexed volume holographic pupils, Fig.2 shows the raw image captured by CCD and its reconstructed image. Fig 2(a) shows the raw data captured by CCD and its reconstructed image without multiplexed volume holographic pupils. Fig 2(b) shows that with multiplexed volume holographic pupils can successfully reconstruct the image and enhanced contrast under incoherent light source.

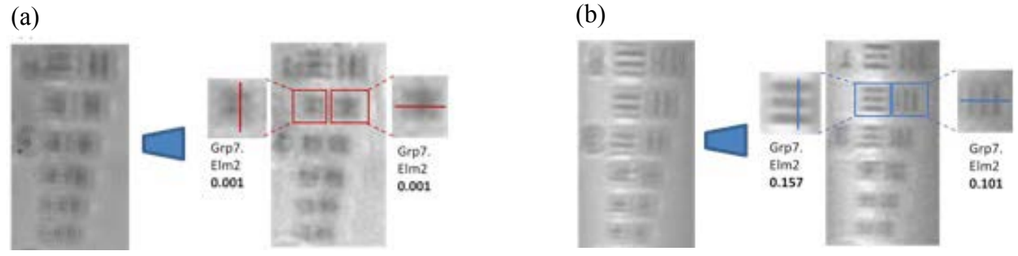

Fig 2. (a) Raw image and reconstructed image in zero order (b) Raw image and reconstructed image in first order.

3. Conclusion

We have demonstrated multiplexed volume holographic pupils in microscopic imaging system with multiplexed volume holographic pupils. The image can be well reconstructed under incoherent light source by digital holography in our system.

References

[1] L. Repetto, E. Piano, and C. Pontiggia, “Lensless digital holographic microscope with light-emitting diode illumination,” Optics Letters Vol. 29, Issue 10, pp. 1132-1134 (2004).

[2] Vicente Micó and Javier García, “Common-path phase-shifting lensless holographic microscopy,” Optics Letters Vol. 35, Issue 23, pp. 3919-3921 (2010).

[3] J. Rosen and G. Brooker, “Digital spatially incoherent Fresnel holography,” Opt. Lett. 32(8), 912–914 (2007).

[4] J. Rosen and G. Brooker, “Non-Scanning Motionless Fluorescence Three-Dimensional Holographic Microscopy,” Nat. Photonics 2(3), 190–195 (2008).

[5] Myung K. Kim “Adaptive optics by incoherent digital holography,” Optics Letters, Vol. 37, Issue 13, pp. 2694-2696 (2012).

[6] Myung K. Kim “Incoherent digital holographic adaptive optics,” Applied Optics, Vol. 52, Issue 1, pp. A117-A130 (2013).

[7] J. Hong, M. K. Kim “Overview of techniques applicable to self-interference incoherent digital holography,” Journal of the European Optical Society - Rapid publications, vol 8 (2013).

[8] Wenhai Liu, George Barbastathis, and Demetri Psaltis, “Volume holographic hyperspectral imaging,” Applied Optics, Vol. 43, Issue 18, pp. 3581-3599 (2004).

[9] Luo Y, Gelsinger PJ, Barton JK, Barbastathis G, Kostuk RK. “Optimization of multiplexed holographic gratings in PQ-PMMA for spectral–spatial imaging filters,” Optics Letters, Vol. 33, Issue 6, pp. 566-568 (2008).

[10]Yuan Luo, Juan M. Russo, Raymond K. Kostuk, and George Barbastathis. “Silicon oxide nanoparticles doped PQ-PMMA for volume holographic imaging filters,” Optics Letters Vol. 35, Issue 8, pp. 1269-1271 (2010).

28.

Volume Hologram with Non-axial-scanning Confocal Microscope

Po-Hao Wang,[1)*] Yuan Luo[1,2)]

[1)]Institute of Medical Device and Imaging, National Taiwan University, Taiwan

[2)]Molecular Imaging Center, National Taiwan University, Taiwan

1. Introduction

Wide-field fluorescence microscopy is a commonly used imaging technique by researchers and clinicians. For thick biological samples, background noise caused by out-of-focus light reduces contrast and signal-to-noise ratio of observed images. In general, post-imaging processing such as deconvolution techniques can improve image quality [1]; however, it does not provide true optical sectioning, due to the missing cone in system's transfer function. The most commonly used optical sectioning imaging method with good background rejection in biomedicine is based on point-by-point laser scanning confocal approach [2-4]. Although increasing number of scanning points at a specific depth are ongoing [5], multiple axial foci are barely achieved in confocal microscopy. Here, we demonstrate the first experimental realization of a non-axial-scanning multi-focal confocal microscope for 3D imaging where contrast and speed are achieved from the combination of confocal imaging pinholes and multiplexed holographic Bragg illumination filters.

2. Experimental results

Volume hologram is a photographic recording of light field. The interference pattern diffracts the light of the original light field during reconstruction. We fabricate a multiplexed holographic Bragg illumination filters with multi-focal points to realize a non-axial-scanning confocal system. Figure 1 shows a schematic diagram of the proposed system, where two conjugated pinholes reject out-of-focus light such that corresponding photodetectors simultaneously collect optically sectioned information from different depths. Figure 2 shows experimental results of the point spread function measured by a flat mirror.

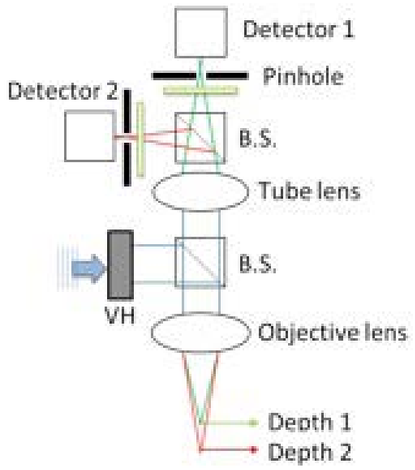

Fig. 1. Non-axial-scanning multifocal confocal system.

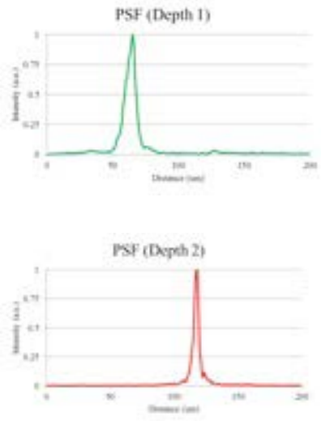

Fig. 2. point spread function measured by a flat mirror.

References

[1] McNally, J.G., Karpova T., Cooper, J., Conchello, J.A., Three-dimensional imaging by deconvolution microscopy, Methods 19, 373-385, 1999.

[2] C.J.R. Sheppard, A. Choudhury, "Image Formation in the Scanning Microscope", Optica Acta, Vol. 24, No.10, pages 1051-1073, 1977.

[3] M.Minsky, "Memoir on inventing the confocal scanning microscope", Scanning, Vol. 10, Issue 4, pages 128–138, 1988.

[4] Yuan Luo, Vijay Raj Singh, Dipanjan Bhattacharya, Elijah Y. S. Yew, Jui-Chang Tsai, Sung-Liang Yu, Hsi-Hsun Chen, Jau-Min Wong8, Paul Matsudaira, Peter T. C. So and George Barbastathis, "Talbot Holographic Illumination Non-scanning (THIN) Fluorescence Microscopy," Laser & Photonics Reviews ,Volume 8, Issue 5, pages L71–L75, September 2014.

[5] Keiichiro Kagawa, Min-Woong Seo, Keita Yasutomi, Susumu Terakawa, and Shoji Kawahito, "Multi-beam confocal microscopy based on a custom image sensor with focal-plane pinhole array effect," Optics Express, Vol. 21, Issue 2, pp. 1417-1429, 2013.

29.

Position Servo of Volume Holographic Disc by Self-Diffraction Signal

Yeh-Wei Yu[1], Po-Kai Hsieh[2], Chung-Mou Hsu[2], Wei-Chia Su[3], Shiuan-Huei Lin[4] & Ching-Cherng Sun[2]*

[1]Optical Science Center, National Central University, Chung-Li, Taoyuan City 32001, Taiwan [2]Department of Optics and Photonics, National Central University, Chung-Li, Taoyuan City 32001, Taiwan [3]Graduate Institute of Photonics, National Changhua University of Education, Changhua City 50091, Taiwan

[4]Department of Photonics, National Chiao Tung University, Hsinchu City 30010, Taiwan

Summary

With the aim of advance the storage capacity on optical disc, using near-field optics or holography to break the bottle neck is a useful method. We make an effort on holographic disc which is a way to achieve better storage capacity and lower recording time. The Bragg condition makes the intensity of recording beam changing, thus we can adjust the position of recording materials to let the data be recorded in several. This paper is thus planned to present the higher precision, stability and efficiency than the traditional disc.

The on-axis holographic data storage system (Figure 1) is easily to miniaturization, integration and downward compatibility by DB/DVD drive and downward compatibility. The coupled mode theory and Born's approximation method which are the calculation method of wave states could be used in the condition of week couple. Unfortunately, those two methods are too intricate to get answer in a short time. Thus, there is a model which is called volume hologram as an integrator of the lights emitted from elementary light source (VOHIL) proposed by Prof. C.C. Sun to have a result of efficiency and relative phase shifting immediately which is. This method could be used in week couple condition, and it is the basic in the simulation on the Bragg degeneracy.

$$D_A \propto \int\left[\left(|S|^2+|R|^2\right)Pe^{i\phi_P}+PS^*Re^{i(\phi_P+\phi_R-\phi_S)}+PSR^*e^{i(\phi_P-\phi_R+\phi_S)}\right]e^{i\phi_d}d\vec{r}$$

The simulation of formula by VOHIL is expressed as

Where the DA is amplitude of diffraction beam, S is amplitude of signal beam, R is amplitude of reference beam, ϕ_P is phase of reading beam, ϕ_S is phase of signal beam, ϕ_R is phase of reference beam, and ϕ_d is phase of diffraction beam.

We change several parameter of recording material which is thicknesses, dimension of interference and focus position. Figure 2 shows the efficiency of self-diffraction signal, the intensity change by the shifting along the Bragg degeneracy axis on disc. With the on-axis system and the simulation, we using the spherical wave as the reference light and signal light to generate the self-diffraction signal from holographic disc, as shows on Figure 3.

In conclusion, after using the standard deviation of several experiments as evaluation criteria, we knows that reference and signal light spot has the larger distance in the X direction, the lower displacement tolerance, but the self- diffraction signal cannot be discriminated if two light spot are too close.

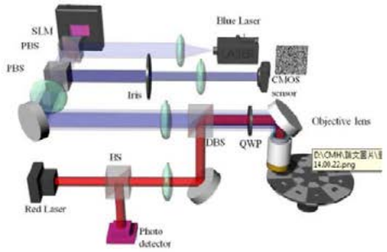

Fig. 1. The system setup of HDS system.

Fig. 2. The simulation in holographic disc by VOHIL.

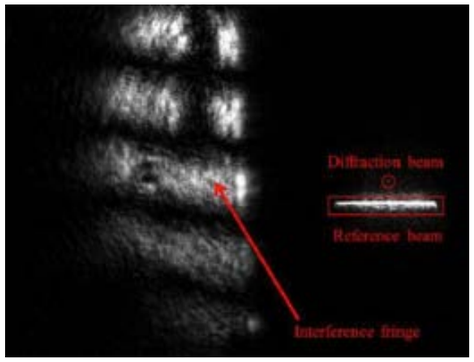

Fig. 3. The self-diffraction beam reading experiment.

References

[1] J. W. Goodman, *Introduction to Fourier Optics*, 3rd eds. (McGraw-Hill, NewYork, 2002).

[2] H. J. Coufal, D. Psaltis, and G. T. Sincrbox, *Holographic data storage*,(Springer, New York, 2000).

[3] C. C. Sun, "*A simplified model for diffraction analysis of volume holograms*," Optical Engineering (Letters) 42, 1184 (2003).

[4] H. Horimai and X. Tan, "*Collinear technology for a holographic versatile disk,"* Appl. Opt. **45**, 910-914(2006).

[5] C. C. Sun and P. P. Banerjee, "*volume holographic optical elements,*" Optical Engineering **43**, 1957 (2004).

[6] C. C. Sun and C. Y. Cheng (2016), "*The study of the collinear holographic data storage system with disc defocus,*" doctoral dissertation , National Central University, Taoyuan

30.

Optimal Angle of Tilted Plane for Diffraction Fields Generated by Diffractive Optical Elements Using Angular Spectrum Method

Shang-Hao Huang, Siou-Jhih Lin, Xin-Yu Xu, and Wei-Feng Hsu*

Department of Electro-optical Engineering, National Taipei University of Technology, Taipei 10608, Taiwan

*Email: whsu@ntut.edu.tw

1. Introduction

In this paper, the diffractive optical elements (DOEs) to generate tilted diffractive fields are designed using the iterative angular spectrum algorithm (IASA) and implemented using a phase-only spatial light modulator (SLM) [1]. IASA adopted the angular spectrum (AS) method to perform fast and exact calculations of the wave propagating not only between two parallel planes but non-parallel planes. This is achieved by modifying and optimizing the spatial frequency [2].

2.Angular Spectrum method and Iterative angular spectrum algorithm (IASA)

In AS method, the light field in a source plane, $U(x, y, 0)$, is decomposed into a angular spectrum,

$$A(f_x, f_y;0) = \int_{-\infty}^{\infty}\int U(x,y,0)e^{-j2\pi(f_x x+f_y y)}dxdy \quad (1)$$

$A(f_x, f_y; 0)$, by Fourier transformation [3]

where f_x and f_y are spatial frequencies with respect to x and y, respectively. When a wave propagates

$$A(f_x, f_y;z) = A(f_x, f_y;0)H(f_x, f_y;z) = A(f_x, f_y;0)e^{j2\pi z\sqrt{1-(\lambda f_x)^2-(\lambda f_y)^2}/\lambda} \quad (2)$$

over a distance of z, the AS undergoes a phase delay specified by the transfer function, given by

To avoid the aliasing error, a band limitation of the spatial frequency is applied to the transfer

$$H'(f_x, f_y;z) = H(f_x, f_y;z)\,rect\left(\frac{f_x}{2f_{x\,\mathrm{limit}}}\right)rect\left(\frac{f_y}{2f_{y\,\mathrm{limit}}}\right). \quad (3)$$

function,$H'(f_x, f_y; z)$, given by

In addition, to obtain the numerical results accurately, the sampling window on the source sampling area needs to be doubled along both the side length, and the extending area will be padded with zeros.

When the spatial frequency coordinates are rotated, the rotated coordinates is calculated by multiplying a rotation matrix M. Rotation of the spatial frequency domain increases the light field of target plane and be non-uniform in cross-sectional area. In order to overcome this problem, a Jacobian term is taken into account to maintain the conservation of energy of light.

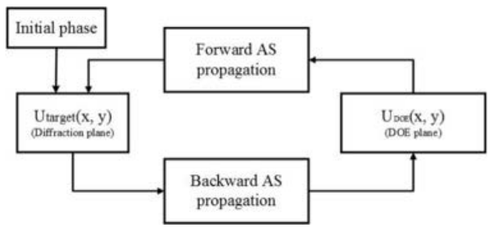

Figure 1. Flowchart of iterative angular spectrum algorithm (IASA)

We designed the DOEs using an iterative angular spectrum algorithm (IASA) which combined an iterative process with the AS theory [1]. As shown in Fig. 1, the rotating spatial frequency domain and the Jacobian are conducted in the process of forward and backward propagations formed by the angular spectrum method.

3. Experimental results

We designed several DOEs using the IASA. Each DOE contains 1920 × 1080 pixels with the display distance z of 30 cm. We changed the tilted angle of the projection plane from 0º to 85º. Figure 2 shows three DOEs and corresponding diffraction images which were captured by displaying the DOEs on an SLM. Figure 3(a) shows the DOE which was designed by setting the propagation distance of 30 cm and the rotation angle of 45 degrees. The diffraction images captured in the observation planes, tilted by the angles of 25º, 45º, and 65º, are shown as in Figs. 3(b) to (d), respectively. The image of tilted angle 45º is coincident with the simulation results, as shown in Fig. 3(c). It is shown that the image quality, including the uniformity and sharpness of the edges, of Fig. 3 (c) is the best among these figures.

4. Conclusion

We designed the DOEs on the basis of AS method to realize the tilted diffractive images. The experimental results show that the best image of rotation was obtained when the observation tilted plane rotated equal to the setting angle. As the tilted angle changed from 0º to 85º, and the maximum angle of the tilted plane of the projection images occurs at 75º.

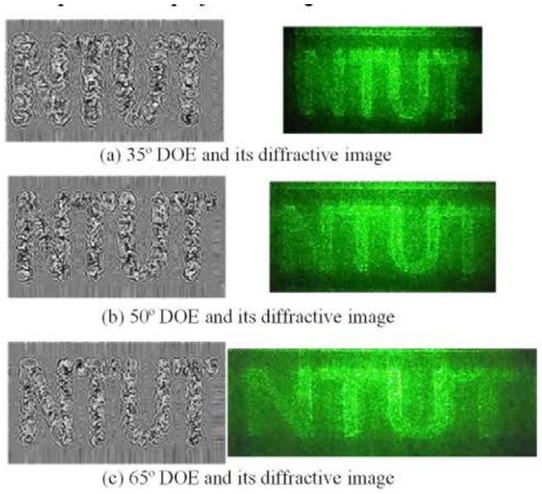

Fig. 2. DOEs of three rotation angle and the corresponding diffractive images

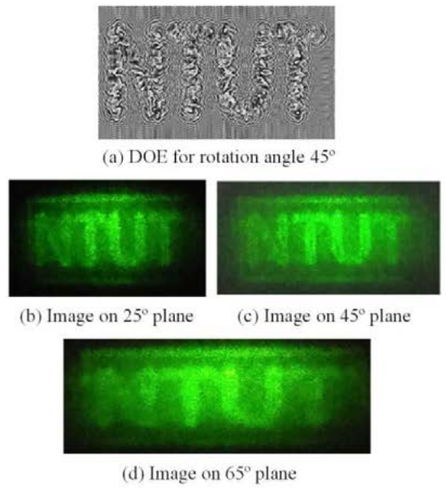

Fig. 3. DOEs of 45 º and its diffractive images on the tilted plane of 25º, 45º, and 65º.

References

[1] T.-Y. Chen, S.H. Huang, and W.-F. Hsu, "Iterative Angular Spectrum Algorithm (IASA) for the Application of 3D Volumetric Projection Display," OPTIC 2015, paper 2015-SAT-P0402-P016.

[2] K. Matsushima and T. Shimobaba, "*Band-limited angular spectrum method for numerical simulation of free-space propagation in far and near fields*," Opt. Express **17**, 19662-19673 (2009).

[3] J. W. Goodman, *Introduction to Fourier optics (3rd ed.)*. 2005: Roberts and Company Publishers, Englewood, Colorado.

31.

Synthesis of PMMA/EGPEA Holographic Materials

Sheng-Kai Juang, Hao-Yu Tsai, Shiao-Wei Kuo, and Wei-Hung Su Department of Materials and Optoelectronic Science,
National Sun Yat-Sen University,
Kaohsiung 804, Taiwan

1. Introduction

Photopolymerizable materials can be used for holographic recording due to their good light sensitivity, real-time image development, large dynamic range, and low cost [1-6]. It typically consists of a specific type of photo-initiated guest monomers and a photo-initiator; both are well dispersed in a host matrix. The light illumination makes the photo-initiators and monomers to produce polymer chains inside the host matrix. Refractive index of this material is therefore modulated by the light illumination. In general, the optical storage properties of these photo-polymeric recording medium rely crucially on the characteristic of the host and guest molecules; the host matrix should be highly porous such that the monomer and the initiator can infiltrate into its pores.

In this paper, an approach to fabricate photopolymerizable materials is presented. The EGPEA (ethylene glycol phenyl ether acrylate) is selected as the monomer, and the Irgacure 784 is employed as the photo-initiator. The porous substrate formed by PMMA [poly(methyl methacrylate)] is then subjected to the subsequent infiltration of the monomers EGPEA and the photo-initiator Irgacure 784. Once it is exposed to photo-illumination, the linear acrylate polymer chains are formed within the PMMA matrix, leading to a change of refractive index.

2. Fabrication method and experiment

Figure 1(a) illustrates the flow chart of the fabrication process. The PMMA uniformly distributed in ethanol is mixed with the monomers EGPEA and the photo-initiator Irgacure 784. The composite gel is then mechanically stirred in circulated condition at room temperature for 15 minutes. After validation for 24 hours, a photopolymerizable material is formed.

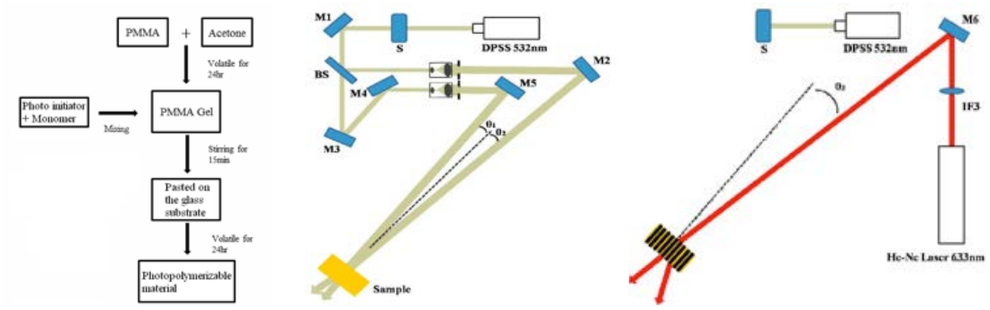

(a) (b) (c)

Fig. 1. (a) Flow chart of the fabrication process. (b) Holographic setup in the recording proceedure. (c) Holographic setup in the reading procedure.

Figure 1(b) shows the optical configuration for holographic recording. A DPSS laser which generates light waves with 532nm wavelength was used as the light source. A beam splitter divided the laser beam into two beams. Directed by two mirrors, these two beams interfered with each other within the holographic medium. The constructive interference made the linear acrylate polymer chains formed within the PMMA matrix, while the destructive interference kept the monomers EGPEA uniformly distributed in the matrix. A phase grating was therefore generated in the matrix. The incident angles of the light waves were $\theta_1 = \theta_2 = 1.5°$, resulting in a grating period of 10.16μm in the holographic medium.

A He-Ne laser with wavelength of 633 nm was used to evaluate the diffraction efficiency. Figure 1(c) depicts the optical configuration. In our experiments, the thickness of the holographic material was 500μm. It was a volume hologram. Thus, the incident angle of the reading beam was approximately 1.8°.

A number of holographic materials with different molar ratios of PMMA/EGPEA composites were fabricated. Figure 2 shows the diffraction efficiencies with the recording time for various diffraction orders. It is found that the diffraction efficiency of the 2nd order was more than 50%, which was higher than the 1st order.

3. Conclusion

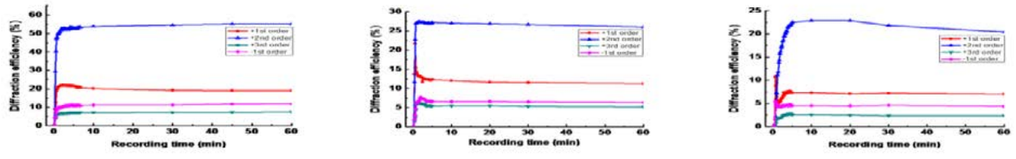

(a) (b) (c)

Fig. 2. Diffraction efficiencies with the recoding time for various diffraction orders. The molar ratio of PMMA/EGPEA was (a) 5/3, (b)5/4, and (c) 5/2.

We have described an approach using PMMA/EGPEA composites to fabricate holographic materials. A holographic configuration has been set up for optical recording and reading on the optical storage materials Diffraction efficiencies of various molar ratios of PMMA/EGPEA have been evaluated. A set of phase gratings with various grating periods by changing the incident angles θ_1 & θ_2 was performed as well. For interference angles $\theta_1 + \theta_2 < 85°$, diffraction efficiency more than 70% can be achieved.

References

[1] K. G. Yager and C. J. Barrett, "All-optical patterning of azo polymer films," Current opinion in solid state and materials science, vol. 5, 2001, pp. 487-494.

[2] I. Khoo, et al., "Observation of orientational photorefractive effects in nematic liquid crystals," Optics letters, vol. 19, 1994, pp. 1723-1725.

[3] Y.M. Chang, S.C. Yoon, M. Han, “Photopolymerization of aromatic acrylate containing phosphine oxide backbone and its application to holographic recording,” Optical Materials, vol. 30, 2007, pp. 662–668.

[4] W. Que, "Azobenzene-containing small molecules organic–inorganic hybrid sol–gel materials for photonic applications," Applied Physics B, vol. 91, 2008, pp. 539-543.

[5] O. Kulikovska, et al., "Smart Ionic Sol. Gel-Based Azobenzene Materials for Optical Generation of Microstructures," Chemistry of Materials, vol. 20, 2008, pp. 3528-3534.

[6] D.Wang, G. P.Bierwagen, “Sol–gel coatings on metals for corrosion protection,” Progress in Organic Coatings, Vol. 64, 2009, pp. 327–338.

32.

Comparisons of Scanning Methods of Pixelization Error Reduction Algorithm (PERA) for Design of Diffractive Optical Elements

Shih-Chih Lin, Kai-Yu Xie, Ho-Ling Chang, and Wei-Feng Hsu*

Department of Electro-optical Engineering, National Taipei University of Technology, Taipei 10608, Taiwan

*Email: whsu@ntut.edu.tw

1. Introduction

Optimization algorithms for design of diffractive optical elements (DOEs) are categorized into two types: inverse method and direct method[1]. The drawbacks of inverse and direct methods are lack of flexibility and inefficiency, respectively. In order to improve these drawbacks, we develop a novel algorithm which combines the features of both inverse and direct methods. In the paper, we introduce the method and compare different scanning methods. Expect for random perturbation, three other scanning methods to ensure the selection of all pixels in the diffraction plane are compared.

2. Pixelization error reduction algorithm (PERA) and scanning methods

Figure 1 shows the schematic of a DOE system in which the DOE and the diffractive planes are connected by Fourier and inverse Fourier transforms. The optimization process starts with the selection of a pixel in the diffractive plane. The amplitude of the pixel is replaced by the value of the corresponding pixel in the target image. The algorithm is thus called pixelization error reduction algorithm or, in brief, PERA. The new diffractive field inverse Fourier transformed to yield a DOE field function. The amplitude of the DOE field is set to a constant for phase-only DOE, and then it is Fourier transformed to produce the diffractive field. The cost is calculated to determine whether the selection of the pixel is accepted. Here, the cost function includes the root-mean-squared error (e), the diffraction efficiency (η), and the signal-to-noise ratio (SNR), defined as

$$e=\sqrt{\frac{\sum_{S+N}\left|I_{target}-\left|U_{diff}(x,y)\right|^2\right|^2}{\sum_{S+N}\left|U_{diff}(x,y)\right|^2}},\quad \eta=\frac{\iint_S\left|U_{diff}(x,y)\right|^2dxdy}{\iint_{S+N}\left|U_{diff}(x,y)\right|^2dxdy},\quad \text{and}\quad SNR=\frac{\min_S\left|U_{diff}(x,y)\right|^2}{\max_N\left|U_{diff}(x,y)\right|^2},$$

respectively, where S is signal region, N is noise region, U$diff(x,y)$ is diffraction field for element, I_{target} is intensity of target, i.e. square to target.

There are various ways to selecting a pixel for perturbation, including random selection, row scanning, snack scanning, and Z-zag scanning, as shown in Fig. 2. Random selection method selects an image pixel randomly. Row scanning changes the pixel value row by row from top to bottom in order. Snack scanning changes the pixel value of a row from one side to another, and then reverses the order in the next row. Z-zag scanning starts with the left-top pixel and then performs snack scanning in diagonal direction.

3. Simulation results

A target image of 128 × 128 pixels was used to design the DOEs of the same resolution using PERA. The number of iterations when conducting PERA was 491,520, i.e., 30 times the number of total pixels. The results of random selection contain e of 0.045, η of 0.8, and SNR of 3.5. The cost functions of the other three sequent selection methods were better than those of random selection, as shown in Fig. 3. Among these scanning methods, the results of row scanning method were the best, but not significant. Especially, the SNRs, exceeding 4.0, show the three sequent scanning methods are much efficient in searching the DOE solution because they ensure that all pixels in the diffractive image are selected.

4. Conclusion

We presented a novel optimal algorithm to designing DOEs, which is called pixelization error reduction algorithm (PERA). The method directly reduces the difference between the target and the temporal state in diffraction plane. PERA is not only flexible in the use of performance parameters but also efficient in searching local DOE solution. We compared three sequent scanning methods with the random selection method. The cost functions were better than those of random selection: e of 0.045, η of 0.8, and SNR of 3.5. In general, row scanning method results into the best DOE. Nevertheless, the SNR of the DOE using Z-zag scanning was the highest because the way of Z-zag scanning improved a DOE from low to high frequencies.

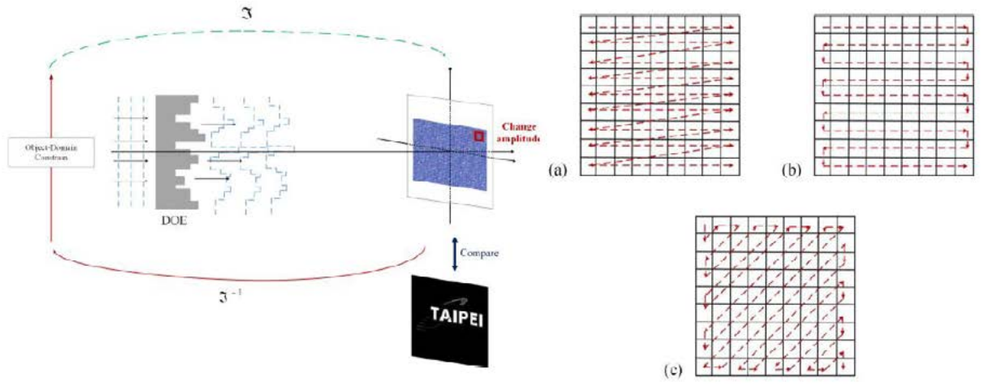

Fig. 1. Schematic diagram of DOE for PERA.

Fig. 2. Different scanning methods: (a) perturbation of a row (b) snack perturbation (c) Z-zag perturbation

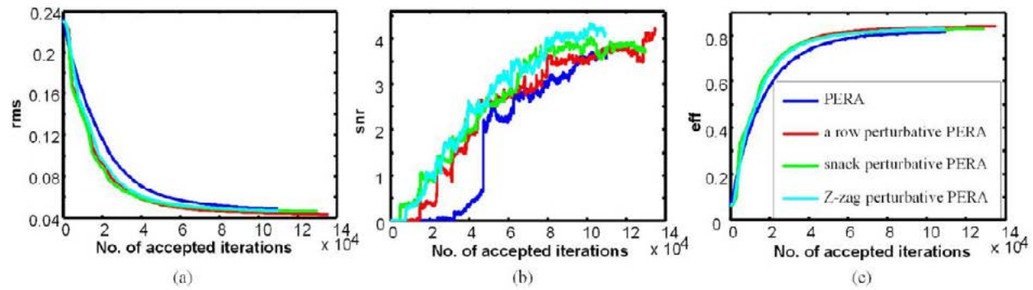

Fig. 3. The cost function of DOEs: (a) root-mean-squared error, (b) signal-to-noise ratio, (c) diffraction efficiency.

References

[1] J. Turunen and F. Wyrowski, Diffractive Optics for Industrial and Commercial Applications: John Wiley & Sons, Limited, 1997.

33.

Optimization of Dynamic Range of Pixelization Error Reduction Algorithm (PERA) for Design of Diffraction Optical Elements

Shih-Chih Lin, Ho-Ling Chang, Kai-Yu Xie, and Wei-Feng Hsu

Department of Electro-optical Engineering, National Taipei University of Technology, Taipei 10608, Taiwan Email: whsu@ntut.edu.tw

1. Introduction

Designing diffractive optical elements (DOEs) requires optimization methods such as simulated annealing algorithm, genetic algorithm, iterative Fourier transform algorithm, and particle swarm optimization. The drawbacks of these algorithms which design DOEs method include low convergent speed, inefficiency, and lack of flexibility. These drawbacks make the methods difficult to be applied in current optoelectronic devices. To overcome these drawbacks, we have developed a novel algorithm which combines the advantages of current optimal algorithms. In the proposed method, the intensity of a pixel in the diffractive image is changed to a specific value close to the intensity of the target pixel. The difference between the specific value and the target intensity is defined as the dynamic range. In the paper, the influence of the dynamic range of the method is studied and the optimal dynamic range is presented.

2. Pixelization error reduction algorithm (PERA)

The proposed algorithm is categorized into an inverse method of DOE design[1], which is applied to an optical framework, as shown in Fig. 1. The DOE domain and the diffractive domain, both are subject to different constraints, are connected by Fourier transform and inverse Fourier transform. The optimization in the proposed approach starts with selecting a pixel in the diffractive image and then changes the value according to the target image. The change of the pixel intensity reduces the error directly, which is thus called pixelization error reduction algorithm (PERA). The new diffractive field is inverse Fourier transformed to result into a complex DOE field. Secondly, the amplitude of the DOE field is set to a constant and the phase remains unchanged, and then is Fourier transformed to yield the diffractive field that actually reveals the effect of the pixel change. The cost of the diffractive field is calculated to evaluate the change of the pixel. When the cost is lower, the diffractive field is saved for the next step. A new pixel is selected randomly, and another loop operations conduct, as shown in Fig. 2.

3. Dynamic range and simulation results

To obtain the DOEs with high performance (large signal-to-noise ratio, low signal variation, and etc), we adopted the dynamic range of amplitude in diffraction field to control the convergence of the optimization operations[2]. The dynamic range is defined as the difference between the target image (a binary image here) and the intermediate image, which is shown as in Fig. 3. In the simulations, we calculated the DOEs using PERA with various dynamic ranges specified in the program. Figure 4 shows the root-mean-square error, the signal-to-noise ratio, and the signal variation of the designed DOEs. When the dynamic range of signal region is set to 0.2, signal variation is approximately 1.3. But, when the dynamic range of signal exceeds 0.3, signal variation increases. However, it is also found that the dynamic ranges in both the signal and the noise regions are needed to be controlled in order to obtain a good DOE using PERA. When the dynamic ranges of both regions exceed 0.1, the three performance parameters, the root-mean-square error, the signal-to-noise ratio, and the signal variation, start becoming worse.

4. Conclusions

In the paper, we introduced a new optimization algorithm PERA for the design of DOEs. PEAR is flexible in using the performance parameters and is effective in reduction of error of the selected pixel. The dynamic ranges less than 0.1 of the signal and noise in the diffractive image were used to result into DOEs with better performance. When dynamic range was between 0.01 and 0.2, we obtained the DOEs with the lowest signal variation among others. In the consideration of converging speed of using PERA, a large dynamic range, such as 0.5, is used in the early phase and then reduces the dynamic range gradually to obtain the DOE of a low signal variation.

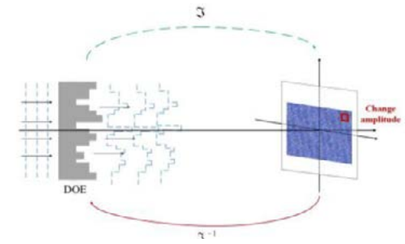

Fig. 1. Framework of DOE usingPERA.

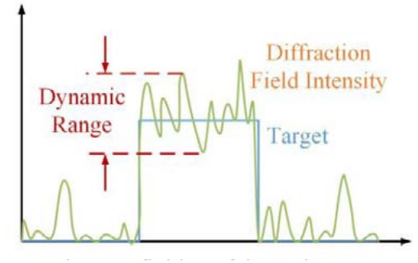

Fig. 3. Definition of dynamic range

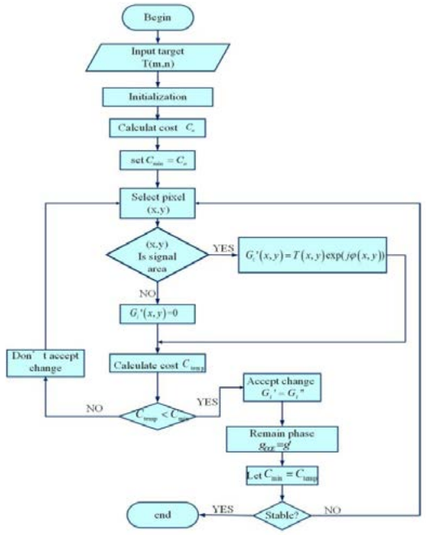

Fig. 2. Flowchart of PERA.

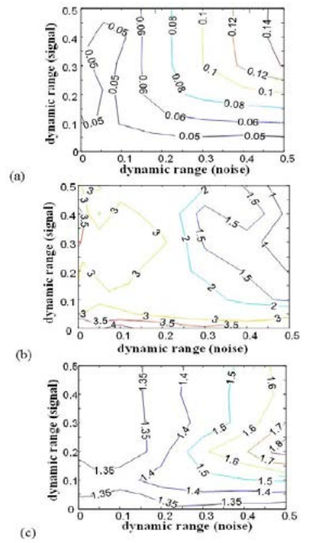

Fig. 4 Cost functions: (a) root-mean-square error (b)signal noise ratio(c) signal variation

References

[1] J. Turunen and F. Wyrowski ed., Diffractive Optics for Industrial and Commercial Applications, Akademie Verlag, Berlin, 1997.

[2] Y.-C. Chiu, W.-C. Lai, T.-Y. Chien, and W.-F. Hsu, “Design and Implementation of the Far Field Phase-Shift Patterns,” in *Proceedings of OPT’08*, Taipei, Taiwan, ROC, Dec. 5-6, 2008, Paper IP-023.

34.

Optical data storage using volume polarization hologram

Shiuan Huei Lin[1], Lun Kuang Lin[1], Vera Marinova[2] and Ken Y. Hsu[2]
[1]*Department of Electrophysics, National Chiao Tung University, HsinChu, Taiwan*
[2]*Department of Photonics, National Chiao Tung University, HsinChu, Taiwan*

In 1963, by studying properties of volume hologram, P. J. van Heerden mathematically demonstrated that storing optical information in solids has huge potentials of capacity and data rate [1]. In the search for "ultra" storage technologies volume holography is therefore considered as a potential candidate. In late 1990s, one can observe intensified research activities concerning various aspects of this field, including the development and theoretical analysis of powerful multiplexing schemes, the availability of suitable recording materials and affordable lasers, modulators, and detectors. Experiments demonstrated the possibilities of 10 TB capacity in a disk and 10 Gb/s data rate [2]. However, for pursuing the commercialization of holographic memories, many of these aspects are still open questions. In addition, new ideas give rise to new innovations and applications. In this paper, we review and discuss the progress of volume polarization holography. Based on the diffraction characteristics of a polarization volume hologram, we propose new holographic data storage scheme using polarization holography.

Polarization hologram records the periodic polarization state of light produced by orthogonally polarized reference and object beams. Permittivity of the recording media is modulated according to polarization states of two writing beams. As a result, the diffraction efficiency and the polarization state of reconstructed signal depend on the polarization of readout beam. This unique property is very useful for data storage application, because the polarization states of the recording and diffracted beams can be considered as new parameters applied into system for either adding new multiplexing scheme or increasing the signal-to-noise ratio of the retrieved data page. Therefore, many investigations have been conducted to understand the characteristics of polarization hologram for achieving a full utilization of advantages of polarization holograms. Further, the holographic properties, such as recording sensitivity and diffraction efficiency, of different polarization schemes have also been studied for different materials. For examples, a vector tensor model has been proposed by Kuroda, …et. al. [3] to analyze particularly recording and readout of a volume polarization hologram in a thick recording medium. We have fabricated thick phenanthrenequinone-doped poly(methyl methacrylate) (PQ/PMMA) photopolymer and investigated experimentally its capability for volume polarization holographic recording [4]. The results were well consist with the theoretical analyses of the polarization dependence diffraction reported by Kuroda. It showed the higher diffraction efficiency and the high degree of distinction of holographic reconstructions under paraxial approximation, for the two writing beams in orthogonal circular polarization configuration.

Those properties provide strategies to design holographic data storage system using polarization hologram in PQ/PMMA photopolymer. The schematic diagram for the optical setup is shown in Figure 1. To fulfill the paraxial approximation, we choose in-line holographic recording. Two SLM devices are placed to two adjoin sides of a polarization beam splitter (PBS) for displaying the signal data page and the reference pattern. They are focused onto an PQ/PMMA disk by a Fourier lens (f=4 cm) together such that intersection angle between the two recording beams can be close to zero. The sample is mounted on a translation stage for implementing the shift multiplexing. During recording, the data page is displayed on SLM1 and the reference pattern is displayed on SLM2, respectively. Two beams are combined by a PBS and then go through a $\lambda/4$ plate. The polarization state of the object beam is transferred into left-handed circularly polarized, and that of the reference beam is transferred into right-handed circularly polarized. They interfere and record a polarization hologram. Multiple holograms are recorded by shifting the recording medium at different positions. During reconstruction, the holograms are reconstructed one by one with a reference pattern displayed on SLM2 and the disk is shifted. Because the reading beam is left-handed circularly polarized, the diffracted signal from the hologram is right-handed circular polarization and then pass through a $\lambda/4$ plate, becoming s-polarized such that it can finally transmits through the analyzer to reach CCD. On the other hand, the reference is p-polarized and blocked by the analyzer.

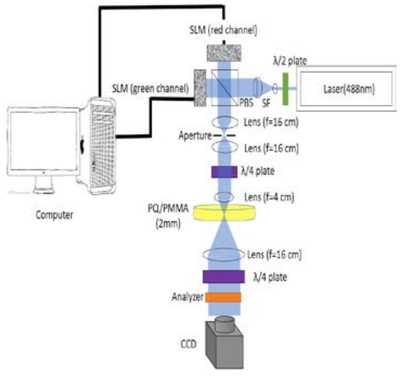

Fig. 1. The schematic diagram of the optical setup of a holographic memory system.

(a) (b)

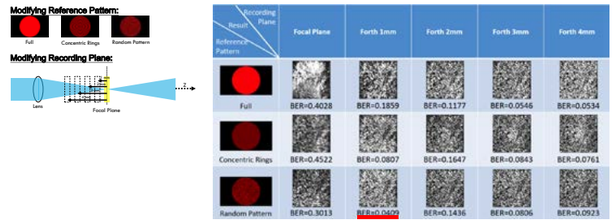

Fig. 2. (a) schematic parameter for testing performance of storage system, (b) experimental reconstructed data page for each testing case

In experiments, we have used three different reference patterns and a data page with random binary bit to test the performance of our storage system. In addition, the recording medium was moved to several positions out of focal plane of Fourier lens with several millimeters, as shown in Fig. 2(a). Three different reference patterns are full circle, concentric rings and random binary bits, respectively. The reconstructed data page for each case is shown in Fig. 2(b). As it can be seen that the reconstructed data page has smaller Bit-Error-Rate (BER) as the recording medium is out of the focal plane. Among them, the case of random-binary-bits reference plus 1-mm away from focal plane gives the best result with BER=0.0409. The further experiments related multiplexed recording and retrieving of the holographic pages will be demonstrated and discussed.

Financial support by the MOST, Taiwan under contracts, 104-2221-E-009-146-MY3, and AUT program, Ministry of Education, Taiwan are gratefully acknowledged.

Reference:

[1] P. J. van Heerden, Appl. Opt. 2, 393-400 (1963)
[2] H. J. Coufal, D. Psaltis, G. Sincerbox, *Holographic data storage* (Springer series in optical sciences, 2000).
[3] K. Kuroda, Y. Matsuhashi, R. Fujimura, T. Shimura, Opt Rev, vol. 18(5), pp. 374-382, 2011.
[4] S. H. Lin, P. L. Chen, C. I. Chuang, Y. F. Chao, and K. Y. Hsu, Opt. Lett. 36(16), pp. 3039-3041 (2011).

35.

Scale Correction of Lens-Less Fourier Digital Holographic Microscope Based on Rayleigh-Sommerfeld Diffraction Integral

Shun Kashiwagi[1)], Daisuke Barada[1,2)], Ryushi Fujimura[2)], Takashi Fukuda[3)], Shigeo Kawata[1,2)], and Toyohiko Yatagai[2)]

[1)]Graduate School of Engineering, Utsunomiya University, 7-1-2 Yoto, Utsunomiya, Tochigi 321-8585, Japan [2)]Center for Optical Research and Education (CORE), Utsunomiya University, 7-1-2 Yoto, Utsunomiya, Tochigi 321-8585, Japan

[3)]Electronics and Photonics Research Institute, National Institute of Advanced Industrial Technology (AIST), Tsukuba Central 5, 1-1-1 Higashi, Tsukuba, Ibaraki 305-8565, Japan

1. Introduction

Holographic data storage is expected for an optical data storage with large capacity and high data transfer rate. In holographic data storage, it is important to adjust complex amplitude patterns of a recording wave at a recording medium for high density recording. However, it is difficult to directly measure the complex amplitude patterns. In our previous study, lens-less Fourier digital holography based on Rayleigh-Sommerfeld diffraction integral is investigated to directly measure the complex amplitude of the signal beam.[1,2)] However, the scale of reconstructed patterns was not coincided with a practical scale. In this paper, the scale correction method is investigated.

2. Principal of proposed lens-less Fourier digital holography

The digital hologram is expressed by an interference image between signal beam U_S and reference beam U_R at an image sensor as

$$H = |U_S + U_R|^2 = |U_S|^2 + |U_R|^2 + U_S U_R^* + U_S^* U_R. \tag{1}$$

In general, by analyzing the third term of eq. (1) in a computer, the complex amplitude U_S' of the signal beamat observation plane is obtained. the complex amplitude U_S of signal beam at the image plane is expressed by Rayleigh-Sommerfeld diffraction integral as follows:

$$U_S(x,y) = \frac{1}{2\pi}\iint_{-\infty}^{\infty} U_S'(\xi,\eta)\frac{d}{dz}\left\{\frac{\exp\left[ik\sqrt{(x-\xi)^2+(y-\eta)^2+z^2}\right]}{\sqrt{(x-\xi)^2+(y-\eta)^2+z^2}}\right\}d\xi d\eta. \tag{2}$$

$$U_R(x,y) = \frac{1}{2\pi}\iint_{-\infty}^{\infty} U_R'(\xi,\eta)\frac{d}{dz}\left\{\frac{\exp\left[ik\sqrt{(x-\xi)^2+(y-\eta)^2+z^2}\right]}{\sqrt{(x-\xi)^2+(y-\eta)^2+z^2}}\right\}d\xi d\eta. \tag{3}$$

The reference beam is expressed by

where U_R' is the complex amplitude of the reference beam at the observation plane. Around $(x, y) = (x_i, y_i)$,

$$V(x_i,y_i) \approx a^2(x_i,y_i)V_R(x_i,y_i)\iint_{-\infty}^{\infty} U_S'(\xi,\eta)\exp\left[-i2\pi\left(\nu_{x,i}\xi+\nu_{y,i}\eta\right)\right]d\xi d\eta \tag{4}$$

in which i is an identifier number of a pixel position, $V = U_S U_R^*$ is expressed by

$$V_R(x_i,y_i) = \iint_{-\infty}^{\infty} U_R'(\xi,\eta)\exp\left[-i2\pi\left(\nu_{x,i}\xi+\nu_{y,i}\eta\right)\right]d\xi d\eta \tag{5}$$

where $(\nu_{x,i}, \nu_{y,i})$ is the position of a Fourier space at the observation plane. When U_R' expressed by is known, U_S' is calculated by inverse FFT with a uniformed sampling point of $(\nu_{x,i}, \nu_{y,i})$. In our previous study, V_R is assumed to 1 so that the scale error was occurred. In this paper, it is investigated that the scale is corrected by using a quadratic phase function.

3. Experimental

Figure 1 shows the experimental setup. A laser beam with a wavelength of 405 nm was split into an illumination beam and a reference beam. The reference beam was reflected by a PZT mirror and focused on a 1951 USAF test target. The PZT mirror was used for four-step phase shifting method. The illumination beam was reflected by a mirror through a lens and illuminated onto a 1951 USAF test target through the objective lens. Then, the illumination area of the illumination beam is adjusted by using the lens at the illumination beam arm. Figure 2 shows the experimental result. The pattern of group 9, element 3 (line width: ~780 nm) was observed and it was confirmed that the scale was corrected.

4. Conclusion

In this paper, a scale correction method was proposed in lens-less Fourier digital holography based on Rayleigh-Sommerfeld diffraction integral and the scale correction was confirmed. However, the phase pattern for scale correction is not experimentally measured pattern. In future, the scale correction accuracy will be improved by using an experimentally measured reference beam pattern.

Acknowledgment

This work has been partially supported by the Japan Science and Technology Agency (JST) under the Strategic Promotion of Innovation Research and Development Program.

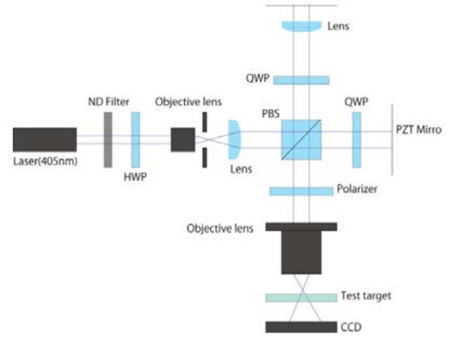

Fig. 1 Optical setup for lens-less Fourier digital holography

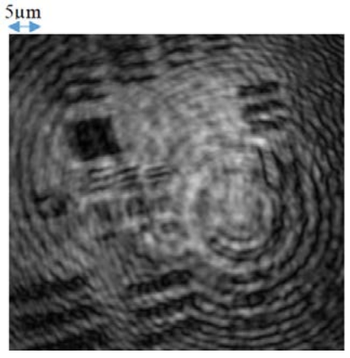

Fig. 2 Experimental result

References

[1] D. Barada *et al*., IWH2015 Digests, Th1-4 (2015).

[2] S. Kashiwagi *et al*., OSA Technical Digest of 2016 Imaging and Applied Optics Congress, JW4A.51 (2016).

36.

A Simply Fabricating Technique for 3D Woodpile Photonic Crystal Structure

Shu-Yu Chen,[1)] Mei-Li Hsieh,[1)] and Shawn-Yu Lin[2) 1)]Department of Photonics, National Chiao Tung University, Hsinchu, Taiwan

[2)]Department of Physic, Applied Physics and Astronomy, USA Rensselaer Polytechnic Institute, Troy, New York 12180

1mlh@cc.nctu.edu.tw

Abstract—We proposed a new technique to fabricate the 3D photonic crystal woodpile structure with double exposure. The advantage of the technique is fast and low cost with in large area manufacture. In optical experiment, we will demonstrate our preliminary results and show the SEM images of our templates.

Photonic Crystal, a periodic dielectric structures, can completely control over light propagation. The concept of how photonic crystal control the light is similar to a periodic potential in semiconductors affects the electrons propagating through the crystal lattice. With photonic bandgap (PBG) [1], photonic crystals offer an immense number of applications, such as localizing the light [2], laser cavity [3], and photonic crystal fiber [4], and so on. Particularly, three-dimensional structures with a diamond symmetry, diamond or diamond-like [5] lattices, offer the most promising approach for creating a large complete photonic bandgap [6]. But the diamond or diamond-like lattices are hard and complex to fabricate. In 1994, Ho et al. introduced the most effective type of 3D photonic crystal - woodpile structure [7]. This structure constructed with dielectric rods and stacked in a periodic array. When the rods are stacked to produce a face-centred cubic lattice , such that their contact points form a diamond-like lattice.To date, there are many method to fabricate woodpile structure, for example, e-beam lithography [8], direct Laser writing [9], and multi- directional etching method [10]. However, these methods are hard to manufacture because the speed is too slow and the equipment is too expensive.

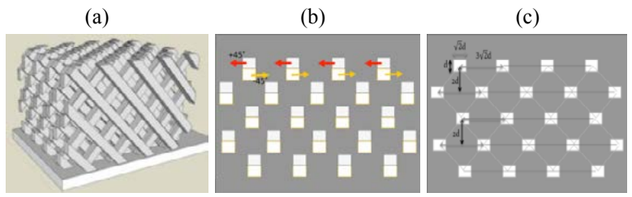

Fig.1. (a) Woodpile structure SP2 with the rods +45° and –45° arrangement. (b)Top view of (a). (c) The Schematic diagram of the mask.

In the paper, we proposed a new technique to fabricate the woodpile structure. The advantage of the technique is fast and low cost with in large area manufacture. In our work, we design and build up the optical double exposure system. For the experiments, a woodpile structure of SP2 was chosen, shown as Fig. 1(a). The SP2 woodpile structure is like some parallel rods formed layer-by- layer with alternating orthogonal direction, with the rods ±45° arrangement. Top view of the structure in Fig. 1(a) is illustrated as Fig. 1(b). No matter +45° or -45° has the same arrangement shown as Fig.1(c). So, first we generate this pattern in Fig.1(c) as our mask for double exposure. The optical lithographic system is shown as Fig. 2. In our experiments, we utilize an Ultra-compact Diode-pumped Q- switched Crystal UV Lasers with 355nm wavelength. A planar light source with 1cm diameter beam size hit on the sample stage, and a switchable mirror located at the pass of laser beam turn the light into different incident. We using

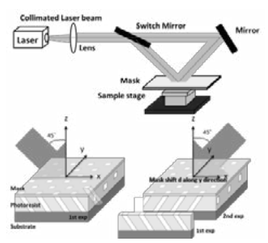

Fig.2. Schematic diagram of exposure optical setup. UV collimated Laser beam reflected by two mirrors, switch mirror and mirror, and expose on sample stage.

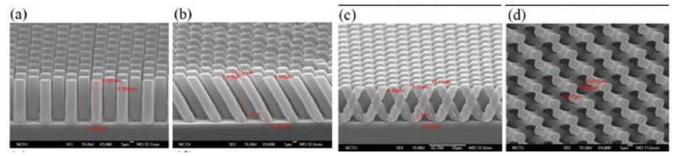

Fig 3. (a) Cross section from SEM image of normal incident structure.(b)Cross section from SEM image of oblique incident structure. (c) Cross section image of oblique double-with-shift exposure structure. (d) Top view image of oblique double-with-shift exposure structure.

the fused silica as the substrate, coated with 10-11μm thickness of photoresist (SU-8 series). With the mask, we expose the photoresist with two steps. First, the incident beam is from –45°, and then shift the mask along y direction after first exposure. Then, the incident beam for second expose is from +45° with same exposure energy as first exposure. Thus, we can form the 3D woodpile by double exposure, shown Fig. 1(a).

The SEM results of our fabrication are shown as Fig. 3(a-d), which are exposed with normal incident, oblique incident, double-with-shift exposure. For normal exposure in Fig. 3(a), the exposure energy is

150 mJ/cm2. For oblique exposure Fig. 3(b), the exposure energy is 250 mJ/cm2 with incident angle 50° in air, the structures' theoretical value of tilt angle is equal 62°. For double-with-shift exposure Fig. 3(c-d), the exposure energy is 130 mJ/cm2 (each). Fig. 3(c) is cross section and Fig. 3(d) is top view. The experimental value of Figure. 3(a-d) and dimension of mask shown in Table.1. The experimental results show that we can successful fabricate 3D woodpile photonic crystal with our simply optical system.

In future, we will invert the PR structure into metallic material to achieve the photonic bandbap and complete the photonic crystal of woodpile structure. Nowadays, the main issue of manufacturing 3D photonic crystal is high cost, and time consuming. We use double exposure method to achieve the 3D woodpile structure. The method we proposed has the advantage of large area manufacture, fast, and low cost.

TABLE I. EXPERIMENTAL DATA

		d	$\sqrt{2}$d	$3\sqrt{2}$d	4d	high	θ
Mask dimension		1.5	2.121	6.364	6	x	x
Exp. Value	a	x	2.559	6.385	x	8.592	x
	b	x	2.036	6.509	6.105	8.679	64.1°
	c	x	2.052	6.266	x	7.931	60.6°
	d	1.221	1.395	6.432	6.105	x	x

ACKNOWLEDGMENT

The authors acknowledge the funding support from the Ministry of Science and Technology under Contract no. MOST-105-2221-E-009-111-MY3. SYL acknowledges the funding support from US Department of Energy-Basic Energy Science under Contract no. DE-FG02-06ER46347 and National Science Council under Contract no. NSC 102-2221-E-009-152-MY3.

References

[1] S. John, "Strong localization of photons in certain disordered dielectric superlattices," Phys. Rev. Lett. 58, 2486, 1987.

[2] M. Tokushima, H. Kosaka, A. Tomita and H. Yamada, "Lightwave propagation through a 120° sharply bent single-line-defect photonic crystal waveguide," Appl. Phys. Lett. 76, 952, 2000.

[3] M. Lončar, T. Yoshie, A. Scherer, P. Gogna and Y. Qiu, "Low-threshold photonic crystal laser," Appl. Phys. Lett. 81, 2680, 2002.

[4] P. Russell, "Photonic Crystal Fibers," Science, vol. 299, no. 5605, pp. 358-362, 2003.

[5] O. Toader, S. John, "Square spiral photonic crystals: Robust architecture for microfabrication of materials with large three-dimensional photonic band gaps," Phys. Rev. E 66, 016610, 2002.

[6]M. Maldovan, E. L. Thomas, "Diamond-structured photonic crystals," Nat. Mater., vol. 3, pp. 593-600, 2004.

[7] K. M. Ho, C. T. Chan, C. M. Soukoulis, R. Biswas, M. Sigalas, "Photonic band gaps in three dimensions: New layer-by-layer periodic structures," Solid State Commun.vol. 89, Issue 5, pp. 413-416, 1994.

[8] J. G. Fleming, S. Y. Lin, I. El-Kady, R. Biswas, K. M. Ho, "All-metallic three-dimensional photonic crystals with a large infrared bandgap," NATURE, vol. 417, 2002.

[9] L. Maigyte, V. Purlys, J. Trull, M. Peckus, C. Cojocaru, D. Gailevičius, M. Malinauskas, and K. Staliunas, "Flat lensing in the visible frequency range by woodpile photonic crystals," OPTICS Lett., vol. 38, No. 14, 2013.

[10] L.Tang, T.Yoshie, "Woodpile photonic crystal fabricated in GaAs by two-directional etching method," JVSTB, vol.28, pp.301-303, 2010.

37.

Projected Fringe Profilometry using Binary-encoded Fringes

Sih-Yue Chen,[2] Nai-Jen Cheng,[1] and Wei-Hung Su[2]

[1]Institute of Photonics and Communications, National Kaohsiung University of Applied Sciences, Kaohsiung 80778, Taiwan

[2]Department of Materials and Optoelectronic Science, National Sun Yat-Sen University,
Kaohsiung 804, Taiwan

1. Introduction

Phase-shifting projected fringe profilometry (PSPFP) is a powerful tool for 3D shape measurements. It projects a fringe pattern onto the inspected object and records the fringe distribution from another point of view. Phase of the projected fringes is distorted by the surface profile, and hence is analyzable retrieve the surface profile.

Phases are extracted with the phase-shifting method. It evaluates phases with the arctangent operation, leading to their principle values constrained within the interval $(-\pi, \pi]$. Unwrapping is therefore required to restore the continuity of the phase map.

In this paper, an encoded fringe projection scheme for PSPFP is proposed. Phase extraction and unwrapping can be directly executed from the sequent projections. Only five-shot measurements are required. Its performance is evaluated by a set of simulation data.

2. Principle

Figure 1(a) shows an example of the encoded pattern. It is alternately assembled by two sets of sinusoidal fringes. Transmittance of one set is ranging from 0.25 to 0.5, and the other set is ranging from 0.0 to 1.0. Figure 1(b) illustrates the corresponding transmittance distribution along one image row. The fringe contrasts are leveled as 0.5 and 1.0. These two contrast values, 0.5 and 1.0, are further represented by two binary numbers, 0 and 1, respectively. Hence the fringes are spatially denoted with a stream of binary numbers. Figure 1(c) shows the fringes with the represented binary numbers. This pattern contains 16 fringes, and therefore fringe orders are labeled from 1 to 16. Figure 1(d) shows the fringe orders with their corresponding binary numbers.

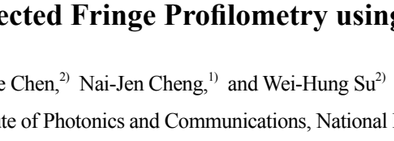

Fig. 1. (a) Appearance of the encoded pattern. (b) Transmittance distribution of the encoded pattern. (c) Fringes denoted with the binary digits. (d) Binary number addressed with the fringe orders.

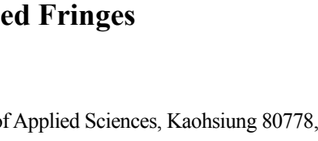

Fig. 2. (a) A stream of 69 binary digits formed by partially overlapping 64 codewords. (b) Correspondence between the fringe orders and the 69 binary digits. (c) Appearance of the encoded pattern generated with reference to the 69 binary digits.

The binary numbers can be spatially permutated to form a codeword. For codewords which contain 6 binary numbers, there are 64 permutations. The 64 codewords can be spatially overlapped by the following way: one codeword is partially overlapped with another, and five digits are overlapped between two codewords.

Hence a stream of 69 binary numbers with their fringe orders can be carried out, and a corresponding fringe pattern can be created. Figure 2 illustrates such an example, in which the length of codewords is 6. Any codewords is unique in 69 sequent digits. Thus, fringe orders can be identified.

The phase-shifting technique can be employed to extract the phase, as described as follows. For a five-step phase-shifting algorithm, the digital projector successfully projects a set of five encoded patterns changed in an incremental phase shift of $2\pi/5$ onto the inspected object. Figure 3(a) shows appearances of the five encoded patterns, in which 6 binary numbers are used to form a codeword.

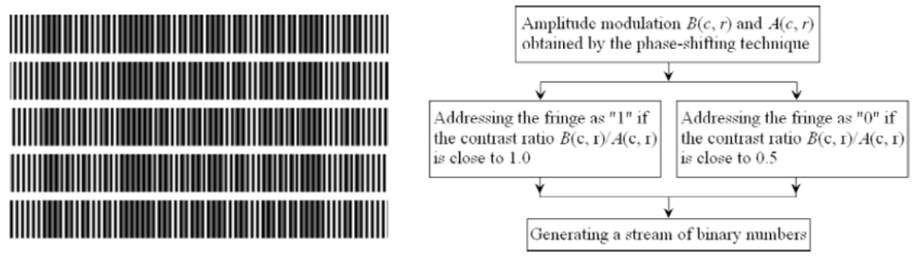

Fig. 3. (a) Appearnce of the five encoded patterns employed for the phase-shifting technique. Each pattern is changed in an incremental phase shift of $2\pi/5$. (b) Flow chart of the decoding procedure.

3. Decoding scheme

Pattern decoding is a task to assign the projected fringes with a stream of binary numbers so that fringe orders can be identified. In our method, this task is achieved by assigning the fringe contrast with a binary number 0 or 1. Figure 3(b) depicts the flow chart of the decoding scheme.

Fringe orders can be identified with a look-up table. The look-up table lists the conversion between the fringe order and the binary number. Actually, it has been addressed in the procedure of encoding the pattern, as shown as Fig. 2(b).

4. Simulation

A flat surface whose reflectivity varied with positions is generated by a computer. Figure 4(a) shows appearance of the inspected object. This object was then illuminated with an encoded pattern. The encoded pattern is shown as Fig. 3(a). Appearance of the fringes projected on the inspected surface is shown as Fig. 4(b). Phase of the projected fringes was extracted with the phase-shifting technique. Figure 4(c) illustrates the extracted result. With the flow chart of the decoding procedure shown in Fig. 3(b), unwrapping was then performed with the look-up table. Figure 3(d) illustrates the unwrapped phase.

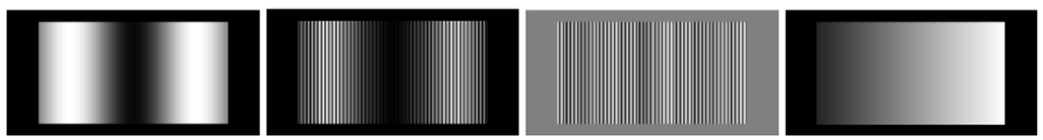

Fig. 4. (a) Appearance of the inspected object. (b) Appearance of the encoded fringes projected onto the inspected object. (c) Phase extracted with the phase-shifting technique. (d) Phase extracted with the Fourier transform method

5. Conclusion

We have presented a pattern encoding method to identify fringe orders for PSPFP. A computer generated image is used to evaluate the performance of the phase unwrapping. Only five-shot measurements are required for processing.

Sub-micron resolution in graphene oxide doped PDLC layer combined with inorganic photorefractive crystal

Vera Marinova,[1,2] Stefan Petrov[3], Shiuan Huei Lin[3] and Ken Yuh Hsu[1]

[1] Department of Photonics, National Chiao Tung University, University Str., 1001, Hsinchu 30010, Taiwan

[2] Institute of Optical Materials and Technologies, Acad. G. Bonchev Str. 109, Sofia, Bulgaria

[3] Department of Electrophysics, National Chiao Tung University, University Str., 1001, Hsinchu 30010, Taiwan

Abstract

The paper reports on Graphene Oxide (GrO) nanoparticles addition in polymer dispersed liquid crystal (PDLC) films combined with $Bi_{12}SiO_{20}$ (BSO) inorganic crystal into hybrid structure and its effect on electro-optical properties and two-beam coupling. It is found that the GrO doping increases the size of LC droplets and leads to decrease of the threshold voltage in comparison with non-doped PDLC samples. Based on the photogenerated space-charge field in BSO substrate and high birefringence of PDLC layer, the hybrid structure allows switching between opaque to the transparent state to be all optically controlled. In addition, GrO addition in PDLC enhances the beam amplification value permitting sub-micron resolution.

1. Introduction

PDLC consists of submicron droplets of liquid crystal (LC) randomly dispersed within a polymer matrix. Due to the refractive index mismatch, PDLC are opaque at their initial state. They can be switched from the light-scattering to the transparent state by application of an electric field, which support the refractive indices match between the LC and the polymer matrix. In general, the switching voltages are excessively high due to strong surface anchoring effects at polymer matrix walls [1].

In order to expand the application ability, enormous efforts have been done to lower the switching voltage. Usually, doping with nanoparticles (NPs) is among the most efficient ways. For example, it was established that nanoparticles as Au, Ag, ZnO and quantum dots significantly alter the LC properties [2]. Recently, the two-dimensional honeycomb structure of graphene shows remarkable interactions with the LC molecules due to the graphene advantages as amazing electrical, optical, chemical and mechanical properties. For example, the rod shapes of LC molecules tend to align along the alternate positions of the graphene hexagons, providing an enhancement of nonlinear properties of PDLC as well as the presence of carbon nanotubes has a favorable impact on LCs' electro-optical switching phenomena [3]. Furthermore, the graphene oxide promotes vertical alignment of the LC without necessity of any surface treatment of the substrates.

Graphene oxide is an oxidized form of graphene, characterized with easy dispensability in water and other organic solvents due to the presence of the oxygen functionalities. This is also a very important property when mixing it with polymer or other organic matrices.

In the present paper, we investigate the effect of GrO addition on the structural and electro-optical properties of PDLC film and establish that GrO doping increases the size of LC droplets, consequently decrease the threshold voltage. A combination of GrO doped PDLC film with BSO inorganic crystal into a functional organic-inorganic hybrid structure is demonstrated. Based on surface activated photorefractive effect, the hybrid structure allows improvement of the beam amplification, permitting realization of new type of all optically controlled devices, operating at Bragg match regime of diffraction.

2. Experimental results and discussion

The proposed hybrid structure consists of photoconductive BSO inorganic crystal substrate and a glass substrate arranged into a cell (10 μm thickness), filled with polymer dispersed liquid crystal (PDLC) doped with Graphene oxide (GrO) nanoparticles. The GrO nanoparticles were added into the LC and LC/GrO suspension was mixed with polymer matrix (NOA 65 UV glue) at 30:70 wt % ratio.

Due to the BSO absorption and high photoconductivity, light illumination caused generation of charge carriers, which migrate inside the substrate and form an inhomogeneous charge distribution. This photo-induced field in BSO plate, can grow strong enough to spread out into the PDLC surface layer and realign the LCs molecules orientation and thus to change the LCs director, consequently the refractive index and transparency of the structure [4]. As a result, the refractive indices between

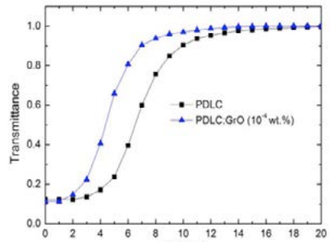

Fig. 1 Voltage-dependence characteristics

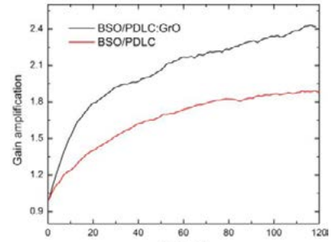

Fig. 2 Two-beam coupling behavior at 532 nm

the LC and polymer matrix changes, and thus the light intensity distribution through the BSO/PDLC:GrO structure could be switched from scattering to the transparent state.

Figure 1 shows the effect of GrO addition in PDLC on the driving voltage and comparison with non-doped PDLC. The two-beam coupling behavior of the studied structures is shown on Figure 2 at 0.8μm.

In a proposed all optically controlled BSO/PDLC:GrO hybrid structure, the charge migration, trap density and space-charge field come from the BSO substrate, whereas the high beam amplification is provided by the LC layer. Therefore, all processes are performed only by the action of light. The proposed structure does not require ITO contacts and alignment layers and all the processes are controlled by light, thus opens further potential for real-time image processing at the near infrared spectral range.

Financial support by the Ministry of Science and Technology (MOST), Taiwan under the contracts: MOST 105-2221-E-009-110, 104-2221-E-009-164; 104-2221-E-009-151 and ATU program under Ministry of Education, Taiwan are gratefully acknowledged.

References

[1] Coates, D., "Polymer-dispersed liquid crystals," J Mater. Chem. 5, 2063-2072 (1995) [2]Yeh, P. and Gu, C., Optics of liquid crystal display, Wiley Interscience, New York (2010).

[3] Li S., Fu M., Sun H., Zhao Y., Liu Y., He D. and Wang Y. "Enhanced photorefractive and third-order nonlinear optical properties of 5CB-Based Polymer Dispersed Liquid Crystal by Graphene doping," J. Phys Chem, 118, 18015-18020 (2014).

[4] Tabiryan, N. V. and Umeton, C., "Surface-activated photorefractivity and electro-optic phenomena in liquid crystals," J. Opt. Soc. Am. B, 15 1912-1917 (1998).

39.

Generation of Depth-Cue-Added Holographic Stereogram with Look-up-Table Method

Sung-Lin Lu,[1)] and Jung-Ping Liu[1)]

[1)]Department of Photonics, Feng Chia University, 100 Wenhwa Rd., Seatwen, Taichung 40724, Taiwan

1. Introduction

Traditional holographic stereogram (HS) consists of multiple two-dimensional images with different viewing angles of a three-dimensional (3D) scene. The merit of HS is that the computing is easy and fast [1, 2]. Nevertheless, HS has the problem of accommodation conflict, which may let the viewers uncomfortable. To solve this problem, depth-cues-added holographic stereogram (DCA-HS) was proposed to retain full depth information of 3D scene [3]. A DCA-HS consists of many tiles called “hogels”. Each hogel contains the 3D information of the object points viewed at the center of that hogel. Therefore, the hogel can be calculated based on the Huygens-Fresnel principle. In other words, each object point generates a spherical wave, and the consequent wave field at the hogel is the superposition of all individual spherical wave fields. This process has to be repeated for all hogels, and thus is time-consuming. Accordingly, we propose to use look-up table [4] to speed up the computing of hogels. By this way, the computing time can be significantly reduced.

2. Theory

To begin with, the DCA-HS is spatially partitioned into many tiles of hogels. Figure.1.(a) shows the geometrical relation between the 3D object and the hologram (HS). For each hogel, the shading image and the depth image, acquired at the center of the hogel, are rendered in computer-graphics software. The 3D location of each object point related to the hogel is obtained from both the shading image and depth image,

$$z_0 = z_p \quad , \quad x_0 = z_0 \tan\theta_x \quad , \quad y_0 = z_0 \tan\theta_y \quad , \tag{1}$$

where (x_0 , y_0 , z_0) is the actual position of the object point, (θ_x ,θ_y) is the angular location defined by the rendered images, and z_p is the object depth. Each object point produces a spherical wave at the hogel, and thus the complete complex amplitude at the hogel is expressed as

$$h_{hogel}(x,y) = \sum_{j=1}^{N} \frac{A_j}{r_j} \exp\left[i(kr_j + \phi_j) \right] \quad , \quad r_j = \sqrt{(x-x_j)^2 + (y-y_j)^2 + z^2} \quad , \tag{2}$$

where N is the number of object points collected in the viewing frustum, A_j is the wave amplitude of the j -th point, $k = 2\pi / \lambda$ is the wave number in free space, ϕ_j is the initial phase, and r_j is the distance between the j -th object point and the sampling point (x, y, 0) at the hogel (HS) plane,

In DCA-HS each object point generates a complex Fresnel zone plate (CFZP) on the hogel plane, as shown in Fig. 1(b). In addition, the shift of the CFZP depends only on the transverse location of the object point. Therefore we pre-computed all possible CFZPs in advance and stored them in the computer memory. In the generaion of a hogel, the contribution of each object point can be quickly looked up from the table (pre-computed CFZP), as shown in Fig. 1(c). By this look-up-table method, the computing time is reduced significantly.

3. Results and Conclusion

Table 1 shows the parameters of the tested DCA-HS. The scene contains two objects: a big football is located at z = 100 mm and a small football at z = 125mm measured from the hologram plane. The reconstructed images calculated by simulating scalar diffraction [5] are shown in Fig.2.

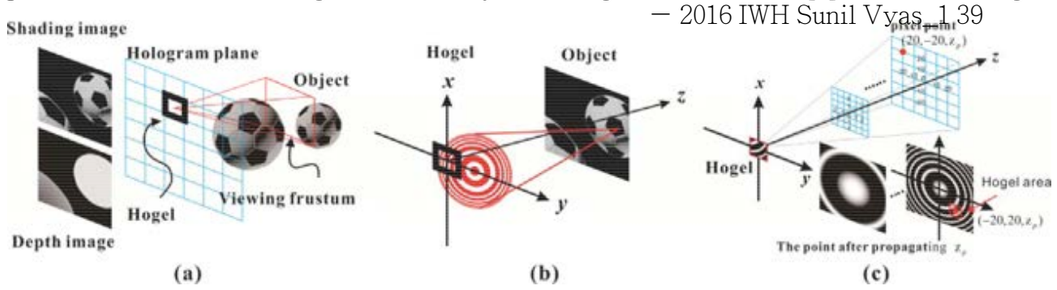

Fig. 1. (a) Geometry of DCA-HS and (b) the CFZP generated from an object point on the hogel plane,(c) Schematic of look-up table.

The holograms have demonstrated significant focus-and-defocus effect. Thus the depth cues are correctly included in the holographic stereogram. The computing time with proposed look-up-table method is only one forty fourth that with conventional point-by-point computation. This work is supported by Ministry of Science and Technology of Taiwan, R.O.C. under contract number 103-2221-E-035-037-MY3.

Table. 1. Parameters of the demonstrated DCA-HS.

Pixel pitch	8 $\mu m \times 8\ \mu m$
Field of view	3.8°
Number of hogels	16 × 16
Number of pixels per hogel	125 × 125
Number of object points per image	200 × 200

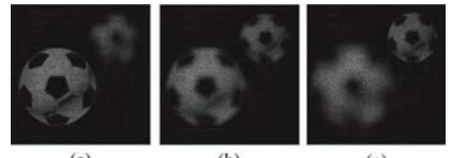

Fig. 2. Reconstructed images by numerical simulations. The focus planes are (a) at the big football (b) between the big football and the small football (c) at the small football.

References

[1] M. W. Halle, S. A. Benton, M. A. Klug, and J. S. Underkoffler, “Ultragram: a generalized holographic stereogram,” Proc. SPIE, **1461**, 142–155, 1991.

[2] M. Lucente and T. A. Galyean, “Rendering interactive holographic images,” Proceedings of the 22nd annual conference on Computer graphics and interactive techniques, 387–394, 1995.

[3] H. Zhang, Y. Zhao, L. Cao, and G. Jin, “Fully computed holographic stereogram based algorithm for computer-generated holograms with accurate depth cues,” Opt. Express, **23**, 3901-3913, 2015.

[4] S.-C. Kim and E.-S. Kim, “Effective generation of digital holograms of three-dimensional objects using a novel look-up table method,” Appl. Opt., **47**, D55–D62, 2008.

[5] J.-P. Liu, “Controlling the aliasing by zero-padding in the digital calculation of the scalar diffraction,” JOSA A, **29**, 1956–1964, 2012

40.

Generation of Doughnut Mode Beam from Volume Holographic Optical Element

Sunil Vyas, Po-Hao Wang, and Yuan Luo
Institute of Medical Devices and Imaging System, National Taiwan University, Taipei, 10051, Taiwan

1. Introduction

Volume holography is one of the key techniques to realize special optical components for creating optical fields with desired properties [1]. With the availability and advancement of spatial light modulating devices, optical beam shaping has become easy and straightforward. One typical example of beam shape is doughnut mode (also known as optical vortex) with a dark center surrounded by a high intensity ring and a phase singularity at the center of the beam. Due to helical shape wavefronts, these beams have property of orbital angular momentum. The doughnut shaped beam can be described as Laguerre-Gaussian modes [2]. The electric field of a doughnut beam can be expressed as $E=E_0\exp(im\varphi)$, where φ is the polar coordinate in the plane perpendicular to the beam axis, and m is the topological charge. The size of the dark core depends upon topological charge m of the beam. These beams find important applications ranging from microscopy to astronomy [2]. There are various direct and indirect methods exist for doughnut beam generation, for example, spiral phase plate, computer generated holograms, optical fiber, or directly from the laser cavity. But all of the above methods are wavelength dependent. Most common method of beam shaping uses computer generated holograms and spatial light modulators to realize desired beam shapes [3]. The beam shape obtained from the SLM is based on thin grating concept where desired beam profile is obtained by selecting particular diffraction orders. It produces multiple diffraction orders and does not have properties of angular and wavelength selectivity which are desirable properties for the multidimensional imaging applications. The purpose of the present work is to make volume holographic optical elements corresponding to unconventional optical beam shapes for their use as advanced pupil functions in volume holographic imaging techniques [4].

2. Experimental Setup

Schematic diagram of holographic recording geometry is shown in Fig.1. In one arm of interferometer a phase spatial light modulator is used (HAMAMATSU-X10468).

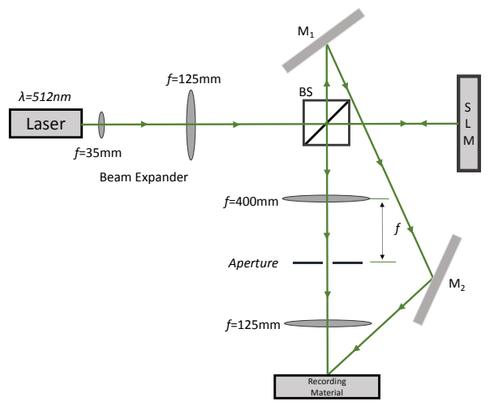

Fig. 1. Experimental setup for recording a volume hologram for different beam shapes.

Here, we used a spiral phase mask coded on to SLM to generate doughnut beam. The diffraction orders are separated from the other orders using spatial filtering setup. Signal beam with doughnut shape intensity distribution interfere with the reference plane wave in the photosensitive recording material. We used PQ-PMMA as recording medium due to its excellent and well-studied properties [5]. The angle between the reference and the signal beam is set around 30 degrees. In order to get maximum contrast in the interference pattern power of the signal and the reference beam is made identical.

3. Results

The first diffraction order of the recorded hologram shows a doughnut mode beam. In order to confirm the presence of phase singularity at the center of the beam, characteristic fork interference fringe was obtained by lateral shearing interferometer. Figure 2 shows reconstructed doughnut beam for two different wavelengths.

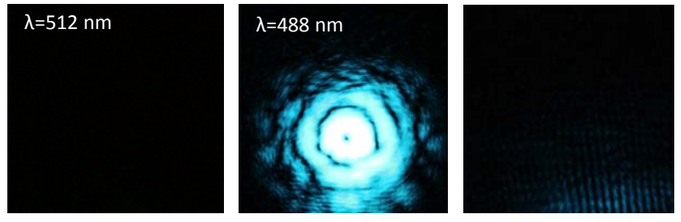

Fig. 2. Intensity distribution of doughnut shape beam generated from a volume hologram (a) reconstruction with λ=512 nm laser (same wavelength as the recorded hologram), (b) reconstruction with λ=488 nm laser. (c) Shearogram of doughnut beam.

4. Conclusions

A volume hologram is recorded to produce a doughnut shaped beam. A thin grating is used to produce beam shapes and a thick grating is recorded corresponding to that. The beam shapes produced by this method offers many advantages. For example, the holographic optical element is simple, and direct way to produce the high quality beam shapes and no other optical components are required. Second they have the property of angle and wavelength selectivity which is highly desirable for microscopy. These optical elements can directly be used to modify the pupil function as comparison to SLM where many optical elements and hardware is required to create beam shapes. In addition, a single optical element is easy to use and always desired for compact imaging system. It can also be extended to multiplex more shaped beams simultaneously within a volume holographic pupil [1,5].

References

[1] H. Coufal, L. Hesselink and D. Psaltis, Holographic Data Storage (Springer-Verlag 2002).
[2] A.M. Yao, M.J. Padgett, “Orbital angular momentum: origins behavior and applications,” Adv. Opt, 2011, pp.161-204.
[3] T. W. Clark, R. F. Offer, S. Frank-Arnold, A. S. Arnold, and N. Radwell, “Comparison of beam generation techniques using a phase only spatial light modulator,” Opt. Express 2016 pp. 6249-6264.
[4] Y. Luo, P J. Gelsinger-Austin, J M. Watson, G. Barbastathis, J. K. Barton, and R. K. Kostuk, “Laser-induced florescence imaging of subsurface tissue structures with a volume holographic spatial-spectral imaging system,” Opt. Lett. 2008, pp. 2098-2100.
5) Y. Luo, P. J. Gelsinger, J. K. Barton, G. Barbastathis, and R. K. Kostuk, “Optimization of multiplexed holographic grating in PQ-PMMA for spectral-spatial imaging filters,” Opt. Lett. 2008, pp.566-568.

41.

Study of coherence wave using lensless Fourier transform holography

Rakesh Kumar Singh[1*], Sunil Vyas[2], and Yoko Miyamoto[2]
[1]Applied and Adaptive Optics Laboratory, Department of Physics, Indian Institute of Space Science and Technology (IIST), Trivandrum, 695547, Kerala, India.
[2]Department of Engineering Science, The University of Electro-Communications, 1-5-1, Chofugaoka, Chofu, Tokyo, 182-8585, Japan.
e-mail address: **krakeshsingh@iist.ac.in*

1. Introduction

Spatial statistical optics deals with the statistical properties of spatial distribution of the random light fields [1]. Low coherence optical fields have important applications in the fields of image processing, astronomy, nonlinear optics and free space communications. A partially coherent light is conventionally described by the coherence function. Similar to the complex amplitude, a coherence function obeys the two four-dimensional wave equations and hence can be considered as a coherence wave [2]. Complete measurement of the coherence wave requires an amplitude-based interferometric setup.

In this work, we examine the interference effect between two complex coherence functions and interpret its impact on imaging from a randomly scattered field. The basis of the present work is derived from an analogy between the optical field and complex coherence wave. The objective of the present work is to experimentally study the interference effect of the coherence waves through the two-point intensity correlation, which contains the square of the modulus of the superposed coherence wave. To experimentally test and examine the interference effect, we generate a spatially fluctuating random field, i.e. laser speckle, which is a coherent superposition of two independently generated laser speckles with well-defined but independent coherence functions. Finally, the interference pattern extracted from the two-point intensity correlation is used to demonstrate an imaging application.

2. Experimental Setup

To study the coherence wave we followed the theoretical treatment given in the reference [4, 5]. Figure 1 shows the experimental setup for a lensless Fourier transform holographic technique to study the coherence wave. A Mach-Zehnder interferometer is used for this purpose. The beam from a He-Ne laser is first spatially filtered and collimated, then sent into the Mach-Zehnder interferometer. In one arm of the interferometer, an object in the form of an amplitude transparency with the shape of a letter C is kept.

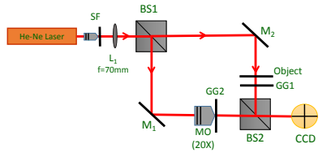

Fig. 1. Schematic diagram for the lensless Fourier transform holography for the study of coherence waves (SF: spatial filter; L1: lens, BS1 and BS2: beam splitters; M1 and M2: mirrors, GG1 and GG2: ground glass plates; MO: microscope objective.

To produce a spatially random object field, the field transmitted from the object is passed through the ground glass plate GG1. After scattering from the GG1, the object field propagates to the recoding plane via a beam splitter BS2. The other arm of the interferometer has a microscopic objective (20×) followed by a ground glass plate GG2. The diverging field coming out of the GG2 act as a reference wave. The distance between the GG1, GG2 and the CCD plane is same. The speckle fields coming from the two arms combine at the CCD plane and form an interference pattern. The combined speckle pattern produced by the object and reference waves is recorded at the CCD plane as shown in the Fig. 2(a). Here we used Hamamatsu CCD camera (C5948 and CT-3000A capture board) with pixel size 13.5 μm and 480×680 pixels.

3. Results

By calculating the spatially averaged two-point cross-covariance of the random intensity distribution, a fringe pattern corresponding to the interference between the two coherence waves associated with the object and reference speckle fields can be obtained as shown in the inset of Fig.2 (a) [3-5]. The pattern can be considered a lensless Fourier hologram of the object coherence wave and can be reconstructed in a similar manner to a lensless Fourier hologram recording complex amplitudes. Reconstructed object transmittance is obtained by suppressing the zero order frequency component as is shown in Fig. 2 (b).

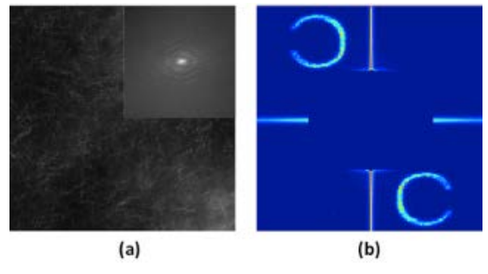

Fig. 2. Experimental results for object (letter C) placed at the GG2 plane: (a) speckle pattern recorded at distance z=150 mm from object using lensless Fourier holography setup in Fig. 1, with inset showing spatially averaged cross-covariance of the intensity pattern; (b) reconstructed object transmittance with suppressed zero order.

4. Conclusions

A new approach to study the interference of the coherence waves is proposed and experimentally tested by considering an example of the spatially fluctuating random field. This is carried out by replacing the ensemble averaging by the spatial averaging for the spatially stationary random fields. Existence of the interference fringes in the two-point intensity correlation highlight the wave nature of the complex coherence functions. The reconstruction of the object transmission demonstrates potential for lensless imaging from randomly scattered fields.

References

[1] J. W. Goodman, Statistical Optics (John Wiley & Sons Inc, New York, 1985).
[2] A. W. Lohmann, D. Mendlovic, and G. Shabtay, "Coherence waves," J. Opt. Soc. Am. A **16**, 359-363 (1999)
[3] M. Takeda, W. Wang, D. N. Naik, and R. K. Singh, "Spatial statistical optics and spatial correlation holography," Opt. Rev. **21**, 849-861 (2014).
[4] D. N. Naik, R. K. Singh, E. Ezawa, Y. Miyamoto, and M. Takeda, "Photon correlation holography," Opt. Express **19**,1408-1421 (2011).
[5] R. K. Singh, R. V. Vinu, and A. M. Sharma, "Retrieving complex coherence from two-point intensity correlation using holographic principle," Opt. Eng. **53**, 104102/1-5 (2014).
[6] M. Takeda, "Spatial stationarity of statistical optical fields for coherence holography and photon correlation holography," Opt. Lett. **38**, 3452-3455 (2013).

42.

Focus error signal obtained at the far-field from a rotational disc and measurement of its positional dependency

Akira Takagi, Takahiro Ishisaka, Satoshi Maruyama and Teruo Fujita

Department of Electrical and Electronics Engineering, Fukui University of Technology, 3-6-1 Gakuen, Fukui 910-8505, Japan

1.Introduction

Holographic data storage system (HDSS) has been studied as one of next-generation optical data storages to realize higher recording density and data transfer rate. Especially colinear HDSS[1]) can be promising one because of its optical stability and recording density. To realize a practical HDSS like a DVD-R recorder, controlling focal and radial positions of signal and reference beams should be necessary because the discs are exchanged in the optical disc jukeboxes. At ISOM'08 we proposed a new focus sensing method using the interference of far-field diffracted waves generated by embedded one-dimensional periodical structure in a disc[2]), which features no additional optics for those error signals' generation as well as non dependency of the irradiation beam's non-uniformity on the focus error signal. As the simulation showed expected results, building up an experiment system with bench optics, analog/digital processing circuits and a disc embedded one-dimensional grating followed to ensure its effectiveness experimentally[3]).

In this paper we brief the principle of this focus sensing method, explain a developed experiment system, and show the focus error signal (FES) obtained from a rotational disc. Also we report FES' dependence on the tangential position of a two element photo-detector (PD) located at the far-field.

2.Principle of the focus error generation

There are areas where the 0th and ±1st order diffracted beams are superimposed on the pupil of the objectives of optical heads for CD and DVD. When the focused spot crosses the grooves of those discs, the optical intensity distribution of those areas changes. If only defocus exists in the irradiation beam, moving linear fringes appear in those areas and its spatial frequency depends on the amount of defocus. Our system uses a two element PD located in the area and samples the intensity variation periodically (constant time period corresponding to $\pi/2$ phase shift of the PD signals). When the PD center in the tangential direction is x_1 on the output pupil of the objective lens, detected intensity from PD element 1 and 2 (D_1 and D_2) are expressed as

$$I_{D1,D2} = I_{01,02} + I_{11,12}\cos\left[\beta_1 + \delta + 2\pi W_{20}\left\{-\frac{2}{q}\left(x_1 \mp \frac{\Delta}{2}\right) + \frac{1}{q^2}\right\}\right], \quad (1)$$

$$I_{DF} = I_{D1} - I_{D2}, \quad I_{SUM} = I_{D1} + I_{D2}, \quad (2)$$

where I_{D1}, I_{D2} are the outputs of the two element PD, W_{20} is a defocus wavefront aberration, β_1 is the initial phase, δ is the normalized lateral shift, q is the normalized groove pitch, Δ is the normalized spacing of the two PD elements' center so that the PD element's centers are expressed as $x_1 - \Delta/2$ and $x_1 + \Delta/2$ respectively. Also $I_{01,02}$ are the DC components and $I_{11,12}$ are the modulation amplitudes. Then, from the difference/sum signals I_{DF}, I_{SUM}, we are able to obtain the FES as follows (FESb shows an opposite DC offset of FESa) ;

$$FESa = \left\{I_{DF}\left(-\frac{\pi}{2}\right) + I_{DF}(0)\right\}\cdot\left\{I_{SUM}\left(-\frac{\pi}{2}\right) - I_{SUM}(0)\right\} + \left\{I_{DF}(0) + I_{DF}\left(\frac{\pi}{2}\right)\right\}\cdot\left\{I_{SUM}(0) - I_{SUM}\left(\frac{\pi}{2}\right)\right\}$$

$$FESb = \left\{I_{DF}\left(\frac{\pi}{2}\right) + I_{DF}(\pi)\right\}\cdot\left\{I_{SUM}\left(\frac{\pi}{2}\right) - I_{SUM}(\pi)\right\} + \left\{I_{DF}(\pi) + I_{DF}\left(-\frac{\pi}{2}\right)\right\}\cdot\left\{I_{SUM}(\pi) - I_{SUM}\left(-\frac{\pi}{2}\right)\right\} \quad (3)$$

$$FES = FESa + FESb, \quad (4)$$

where $I_{DF}(\alpha)$ means the value of I_{DF} at $\delta = \alpha$.

3. Experiments

Figure 1 shows our experiment system we have been developing to verify the dynamic operation of this focus sensing method. First we prepared an optical disc with one-dimensional structure grooved in the radial direction (180,000 grooves/rotation ; groove pitch = 1.3 μm at r = 37 mm so that the 1st order is shifted by the radius of the beam) using a Compact Disc production process, and it was set on a turn table for SP/LP discs. When the disc rotates at 78 rpm (1.3 rps), the frequency of a groove crossing signal becomes 234kHz. To obtain sampling pulses, we use the stroboscopic pattern (160/rotation) caved on the outside perimeter of the rotation table. A He-Ne Laser beam irradiates this pattern so that the reflected light frequency is modulated at 208Hz. Then a Phase Lock Loop (PLL) circuit, which was composed of a digital VCO and MaxII CPLD, multiplies this signal by 4,500 for getting the sampling pulse whose frequency is 234KHz x 4 = 936kHz. The defocus fringes on the exit plane of the objective lens (NA=0.53) are projected onto the two-element PD through a macro lens with equal magnification. The PD width in the tangential direction is 155μm (width of 1 element) x 2 + 27μm (space between elements) = 337μm and the beam diameter is 4mm. I_{D1} and I_{D2} from the PD are sampled simultaneously at the rate of 936 kS/sec with two A/D converters and then 16 values of I_{D1} (I_{D2}) which correspond to 4 periods, are transferred to a TI's DSP. The DSP averages those data to reduce the noise and calculates FES. Finally the FES is put out from a D/A converter with a period of around 17 μsec. We acquired well-shaped FES curves twice per one disc rotation due to the disc vertical vibration (Fig.2).

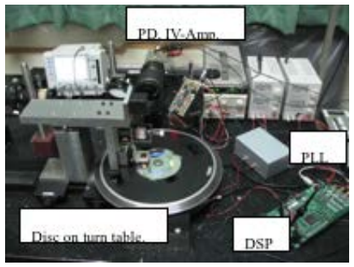

Fig. 1. Experimental setup. Red (690nm) laser beam comes from the left side, is reflected down by 90 degree and focused on the grating surface in the disc. Reflected/ diffracted beams by the disc go up and are conducted to the PD by a beam splitter and a macro lens behind it.

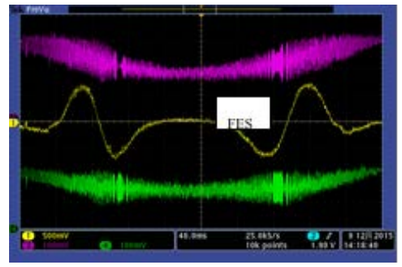

Fig. 2. obtained FES (yellow line in the middle) and input signals (upper and lower lines, proportional to I_{D1} and I_{D2}). Horizontal grey line indicates a reference level for the FES, and the input signals are shifted up and down just not to be superimposed each other.

Next we evaluated the influence of the tangential location of the PD on the FES offset. In this experiment, PD was shifted ±300μm in the tangential direction from the best position (Fig.3(a)), where the offset was zero. The maximum offset case (around 1.5μm offset at -250μm PD shift) was shown in Fig.3(b). In these figures blue line is the modulated light intensity, and the distance between a point of FES=0 and that of SUM=MAX gives the focus offset. Please note that the symmetry of the FES curves was not lost according to the PD position shift. As our simulation including the third order spherical/coma aberration had predicted such small offset4), residual aberrations of the diffraction-limited optics' components seem to cause this offset.

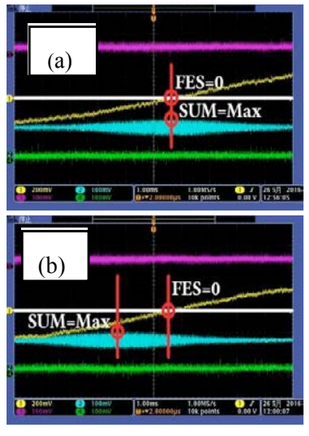

Fig.3. Focus offset dependency on the PD position, left: best position, right: shifted position by -250μm.

4. Summary

Focus offset of the FES generated by interference fringes at the far-field was verified by an actual optics and electronics system. A position where the offset became zero was confirmed, and small offset's dependence on the PD position was observed.Also FES curves' symmetry was not affected by the PD position.

References

[1] H.Horimai et al. : Appl. Opt. **44**, p.2575 (2005).
[2] T.Fujita and H.Horikoshi : Jpn.J.Appl.Phys. **48**, 03A037 (2009).
[3] T.Sawada, A.Takagi and T.Fujita : ODF2016,1PDb-06 (2016).
[4] T.Fujita : Jpn.J.Appl.Phys.**49**, 08KD08 (2010).

Acknowledgment This work was supported by JSPS KAKENHI Grant Number JP15K06040.

43.

Shift Multiplexed Recording in Holographic Data Storage Based on a Computer-generated Hologram with a Conical Wave

Teruyoshi Nobukawa[1] and Takanori Nomura[2]

[1]Graduate School of Systems Engineering, Wakayama University, 930 Sakaedani, Wakayama, 640-8510, Japan

E-mail: s132072@sys.wakayama-u.ac.jp

[2]Faculty of Systems Engineering, Wakayama University, 930 Sakaedani, Wakayama, 640-8510, Japan

1. Introduction

Holographic data storage is capable of storing huge information owing to the multiplexed recording. To realize a practical and huge-capacity recording system, a large number of recording setups have been proposed. Among them, holographic data storage based on a computer-generated hologram (CGH) can realize a simple, compact, and cost-effective recording system [1]. In this system, the complex amplitude distribution of a beam can be modulated with a single amplitude-only spatial light modulator (SLM). Moreover, a reference beam is generated from a CGH. However, multiplexed recording is not applicable in the conventional system because a reference beam is a plane wave on a recording medium and its angle is fixed. To solve this problem, we have proposed and demonstrated angular [2] and shift multiplexing [3] methods for holographic data storage based on a CGH.

In this study, to further extend the capability of the holographic data storage based on a CGH, we propose an alternative recording setup using a CGH with a conical wave. Owing to the CGH, it is possible to generate a ring-shaped reference beam, and thus the configuration of signal and reference beams is similar to a collinear system [4]. This allows us to implement shift multiplexing. We numerically demonstrated the proposed method.

2. Holographic memory using a computer-generated hologram with a conical reference wave

Figure 1 shows the schematic of the proposed system. In conventional holographic data storage based on a CGH, a plane wave is used as a reference beam for generating a CGH [1]. Unlike the conventional system, we use a conical wave for generating a CGH. The conical wave is given by

$$r(x_0, y_0) = \exp\left\{i2\pi\rho\sqrt{x_0^2 + y_0^2}\right\}, \tag{1}$$

where ρ is a radial spatial frequency. Let $s(x, y)$ denotes the complex amplitude distribution of a signal beam. A CGH $I(x_0, y_0)$ between a signal beam and the conical wave is given by

$$I(x_0, y_0) = |\mathcal{F}[s(x, y)] + r(x_0, y_0)|^2, \tag{2}$$

where F [· · ·] is the Fourier transform operator. Figure 1(a) shows a sample CGH based on Eq. (2). During recording process, the CGH is displayed on an amplitude-only SLM, as shown in Fig. 1(b). To generate a conical wave of Eq. (1), an axicon lens is placed in the front of the SLM. A conical wave from an axicon lens is incident on the CGH, and its amplitude distribution is modulated. The modulated beam is Fourier transformed by a lens. In the Fourier plane, a desired signal beam and a ring-shaped beam are generated. The ring-shaped beam serves as a reference beam. The configuration of signal and reference beams is similar to a collinear system. This allows us to implement shift multiplexing in a holographic data storage system based on the CGH. These beams are Fourier transformed again, and a hologram between signal and reference beams is recorded in a recording medium. During reading process, the hologram is illuminated by a reference beam, and thus a signal beam is reconstructed. The reconstructed signal beam is captured with an image sensor, and the original data can be obtained.

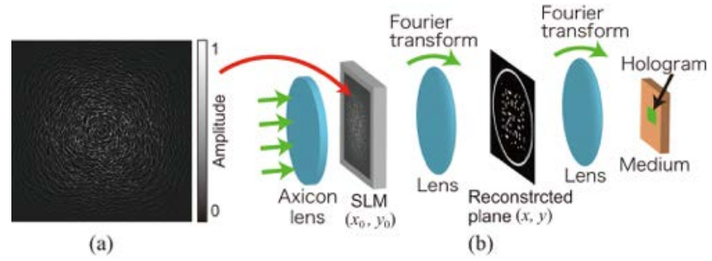

Fig. 1. Holographic data storage system based on a CGH with a conical wave. (a) CGH with a conical wave and a (b) recording setup.

3. Numerical simulation

We carried out a numerical simulation to confirm the feasibility of the proposed method. In this numerical simulation, the propagation of beams is based on a scalar diffraction, and a recording medium is represented by voxels [5]. We first evaluated shift selectivity in the proposed and conventional systems by the numerical simulation. Figure 2(a) shows the obtained shift selectivities. It can be seen that the narrow shift selectivity is obtained by the proposed system. The intensity of the reconstructed data page is reduced to 20% at the shift distance of 150 μm. We subsequently evaluated shift multiplexed recording of two data pages at an interval of 150 μm. Figure 2(b) shows two reconstructed data pages. Each data page was successfully retrieved without error. The numerical results show that the proposed method allows us to implement shift multiplexed recording.

4. Conclusion

We have proposed and numerically demonstrated holographic data storage system based on a CGH with a conical reference wave. In the proposed system, the configuration of signal and reference beams is similar to a collinear setup. This allows us to implement shift multiplexing, unlike to the conventional holographic data storage system based on a CGH.

This work was supported by Grant-in-Aid for JSPS Fellows from Japan Society for the Promotion of Science (Grant No. 15J11996).

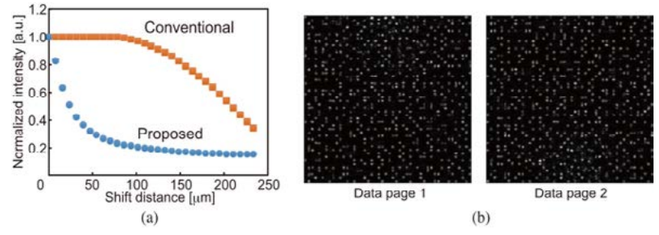

Fig. 2. Numerical results. (a) Shift selectivity. (b) Two reconstructed data pages by shift multiplexed recording.

References

[1] A. Yu. Betin, et al., Appl. Opt **52**, 8142–8145 (2013).
[2] T. Nomura, T. Morimoto, and T. Nobukawa, IWH 2015, Digest, We1-2 (2015).
[3] T. Nobukawa and T. Nomura, Proc. SPIE **9959**, 9959-11 (2016). 4) H. Horimai, et al., Appl. Opt. **44**, 2575–2579 (2005).
[5] S. R. Lambourdiere, et al., Jpn. J. Appl. Phys. **45**, 1246–1252 (2006).

44.

Ultra High Speed Printing of Large Size Holographic Optical Elements for Solar Power Generation Window Module

Tomoyasu Saigo, [1] Toshihiro Kasezawa,[2] Hideyoshi Horimai,[2),3),4)] Ryo Taguchi[1)] and Taizo Umezaki[1),3),5)]

[1)] Nagoya Institute of Technology, Gokiso-cho, Syowa-ku, Nagoya-shi, Aichi 466-8555, Japan

[2)] Egarim Co., Japan, 330 Shibukawa, Shimizu-ku, Shizuoka-shi, Shizuoka 424-0533, Japan

[3)] 3Dragons Llc., 12-2 Tashirohondori, Chikusa-ku, Nagoya-shi, Aichi 464-0827, Japan

[4)] HolyMine Ltd., 2301 Oooka, Numazu-city, Shizuoka 410-0022, Japan

[5)] Tokyo University, 7-3-1 Hongo, Bunkyo-ku, Tokyo 113-8656, Japan

1. Introduction

Volume holographic optical elements (HOEs) have wide-spread application, e.g. 3d display, solar concentration[1,2]. The window type unit, called “Holo-Window”, is candidate technology for photovoltaic generation because this is able to be integrated into buildings after construction[1]. In order to increase electric-generating capacity, it is important to decrease optical power loss when propagating in glass plate of windowpane and to expand the sunlight capturing area. In this paper, we show ultra high speed HOE printer and describe the optical configuration. And we propose HOE to decrease propagating loss.

2. HOE Printing System

Some holographic printing technologies were proposed[3], however those recording processes were obeyed “Step-by-Step” architecture because of avoiding the effects of vibrations. In order to decrease the recording time, we developed collinear printing system, which is able to withstand considerable vibration, and realized ultra high speed HOE printer with “on-the-fly” recording architecture.

Figure 1 shows a schematic diagram of the developed holographic printer. The developed holographic printer is able to print transmission type volume HOEs. The laser which is introduced optical head is branched into a reference beam and an object beam by beam splitter (BS). Each beam is reflected by mirrors and both are introduced to same objective lens and superimposes at front focal plane of objective lens. In this collinear optical configuration, the object and reference beams pass thorough same optical path except for the branched path between the BS and the mirror, which distance is less than 100mm. The effects of vibration are almost canceled out by this optical configuration, and the interference fringes are hard to change even if there is vibration by the optical head movement. The optical head is able to move 300mm stroke at 300mm/s along laser direction.

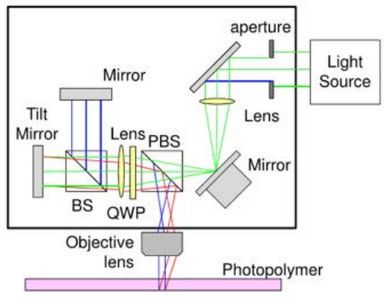

Fig.1. optical configuration

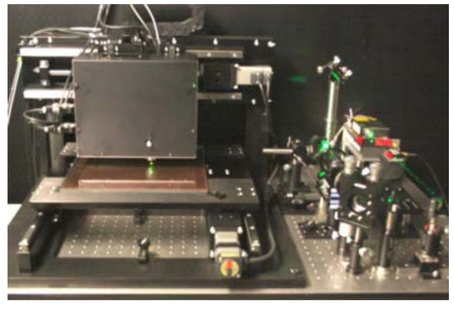

Fig.2. HOE printer

Figure 2 shows the developed printer. Laser source for hologram recording is used Q-switched YAG laser VECTOR-532-1000-20, made by Coherent Inc. This laser instrument is able to generate green light (wavelength is 532nm) with pulse width 10ns. The recording hologram materials are used Bayfol HX, made by Covestro AG (formerly Bayer Material Science AG) and DAROL, produced by Egalim co.jp. The max diffraction efficiency is 74% with 240mm/s head speed in condition that material is double exposed.

3. Printing HOE for Solar Window

Figure 3 shows the improved optical structure of Holo-Window we proposed. The sunlight is diffracted by reflective HOE film at innermost layer. The angle of diffracted light is **increased by** passing through trans- missive HOE film at middle layer. By the effect of larger angle, the optical power loss would decrease when propagating in glass plate.

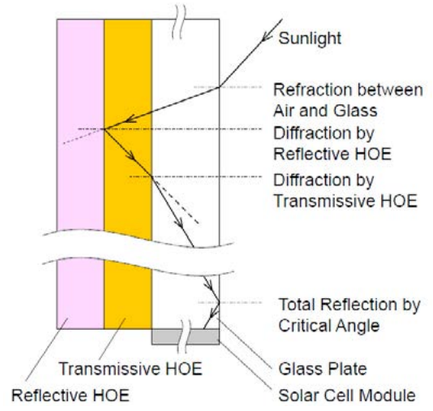

Fig. 3 Structure of improved Holo-Window

This suggested transmissive HOE at middle layer requires the diffractive efficiency to large incident angle form high refractive index(n~1.58) region. The liquid immersion method is preferable in order to produce the recommended HOE using objective lens, however, immersion method is hard to apply in this printer because of moving optical head with ultra high speed. Then we set the planar prism on photopolymer as shown in Figure 4. In this method, grating pattern by high angle beams is able to be recorded in photopolymer.

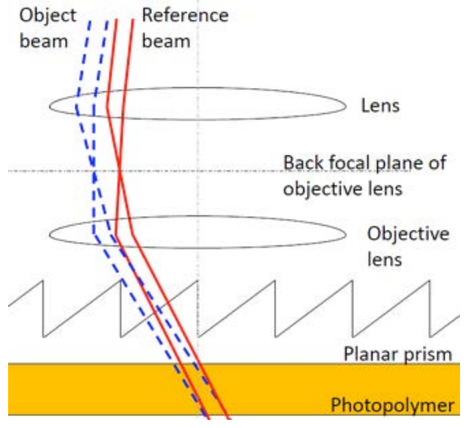

Fig. 4 optical diagram for HOE printing

4. Conclusion

In this paper we describe high speed holographic printing system. This printer is able to produce trans-mission type HOEs using photopolymer. The optical head in this printer is able to move high speed when recording HOEs. The diffraction efficiency is achieved 74% with 240mm/s head speed. And we propose the improved optical structure of Holo-Window in order to decrease propagating optical power loss. And technique to produce the required HOE is suggested.

References

[1]T. Kasezawa, H. Horimai, H. Tabuchi, and T. Shimura, ”Holographic window for solar power generation”, Opt. Rev.(2016), pp.1-7, doi: 10.1007/s10043-0257-z.

[2] M. V. Collados, D. Chemisana, and J. Atencia: “Holographic solar energy systems: the role of optical elements”, Renew. Sustain. Energy Rev. Vol.59 (2016) pp.130-140.

[3] A. V. Morozov, A. N. Putilin, S. S. Kopenkin, Y. P. Borodin, V. V. Druzhin, S. E. Dubynin, and G. B. Dubinin, “3D holographic printer: Fasy printing approach”, Optics Express. Vol.2, No. 3(2014) pp.2193-2206.

45.

1mm-thick See-through Holographic Lighting Unit ~ Ega-rim ~

Toshihiro Kasezawa,[1)] Hideyoshi Horimai,[1)] Hiroshi Tabuchi,[2)] Toshitaka Nara,[2)] and Tsutomu Shimura[3)]
[1)] Egarim Co., Japan, 330 Shibukawa, Shimizu-ku, Shizuoka-shi, Shizuoka 424-0533, Japan
[2)] Okamoto Glass Co., Ltd., 380 Toyofuta, Kashiwa-shi, Chiba 277-0872, Japan
[3)] The University of Tokyo, 4-6-1 Komaba, Meguro-ku, Tokyo 153-8505, Japan

1. Introduction

In the field of the hologram, there are two big walls to disturb the development and market growth. First big wall is the holographic media production issue. Such as a photopolymer material is very useful for creating the hologram contents, however, available products and supply roots are strictly limited in the world. To make a solution to this first wall, we have started photopolymer production in Japan with an overseas photopolymer development company by the technological cooperation. We intend to present these items separately in near future.

Second big wall is the limitation of the expression methods for hologram contents and holographic pictures. As shown in Figure 1, an external light source is mandatory for observing the sufficient quality of External Lighting Unit Holographic Picture holographic image. In this paper, we propose the brand-new solution to solve the second wall problem by using holographic technology.

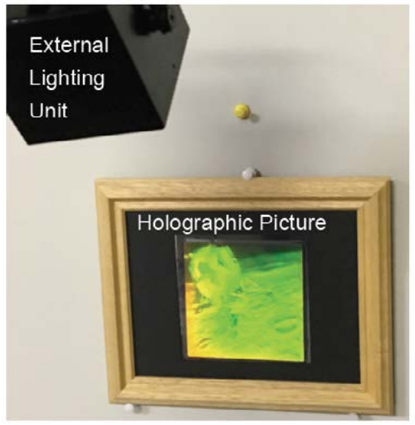

Fig. 1 Commonly used lighting method for holography.

Figure 2 (b) shows the design concept of the holographic lighting unit compare to the conventional expression method as shown in Fig.2 (a). Illumination part looks like a thin plane glass with only 1mm thick. In spite of this, the light can be lead from the edge of this glass and the emitted light from the plane glass surface illuminate the hologram picture with certain angle. This holographic lighting unit enables to combine with the photo-frame. In Japanese, usually the picture pronounces /e/ or /ga/, and a frame is a rim in English. Therefore, this unit is so-called “Ega-rim”.

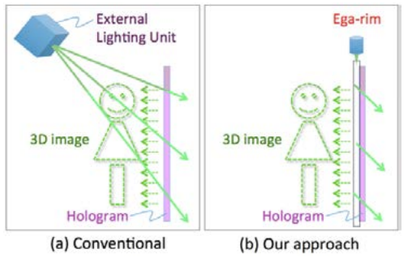

Fig. 2 Design Concept in Ega-rim

2. Realizing approach of holographic lighting unit “Ega-rim”

In IWH2015, Holo-Window has been proposed and its concept was proved by experimentally. The Capturing Efficiency in 532nm was achieved approximately 53% at proto-type unit [1]. This time, we did the reversal Holo-Window’s idea. Since it take in much light from the surface of the glass and lead it to the end edge, that means, take in the light from the end edge and lead it to the surface will also enable, as shown in Fig. 3. These are the design parameter of Ega-rim. The effect demanded from the hologram attached to Ega-rim is to diffract the light that was incident at an angle of 3 degrees at the internal of the glass material. This is impossible to create the interference pattern by using the normal optical elements and setting. Figure 4 shows the main part of optical configuration for hologram exposure schematically and its actual optical components.

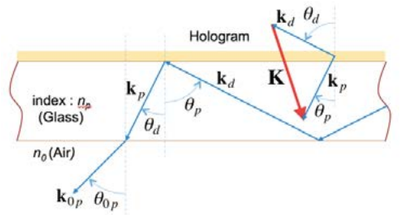

Fig. 3 Hologran design parameter of Ega-rim.

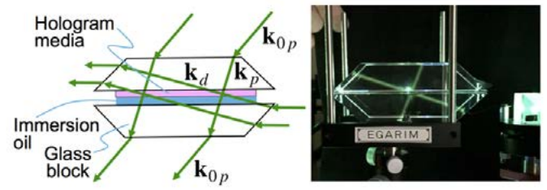

Fig. 4 Optical configuration and actual optical components for Ega- rim

3. Ega-rim Laboratory Proto-type

Figure 5 shows the optical simulation result of 1mm-thick glass inside reflection of Ega-rim. Figure 6 shows the laboratory proto-type of Ega-rim. The exposed hologram, made as in Fig. 4, was set up on the 1mm-thick transparent glass surface. Figure 7 proves experimentally the concept of Ega-rim that we can take in the light from the end edge and lead it to the surface, as explained in Fig. 3. The detailed characteristics will be discussed in this conference.

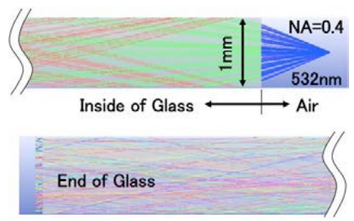

Fig. 5 Beam propagation: 1 mm-thick glass inside

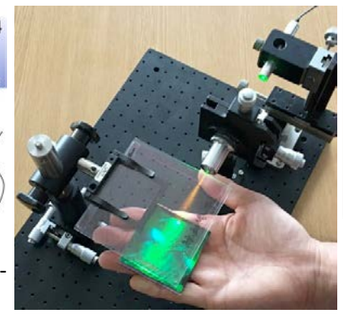

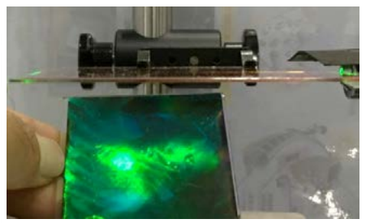

Fig. 7 Side view of Ega-rim and Hologram : Proof of Concept.

Fig. 6 Laboratory proto-type.

4. Conclusion

The brand-new see-through holographic illumination unit called Ega-rim was proposed. The thickness was only 1mm and has a transparency; it looks like a just plane glass. In spite of this, the light can be lead from the edge of this glass and emit from the surface with certain angle. Therefore, this illumination unit can be set very close to the hologram content or hologram picture, i.e. enables to combine with the photo-frame. By using the laboratory proto-type, its performance was proven experimentally. We hope everybody can enjoy a hologram easily by using Ega-rim, and open up the hologram market worldwide.

References

[1] T. Kasezawa, H. Horimai, H. Tabuchi, and T. Shimura, “Holographic Window for Solar Power Generation”, International Workshop on Holography and related Technologies 2015 (IWH2015).

46.

Wide wavelength range of Holographic Window for Solar Power Generation ~ Holo-Window II ~

Toshihiro Kasezawa,[1)] Hideyoshi Horimai,[1)] Hiroshi Tabuchi,[2)] Tomoyasu Saigo,[3)] and Tsutomu Shimura[4)]
[1)] Egarim Co., Japan, 330 Shibukawa, Shimizu-ku, Shizuoka-shi, Shizuoka 424-0533, Japan
[2)] Okamoto Glass Co., Ltd., 380 Toyofuta, Kashiwa-shi, Chiba 277-0872, Japan
[3)] Nagoya Institute of Technology, Gokiso-cho, Syowa-ku, Nagoya-shi, Aichi 466-8555, Japan
[4)] Tokyo University, 4-6-1 Komaba, Meguro-ku, Tokyo 153-8505, Japan

1. Introduction

In IWH2015, our Holo-Window was proposed and its concept was proved by experimentally. The Capturing Efficiency in 532nm was achieved approximately 53% at proto-type unit [1].

Figure 1 shows Holo-Window Demo Building. We stuck our prototype on the side of this building. And Holo light was utilized simulated sunlight. The light through windowpane is captured into the glass plate. And the prototype leads it to the edge of the side of the Demo Building. Finally green wavelength color component emitted the edge. The concept of Holo-window has been proved by this Demo building again.

We proposed the next challenge. Since actual sunlight has a wide wavelength range, we are planning to improve the holographic performance for whole visible light. Therefore the field test of proto-type unit for wide wavelength range and development of the large size “Holo-window”.

Therefore, we advance becoming it by correspondence to the wide wavelength range and large size of the material of the hologram. We perform the original production of the color photo polymer. And we do the proof experiment of those problems with the super-high-speed exposure machine of Nagoya Instisute of Technology.

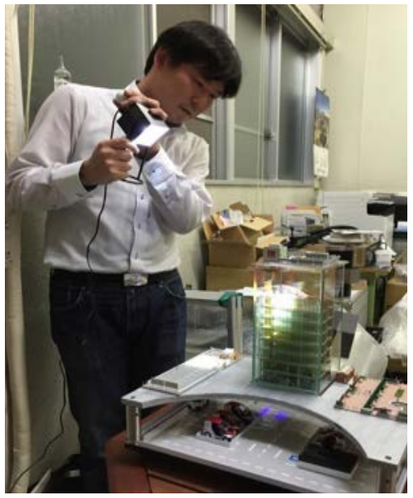

Fig. 1. Holo-Window Demo

2. Correspondence to a wide wavelength range with the original production of the color photo polymer.

Figure 2 shows schematic illustration of hologram exposure system to investigate the sunlight capturing characteristics. Green laser (532nm) was used to create these holograms with custom designed optical components. Photopolymer was used to create the hologram; it was sandwiched between dove prisms. Including this photopolymer surface, all of the contacted surfaces were filled with matching oil to prevent the surface reflection. In this setting, the reflection type holograms were fabricated with the function as described in basic principle, θ_d was more than a critical angle of total reflection on the window glass. In the “A” position, additional optical components can be inserted. This time we exposed it with RGB laser. In this way, we correspond to the wide wavelength range of sunlight. The result is shown in this meeting.

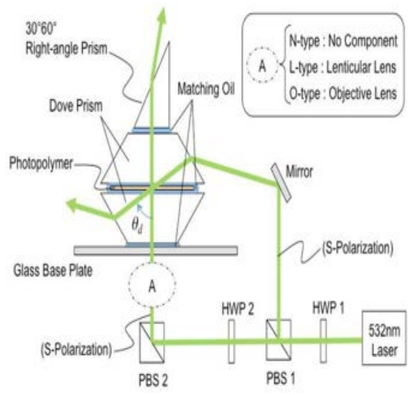

Fig. 2 . Schematic illustration of hologram exposure system to investigate the sunlight capturing characteristics

3. Ultra-High Speed Printing of Large Size Holographic Optical Elements

Figure 3 shows the developed printer, which have collinear optical head. This printer is able to record hologram with 240mm/s head speed. Laser source for hologram recording is used Q-switched YAG laser VECTOR-532-1000-20, made by Coherent Inc. This laser instrument is able to generate green light (wavelength is 532nm) with pulse width 10ns. The recording hologram materials are used DAROL, produced by our original production of the color photo polymer.

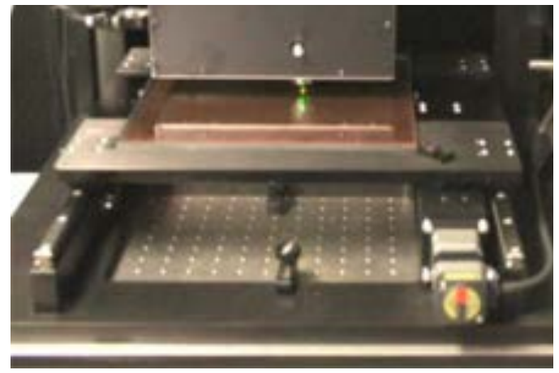

Fig. 3. HOE printer

4. Conclusion

Since actual sunlight has a wide wavelength range[2], we are planning to improve the holographic performance for whole visible light. So we established production and the exposure technology of the materials which were a problem of Holo-Window.

References

[1] T. Kasezawa, H. Horimai, H. Tabuchi, and T. Shimura, “Holographic Window for Solar Power Generation”, International Workshop on Holography and related Technologies 2015(IWH2015).
[2] S.N.Singh, P.Saw, and R.Kumar: *HOLOGRAPHY : NEW BREAKTHROUGH IN SOLAR POWER CONVERSION TECHNOLOGY* (International Journal of Engineering Science and Technology. Vol. 4 No.06 June 2012), p. 2485-2492.

47.

Study of 3D Human Face Imaging and Identification With Projection Grating Fringe

Yeh-Wei Yu[1,2], Wei-Wen Ni[2], Li-Wen Chiu, Che-Chu Lin, Tsung-Hsun Yang[2]and Ching-Cherng Sun[2]
[1]Optical Science Center, National Central University, Chung-Li, Taoyuan City 32001, Taiwan
[2]Department of Optics and Photonics, National Central University, Chung-Li, Taoyuan City 32001, Taiwan

Summary

The fringe projection profilometry (PFP) has great advantages on non-contact measuring method and is widely used for analyzing the three-dimensional objects nowadays. There are many ways for us to generate our projecting fringe, and holography is one of the approaches.

In this study, we apply Fourier transform profilometry (FTP) to reconstruct the three-dimensional object since it is fast, high-accurate and merely a single image that can restore the three-dimensional shape of an item. Therefore, we operate FTP to reinstate the three-dimensional shape of humans' physiognomy in order to get the feature value. Owing to the fact that, each person has individual attribute of themselves, we propose the routine of double-identification.

In the calculating process, there are some artificial errors, which occur because of tilting and shifting of human face. To solve this problem, we suggest two kinds of tilt-correction practices to normalize each human profile and compute the actual distance by utilizing optical triangulation [2]. On that account, it allows a small tilt angle tolerance for system and extends the shooting distance to 35~55 centimeters. In closing, we compare 85 people with each other from the database, with 3570 times of comparison. By making use of double-identification approach to single out 85 people from each other, the recognition rate could reach 99.91%.

To reconstruct the structure of the object, triangulation survey helps us acquire the relationship between fringes and the item's degree of curve (Fig. 2). With Fourier Transform, the image will transfer from spatial domain to frequency domain. Obviously, the first order and the zero order have a crystal clear separation. To obtain the frequency of first order, a circular widow is made (Fig. 1). As a result, we are able to access the wrapped phase of the face. By applying phase-unwrapping technique [1], the differences of the original phase that carry depth information will be revealed.

In order to recognize the variation from person to person, the selection of characteristic point [3] will be put on our highest agenda. As far as we know, eyes, the root of nose, forehead, etc., can be seen as feature points of humans' face. By utilizing the association from each characteristic point, we are capable of obtaining the magnitude of each profile in the database (Fig. 3). For the reason that each very one possess non-identical trait value, every characteristic figure can be a great term to identify humans' countenance. With the aid of comparing the attribute value we determine, the liminal value can be qualified and collated.

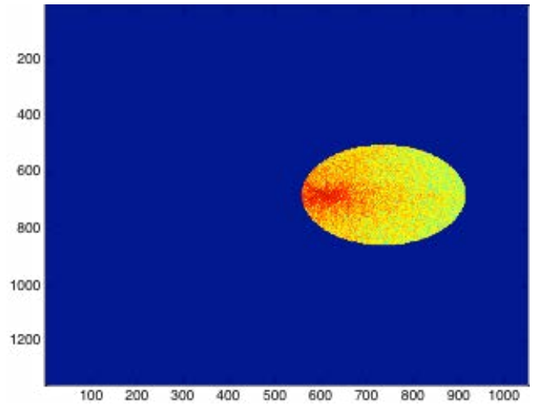

Fig.1 to extract the first order frequency

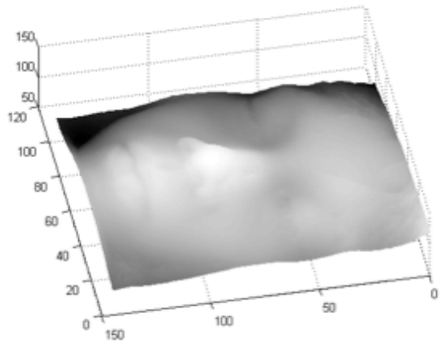

Fig.2 human face after reconstruction

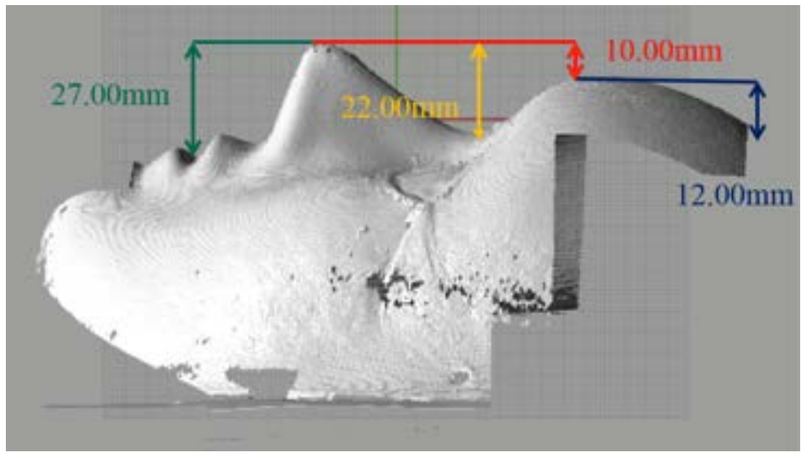

Fig.3 analyzing the relationship between characteristic points

References

[28]D. C. Ghiglia and L. A. Romero, "Robust Two-dimensional Weighted and Unweighted Phase Unwrapping that Uses Fast Transforms and Iterative Methods," JOSA A **11**, 107-117 (1994).

[2] M.F. Costa, "Surface Inspection by An Optical Triangulation Method," Opt. Eng. **35**, 2743 (1996).

[3] R. Brunelli and T. Poggio, "Face Recognition: Features Versus Templates," IEEE Trans Pattern Anal Mach Intell. **15,** 1042-1052 (1993).

48.

Holographic Image Reconstruction in front of polarization-dependent Diffuser.

Wen-Kai Lin[1,2] , Wai-Tin Liu[1] , Bor-Shyh Lin[2] , Wei-Chia Su*[1]

*[1] Graduate Institute of Photonic, National Changhua University of Education, Changhua, 50007, Taiwan

[2] College of photonics, National Chiao Tung University, Tainan, 71150, Taiwan

1. Abstract

A holographic image is reconstructed successfully in front of a diffuser based on transmission type holograms. The reconstruction of the hologram is clearly when the reference beam passes through a diffuser. The diffuser is a polarization-dependent diffuser based on liquid-crystal and polymer.

2. Introduction

In 2014, we presented a research about the reconstruction of holograms in front of a diffuser [1]. It used the reversibility of light to reconstruct the hologram through a diffuser by the conjugate wave. However, there is a disadvantage that the system setup is very difficult in the reconstruction process. In this paper, a polarization-dependent diffuser is used to replace the general diffuser. This diffuser does not affect the light transmission for one specific polarization of light [2-4]. The hologram is attached on the diffuser, and the holographic image is reconstructed in front of the diffuser successfully.

3. Experiment

In this paper, the diffuser is generated from NOA65-Doped E7 as shown in Ref.3. The recording experimental system is shown in Fig.1. In this work, we used a 532nm laser as the light source. The HWP1 is used to modulate the beam ration between the object beam and the reference beam. The HWP2 modulates the object beam to become an s-polarized wave. Then the light passing through the S.F. and lens becomes a collimation beam. And then we use the lens to generate the real image of pattern1 and pattern2, and they will locate in front of the hologram. The information of these two real images will be recorded in the hologram.

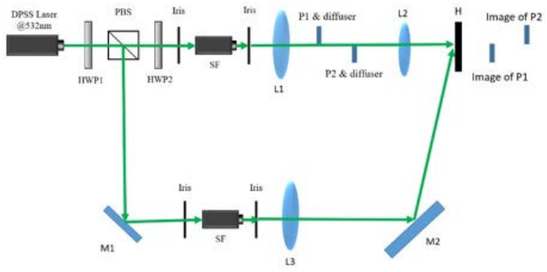

Fig.1 The holographic recording system.
HWP, half-wave plate; PBS, polarization beam splitter; P, pattern; H, hologram

The method of holographic reconstruction is shown in Fig.2.Once the hologram is recorded, we can use the reference light to reconstruct the hologram. Figure 2(a) shows the traditional holographic reconstruction process. Figure 2(b) show the setup for the proposed system. The hologram attached in front of the polarizations dependent diffuser. And we still use the same reference beam for reconstruction.

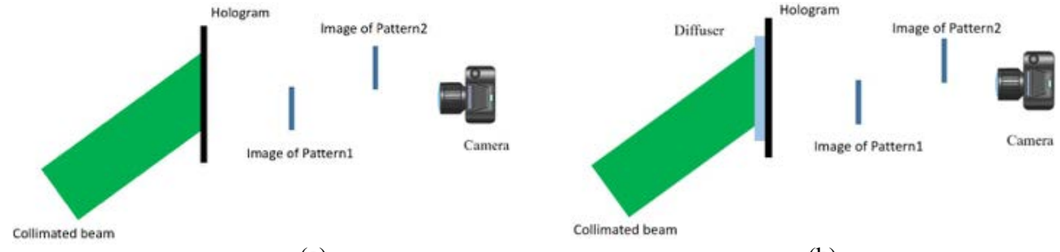

Fig.2 The holographic reconstruction (a) without diffuser; (b) with diffuser.

4. Results

As shown in Fig.3(a), if we reconstruct the hologram without using the diffuser, the image will be diffracted regardless of the polarization of the reading beam. When the diffuser is attached in back of the hologram, the property of light transmission will be different. The s-polarized wave

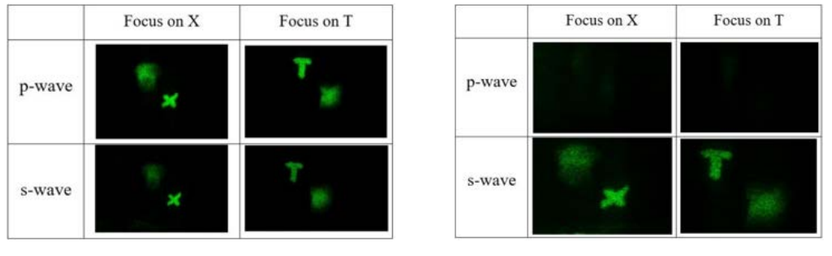

Fig.3 The results of image reconstruction (a) without diffuser; (b) with diffuser

will propagate through the diffuser, and the p-polarized wave will be scattered. Therefore, the p-polarized wave can't be used to access the hologram, and only the s-polarized wave can be used for reconstruction. These results are in Fig. 3(b).

5. Conclusion

Based on architecture of transmission type hologram, holographic images are successfully reconstructed in front of a polarization-dependent diffuser. Once the polarization of the probe beam is properly arranged, the hologram can be reconstructed clearly, otherwise no diffraction will be obtained from the hologram.

Acknowledgment

This work is supported by the Ministry of Science and Technology of Taiwan under contract NO.104-2221-E- 018-018-MY2.

References

[1] J.-F. Chang and W.-C. Su, "3D Hologram Reconstruction in the Front of a Transmission Diffuser Screen," proceeding of IDW'14, 3D1-3, Niigata, 2014.

[2] W.-K. Lin and W.-C. Su, "The See-Through Screen Based on a Polarization-Dependent LC Device," proceeding of IDW'14, LCTp2-1, Niigata, 2014.

[3] W.-K. Lin and W.-C. Su, "The Optical Characteristic of a Polarization-Dependent Diffuser Based on NOA65- Doped E7," proceeding of IDW'15, LCTp3-1, Otsu, 2015.

[4] W.-K. Lin, W.-C. Su, and B.-S. Lin, "Polarization-Dependent Diffuser Based on Liquid-crystal Lens Array," proceeding of IDW'15, PRJp1-6L, Otsu, 2015.

49.

Generating 3D Photonic Crystal Structure by Holographic Lithography

Mei-Li Hsieh,[1],* Wen-Tse Shih,[2] and Shawn-Yu Lin[3]
[1] Department of Photonics, National Chiao Tung University, Hsinchu, Taiwan
[2] Department of Opto-Electronic System Engineering, Minghsin University of Science and Technology, Hsinchu, Taiwan
[3] Department of Physics, Applied Physics and Astronomy, Rensselaer Polytechnic Institute, Troy, New York 12180, USA
*mlh@cc.nctu.edu.tw

Abstract
We proposed a hybrid technique with holographic lithography to generate the 3D photonic crystal structure. By modifying the 1D or 2D structure along the vertical direction, 3D photonic crystal structure can be easily fabricated, which provides a simple, low cost, and large area maintainable process.

Photonic crystals possess many unique properties due to their periodic structures with lattice periods comparable to the light wavelength. The interaction between light and the photonic crystal results to the redistribution of energy, such as diffraction, absorption, focusing, and photonic bandgap.[1] The responses of photonic crystals depend on the structure and the lattice period, providing the possibility to fit the response to the spectrum of interest. Many applications of the photonic crystal have been made owing to the features of trapping and localization of light, including wave guiding,[2] laser cavity,[3] photonic crystal fiber,[4] and thin film photovoltaics. [1,5,6] Recently, combining the nanowire and the 3D photonic crystal structure, sinusoidaly modulated nanowires have been proposed due to their strong light trapping effect.[7,8] The conventional photolithography with mask exposure can be used to fabricate the 1D or 2D structure. For 3D structure, it only can be done layer by layer. However, the issues of the layer to layer processing include the time consuming, complex, and high cost. Thus, we propose a hybrid technique with holographic lithography to modify the 1D or 2D photonic crystal structure along the vertical direction. By using our hybrid technique, the 3D photonic crystal structure can be easily fabricated within large area and simple process.

In this paper, we proposed a hybrid technique to fabricate the 3D photonic crystal structure. Using holographic lithography, the 1D/2D structure can be modified along the vertical direction and become 3D photonic crystal structure. To obtain the modulated structured photonic crystal, we proposed the multiple exposure method on a photoresist. Fig.1 (a) shows the schematic diagram of the holographic system. 1D structure can be obtained by the optical setup shown in Fig.1(b). For the modulated structure along the vertical direction, a 90° vertical rotation of the sample is needed, and then the two laser beams incident into the sample from the opposite sides. Therefore, the modulated structure can be achieved by the optical setup in Fig.1(c).

The period of photonic crystal structure depends on the wavelength and the incident angle of the laser beam. The relations between the period Λh and Λv, wavelength, and incident angle θh and θv in Fig. 1(b) and

(c) are shown in Fig.2.(a) and (b), respectively. The period can be adjusted by selecting the wavelength of

light source or changing the incident angle. For example, assume that the wavelength of the laser beam used is 355nm, the simulated results of the period corresponding to the incident angle are shown in Fig.2. By setting the incident angle θh and θv as 6.5° and 30°, the period Λh and Λv result to 1568nm and 145nm, respectively.

The hybrid technique we proposed is capable to generate the 3D photonic crystal structure by modifying the 1D or 2D structure along the vertical direction with holographic lithography. The obtained photonic crystal also can be used as a template and further inverted into other material with photonic bandgap of interest. The holographic lithography can improve the cost issue on manufacturing 3D photonic crystal, and provides a fast, simple, and large area maintainable approach.

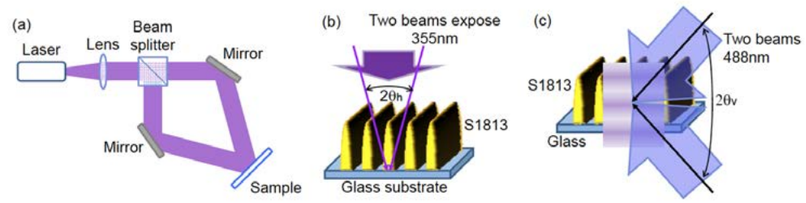

Figure 1. (a) The schematic diagram of optical system. The optical setup of (b) the 1D structure and (c) the modulated structure along the vertical direction.

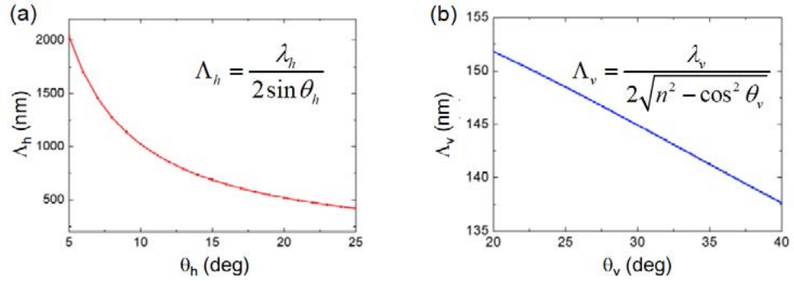

Fiure 2. (a) The period Λ_h vs. the incident angle θ_h. (b) The period Λ_v vs. the incident angle θ_v, where the index of refraction n is 1.5.

References

[1] S. John, "Strong localization of photons in certain disordered dielectric superlattices," Phys. Rev. Lett. 58, 2486, 1987.
[2] M. Tokushima, H. Kosaka, A. Tomita and H. Yamada, "Lightwave propagation through a 120° sharply bent single-line-defect photonic crystal waveguide," Appl. Phys. Lett. 76, 952, 2000.
[3] M. Lončar, T. Yoshie, A. Scherer, P. Gogna and Y. Qiu, "Low-threshold photonic crystal laser," Appl. Phys. Lett. 81, 2680, 2002.
[4] P. Russell, "Photonic Crystal Fibers," Science, vol. 299, no. 5605, pp. 358-362, 2003.
[5] E. Yablonovitch, "Inhibited Spontaneous Emission in Solid-State Physics and Electronics," Phys. Rev. Lett. 58, 2059–2062 (1987).
[6] J. D. Joannopoulos, S. G. Johnson, J. N. Winn, and R. D. Meade, Photonic Crystals: Molding the Flow of Light (Princeton University, Princeton, NJ, 2008).
[7] G. Demésy, and S. John, "Solar energy trapping with modulated silicon nanowire photonic crystals," J. Appl. Phys. 112, 074326 (2012).
[8] A. Deinega, and S. John, "Solar power conversion efficiency in modulated silicon nanowire photonic crystals", J. Appl. Phys. 112, 074327 (2012).

50.

Photopolymerizable Silica using Ionic Liquids as Solvents by Sol-Gel Process

Xin-De Xie, Tzu-Chien Hsu, and Wei-Hung Su
Department of Materials and Optoelectronic Science, National Sun Yat-Sen University, Kaohsiung 804, Taiwan

1. Introduction

Photopolymerizable holographic materials have the great advantage of recording and reading holograms in real time due to their good light sensitivity, real-time image development, large dynamic range, and low cost [1-8].

In this paper, an sol-gel process using ionic liquids as solvents to fabricate photopolymerizable silica for optical storage is proposed. It uses tetraethylorthosilicate (TEOS) to form the SiO2 network structure, and the ethylene glycol phenyl ether acrylate (EGPEA) as the monomer. The silane coupling agent γ-glycidoxypropyltrimethoxysilane (GPTMS) connects organic and inorganic phases to avoid the phase separation. This makes the monomer and photoinitiator (IRGACURE 784) uniformly distributed in the silica. To enhance the diffraction efficiency, the high refractive index species, zirconium isoproxide isopropanol complex (ZPO), is filled into this composite material.

2. Fabrication method and experiment

The flow chart of the sol-gel process is illustrated as Fig. 1(a). Figure 1(b) shows the optical configuration for holographic recording. A DPSS laser with a wavelength of 532 nm was used as the light source. The photopolymerizable silica is illuminated by interference of the two plane waves. The power of the plane wave is 5 mW/cm2. A He-Ne laser with wavelength of 633 nm was used to evaluate the diffraction efficiency. Figure 1(c) depicts the optical configuration.

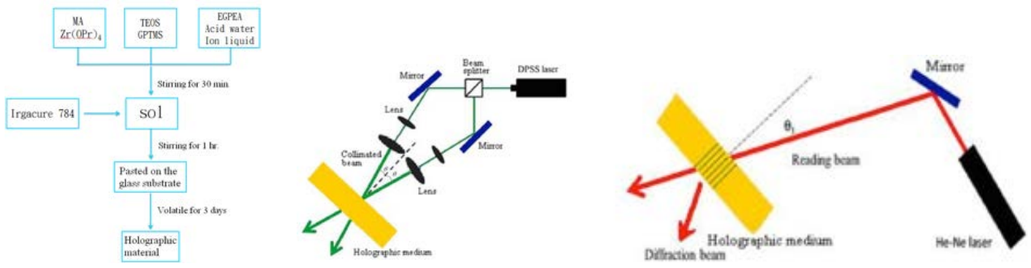

(a) (b) (c)

Fig. 1. (a) Flow chart of the fabrication process. (b) Holographic setup in the recording proceedure. (c) Holographic setup in the reading procedure.

A number of holographic materials with various proportions of EPGEA, ZPO, and TEOS were fabricated. For the case that the incident angle θ was 1.5°, the grating period is 10.16 μm. The thickness of this hologram was measured as 0.27mm. Figure 2 shows the mole ratio for each component. diffraction efficiencies for various diffraction orders is shown as Fig. 3(a). It is found that the diffraction efficiency of the 2nd order was more than 50%, which was higher than the 1st order. The reason might be the Bragg's mismatch appeared within this material. Figure 3(b) shows the diffraction efficiency for +1 order at various incident angles θ. It shows that the highest diffraction efficiency is 92.36% when ionic liquid is employed as solvents.

3. Conclusion

	TEOS	GPTMS	EGPEA	MA	$Zr(OPr)_4$	Irg784	Acid water	Ion Liquid	EtOH	0 order η (%)	+1 order η (%)	+2 order η (%)
GIe-2	1	6.56	1.86	3.89	0.83	0.06	0.61	0.53	-	9.76	19.53	54.29

Fig. 2. The mole ratio for the components.

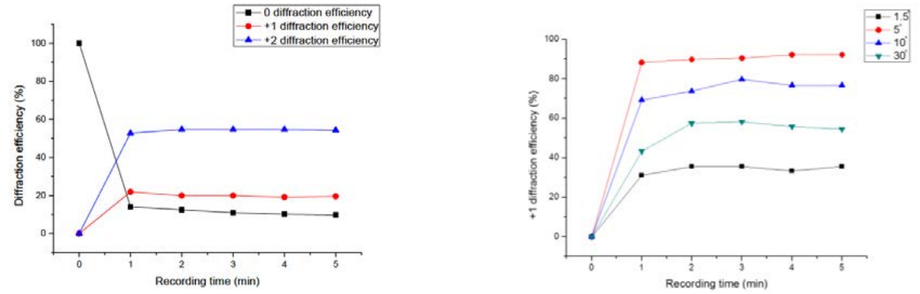

(a) (b)

Fig. 3. (a) Diffraction efficiencies for various diffraction orders. (b) Diffraction efficiencies at different recording time for various θ.

A set of silica glass photopolymerizable materials has been fabricated for optical storage. Performances of their diffraction efficiencies have evaluated as well. The optimization of the composition for the proportion of the components has been illustrated as Fig. 2. The diffraction efficiency could be 92.36%.

References

[1] D.Wang, G. P.Bierwagen, "Sol–gel coatings on metals for corrosion protection," Progress in Organic Coatings, Vol. 64, 2009, pp. 327–338.
[2] P. Hariharan "Basic of holography" Cambridge University Press, Cambridge, 2002.
[3] W. S. Colburn, K. A. Haines, "Volume hologram formation in photopolymer Materials," Applied Optics, vol. 10, 1971, pp.1636-1641.
[4] Y.M. Chang, S.C. Yoon, M. Han, "Photopolymerization of aromatic acrylate containing phosphine oxide backbone and its application to holographic recording," Optical Materials, vol. 30, 2007, pp. 662–668.
[5] G. Ramos, A. Alvarez, T . Belenguer, "Shrinkage Control in a Photopolymerizable Hybrid Solgel Material for Holographic Recording," Applied Optics, vol. 43, 2004, pp. 4018-4024.
[6] P.Cheben, M.Clavo, Appl.Phys.Lett, vol. 78, 2001, pp. 1490-1492.
[7] M. L. Calvo, P. Cheben, "Photopolymerizable sol–gel nanocomposites for holographic recording," Journal of optics. A, Pure and applied optics, vol. 11, 2009.
[8] C.Y Kuo. "Fabrication of volume holograms using sol-gel technology and its application to 3D profile measurement", doctorate dissertation, National Sun Yat-sen University, Taiwan, 2012

51.

Mirror-assisted Tomographic Phase Microscopy

Yeh-Wei Yu[1,2], Xing-Chen Liu[1], Wei-Mao Hsu1, Sih-Yu Chen[1], Tsung-Hsun Yang[1] and Ching-Cherng Sun[1]
Department of Optics and Photonics, National Central University, Taoyuan City 32001, Taiwan
[1]Department of Optics and Photonics, National Central University, Chung-Li, Taoyuan City, 32001 Taiwan.
[2]Optical Science Center, National Central University, Chung-Li, Taoyuan City, 32001 Taiwan.
Correspondence and requests for materials should be addressed to C.-C.S. (email: ccsun@dop.ncu.edu.tw)

Summary

The motivation of this study is to improve the tomographic phase microscopy (Fig.1) (TPM) [1] by adding a mirror at the sample plane and using the off-axis holographic configuration(Fig.2). These improvements can help to reduce system complexity and scanning time based on the traditional TPM. The phase projections of sample in different directions are obtained by using the off-axis digital holography. The wrapped phase has to be unwrapped to obtain successive phase distribution by applying phase unwrapping algorithm (Fig.3) [2]. We use discrete cosine transform (DCT) [3] to unwrap wrapped phase. Polymer beads with known diameter and refractive index are used as samples to verify the system performance and algorithm accuracy. Finally, the three-dimensional refractive index distribution (Fig.4) of the sample is reconstructed through filtered backprojection (FBP) [4] algorithm.

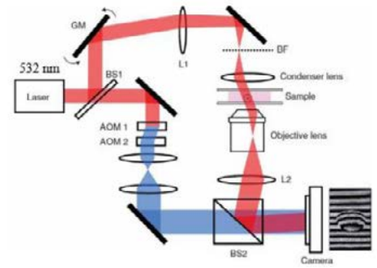

Fig. 1. Tomographic phase microscopy

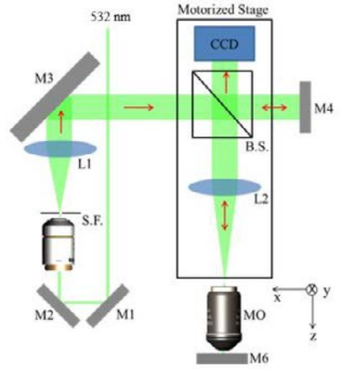

Fig. 2. Mirror-assisted TPM

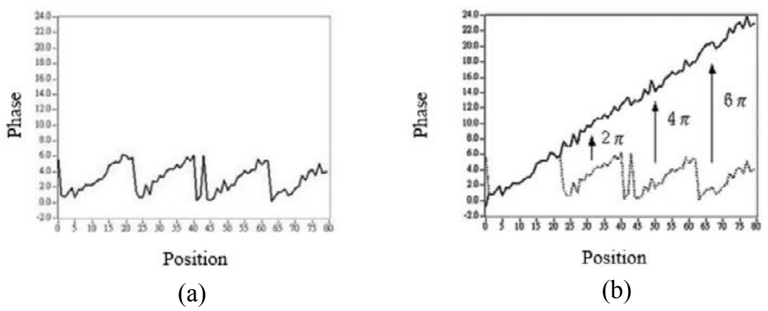

Fig. 3. One dimensional phase unwrapping (a)Wrapped phase (b) Unwrapping phase

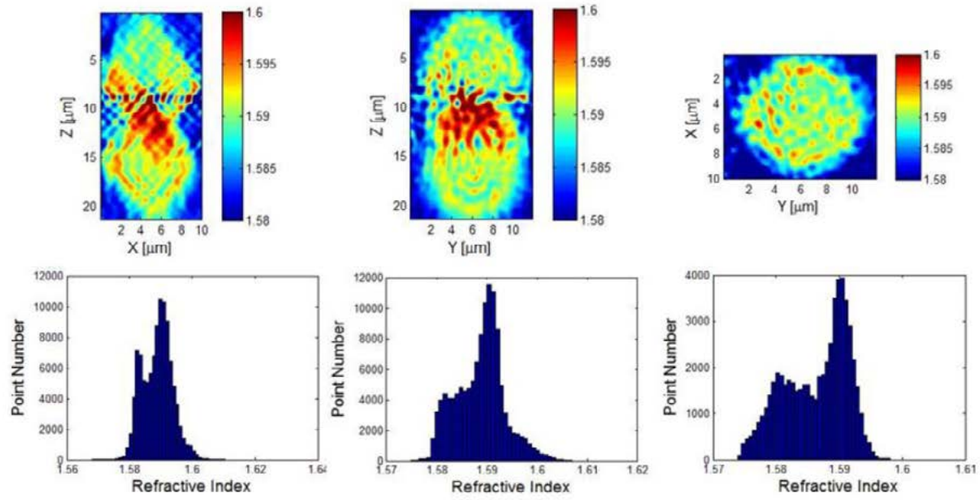

Fig. 4. Tomogram and histogram of 10 mm bead in different. (a) Distribution of refractive index in Y direction, (b)in X direction, (c)in Z direction.

References

[1] F. Charrière, A. Marian, F. Montfort, J. Kuehn, T. Colomb, E. Cuche, P. Marquet, and C. Depeursinge, "Cell refractive index tomography by digital holographic microscopy," Opt. Lett. **31**, 178-180 (2006).
[2] D. C. Ghiglia and M. D. Pritt, *Two-dimensional phase unwrapping: theory, algorithms, and software* (Wiley New York, 1998).
[3] D. C. Ghiglia and L. A. Romero, "Robust two-dimensional weighted and unweighted phase unwrapping that uses fast transforms and iterative methods," JOSA A **11**, 107-117 (1994).
[4] A. C. Kak and M. Slaney, *Principles of computerized tomographic imaging* (Siam, New York, 1988).

52.

Resolution enhancement of digital holographic microscopy based on structured-illumination induced moiré fringes

Xin-Ji Lai[1)], Han-Yen Tu[2)], and Chau-Jern Cheng[1)]

[1)]Institute of Electro-Optical Science and Technology, National Taiwan Normal University, Taipei 11677, Taiwan

[2)]Department of Electrical Engineering, Chinese Culture University, Taipei 11114, Taiwan

**E-mail:* cjcheng@ntnu.edu.tw

Abstract—**This study presents a resolution enhancement in digital holographic microscopy based on structured-illumination induced moiré fringes. The high-resolution information can be retrieved by low-frequency moiré fringes and known regular structured patterns. The spectral bandwidth modulation and zero-order suppression methods are applied to reduce the spectral overlapping of each diffraction orders.**

***Keywords*— resolution, digital holographic microscopy, structured-illumination, moiré.**

1. Introduction

Digital holographic imaging has been investigated for decade in applications of biological specimen, micro-optical elements and industrial inspection [1]. The infinite aperture size and wavelength of light have restricted the spatial resolution of optical imaging system. In recent, the synthetic aperture (SA) method is widely used in quantitative imaging for overcome the diffraction limit and resolution enhancement [2,3]. Moreover, a structured-illumination (SI) light is proposed to deflect the illumination angle by spatial light modulator (SLM) without mechanical movement [4]. Thus, in this study, we present the resolution enhancement in digital holographic microscopy (DHM) by structured-illumination induced moiré fringes. Compared to conventional method, proposed approach can obtain low-frequency moiré fringes for enlarging the spectral bandwidth coverage.

2. Principle

The schematic representation of the resolution enhancement by structured-illumination in digital holographic microscopy is indicated in Fig. 1. The known regular structured pattern is used to projection onto the object plane by telescope system. The transmitted wavefront is imaged and magnified at the intermediate image plane and interference with the spherical reference wave as an off-axis Fresnel hologram. Figure 2 indicates the conception of SI induced moiré fringes, which can shift the spectral bandwidth of unsolved object through convolution with the known regular SI as in Fig. 2(c). The known regular SI in Fig. 2(b) is projected onto an unresolved object as shown in Fig. 2(a). By this approach, the spectral bandwidth coverage would be enlarged than the original cut-off frequency by detecting the low-frequency moiré fringes.

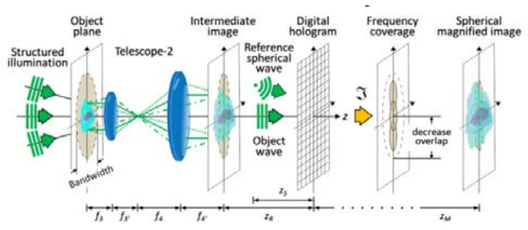

Fig. 1. Schematic diagram of the resolution enhancement in digital holographic microscopy based on structured illumination.

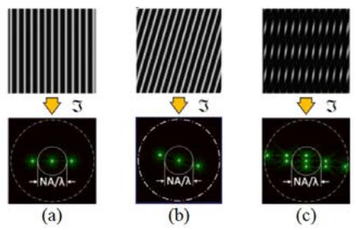

Fig. 2 Concept of SI induced moiré fringes (a) unresolved object (b) known regular SI and (c) is (b) projected onto (a) for producing moiré fringes.

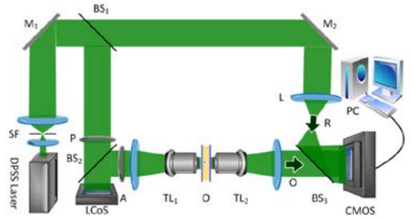

Fig. 3. Experimental setup of structured-illumination digital holographic microscopy. SF: spatial filter, M: mirror, BS: beam splitter, MO: microscope objective, L: lens, O: object, TL: telescopic imaging, P: polarizer, A: analyzer, PC: personal computer.

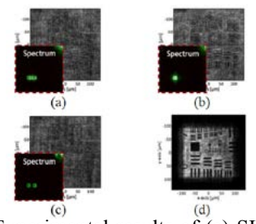

Fig. 4. Experimental results of (a) SI hologram and (b) normal aperture hologram and (c) zero-order suppressed hologram after (a) subtract with (b), and (d) synthesized reconstruction amplitude image.

3. Experimental setup and results

The experimental setup of structured-illumination induced moiré fringes in digital holographic microscopy for resolution enhancement is shown in Fig. 3. The SI-DHM was constructed by a modified Mach-Zehnder interferometer with an CMOS image sensor (pixel number: 1,280(H)×1,024(V) and pixel size: 5.2×5.2 μm^2). The display mode LCoS-SLM (native resolution: 1,920(H)×1,080(V) and pixel size: 6.4×6.4 μm^2) was used in the object arm to display binary amplitude grating pattern. The DPSS laser (λ=532 nm) was applied as the light source for producing interference between object and reference beams. In reference arm, a lens (*f*: 50 mm) was employed to encode a spherical wave and then recorded as an off-axis Fresnel hologram. In experiments, we constructed two telescopic imaging system ($TL_{1,2}$) to enlarge the diffraction angle by TL_1 and then imaging the SI projected object by TL_2. The TL_1 was consisted by microscope objective (10×, NA: 0.25) and a lens (*f*: 200 mm), and the TL_2 was consisted by a microscope objective (4×, NA: 0.10) and a lens (f: 250 mm). Experimental results of resolution target by SI-DHM were shown in Fig. 4. In Fig. 4(a), the spectral bandwidth of SI hologram was decreased by spherical factor encoding. And the normal aperture hologram in Fig. 4(b) was applied to subtract with SI hologram for zero-order suppression, thereby the ±1st order diffraction can be separated as in Fig. 4(c). Under this condition, the line-width of G7-E5 can be resolved because of the resolution enhancement by SI induced moiré fringes. However the diffraction efficiency of 0th and ±1st order was greatly differences that degraded the interference fringe visibility of hologram and cause the high-frequency noise in the reconstruction amplitude image as Fig. 4(d).

Acknowledgment

This work was financially supported in part by the Ministry of Science and Technology, Taiwan (MOST 105-2221-E-003 -015 -MY3 and MOST 104-2221-E-034-010-MY3).

4. Conclusions

This work has proposed and demonstrated a resolution enhancement method by SI induced moiré fringes in DHM. The spherical factor from reference arm was used to reduce the spectral bandwidth of each diffraction order and the normal aperture hologram subtraction with SI hologram was applied to decrease spectral overlapping. Experimental results have implemented to synthesize the low-frequency moiré fringes with normal aperture for resolution enhancement. The numerical compensation of intensity ratio at each diffraction order and high-frequency noise will be discussed and analyzed in the near future.

References

[1] M. K. Kim, Digital Holographic Microscopy: Principles, Techniques, and Applications (Springer New York, 2011).

[2] M. G. L. Gustafsson, D. A. Agard, and J. W. Sedat, "Sevenfold improvement of axial resolution in 3D widefield microscopy using two objective lenses," Proc. SPIE 2412, 147-156 (1995).

[3] X. J. Lai, H. Y. Tu, C. H. Wu, Y. C. Lin, and C. J. Cheng, "Resolution enhancement of spectrum normalization in synthetic aperture digital holographic microscopy," Appl. Opt. 54, A51-A58 (2015).

[4] J. Zheng, G. Pedrini, P. Gao, B Yao, and W. Osten, "Autofocusing and resolution enhancement in digital holographic microscopy by using speckle-illumination," J. Opt. 17, 085301 (2015).

53.

Synthetic aperture common-path digital holographic microscopy based on spiral phase filter

Xin-Ji Lai[1)], Wei-Jen Hsiao[1)], Yu-Chih Lin[1)], Han-Yen Tu[2)], and Chau-Jern Cheng[1)]

[1)]Institute of Electro-Optical Science and Technology, National Taiwan Normal University, Taipei 11677, Taiwan

[2)]Department of Electrical Engineering, Chinese Culture University, Taipei 11114, Taiwan

**E-mail*: cjcheng@ntnu.edu.tw

***Abstract*—**This work purposes a common-path digital holographic microscopy based on spiral phase filter to enhance the phase stability and spatial resolution. The phase-mode liquid crystal on silicon spatial light modulator is used to produce a spiral phase with an optical aperture on the Fourier plane. The convergence wave is filtered by optical aperture as reference wave and the scattering wave is modulated by spiral phase as object wave. Experimental results illustrate that the reflective nano-structure can be numerical reconstructed.

Keywords— synthetic aperture, common-path, digital holographic microscopy, spiral phase.

1. Introduction

Digital holographic imaging is a useful technique that can quantitative analyzed the amplitude and phase information. However, the interference phenomenon requires additional reference wave to interfere with object wave, which has increased the mass of optical architecture and sensitive in environment perturbation. Even though the off-axis recording setup [1] is extensively constructed, the phase stability still affects the wavefront reconstruction quality. Therefore, the common-path interferometer architectures [2] were demonstrated to strength the phase stability without phase retrieval algorithm. In this work, we purposed to integrate the spiral phase contrast microscopy [3,4] into the synthetic aperture (SA) digital holographic microscopy (DHM) for upgrading the phase stability and spatial resolution.

2. Principle

The schematic diagram of SA common-path spiral DHM is illustrated in Fig. 1. The plane wave is used to illuminate on the object and the diffraction object pass through the first lens to the Fourier plane. The convergence wave is filtering by an optical aperture as reference wave (E_r), and the scattering wave is mapped with spiral phase as modulated object wave (E_o). Then, the intermediate image plane after second lens can be formed as an interference image as $E_i=E_o\otimes Se^{i\phi}+E_r$ and the rotation of the spiral phase plate is applied to produce phase-shift of φ=0, π/2, π, 3π/2. The intensity wave field with a sequence of phase-shifting interference image on

the hologram plane. In the numerical reconstruction process, the complex average method is used to calculate the modulated object wave. Finally, the complex average result (I_A) with inverse numerical phase spiral phase (S^{-l}) and conjugate reference wave (E^*_r) are calculated and numerical propagated by convolution approach as

$$E_i = \Im^{-1}\left\{\Im\left(\frac{I_A \otimes S^{-1} + |E_r|^2}{|E_r^*|}\right)\cdot CTF\right\}, \tag{1}$$

where *CTF* is the coherent transfer function and $\Im$ represents Fourier transform symbol. In SA process, consider the different angle plane wave is used to illuminate on the object thereby the spiral phase is shifted

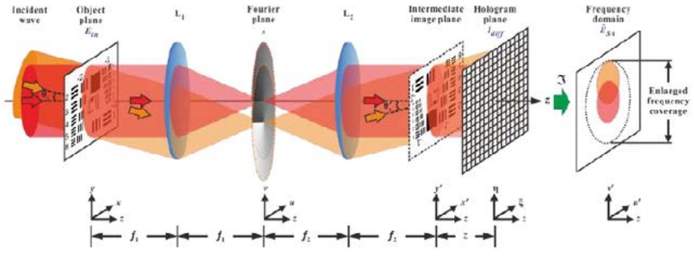

Fig.1 Schematic diagram of the synthetic aperture common-path digital holographic microscopy based on spiral phase filter.

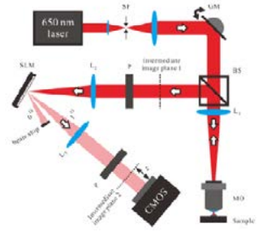

Fig. 2 Experimental setup of synthetic aperture common-path spiral digital holographic microscopy. (SF: spatial filter, MO: microscope objective).

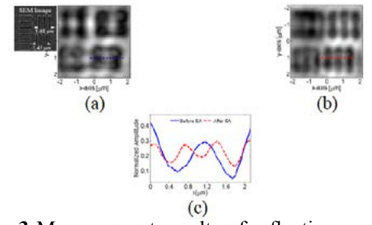

Fig. 3 Measurement results of reflective nano-structure. The reconstruction amplitude map of (a) normal aperture and (b) SA and cross-section profile of ROI in (c).

for mapping with the covergence and scattering wave of the object wave as follow:

$$E_o(x',y') = \Im^{-1}\left\{\tilde{E}_o(u,v)\cdot s(u,v)\cdot\left[H(u,v)\otimes\delta\left(u+\frac{\alpha}{\lambda},v+\frac{\beta}{\lambda}\right)\right]\right\} \tag{2}$$

where $H(u,v)$ is the cut-off frequency of telescope system, $s(u,v)$ is the spiral phase and α and β represent the incident angle. The convergence and scattering wave would be modulated and formed as the digital hologram without using additional reference arm. Thus, purposed common-path spiral phase digital holographic microscopy can improve the phase stability; moreover, the spatial resolution can be improved by synsthetic aperture method.

3. Experimental setup

The experimental setup of SA common-path spiral phase DHM is shown in Fig. 2, it was mainly consisted of two telescopic imaging system (TL_1:L_1-MO; TL_2:L_2-L_3), which can record the hologram at different illumination direction by use of the Galvo-mirror. The wavelength of laser diode is 650 nm and the object arm and reference arm would be modulated by spiral phase filter at the Fourier plane. The LCoS-SLM (pixels size: 6.4×6.4 μm^2, pixel number: 1,920×1,080) was employed to output a phase-shifting blazed spiral phase. Then, the convergence wave would be filtering by optical aperture as reference wave and the scattering wave would be modulated by a serious phase-shifting blazed spiral phase as modulated object wave. Finally, the CMOS sensor (pixel size: 5.2×5.2 μm^2) was used to record the Fresnel holograms. In experiment, we made a reflective nano-structure by NDL, which was fabricated by E-beam lithography and etching of the photo-resist on the glass substrate with 100 nm thick of TiN. The measurement results were shown in Fig. 3. In Fig. 3(a) shows the SEM image and reconstruction amplitude map at normal aperture condition. After SA procedure, the line-width 280 nm of reconstruction amplitude map can be resolved as shown in Fig. 3(b) and the cross-section profile of (a) and (b) were indicated in Fig. 3(c). These results could indicate the effective of resolution enhancement and phase stability improvement in SA common-path spiral phase DHM.

4. Conclusions

We have demonstrated a synthetic aperture common-path digital holographic microscopy based on spiral phase filter to measure the reflective nano-structure. Experimental results illustrate that the lateral resolution was enhanced from 560 nm to 280 nm and the phase sensitivity was down to 4 nm. The purposed common-path spiral digital holographic microscopy has potential applications in real-time measurement and industrial inspection.

Acknowledgment

This work was financially supported in part by the Ministry of Science and Technology, Taiwan (MOST 105-2221-E-003 -015 -MY3 and MOST 104-2221-E-034-010-MY3).

References

[1]E. Cuche, F. Bevilacqua, and C. Depeursinge, “Digital holography for quantitative phase-contrast imaging,” Opt. Lett.**24**(5), 291-293 (1999).

[2]G. Popescu, T. Ikeda, R. R. Dasari, and M. S. Feld, “Diffraction phase microscopy for quantifying cell structure and dynamics,” Opt. Lett. **31**(6), 775-777 (2006).

[3] C. Maurer, A. Jesacher, S. Bernet, and M. R. Marte, “What spatial light modulators can do for optical microscopy,” Laser Photonics Rev. 5(1), 81-101 (2011).

[4] C. Maurer, S. Bernet, and M. R. Marte, “Refining common path interferometry with a spiral phase Fourier filter,” J. Opt. A: Pure Appl. Opt. 11, 094023 (2009).

54.

GPU Implementation of Phase Retrieval with Fourier Transform

Yang-Hsien Lin,[1)] and Kung-Bin Sung[1,2,3)]

[1)] Institute of Biomedical Electronics and Bioinformatics, National Taiwan University, Taipei, Taiwan

[2)] Department of Electrical Engineering, National Taiwan University, Taipei, Taiwan

[3)] Molecular Imaging Center, National Taiwan University, Taipei, Taiwan

1. Background

Common-path tomographic diffractive microscopy (cTDM) has been used to investigate the optical properties and structural details of biological samples [1-2]. The quality of 3-D refractive index maps highly depends on the two-dimensional quantitative phase image (QPI) [3]. The QPI can be extracted from interference patterns generated by the sample beam interfering with a unform reference beam. In order to quantitatively retrieve the phase and the amplitude of the wave front after the sample beam passes through the specimen, the process contains phase extraction and 2-D phase unwrapping to solve 2π ambiguities. Typically, the extraction process of a hologram with one mega pixels takes half a minute. To develop real-time analysis for clinical applications such as disease diagnosis, fast holographic processing and visualization is important. Therefore, in this study we integrate parallel computing with a graphics processing unit (GPU) into the phase retrieval to improve the efficiency of computations.

2. System Setup

cTDM was used to acquire a series of two-dimensional phase images of 10 μm polystyrene bead. The details of the system architecture were described in [3]. cTDM illuminates the sample using a 532 nm continuous-wave diode-pumped solid-state laser with angles ranging from -65° to 65°. The laser beam is expanded by a spatial filter and then focused by a scan lens to the back focal plane of an oil-immersion condenser to generate plane wave illumination. An oil immersion objective lens collects transmitted illumination light and forwardly scattered light of the specimen. A transmission grating is placed at about 70 mm in front of an intermediate image plane to generate multiple diffraction orders of the transmitted light. A window allows the zeroth-order and the first-order beams to pass. An image of the specimen in the zeroth-order beam interferes with a uniform first-order beam serving as the reference beam. Interference images of the specimen are acquired by a high-speed CMOS camera.

3. Phase Retrieval

The digital hologram recorded by the camera can be expressed as follows [4]:

$$I = |O^2| + |R^2| + O^* R + R^* O,$$

where I is the image irradiance, O* and R* are complex conjugates of the fields of the sample beam and the reference beam, respectively. The phase extraction process consists of the following steps:

Step 1. We convert the hologram (NxN pixels) to the 2-D Fourier domain using a built-in CUDA 2-D FFT function (cuFFT), and the resulting matrix contains NxN complex pixels.

Step 2. The cross-correlation term with N/4 x N/4 complex pixels is cropped into a new matrix. Step 3. Convert the cropped cross-correlation back to the image domain using 2-D inverse FFT.

Step 4. To solve 2π ambiguities, we apply a 2-D Fourier-based phase unwrapping algorithm (FFT-based) to calculate forward/inverse Laplacian operators and solve the phase jump problem on the N/4 x N/4 image matrix. [5] The unwrapped phase map is expressed as

$$\phi'(x,y) = FFT^{-1}\left(\frac{FFT\left\{\cos\phi_w FFT^{-1}\left[\left(p^2+q^2\right)FFT\left(\sin\phi_w\right)\right]\right\}}{\left(p^2+q^2\right)}\right)$$

$$-FFT^{-1}\left(\frac{FFT\left\{\sin\phi_w FFT^{-1}\left[\left(p^2+q^2\right)FFT\left(\cos\phi_w\right)\right]\right\}}{\left(p^2+q^2\right)}\right)$$

Step 5. Enlarge the unwrapped phase image to the original size (N x N).

4. Results

We used NVidia's GeForce GTX 970 GPU on a personal desktop computer with Intel Core i7-3820 3.60 GHz 8GB RAM CPU. Single-precision floating-point format was used on the cuFFT processing. The results of calculation time are list on Table 1. All the calculation time of phase map contains the processing of sample and background images. Compared to the CPU (C++) processing time, the GPU processing time has significant shorter as expected. For 1024 × 1024 pixel holograms, the speed factors can be achieved to 50× and 19× with Goldstein's method and FFT-based method on CPU.

Table 1. Comparison of the calculation time (in second) on the CPU (C++) and the GPU (CUDA)

		Data Transfer	Wrapped Phase Extraction	Phase Unwrapping	Total Time
CPU	Goldstein's method	--	1.64	30.37	32.01
	FFT-based	--	1.64	10.47	12.11
GPU	FFT-based	0.541	0.072	0.023	0.636

5. Discussion and Conclusion

In general, parallelizing the multi-step algorithm (path-dependent algorithm) might be a challenging task since some steps might be sequential and impossible to parallelize. In the current results, we implement the FFT-based phase retrieval with CUDA for extracting the quantitative phase images from the interference patterns. Our GPU implementation is significantly faster than the commonly used Goldstein's method implemented on the conventional computer. The results demonstrate the potential of the implementation for real-time extraction and quantitative visualization of phase maps.

References

[1] Su JW, Hsu WC, et al (2014). J Biomed Opt, 19(7):75007.

[2] Su JW, Lin YH, et al (2015). Biomed Opt Express. 6(10): 3795–3805.

[3] Hsu WC, Su JW, et al (2014). Opt Lett, 39(7):2210-13.

[4]Ikeda T, Popescu G, et al (2005). Opt Lett, 30(10):1165-7.

[5] Schofield MA, Zhu Y (2003). Opt Lett, 28(14):1194-6.

55.

Single Light Source Tracking Method for Collinear Holographic Data Storage System

Yawara Kaneko[1)2)]
Teikyo Heisei University, 2-51-4 Higashi Ikebukuro, Toshima-ku, Tokyo 170-8445, Japan[1)]
TechnoConsulting, Inc., Chigasaki 253-0056, Japan[2)]

Introduction

Collinear holographic data storage system has been invented[1)] and proposed[2)] as one of the next generation data storage systems with large data capacity and high data transfer rate. The collinear system has a simple optical pick-up and data is recorded on rotating disk so called on-the-fly like as conventional optical disk storage system.

Consequently, as the first step of industrialization of the collinear system, 200 Gbyte holographic disk has been defined as international standard of ecma-377 titled of “Information Interchange on Holographic Versatile Disc (HVD) Recordable Cartridges – Capacity: 200 Gbytes per Cartridge” by ecma international[3)]. People can image and discuss a practical production of the collinear system by taking the standard ecam-377 into account.

The 200 Gbyte system has two light sources. One is green LASER for holographic data recording and retrieving. The other is red LASER for focusing and tracking while a recording medium consists of a holographic recording layer and a conventional pit layer[4)]. The pit layer is used for tracking of sequence of recorded holographic data pages. The above is an outstanding way because it introduces well-established tracking technology of the conventional optical disk storage system into the collinear holographic data storage system.

However if there is another tracking method without using a red light nor a pit layer, the system should become more simple and more mass productive. Actually one of challenges of the standard ecma-377 is that the axis of the green LASER beam and the red LASER beam should be precisely aligned for keeping media interchangeability among more than one collinear holographic data storage drives. In addition, a recording medium with only holographic recording layer but without pit layer costs much less and yields much more than a medium with layers for holographic recording and tracking pits.

In this paper the author proposes a method of tracking of sequence of recorded holographic data pages along rotation of a disk using only green LASER without using a red LASER nor a pit layer.

Discussion

In the proposal a singal for the tracking is to be recorded by green LASER and in the holographic recording layer instead of the pit layer right before or after recording of holographic data page.
The tracking signal is going to show up somewhere between the data page pattern area and reference pattern area or somewhere within data page pattern area. The figure 1 shows a layout of data page pattern and reference pattern on the 358 pixels by 358 pixels spatial light modulator defined in the standard ecma-377. The pitch of spatial modulator elements is defined as 13,68 μm ± 0,02 μm. The data page pattern is defined in the 192 pixels by 192 pixels area. The annular reference pattern surrounds the data pattern area. The outer diameter of the annular reference pattern is defined as 358 pixels and the inner diameter is defined as 230 pixels. Note that the width of the annular reference pattern is 65 pixels.
The position error sensitivity should be relaxed for tracking signal for continuous servo control while the position error sensitivity should be strict for low cross talk noise from adjacent data pages. The author previously proposed a way of controlling sensitivity of retrieving intensity on position error[5)] in a range from less than 3 μm to more than 9μm.

Conclusion

A method of tracking of sequence of holographic data pages of collinear holographic data storage system is proposed. It uses single LASER source in a drive for tracking and data recording/ retrieving and single holographic recording layer in a medium.

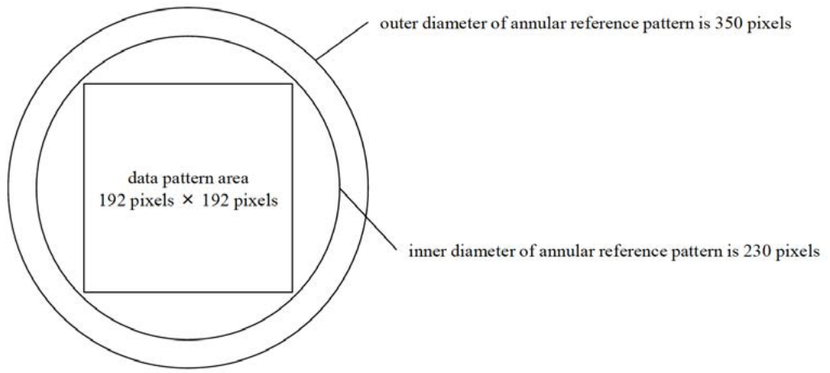

Figure 1. Layout of data page pattern and reference pattern.

References

[1] H. Horimai and K. Saito, “OPTICAL INFORMATION RECORDING DEVICE AND METHOD, OPTICAL INFORMATION REPRODUCING DEVICE AND METHOD, AND OPTICAL INFORMATION RECORDING MEDIUM”, Japan Patent,10-124872,A, published in 1998.
[2] Horimai H, Tan X. Collinear technology for a holographic versatile disk. Applied Optics, 2006, 45(5): 910–914
[3] ecma international, “Information Interchange on Holographic Versatile Disc (HVD) Recordable Cartridges – Capacity: 200 Gbytes per Cartridge”, http://www.ecma-international.org/publications/standards/Ecma-377.htm
[4] H. Horimai, “OPTICAL INFORMATION RECORDING MEDIUM”, Japan Patent, 11-311936,A, published in 1999.
[5] Y. Kaneko, “Asymmetric shift selectivity control and application for hologram position sensing in collinear holographic information storage system”, TuE08, ODS2007, Portland Oregon.

56.

Scanning Projected Fringe Profilometry for Shape Measurements

Yi-An Lin,[1)] Nai-Jen Cheng,[1)] and Wei-Hung Su[2)]

[1)]Institute of Photonics and Communications, National Kaohsiung University of Applied Sciences, Kaohsiung 80778, Taiwan

[2)]Department of Materials and Optoelectronic Science, National Sun Yat-Sen University, Kaohsiung 804, Taiwan

1. Introduction

Fringe projection schemes [1-2] are one of the powerful tools to describe the 3D surface profile due to its properties of full-field inspection and high sampling density. A fringe pattern is projected onto the inspected object and a CCD camera is used to observe the projected fringes. It can be further divides into two categories: the off-axis schemes and the on-axis schemes.

In the method of on-axis schemes, the line of sight of the CCD camera is the same as fringe projector. The depth-of-field of the camera lens and the depth-of-focus of the projector lens are so short that only the projected fringes located at the image-focused area can be clearly observed. Fringes outside the image-focused area are blurred. Thus, the focused fringes address the contour of the object at a specific depth position. By moving the inspected object around the focused area along the depth direction, a set of images, which addresses the contour of the object by the focused fringes, is obtained. The 3D surface profile is retrieved by assembling the image contours with their corresponding depths.

In this paper, a scanning approach based on the on-axis schemes is proposed. With the proposed image processing algorithm, noises and errors are efficiently detected and reduced.

2. Principle and experiment

Figure 1(a) illustrates the optical configuration of the on-axis scheme. A sinusoidal fringe pattern is illuminated by the light source and then projected onto the inspected object by a projecting lens and a beam splitter. Fringes projected on the inspected object are observed by a CCD camera. In our setup, a halogen lamp is used as the light source.

A seremban plant posited on a translation stage was selected as an inspected sample. Figure **1(b)**

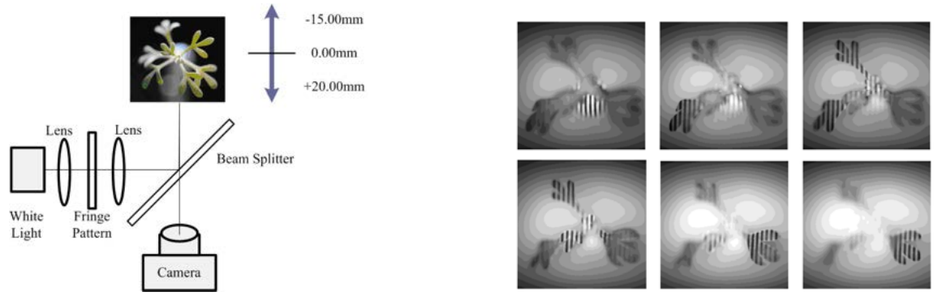

Fig. 1. (a) Schematic setup of the scanning fringe projection. (b) Appearance of the focused plane located at various depth positions

illustrates

some examples of the obtained images. Only the projected fringes located at the image-focused area can be clearly observed. Outside the image-focused plane, the fringe contrast is getting worse. Thus, the contour of the object is addressed by means of the fringe contrast.

Amplitude of the fringes can be extracted in the frequency domain. Figure 2(a) illustrates the amplitude extracted from Fig. 1(b). Compared with the image-focused area, the amplitude of the misfocused fringes is getting worse. Now that the scanning approach have taken a couple of measurements to extract the amplitudes with their associated depth positions, a relationship between the depth and the amplitude can be determined by a proper curve-fitting algorithm. Finding the depth position for each image pixel becomes searching for the location of the maximum amplitude from the fitted curve.

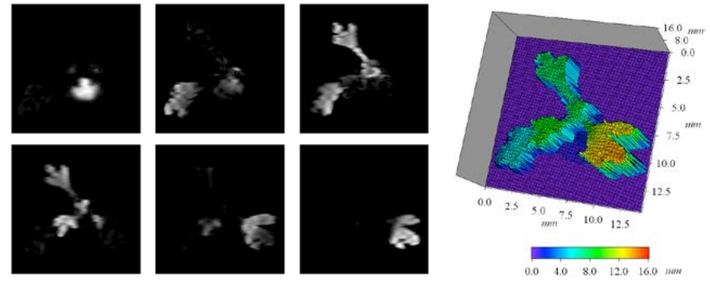

Fig. 2.(a) Amplitude map extracted from the frequency domain. (b) The retrieved profile.

By assembling the available data points for each depth position, the profile can be retrieved, as illustrated as Fig. 2(b). Depth positions at the inspected object's edge area cannot be accurately described. The reason comes from that the band-pass filtering algorithm always fooled by the change of gray-levels at the edge area. It always assigns a wrong amplitude value to the edge area, even though that area is only the background. On the other hand, accuracy is limited not only by the accuracy of the band-pass filter, but also by the precision of the curve-fitting algorithm. In our system, the accuracy was approximately 300 microns

3. Conclusion

A one-dimensional scanning method based on fringe projection to describe the profile of the inspected object is presented. Shadowing caused by tilted fringe projection can be eliminated. Even though a lot of depth discontinuities appear on the obtained image, the proposed method describes the 3D profile very well. The overall hardware is simple, robotic, and compact. Systematic accuracy is mainly limited by the precision of the curve-fitting algorithm and accuracy of the band-pass filter.

References

[1] V. Srinivasan, H. C. Liu, and M. Halioua, "Automated phase-measuring profilometry of 3-D diffuse objects," Appl. Opt. Vol. 23, 1984, pp. 3105-3108.

[2] M. Takeda, T. Aoki, Y. Miyamoto,; H. Tanaka, R. Gu, Z. Zhang, "Absolute three-dimensional shape measurements using coaxial and coimage plane optical systems and Fourier fringe analysis for focus detection," Opt. Eng. 39, 2001, pp. 61-68.

57.

Multiwavelength Meta-hologram

Yi-Chieh Lai, [1] Hisang-Chu Wang, [2] Yao-Wei Huang, [2,5] Cheng Hung Chu, [5] Pin Chieh Wu, [2,5] Hui Jun Wu, [5] Wei-Yi Tsai, [2] Chih-Ming Wang, [3] Greg Sun, [4] and Din Ping Tsai[2,5]

[1]Department of Photonics and Advanced Optoelectronic Technology Center, National Cheng Kung University, Tainan 701, Taiwan

[2]Department of Physics, National Taiwan University, Taipei 10617, Taiwan

[3]Institute of Opto-electronic Engineering, National Dong Hwa University, Hualien 97401, Taiwan

[4]Department of Engineering, University of Massachusetts Boston, Boston, Massachusetts 02125, United States

[5]Research Center for Applied Sciences, Academia Sinica, Taipei 11529, Taiwan

** L78021020@mail.ncku.edu.tw*

1. Introduction

In the past decade, metamaterials/metasurfaces composed of sub-wavelength artificial structures show tailored optical properties in electromagnetic regions, enabling us to develop holograms in any electromagnetic wavelength region [1, 2]. Metamaterials with tunable effective refractive indices by design have been applied to holograms in which switchable polarizations and dual images of different wavelengths were demonstrated in the near IR region [3, 4]. The spatial phase and amplitude modulation of metasurfaces have a better employment to achieve the spatial light modulators (SLM) and have been explored to realize polarization- controlled dual images at arbitrary electromagnetic wave region in referred to as broadband metasurface hologram or meta-hologram [5-7]. What remains elusive is the demonstration of a full-color meta-hologram because of the inherent loss of gold in the visible range that had been commonly used in the above-mentioned literatures. Metasurfaces incorporating metal with higher plasma frequency like aluminum offer the unique opportunity to extend the working wavelength to cover the entire visible spectrum for the generation of full-color meta-hologram [8].

2. Results

Here we present a phase-modulated full-color meta-hologram based on a thin reflective metasurface that projects polarization switchable images in three primary colors. Figure 1(a) shows the schematic setup of meta-hologram under y-polarized white light illumination (consisting of 405, 532, and 658 nm laser beams) that reconstructs images “R” in red, “G” in green, and “B” in blue, respectively. The meta-hologram consists of 180 × 180 pixels, and each pixel of it consists of 4 sub-pixels; one for blue, one for green, and two for red because of the lower reflectance of red light. The metasurfaces with patterned nanoantenna array in each pixel yield the required phase distribution of a computer-generated hologram (CGH) designed by iterative Fourier-transform algorithm (IFTA). Each sub-pixel has 4 × 4 aluminum nanoantennas patterned on top of a thin SiO_2 layer on a thick aluminum mirror. All nanoantennas are designed to have the same width of 50 nm and thickness of 25 nm with only their lengths varied to generate the required phase and reflectance.

We have calculated the phase and reflection of the periodic aluminum nanoantennas on top of SiO_2 and aluminum layer under the normal illumination of a y-polarized light. To reduce the crosstalk in projected images between these three operating wavelengths, we have selected the scheme of 2-level phase modulation in meta-hologram. Two different rod lengths were chosen for each wavelength in such a way that they yield a phase difference of π while maintaining approximately the same reflectance. Therefore, there are total 6 kinds of length of nanoantenna with their corresponding reflection and phase modulations we have selected to realize the meta-hologram. Narrower resonances of the nanoantennas are common for minimizing crosstalk, but it is more challenging in fabrication to suffering from lower reflectance. Considering this trade-off, our design of nanoantenna pixels has yielded resonances of adequate bandwidths with acceptable reflectance and reasonably low crosstalk.

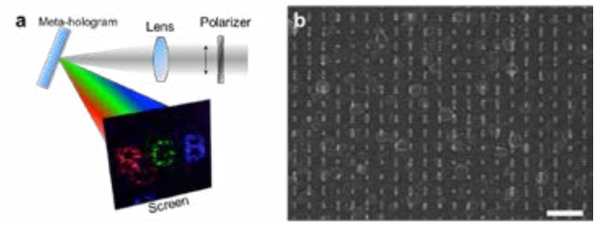

Fig. 1. (a) Illustration of the meta-hologram under linearly polarized illumination. The structure produce images R, G, and B in three primary colors (405 nm, 532 nm, and 658 nm), respectively. (b) SEM image of the fabricated structure. The scale bar is 500 nm.

The meta-hologram was fabricated with standard e-beam lithography. Figure 1(b) shows the scanning electron microscope (SEM) image of a small region of the fabricated sample. The corresponding lengths of nanoantenna for the binary phases are used to form the sub-pixels, each of them occupies an area of 800 × 800 nm^2 consisting of 4 × 4 aluminum nanoantennas of equal dimensions.

Figure 1(a) shows the optical measurement setup to measure the projected image of fabricated structure. We employed white light illumination consisting of three laser diodes emitting at 405, 532, and 658 nm. The laser beam of any linear polarization can be select by rotating the polarizer. The meta-hologram was placed onto the focal plane of lens where the reconstructed images are recorded directly by a CCD camera. The image in the screen of Fig. 1(a) shows the CCD recording of reconstructed images, where the three letters of different colors and equal size are positioned in a row. Because the diffraction angle varies with the wavelength, the appearance location of a letter image depends on its working wavelength. Therefore, we have designed the sizes of letters with the normalization factor to make the reconstructed images fall into the right positions with the equal size. We note that, the nanoantennas array of the meta-hologram are align along the y-direction, which works under the y-polarized illumination. Therefore, as the laser beam polarization being rotated from y- to x-direction, the recorded image gradually disappeared, which makes a polarization switchable and capable of producing images.

3. Conclusion

We have demonstrated original approach of a phase-modulated full color meta- hologram with polarization switchable property using aluminum nanoantennas with resonances in three primary colors of the visible range. Working with the proper pixel arrays of nanoantennas and material combination, we have designed narrow- bandwidth meta-hologram. This design allowed us to implement the full color scheme with the three primary colors. We can project images to specific locations with pre-determined size by taking into account of the wavelength dependence of the diffraction angle. The phase modulated device can be easily link to fully developed SLM. The low-coast materials of aluminum and silica make MCMH mass- producible. The polarization switchable meta-hologram presented here can be expanded to yield dual images with the design of cross nanoantennas. Therefore, each direction of nanoantenna can be used to produce one image under a particular polarized illumination, with potential applications in performing polarization analyzer, data storage, and glass-free 3D imaging.

References

[1] N. Yu et al. Science 334, 333-337 (2011)
[2] S. Sun et al., Nano Lett. 12, 6223-6229 (2012).
[3] S. Laroucheet al., Nat. Mater. 11, 450-454 (2012).
[4] B. Walther et al., Adv. Mater. 24, 6300-6304 (2012).
[5] X. Ni et al., Nat. Commun. 4, 2807 (2013).
[6] L. Huang et al., Nat. Commun, 4, 2808 (2013)
[7] W. T. Chen et al., Nano Lett. 14 , 225-230 (2014). [8] Y.-W. Huang et al., submitted (2014).

58.

Spatial and temporal imaging in digital holographic microscopy for quantitative analysis

Yu-Chih Lin,[1] Xin-Ji Lai,[1] Han-Yen Tu[2], and Chau-Jern Cheng[1]

[1] Institute of Electro-Optical Science and Technology, National Taiwan Normal University, Taipei 11677, Taiwan

[2]Department of Electrical Engineering, Chinese Culture University, Taipei 11114, Taiwan

**E-mail: yclin_ioplab@ntnu.edu.tw*

***Abstract*— This study presents the spatial and temporal imaging in digital holographic microscopy for high resolution quantitative analysis. The applications in biological and physics research has been achieved with sub-micron and picoseconds resolution. The novel method and potential applications for ultrafast, super-resolution wavefronts recording and reconstruction will be discussed in this study.**

***Keywords*— resolution, time-resolved, digital holographic microscopy**

1. Introduction

Digital holographic microscopy (DHM) [1-3] has been wid ly used in quantitative measuremen s for optical micro-elements or biological samples. Quantitative complex imaging (amplitude and phase) is an important issue in recently studies, becaus the complex wavefronts can serve the analysis for detecting the three-dimensional optical thickness profile with high phase accuracy in sub-wavelength range. Compare to the high phase accuracy in DHM, the spatio-temporal resolution becomes more and more important when applied DHM system to the precise researches as biological and physics applications. For spatial domain, the infinite aperture size and wavelength of light have restricted the spatial resolution of optical imaging system. In recent, the synthetic aperture (SA) method is widely used in quantitative imaging for overcome the diffraction limit and resolution enhancement [4]. Then, the Ultrashort pulse laser is well established as a convenient tool for surface processing and optical excited of several different materials [5,6], such as optical absorption, heat conduction, phase transitions, evaporation kinetics and plasma dynamics. And the ultrashort duration in pulse laser has a good potential for ultrafast time-resolved measurement and improve the temporal resolution up to sub-picoseconds time scales [7].

2. Resolution enhancement in spatial imaging

The schematic representation of the resolution enhancement by synthetic aperture in digital holographic microscopy is indicated in Fig. 1(a). The synthetic aperture task was achieved by the scanning of the galvo mirror with the 4-f imaging architecture in object arm. In this experiment, the scanning angles could attain a scanning range of ±65°. Experimental results of the resolution enhan ement are shown in Fig. 1(b). The spatial resolution was improved to 200 nm and the finest structure in the cell body can be observed as in he magnified area in Fig. 1(b) after employed the synthetic ape ture in digital holographic microscopy.

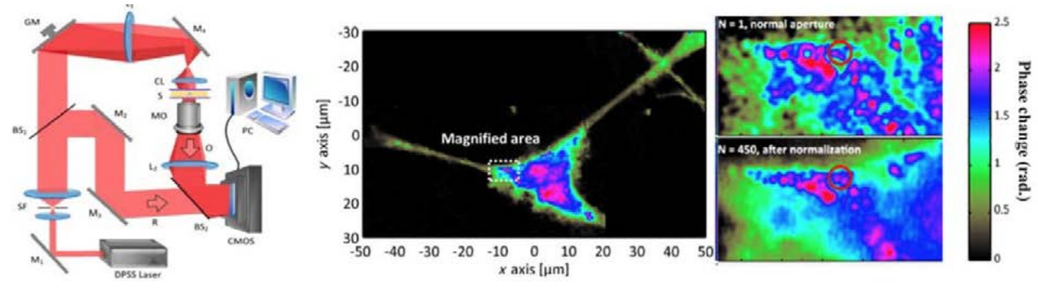

Fig. 1. (a) experimental setup of synthetic aperture DHM and (b) its resolution enhancem nt results for measuring the living cell.

3. Ultrafast time-resolved imaging by pulsed digital holographic microscopy

We propose and demonstrate a time-resolved pump-probe pulsed digital holographic microscopy as in Fig. 2 to observe the ultrafast phenomenon of photoexcited phase change in dielectric material. The reconstructed pulse-induced phase is shown in Fig. 3, where the ultrafast excited in graphene was obtained and analyzed in femtosecond scale. The pulse-induced phase variation would be start in 0 fs as in Fig. 3(a), and achieve to higher variation in 100 fs as in Fig. 3(c). The phase variation

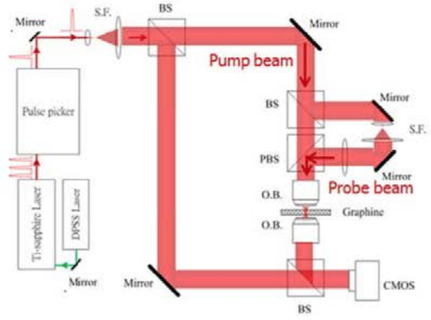

Fig. 2 Experimental setup of the time-resolved pump-probe pulsed digital holographic microscopy. S.F.: spatial filter; BS: beam splitter; PBSpolarized beam splitter; O.B.: objective.

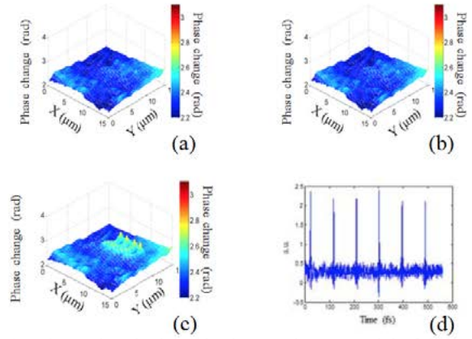

Fig. 3. Pulse-induced phase change with fringes structure in the sample at (a) 0 fs, (b) 50 fs, (c) 100 fs, and intensity of diffraction tem from the pulse-induced phase fringe on materia l by far-field measurement

would be decreased and disappeared after 300 fs in following experiments. The diffraction from this fringe has been analysis in far-field diffraction by high frequency photodetector as in Fig. 3(d). The diffraction angle of firs order term is 16 degree, which is similar with the frequency of reconstructed phase fringes by near-field (DHM) measurement.

4. Conclusions

We have proposed and demonstrated different techniques to enhance the spatial and temporal resolution in digital holographic microscopy an applied to biological and physics studies. The high spatial resolution information by synthetic aperture method is served for the living cell measurement. With employed the pulsed laser, the ultrafast time-resolved imaging can also applied to analyze the photoexcited phenomenon.

Acknowledgment

This work was financially supported by the Ministry of Science and Technology, Taiwan (MOST 102-2221-E-003 -025-MY3, MOST 105-2221-E-003 -015 -MY3, MOST 105-2923-E-003-001, and MOST 104-2221-E-034-01 -MY3).

References

[1] M. K. Kim, Digital Holography and Microscopy: Principles, Techniques, and Applications (Springer Verlag, 2011).

[2] L. Miccio, P. Memmolo, F. Merola, S. Fusco, V. Embrione, Chip 14(6), 1129–1134 (2014). . Paciello, M. Ventre, P. A. Netti, and P. Ferraro, Lab

[3] X. J. Lai, H. Y. Tu, C. H. Wu, Y. C. Lin, and C. J. Cheng, Appl. Opt. 54, A51-A58 (2015).

[4] Y. Cotte, F. Toy, P. Jourdain, N. Pavillon, D. Boss, P. Magistretti, P. Marquet, and C. Depeursinge, Nat. Photonics 7, 113–117 (2013).

[5] R. Kammel, R. Ackermann, J. Thomas, J. Götte, S. Skupin, A. Tünnermann, and S. Nolte, Light: S i. Appl. 3(5), e169 (2014).

[6] K. J. Tielrooij, J. C. W. Song, S. A. Jensen, A. Centeno, A. Pesquera, A. Zurutuza Elorza, M. Bonn, L. S. Levitov, and F. H. L. Koppens, Nat. Phys. 9, 248–252 (2013).

[7] Y. Hayasaki, M. Isaka, A. Takita, and S. Juodkazis, Opt. Express 19, 5725-5734 (2011).

59.

The Implementation of Real-Time Tracking and Time Reversal of Random Scattering in Diffused Media Based on Kitty Self-Pumped Phase Conjugate Mirror

Yeh-Wei Yu1[2], Yu-Heng Chen[1], Wei-Hsin Chen[1] and Ching-Cherng Sun[*1]
[1]Department of Optics and Photonics, National Central University, Chung-Li, Taoyuan City 32001, Taiwan
[2]Optical Science Center, National Central University, Chung-Li, Taoyuan City 32001, Taiwan

Summary

In the past few decades, there are large amounts of academic references which showed the reversing techniques of random scattering in turbid media [1,2]. With the aid of the technique, we are able to inject the laser beam into the biological tissue and produce a high-density power focusing point in order to kill the unwanted malignant cells. Optical phase conjugation (OPC) is one of the methods which successfully implements the technique of optical conjugation. Based on the technique of reversing of random scattering in turbid media, we hereby demonstrate a brand-new phase conjugate time differentiator which features self-tracking in vivo. Applied with the concept of phase conjugate time differentiator and the reversing technique of random scattering in turbid media through optical conjugation, we verify the fidelity and the availability of our structure by experiments. Additionally, we successfully focus the conjugate signal inside a simulated bio-tissue. The research will definitely make a tremendous contribution towards the observation of moving creatures in the field of bio-imaging.

Signal recoded inside the barium titanate forms gratings. The readout beam reads out the gratings which has been recorded to obtain the signal. The former descriptions occur with only few milliseconds. One of the unique behavior of barium titanate is that it can promptly clean out the signal being input at last moment and record the signal being input at next moment. We bring a barium titanate as a self-pumped phase conjugate mirror (SPPCM), a liquid crystal panel within a circle signal as a simulated bio-tissue and an Electro-optic modulator (EOM) periodically input whole pages of 0, pi signals at different time into our structure, shown in figure 1. If the simulated bio-tissue has no movement, the recorded gratings at last moment and next moment inside the barium titanate stagger completely, which causes no conjugate signal reversing back on the CCD. If the simulated bio-tissue has little movement, the recorded gratings at last moment and next moment inside the barium titanate stagger incompletely. Therefore, there are still some conjugate signals reversing back on the CCD (figure 2). We can then apply our structure to in vivo tracking.

Based on the above structure, we apply the phase conjugate time differentiator to the technique of reversely focusing a spot inside turbid media and real-time self-tracking. Considering the issues of étendue and the limited active incident angle of barium titanate, we place a lens in the middle of two diffused objects in order to collect more scattering signals. Preventing from obtaining the fake conjugate signals during reconstruction, we especially design our original signals as a three-spot circle and a complete circle. We put both signals in the EOM periodically and then observe the conjugate signals on the CCD. Also, we simply observe the axial tolerance of the conjugate signal on the CCD including 0 mm, 1 mm, 2 mm, 3 mm, 4 mm and 5 mm axial shift away from the focal plane, shown in figure 3.

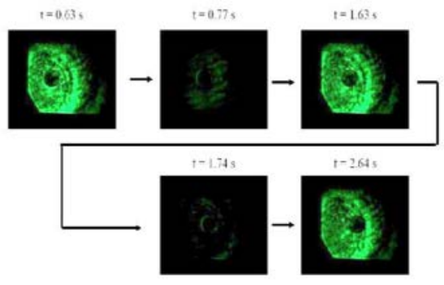

Fig. 1. shows that the conjugate signal keeps reversed once per 1.63 seconds.

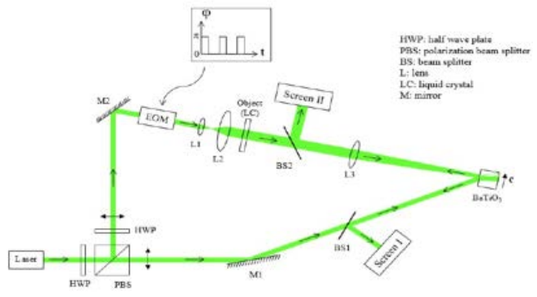

Fig. 2. The experimental setup of phase conjugate time differentiator with kitty-SPPCM.

Fig. 3 shows the conjugate signal observed on the CCD. We place the CCD at the difference places to check tolerance of the system including (a) on-focus, (b) 1 mm, (c) 2 mm, (d) 3 mm, (e) 4 mm and (f) 5 mm away from the focus.

References

[1] M. Cui and C. Yang, “Implementation of a digital optical phase conjugation system and its application to study the robustness of turbidity suppression by phase conjugation,” Opt. Express **18**, 3444-3455 (2010).

[2] Y. M. Wang, B, Judkewitz, C. A. DiMarzio, and C. Yang, “Deep-tissue focal fluorescence imaging with digitally time-reversed ultrasound-encoded light,” Nat. Commun. **3**, 928 (2012).

60.

Multi-Layered Holographic Memory using Virtual Phase Conjugation

Yuta Goto[1)], Atsushi Okamoto[1)], Kazuhisa Ogawa[1)], Akihisa Tomita[1)] and Kunihiro Sato[2)]

[1)] Graduate School of Information Science and Technology, Hokkaido University, Sapporo, 060-0814, Japan

[2)] Faculty of Engineering, Hokkai-Gakuen University, Sapporo, 064-0926, Japan

1.Introduction

Until now, although various multiplexing techniques, e.g. an angular multiplexing[1)], a shift multiplexing[2)] has been proposed, these cannot utilize a whole of a recording area in a medium effectively because only the cross-sectional (*xy*-) direction is used for multiplexing holograms. By contrast, a multi-layered holographic memory[3,4)] has been proposed as a technique for effectively utilizing the three-dimensional recording area in a medium. However, the multi-layered holographic memory requires the sequential recording and reading of holograms while scanning a medium along the depth (*z*-) direction.

To solve the problem, we propose a multi-layered holographic memory using a virtual phase conjugation (VPC). In this method, multiple signal beams are added lens phase factors, which has a different curvature, and are combined. Hence, each signal beam is focused into different z-positions in a medium, respectively. After simultaneous recording and reading these signal beams by a single reference beam, each signal beam is selectively demodulated using the VPC based on the effect of the phase modulation of a random diffuser and an optical phase conjugation. Thus, our method enables us to simultaneously record and read multiple signal beams in each layer of a medium. In the following, we describe the basic principle of our method and numerically analyze the recording and reading characteristics of our method. In addition, we also compare the achievable multiplexing number of our method and that of the conventional method.

2.Method

Proposed method as shown in Fig. 1 includes the generation process for a multiplexed diffusion-signal-beam [Fig 1(a)], the processes for recording and reading of hologram [Fig. 1(b)] and the demodulation process using the virtual phase conjugation [Fig. 1(c)]. In addition, generation and demodulation processes are performed as an electronic process in a computer.

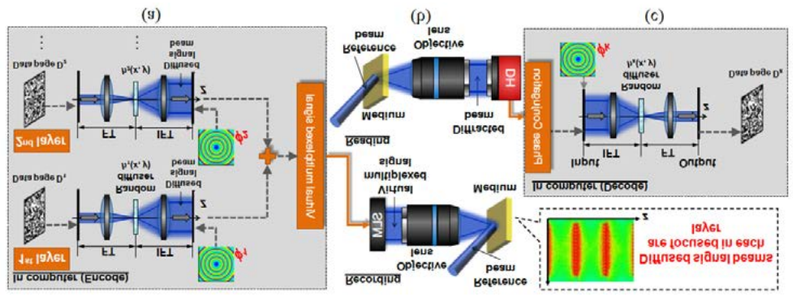

Fig. 1. Schematic diagram of

First, during the generation process, a spatial spectral distribution of a two-dimensional data page D_k (k = 1, 2, 3, …, M) carried out the fast Fourier transform (FFT) is modulated by a random diffuser $h_k(x, y)$. Here, M is a layer number. Then, a diffusion-signal-beam is calculated by applying the inverse FFT (IFFT) to the modulated spatial spectral distribution. Depending on number of M, diffusion-signal-beams are generated and added the lens phase factor $\phi_k(x,y)$ which has different curvature. Then, a multiplexed diffusion-signal-beam is generated by combining these diffusion-signal-beams. Next, during the process for recording and reading of hologram, the multiplexed diffusion-signal-beam is reproduced on an actual optical system using a spatial light modulator (SLM). After that, the interference fringes of multiplexed diffusion-signal-beam and the reference beam is recorded into a medium. It is noteworthy that components of each diffusion-signal-beam is focused into different *z*-positions of the medium by the influence of lens phase factors. In the reading of the holograms, the multiplexed diffusion-signal-beam is diffracted by irradiating the reference beam to the medium again. Then, the complex amplitude distribution of the diffracted beam is detected by digital holography (DH). Finally, during the demodulation process, the phase conjugation, inverting the sign of the phase term, is implemented to the beam detected by DH. After adding the lens phase factors $\phi_k(x,y)$ again, FFT, the phase modulation by random diffuser and IFFT are applied to the phase conjugated detection beam. At the time, the only desired signal beam is demodulated as the original data page. As mentioned above, since our method has capable of simultaneous recording and reading of holograms along *z*-direction, a multi-layered holographic memory with simplified optical system can be realized.

3.Numerical analysis

In this simulation, we used the FFT beam propagation method[5)]. Parameters used in this simulation are shown in Table I. In addition, the layer number M is 2. First, we demonstrate the simultaneous recording of 2 holograms in different z-position (−200 μm and 200 μm) using our method. Figure 2 shows the normalized diffraction efficiency in each z shift position by varying the curvature of the lens factor. According Fig. 2, it can be seen that each hologram is recorded in different *z*-positions, respectively. Next, we analyze a signal-to-noise ratio (SNR)[6)] when our method and conventional method are applied to the speckle shift multiplexing method. For each recording, the first data page is read and its SNR is calculated. Figure 3 shows the relation between the SNR of the first data page and multiplexing number. According to Fig. 3, when 100 data pages are recorded in each layer (200 data pages in total), the achievable SNR of our method is good agreement with the conventional method. It is evident that our method can perform the simultaneous recording and reading of holograms in multiple layers while maintaining the achievable multiplexing number.

Table I. Numerical parameters.

Wavelength, λ	405 nm
Numerical aperture, NA	0.53
Pixel pitch of SLM, $d_x \times d_y$	10 × 10 μm²
Pixel number of SLM, $N_{px} \times N_{py}$	32 × 32
Thickness of medium, L	400 μm
Analytical sample number, $N_x \times N_y \times N_z$	2048 × 2048 × 512
Diffusion angle of diffuser, θ_{diff}	2.0 deg
Incident angle of ref. beam, θ_{ref}	32.0 deg

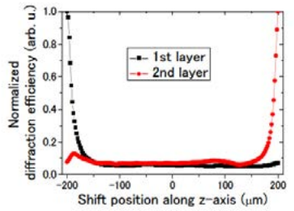

Fig. 2. Normalized diffraction efficiency along *z*-direction.

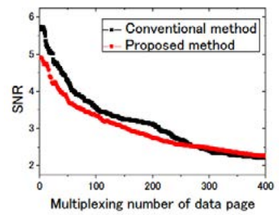

Fig. 3. Relation between SNR and multiplexing number.

References

[1] J. Liu, J. Opt. Soc. Am. A **28**, 229 (2011).
[2] D. Psaltis, *et al*., Opt. Lett. **20**, 782 (1995).
[3] A. Shibukawa, *et al*., Jpn. J. Appl. Phys. **50**, 09ME10 (2011).
[4] T. Nobukawa, *et al*., Opt. Lett. **40**, 5419 (2015)
[5] J. Tanaka *et al*., Jpn. J. Appl. Phys. **48**, 03A028 (2009).
[6] S. R. Lambourdiere *et al*., Jpn. J. Appl. Phys., **45**, 1246 (2006).

61.

Panoramic 3-D Image Projection Using Computer Generated Phase-Only Hologram

Chien-Yu Chen[1)], Wu-Chun LI[2)], Hsuan-Ting Chang[2)], Chih-Hao Chuang[3)], Yu-Ting Wang[2)], and Tsung-Jan Chang[4)]

[1)]Graduate Institute of Color and Illumination Technology, National Taiwan University of Science and Technology, Taipei 10607, Taiwan
[2)]Photonics and Information Laboratory, Department of Electrical Engineering, National Yunlin University of Science and Technology, Yunlin, Taiwan
[3)]Graduate Institute of Photonics and Optoelectronics, National Taiwan University, Taipei 106, Taiwan
[4)]Electronic and Optoelectronic Engineering, National Yunlin University of Science & Technology, Yunlin, Taiwan

Abstract

In this study, a novel computer-generated holography based on the three-dimensional (3-D) modified Gerchberg-Saxton algorithm (MGSA) for phase retrieval is proposed and demonstrated in a panoramic projection system. The point-based Fresnel transform in the 3-D space is utilized in the MGSA in order to retrieve the panoramic computer-generated phase-only hologram (CGPOH) of a 3-D object. Consider the different viewing angles of the 3-D object. The panoramic CGPOH capable of panoramic 3-D image projections can be determined by using the rotation matrices and illuminating the light sources at the corresponding viewing angles. The computer simulation and optical experiments are conducted to verify that the determined panoramic CGPOH can successfully generate the panoramic projection images with various depths and under the different viewing angles. The computation complexity of the proposed method and the image quality assessment are also provided. The zero order light has been avoided in our experimental results. However, some detailed structures with complicated depth information cannot be clearly reconstructed. Our future work will focus on improving the reconstruction of the detailed structures/patterns in the 3-D projection images. In addition, the speckle effects obtained from the constructive or destructive interference between neighboring light spots in the experimental results are still obvious due to the coherent laser light source.